NEDO-21878
79NED71
CLASS I
SEPTEMBER 1979

MARK I CONTAINMENT PROGRAM ANALYTICAL MODEL FOR COMPUTING AIR BUBBLE AND BOUNDARY PRESSURES RESULTING FROM AN S/RV DISCHARGE THROUGH A T-QUENCHER DEVICE

TASK NUMBER 7.1.1.2

P. VALANDANI
W. T. HSIAO

GENERAL ELECTRIC

NEDO-21878
79NED71
Class I
September 1979

MARK I CONTAINMENT PROGRAM
ANALYTICAL MODEL FOR COMPUTING AIR BUBBLE AND BOUNDARY PRESSURES RESULTING FROM AN S/RV DISCHARGE THROUGH A T-QUENCHER DEVICE

Task Number 7.1.1.2

P. Valandani
W.T. Hsiao

Reviewed by: _____
H. E. Townsend, Manager
Containment Methods

Approved by: _____
A. E. Rogers, Manager
Containment Technology

Approved by: _____
E. Kiss, Manager
Applied Mechanics

NUCLEAR ENGINEERING DIVISON • GENERAL ELECTRIC COMPANY
SAN JOSE, CALIFORNIA 95125

GENERAL ELECTRIC

DISCLAIMER OF RESPONSIBILITY

Neither the General Electric Company nor any of the contributors to this document makes any warranty or representation (express or implied) with respect to the accuracy, completeness, or usefulness of the information contained in this document or that the use of such information may not infringe privately owned rights; nor do they assume any responsibility for liability or damage of any kind which may result from the use of any of the information contained in this document.

TABLE OF CONTENTS

TABLE OF CONTENTS (Continued)

APPENDICES

LIST OF ILLUSTRATIONS

LIST OF ILLUSTRATIONS (Continued)

LIST OF ILLUSTRATIONS (Continued)

1764 172

LIST OF ILLUSTRATIONS (Continued)

1764 173

LIST OF ILLUSTRATIONS (Continued)

1764 174

LIST OF ILLUSTRATIONS (Continued)

LIST OF TABLES

ABSTRACT

This report describes the methodology for calculating the loads on the boundaries of a pressure suppression pool due to safety/relief valve actuation. The methodology is applicable to Mark I plants equipped with T-Quencher discharge devices.

Model predictions are compared with full scale in-plant and 1/4 scale test data, the latter covering the range of the important parameters for Mark I plants.

NOMENCLATURE

SYMBOL	DESCRIPTION
A	Flow area
A_p	Pool area per quencher
G	Mass Flux
G_{ao}	Initial mass flux
G_{am}	Maximum mass flux
H	Pool depth
h	Enthalpy
h_o	Stagnation enthalpy
L_a	Quencher arm length
L_f	Length of perforated portion of quencher arm
M	Molecular weight
m	Mass
m_o	Total air mass per bubble
n	Number of moles or polytropic exponent
P	Pressure
P_B	Bubble pressure
P_o	Maximum interface pressure
P_r	Reference pressure
P_∞	Absolute pressure at the level of quencher arm centerline
R	Gas constant or bubble radius
$\tilde{R}$	Universal gas constant
R_m	Torus major radius
T	Temperature
T_i	Initial air temperature

NOMENCLATURE (Continued)

T_o	Air temperature inside the quencher arm
T_p	Pool temperature
t	Time
t_c	Time at which flow is choked
t_r	Reference time
t_{wc}	Water-clearing time
V	Volume
$\overline{V}$	Average speed
v	Specific volume
$\overline{X}$	Mean of x's
Z	Bubble elevation

Subscripts

a	Air
b	Bubble
g	Vapor
p	Pool
r	Reference
s	Steam
w	Water
wc	Water clearing
t	Temperature
x	Length

NOMENCLATURE (Continued)

Greek Letters

α	Azimuthal angle
β	Polar angle
λ	Scale factor
σ	Standard deviation
ρ	Density

1.0 INTRODUCTION

1.1 SCOPE

This report describes the analytical model developed by the General Electric Company for calculating torus shell pressures in Mark I plants due to safety/relief valve (S/RV) actuation. This model is applicable to Mark I plants equipped with the T-Quencher discharge device shown in Figure 1-1. The analytical model provides pressure-time histories for any number of locations on the torus shell, as well as the time dependent dynamics of the S/RV air bubbles.

1.2 SAFETY/RELIEF VALVE DISCHARGE PHENOMENA

When a safety/relief valve (S/RV) is actuated, the following sequence of events takes place.

1.1.1 Water Clearing

Prior to valve actuation, the S/RV discharge line contains a mixture of air and water-vapor. The submerged portion of the line is normally filled with water. When the valve is actuated, the flow of steam into the lines causes rapid pressurization of the gaseous contents of the line and acceleration of the water column. The water is expelled from the line in less than half a second after the valve opens.

1.1.2 Bubble Formation

The gaseous contents of the S/RV discharge line follow the water into the pool. As the compressed air is expelled from the pipe, it forms bubbles which expand by accelerating the surrounding water. The momentum of the water causes the bubbles to expand beyond the equilibrium pressure; i.e., the bubble pressure drops below the local hydrostatic pressure. The magnitude of this

underpressure depends on the initial bubble pressure and diameter, the duration of the discharge and on the energy flow rate into the bubble. The duration of the discharge and the energy flow rate depend on the discharge device employed. Ideally, the mixture is cooled down to the pool temperature and is introduced gradually into the pool.

1.1.3 Bubble Oscillation

When all the air is out of the line, the bubble formation phase is complete and the bubble oscillation phase begins. At this time, each bubble is at its maximum size and minimum pressure, which is below the local equilibrium pressure. The low pressure region created by a bubble causes the surrounding water to accelerate toward the center of the bubble. As the water moves inward, it compresses the bubble until the pressure is high enough to halt the inward motion. The bubble then expands again and a new cycle of oscillation begins. These expansions and contractions create oscillating pressure and velocity fields in the pool. The pressure magnitude decreases with distance from the center of the bubble and with time. As the bubble rises due to its buoyancy and as it dissipates energy by various mechanisms, local pressure magnitudes decrease and finally become negligible when the bubble reaches the surface of the pool.

1.1.4 Steam Condensation

After the discharge line is cleared of water and air, steam discharge begins. Steam condensation is generally smooth and the pressure oscillations associated with it are of low magnitude. This phase is not addressed by the analytical model described herein.

1.1.5 Valve Closure and Reflood

Steam condensation in the pool continues until the relief valve is closed manually or a preset vessel pressure is reached, at which point the S/RV automatically closes and the flow of steam through the S/RV stops. However, steam condensation at the steam-water interface continues and causes rapid

depressurization of the discharge line. The reduced line pressure thus created causes the water to move up the discharge line and the air from the drywell to flow in through a vacuum breaker that is installed on each S/RV line. The vacuum breaker closes when the pressure in the discharge is equalized with the drywell pressure. The flow of water toward the S/RV compresses the mixture of air and steam until the water column motion is halted and then reversed. After several oscillations, the water level gradually settles at the equilibrium level. But the composition of the gaseous contents of the discharge line keeps changing as steam condenses and is replaced by air coming through the vacuum breaker. Eventually, a steady state is reached where the partial pressure of the steam in the line reduces to the vapor pressure corresponding to the mean temperature of the air.

Should the S/RV be actuated before steady state is reached, the resulting pressure, both in the discharge line and in the pool will be different from the steady state case. The difference is due to higher temperatures and the amount of steam in the line.

1.2 THE T-QUENCHER

The T-Quencher is an S/RV discharge device developed by the General Electric Company (see Figure 1-1). The main features of this new discharge device are:

a. Low air-clearing wall pressures. The four-hole fields (A, B, C, and D on Figure 1-1) are designed to give a uniform and gradual discharge of air over the quencher arms. This, plus the cooling of the compressed air, lead to much lower bubble and shell pressures than would be obtained if the air were introduced into the pool suddenly and in the form of one large bubble.

b. Good condensation characteristics. The large contact area between steam and water results in effective and smooth condensation.

The details of the hole fields are shown in Figure 1-2 and a typical installation in Figure 1-3.

1764 183

The T-Quencher was first installed and tested in the Monticello power plant in 1977. Results of that test program are given in Reference 1.

In 1978 a 1/4 scale test program was conducted to determine the effects of the following parameters on wall pressures:

a. Steam flow-rate

b. Discharge pipe diameter

c. Discharge pipe air length

d. Submergence of the quencher

e. Distance of the quencher from the pool floor

f. Initial pipe and wetwell pressure

g. Length and geometry of the water column in the discharge line.

For the details of the 1/4 scale T-Quencher Test Program and the test results, see Reference 2. The results of the Monticello in-plant test and the 1/4 scale test were used to verify the analytical models described below.

1.3 ANALYTICAL MODELS

The following models are used in determining pressure-time histories for various points on the torus shell due to S/RV air bubbles.

1.3.1 The Water Clearing Model

This model describes that part of the phenomenon which starts with the opening of the S/RV and ends when all the air is expelled from the discharge line. A description of this model is contained in Reference 3. For the purpose of developing pressure-time histories, only the maximum air pressure prior to

discharge and the water clearing time predicted by the water clearing model are used in the subsequent analysis. This information is used in calculating the rate at which the air is discharged into the pool.

1.3.2 The Bubble Dynamics Model

This model describes the phenomena that take place in the pool from the time the air discharge begins until the air bubbles reach the pool surface. It consists of two phases:

a. Charging Phase — This part of the model describes the formation of the bubbles around the quencher arms. It is important to know the rate and the temperature at which the air is discharged. The magnitudes of the bubble pressure oscillations depend strongly on the enthalpy flow rate into the bubble.

b. Bubble Oscillation — Once all the air is out of the discharge line, the bubble formation phase is completed and bubble oscillation continues. This part of the model describes the dynamics of an oscillating bubble in a finite pool. Bubble pressure, radius, radial velocity and bubble elevation are calculated as functions of time.

1.3.3 Pressure Distribution Model

The pressure-time history for any point on the torus shell can be obtained from the output of the bubble dynamics model. The dependence of local pressures on bubble pressure has been determined empirically. The empirical correlation is used to construct local pressure time-histories that are used in structural analysis.

1.3.4 The Reflood Model

This model describes the hydraulic and thermodynamic phenomena that occur after the valve is closed. It determines the water level as well as the composition of the air-steam mixture in the discharge line as functions of time (see Reference 4). This information is needed for predicting torus shell pressures for the case when the valve is actuated before normal conditions in the discharge line are established.

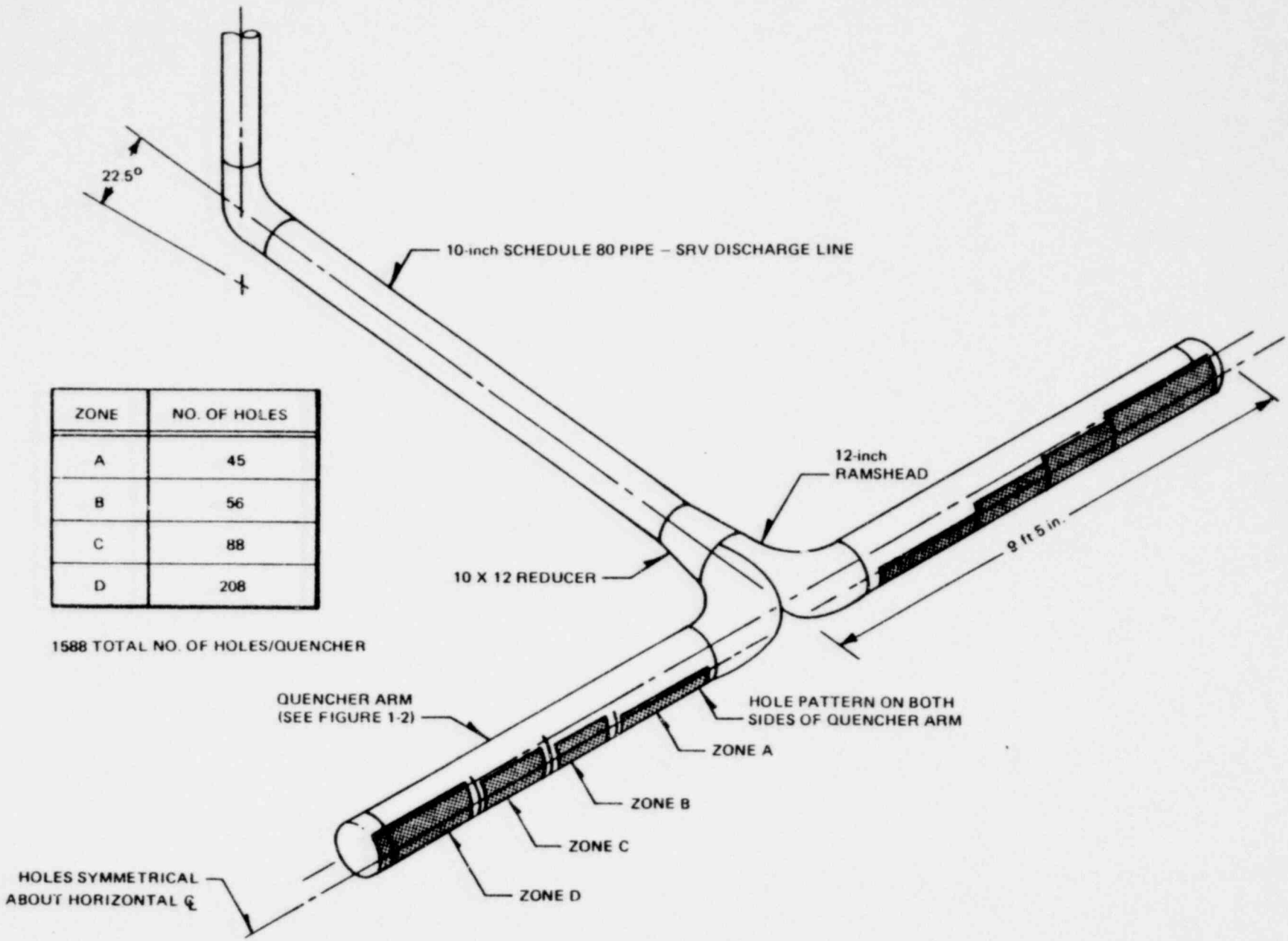

ZONE	NO. OF HOLES
A	45
B	56
C	88
D	208

1588 TOTAL NO. OF HOLES/QUENCHER

Figure 1-1. Monticello T-Quencher

Figure 1-2. Quencher Arm

* Proprietary information has been deleted.

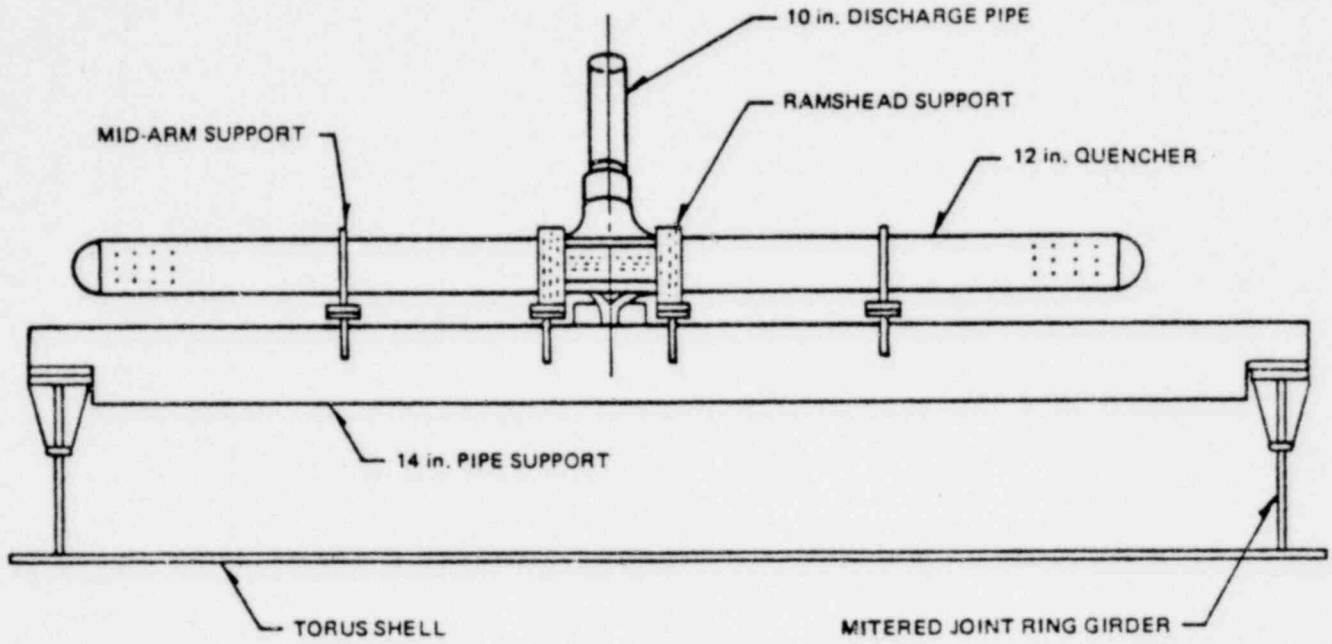

Figure 1-3. Quencher Installation

2.0 BUBBLE DYNAMICS AND PRESSURE DISTRIBUTION MODELS FOR THE T-QUENCHER

2.1 INTRODUCTION

Discharge of air from S/RV discharge line with the T-Quencher device can be analyzed only by some idealizing assumptions. The actual phenomenon is complicated by uneven distribution of the air between the arms, the shape of the air-water interface, which varies with the orientation of the S/RV discharge line, and the formation and coalescence of a multitude of small bubbles. However, the main objective of the bubble dynamics model is to provide the information necessary to develop pressure-time histories for predetermined points on the torus shell. The crucial test of the model is to predict the correct amplitude and frequency of bubble and shell pressure oscillations. The analytical model described herein predicts bubble pressure and bubble frequency, and their variations with different parameters, with a good degree of accuracy over the entire range of parameters encountered in Mark I plants.

2.2 BASIC ASSUMPTIONS

The following assumptions are incorporated in the bubble dynamics model:

a. There is no mixing of the initial gaseous mixture in the line with the steam coming through the S/RV. This is a conservative assumption, since any mixing of this kind will prolong the discharge time of the mixture and result in lower bubble pressure.

b. Air enters the pool at the pool temperature and the vapor pressure of the air corresponds to the pool temperature. Any additional vapor initially present in the line is condensed during the air discharge. These assumptions regarding the air temperature and its vapor pressure are also conservative assumptions that minimize the discharge time by maximizing the air density. The shorter the discharge time the higher the resulting bubble pressure.

c. During the air discharge phase, the water is discharged through the quencher holes at a constant velocity. This average velocity, corresponding to steady state, frictionless flow of water with an upstream pressure equal to the maximum pressure at the air-water interface is modified by an empirical coefficient as described in Section 2.3. The maximum pressure is calculated by using the water clearing model (Reference 3). The downstream pressure is the pressure at the elevation of the center line of the quencher arm prior to valve actuation. The air is assumed to be at its maximum calculated pressure and at pool temperature. The mass flux of air through the quencher holes increases with time until a maximum flux, corresponding to choked flow, is reached; then it remains constant thereafter. The form of the function describing the air mass flux vs time was obtained empirically and is given in Section 3.2.

d. Four identical bubbles are formed per quencher. The small bubbles on each side of each arm are coalesced into one bubble. This assumption is supported by the agreement between predicted and measured bubble oscillation frequencies, which strongly depend on bubble size. The uneven clearing of the quencher arms in the real case may lead to bubbles that are not identical in size or pressure. However, the shell pressures can be predicted with reasonable accuracy when four identical bubbles are assumed.

e. The initial diameter of a bubble nucleus is assumed to be equal to the diameter of one quencher hole. The results are not sensitive to the initial bubble nucleus size if a reasonable initial diameter is assumed.

f. The initial bubble pressure is assumed to be the same as the maximum air-water interface pressure calculated by the pipe clearing model. The results are not sensitive to this initial pressure of the nucleus.

g. Air and water vapor in the bubble are treated as ideal gases.

h. During the charging phase, the bubble temperature is assumed to be the same as the pool temperature. After the completion of the charging phase, subsequent expansions and contractions of the bubble take place polytropically according to PV^n = constant. The exponent n was determined empirically to be 1.2.

i. The bubbles are assumed to be spherical. This simplifying assumption is necessary for the analytical solution of the problem.

2.3 BASIC EQUATIONS

During the charging phase, the bubble temperature is constant and equal to the pool temperature. Bubble radius and bubble mass (both air and water vapor) must be known to calculate bubble pressure. Following the charging phase, the process is polytropic and the pressure is defined once the bubble radius is known.

2.3.1 Conservation of Mass

The mass of the bubble includes the air mass and the water vapor. The air mass increases during the charging phase until all the air is out of the line. It then remains constant for the rest of the time. The mass of the water vapor increases in parallel with the increase in the air mass; i.e., the bubble remains saturated with water vapor during the charging phase. After the charging phase is completed, condensation of vapor is allowed (due to compression of the bubble) but not evaporation. Evaporation is too slow a process and is not expected to take place instantaneously.

Bubble dynamics are determined by the rate at which the bubble is charged. The charging rate depends on density of the air, its velocity and the flow area. The flow area, in turn, is determined by the water velocity through the quencher holes, the geometries of the air-water and air-steam interfaces and the pressure and temperature of the air in the quencher arm. The problem is further complicated by the air forming many small bubbles before the bubbles coalesce to form four large ones. Furthermore, the velocity at which the air is discharged into the pool varies with time.

Since this phase of the problem was complex, a semi-empirical approach was taken. The justification of this approach is that it gives results that are in excellent agreement with measured data and with in-plant test data, over a wide range of parameters.

During the charging phase, the mass of air in the bubble is calculated from the following equation:

$$\frac{dm_a}{dt} = G_a A_a \tag{2-1}$$

Where both G_a and A_a are functions of time.

At the beginning of the charging phase, the flow area (A_a) for a bubble is determined from the location of the air-water interface (see Figure 2-1). The velocity of the interface is calculated from the continuity equation by assuming the velocity of water through the quencher holes to be equal to $\overline{V}_w$ given below:

$$\overline{V}_w = 0.00867 \frac{P_o}{P_r} (2 (P_o - P_\infty)/\rho_w)^{1/2} \tag{2-2}$$

Where

$$P_r = \rho_w g L_f \tag{2-2a}$$

is a reference pressure, which obeys the scaling laws (Reference 5). The term 0.00867 Po/Pr was determined empirically. Its numerical value is $\simeq$ 1 for Monticello and the 1/4 scale base case and varies from 0.6 to 1.2. The term $(2 (Po-P\infty)P_w)^{1/2}$ is the maximum steady-state water velocity due to a pressure difference P_o-P_∞. Equation (2-2) is significant only in that, combined with other assumptions, it gives a charging rate that leads to correct bubble pressure and frequency.

1764 192

Knowing the distribution of holes on an arm and the location of the interface, the area A_a can easily be calculated. In stage 2 of the charging phase, water, air and steam are discharged into the pool (Figure 2-2). Locations of air-water and air-steam interfaces must be predicted. The air-water interface is determined as before. The air-steam interface is determined by applying the continuity equation to the air. The amount of air left in the pipe determines the distance between the two interfaces. Knowing this distance and the location of the air-water interface, the flow area A_a can be calculated.

The mass flux of air (G_a) is calculated from the following empirical equation:

$$G_a = G_{ao}\left[1 + \left(\frac{G_{ao}}{G_{am}} - 1\right)\left(\frac{t}{t_c}\right)^2\right] \qquad (2\text{-}3)$$

With the constraint: $G_a \leq G_{am}$

Where:

$$G_{ao} = \frac{0.02}{\tau} P_o^{1.5} \qquad (2\text{-}4)$$

In this equation, P_o is in psi, G_{ao} is in lbm/sec./ft^2 and τ is a dimensionless time:

$$\tau = \frac{t_{wc}}{t_r} \qquad (2\text{-}5)$$

The water clearing time (t_{wc}) is obtained from the water clearing transient analysis (Reference 3). The reference time t_r is defined as:

$$t_r = \left(L_f/g\right)^{1/2} \qquad (2\text{-}6)$$

and obeys the scaling laws. It is reasonable to assume that the initial mass flux is proportional to $P_o^{1.5}$, since the density is proportional to P_o (absolute

air temperature = absolute pool temperature being about the same for all cases) and the velocity is proportional to $P_o^{0.5}$. The dependence of G_{ao} on water clearing time was determined empirically.

Equation (2-3) indicates that the mass flux starts at G_{ao} at the beginning of the charging phase and increases parabolically to G_{am} at the time t_c. The maximum mass flux (G_{am}) corresponds to choked flow and is calculated as follows:

$$G_{am} = 0.532\ P_o/\sqrt{T_o} \tag{2-7}$$

Where G_{am} is lbm/sec./ft^2, P_o is in psf and $T_o = T_p$ is in ^oR. The mass flux is not allowed to exceed G_{am}. The time (t_c) at which the average flux reaches G_{am} depends on the amount of air initially in the line. This is because the flux through a given quencher hole increases with time, so the instantaneous mass flux for the quencher depends on how many of the holes have been discharging air and for how long.

To account for the effect of air mass, t_c is defined in terms of this mass and is determined empirically to be:

$$t_c = 0.156/(m_o/m_r)^{0.3} \tag{2-8}$$

Where m_o is the total air mass in the discharge line, m_r is a relative mass defined as:

$$m_r = P_r\ V_r/RT_r \tag{2-9}$$

Where P_r is defined by Eq. (2-2a)

$V_r = (L_f)^3$

$T_r = T_i$ = Initial absolute temperature of the air

1764 194

Air mass in the bubble is calculated numerically at each time step. The bubble radius is calculated from the equations of motion described in the following section. The mass of the water vapor is calculated by the following equation:

$$m_s = V_B/v_g$$

where V_B is the instantaneous bubble volume and v_g is the specific volume of saturated vapor at pool temperature.

After the charging phase is over, m_s is not allowed to increase any further, but it can decrease as V_B decreases.

After all the air is out of the quencher, the air mass in the bubble remains constant for the rest of the time.

2.3.2 Equations of Motion

The radial expansion (or contraction) and the vertical motion of the bubble are described by the following equations (for derivation of these equations, see Appendix D):

$$R\ddot{R}\left(1+R/2Z-R/2\ (H-Z)+4R/\sqrt{A_p}\right)+\frac{3}{2}\dot{R}^2\left(1+2R/3Z-2R/3\ (H-Z)\right.$$

$$\left.+\ 16R/3\sqrt{A_p}+2\dot{R}/3C\right)=\left(P_B-P_\infty\right)/\rho-2\dot{R}\left(P_B+P_\infty\right)/\rho c+\frac{R\dot{Z}}{3\dot{R}}\left(g-\ddot{Z}/2\right)$$

$$-\dot{Z}^2/4+(R^2\dot{R}\dot{Z}/4)\ (1/Z^2-1/(H-Z)^2) \qquad (2\text{-}10)$$

Equation (2-10) describes the radial motion of the bubble. Notice that if Z, H and A_p are infinitely large and $\dot{Z}$ is negligible and $\dot{R}<<C$, then Equation (2-10) reduces to Raleigh's Equation; i.e.,

$$R\ddot{R}+3\dot{R}^2/2 = (P_B-P_\infty)/\rho \qquad (2\text{-}11)$$

1764 195

The vertical acceleration of the bubble is caused by the difference in the average radial acceleration $\ddot{R}$ and the acceleration of the apex of the bubble $\ddot{R}_1$ (see Appendix D for derivation).

$$\ddot{Z} = \ddot{R}_1 - \ddot{R} \tag{2-12}$$

$\ddot{R}_1$ is different from $\ddot{R}$ because the hydrostatic pressure at the apex of the bubble is an amount ρRg smaller than the average hydrostatic pressure on the bubble boundary. It is this pressure difference that makes the bubble buoyant. As shown in Appendix D, the radial velocity $\dot{R}_1$ is greater than $\dot{R}$ by an amount $\dot{Z}$. Therefore, the acceleration $\ddot{R}_1$ can be calculated by using the following equation:

$$R\ddot{R}_1\left(1+R/2Z-R/2\ (H-Z)+4R/\sqrt{A_p}\right)+\frac{3}{2}\left(\dot{R}+\dot{Z}\right)^2\left(1+2R/3Z-2R/3\ (H-Z)\right.$$

$$\left.+16R/3\sqrt{A_p}+2\left(\dot{R}+\dot{Z}\right)/3C\right)=\left(P_B-P_\infty-\rho Rg\right)/\rho-2\left(\dot{R}+\dot{Z}\right)\left(P_B+P_\infty+\rho RG\right)/\rho c+\frac{R\dot{Z}}{3(\dot{R}+\dot{Z})}\left(g-\ddot{Z}/2\right)$$

$$-\dot{Z}^2/4+R^2\dot{Z}\left(\dot{R}+\dot{Z}\right)\left(1/Z^2-1/\ (H-Z)^2\right)/4 \tag{2-13}$$

Equation (2-13) is identical to Equation (2-10) except P_∞ is replaced by $P_\infty+\rho RG$ and $\dot{R}+\dot{Z}$ is substituted for $\dot{R}$. However, R remains the same, implying that in spite of a different acceleration at the top and the bottom of the bubble, the shape of the bubble remains spherical at all times.

Simultaneous solution of Equations (2-10), (2-12) and (2-13) gives the time history of R and Z, provided P_B is known at each time step. During the charging phase, the bubble pressure is calculated from the equation of state:

$$P_B V_B = n\tilde{R}T_p \tag{2-14}$$

where

$$n = m_a/M_a + m_s/M_s \tag{2-15}$$

Following the charging phase, bubble pressure is calculated from the following equation:

$$PV^{1.2} = \text{constant} \tag{2-16}$$

2.4 PRESSURE DISTRIBUTION MODEL

Based on the Monticello T-Quencher test data, a semi-empirical model was developed for calculating local pressure-time histories at various points on the torus shell. The model was developed in three steps. First, the maximum shell pressure was correlated with bubble pressure, bubble radius and distance between the bubble and a point directly below the center of the quencher. The second step was to find an empirical fit to the circumferential attenuation of the shell pressure for the points directly below the quencher. Finally, the variation of pressures with the angle β (see Figure 2-3) were formulated. This turned out to be dependent on the azimuthal angle α (Figure 2-4).

2.4.1 Maximum Shell Pressure

The maximum shell pressure depends on the product $P_B R_B$ and is inversely proportional to the distance r between the bubbles and the point where the maximum pressure occurs. Selecting point B (Figure 2-5) as a representative point where the shell pressure is assumed to be maximum (although the maximum may not always occur at B, the pressure at B is close to the maximum shell pressure):

$$r = \left[\left(L_a/2\right)^2 + Z^2 + R_m^2\right]^{1/2}$$

where R_m is an average bubble radius corresponding to a temperature equal to the pool temperature and a pressure equal to the initial value of P_∞. It was found empirically that the maximum shell pressure P_{max} is:

$$\left.P_{max}\right]_{\text{point B}} = \frac{4P_B R_B}{r} \tag{2-17}$$

2.4.2 Attenuation in the Circumferential Direction

It was assumed that from point B (Figure 2-5) to a distance of $0.7L_a$ from B in the circumferential direction, there would be no pressure attenuation. Beyond that point, pressures attenuated as the inverse of the distance, i.e.:

$$P_{max} = P_{max}\Big]_{\text{point B}} \quad \text{for } |\alpha| R_m \leq 0.7L_a \tag{2-18}$$

$$P_{max} = P_{max}\Big]_{\text{point B}} \frac{0.7L_a}{R_m|\alpha|} \quad \text{for } |\alpha| R_m > 0.7L_a \tag{2-19}$$

where R_m is the torus major radius.

2.4.3 Variation of Local Pressure with β

The following empirical formula describes the dependence of local pressure on β.

$$P = P_{max} (\text{Cos } \beta)^{(2.-1.65|\alpha|)} \quad |\alpha| \leq 1.2 \text{ Rad.} \tag{2-19}$$

$$P = P_{max} \quad |\alpha| \leq 1.2 \text{ Rad.} \tag{2-20}$$

2.4.4 Summary

Combining Equations (2-17) through (2-20), one obtains the following formulas for calculating local pressures:

$$P = \left[4P_B R_B / \left(L_a^2/4 + Z^2 + R_m^2\right)^{1/2}\right] (\text{Cos } \beta)^{(2-1.65\ |\alpha|)} \tag{2-21}$$

For

$$|\alpha| R_m \leq 0.7\ L_a$$

1764 198

$$P = \left[4P_B R_B \left(7L_a/R_m \ |\alpha|\right)/\left(L_a^2/4+2^2+R_m^2\right)^{1/2}\right] (\text{Cos } \beta)^{(2-1.65\ |\alpha|)} \quad (2\text{-}22)$$

For

$$1.2R_m \geq |\alpha| \ R_m > 0, \ 7L_a$$

$$P = \left[4P_B R_B \left(0.7L_a/R_m \ |\alpha|\right)/\left(L_a^2/4+Z^2+R_m^2\right)^{1/2}\right] \quad (2\text{-}23)$$

For

$$|\alpha| > 1.2 \text{ Rad.}$$

The time dependent quantities P_B,R_B and z are calculated using the bubble dynamics model. Using Equations (2-21), (2-22) and (2-23), pressure time histories for various points on the torus shell are developed.

It will be shown in Section 3 that this semi-empirical model, which accounts for the important parameters (P_B,R_B,A,R_M), is a good approximation for the actual pressure distribution.

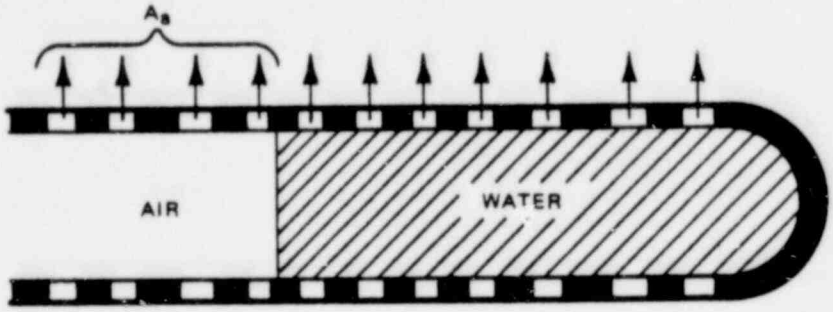

Figure 2-1. Stage 1 of the Charging Phase

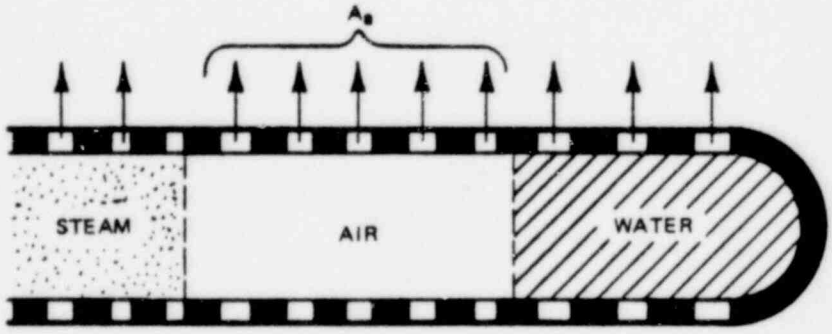

Figure 2-2. Stage 2 of the Charging Phase

1764 200

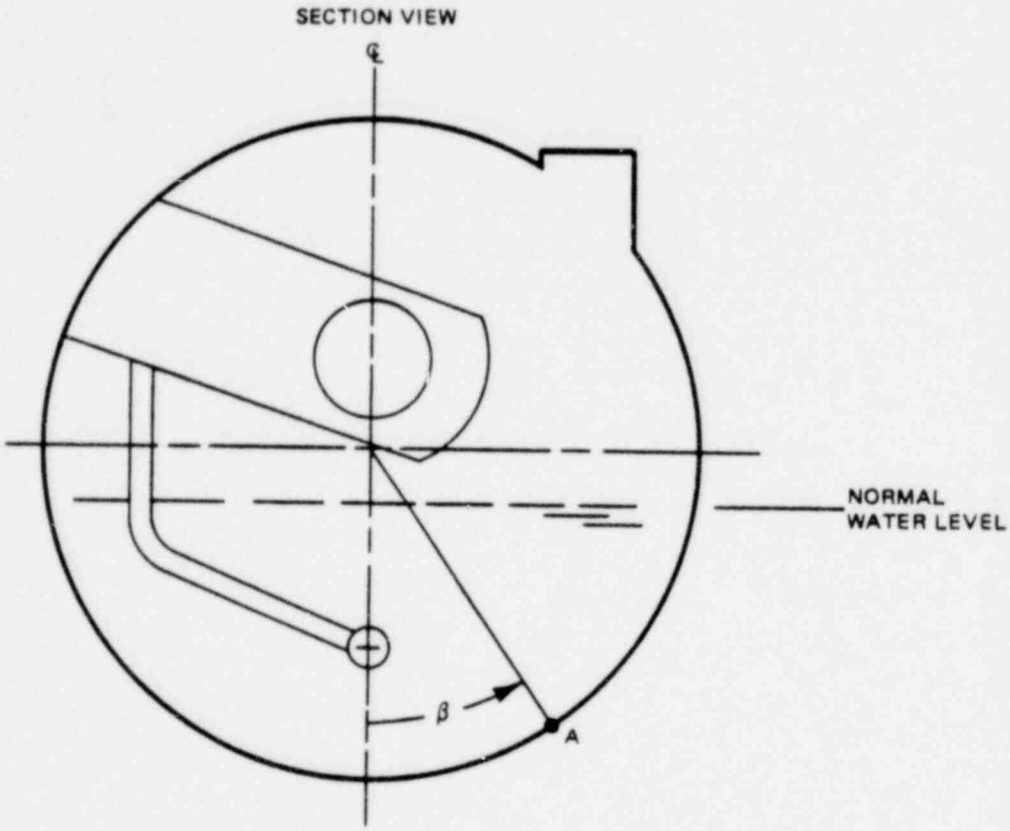

1764 201

Figure 2-3. Definition of Angle β for Point A

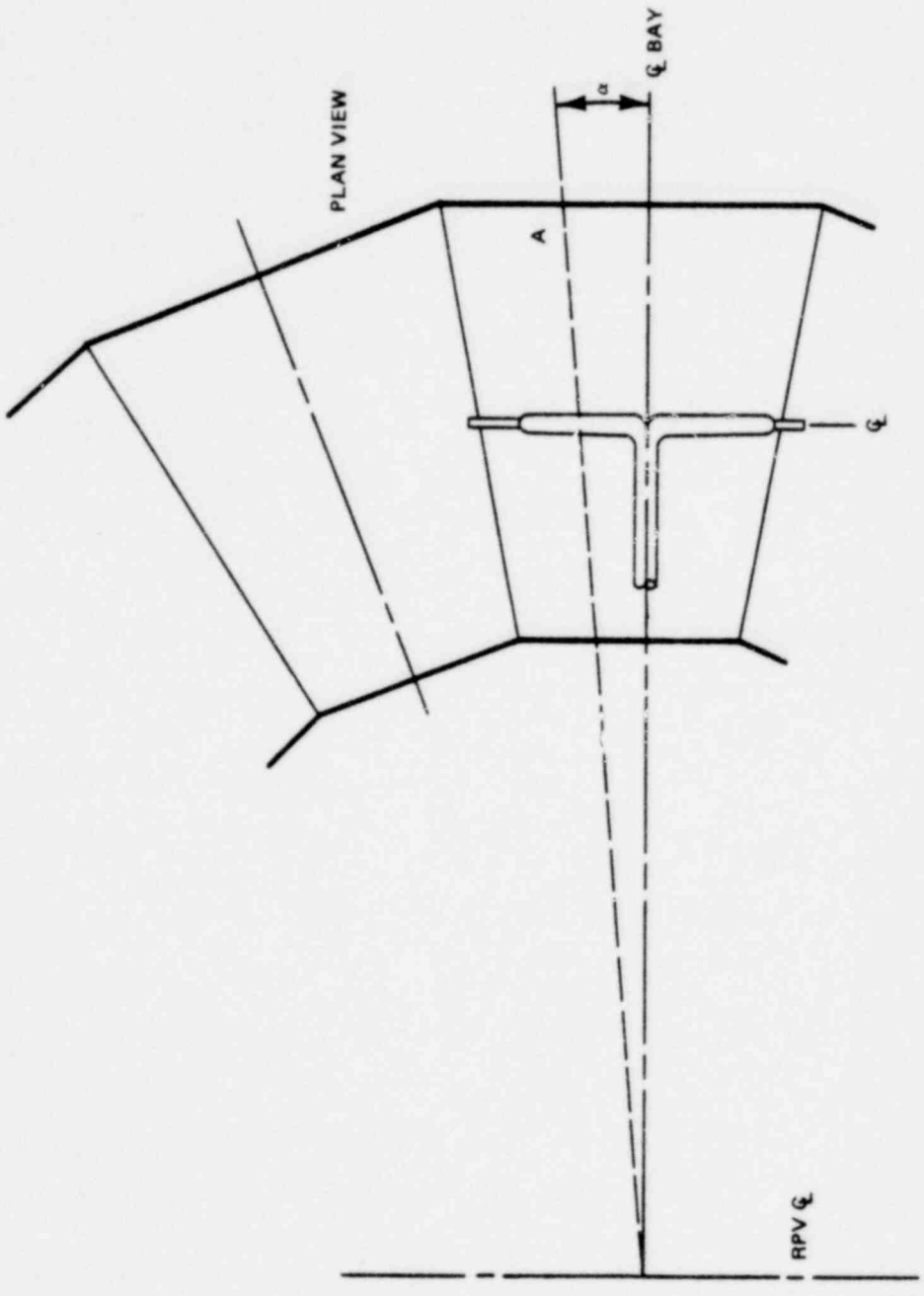

Figure 2-4. Definition of Angle α For Point A

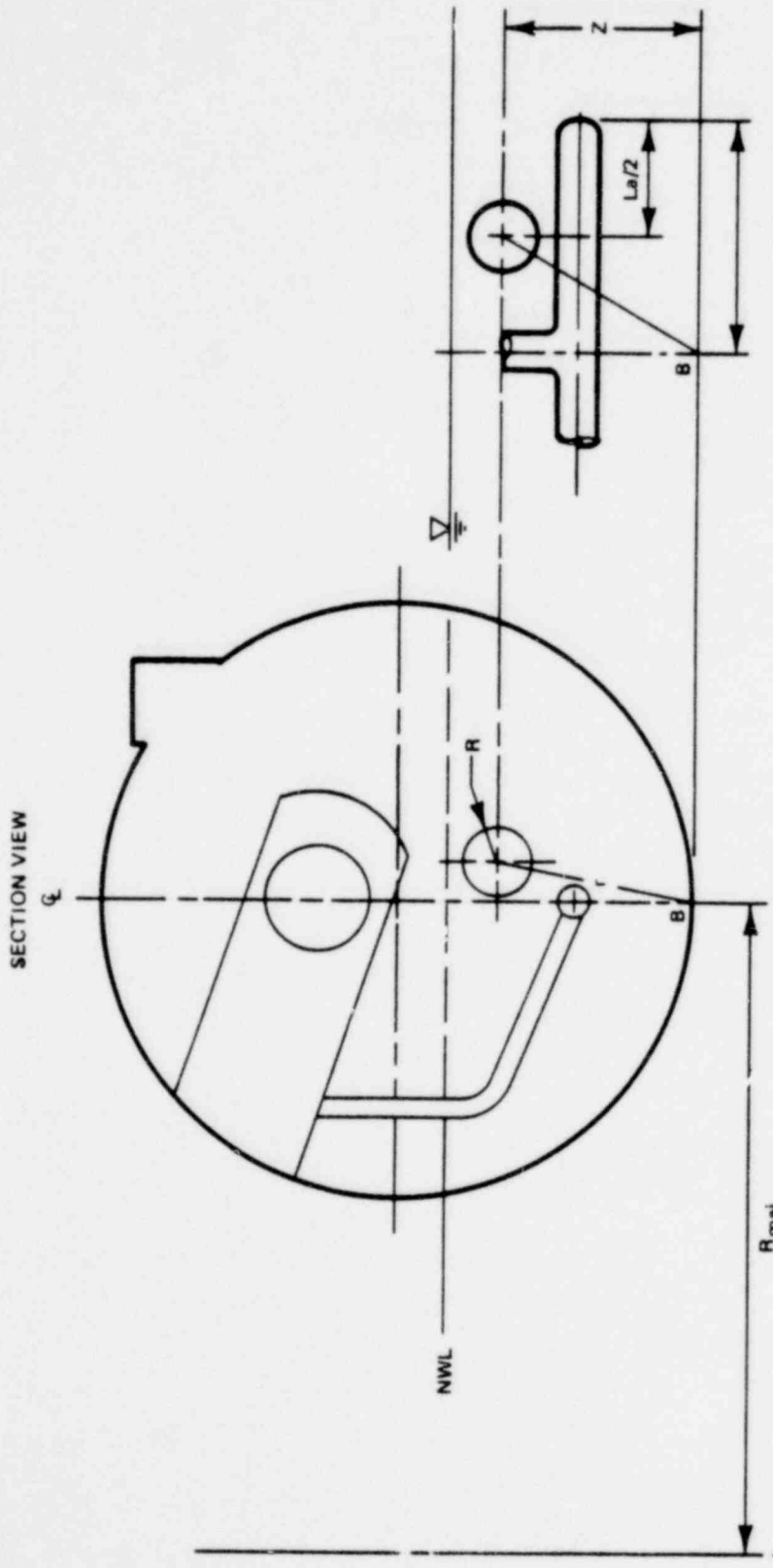

Figure 2-5. Definition of the Distance r

3.0 MODEL VERIFICATION

3.1 VERIFICATION OF METHODOLOGY

The analytical model, described in Section 2, predicts bubble properties such as pressure, radius, oscillation frequency, breakthrough time and containment wall pressures as the bubble rises toward the pool surface.

In this section, the model predictions are compared with full scale and small scale test data. The full scale data were obtained from Monticello T-Quencher test results described in Reference 1. The small scale data consist of 21 tests (over 80 runs) conducted in a 1/4 scale test facility. These tests were designed to cover the entire range of parameters for Mark I plants. Additional information about the 1/4 scale test program is contained in Reference 2.

Since the final output of the model is pressure-time histories for various points on the torus, comparisons are made between predicted and measured pressures on the torus shell. Comparisons of predicted bubble pressures and frequencies with the measured data are also included.

3.2 MONTICELLO T-QUENCHER TEST

The various test conditions selected for verification and the corresponding test runs are given in Table 3-1. The test runs for each case were selected based on two criteria:

a. Completeness of data - whenever possible, only those tests with well defined initial conditions were selected.

b. Within each case, test runs that were similar enough to justify averaging the parameters were chosen.

The initial conditions for the selected test runs and their averages for each group are given in Table 3-2. These averaged initial conditions were used in the analytical model to predict bubble and shell pressure for each case.

3.2.1 Bubble Pressure Comparisons

Bubble pressures were measured at four locations on the arm where pressure transducers P8, P9, P10, and P11 were located (see Figure 3-1). These pressures are given in Table 3-3.

In addition to the initial conditions listed in Table 3-2, the model requires input specifying pool and quencher geometries. These are listed in Table 3-4 and are common to all cases.

Finally, the maximum absolute pressure (P_o) at the air-water interface and the water clearing time (t_{wc}) are also input to the analytical model. These were obtained from the water clearing transient analysis (Reference 3) and are listed in Table 3-5.

The results of bubble pressure comparisons are shown in Table 3-6. In this table P_B+ stands for maximum positive bubble pressure (psid), $P_{\overline{B}}$ stands for maximum negative bubble pressure (psid), and f stands for frequency. The combination of water clearing model and bubble dynamics model, in general, gives results that agree reasonably well with measured data. However, to bound the data, it was necessary to use either multipliers on positive and negative peak pressure predictions or on the bubble charging rate. The latter method was preferred because it adjusts the velocity field as well as the pressure field. Since both the water velocity and the air discharge velocity affect the bubble charging rate, the multiplier was applied to both velocities. A multiplier of 2.5 applied on flow rates of air and water was found to give bubble pressures that were bounding on both positive and negative sides. This method of adjustment not only increases the magnitudes of predicted bubble pressures but also adjusts bubble radial velocity and acceleration accordingly.

The effect of reducing the number of holes in zone D of the quencher arm (Figure 1-1) from 208 per ride to 188 per ride and drilling 40 holes in one endcap to maintain the same total hole area per arm was studied. This modification did not have a significant effect on bubble pressure or shell pressures.

3.2.2 Shell Pressure Comparisons

The measured maxima and minima of shell pressures for transducers P12 through P46 (except for P25, P28, P32, P44, and P45, which for reasons explained in Reference 1 are not included), are given in Table E-1 of Appendix E for all Monticello test program runs. Locations of these transducers are shown in Figures 3-2 and 3-3.

Typical shell pressure traces from Reference 1 are shown in Figure 3-4 and a typical shell pressure prediction in Figure 3-5. The empirical shell pressure distribution model was developed based on the Monticello test data. Cold pipe tests, which resulted in highest shell pressures, were chosen for this purpose. Comparisons of model predictions with Monticello cold pipe data are shown in Figures 3-6 through 3-13.

Each figure represents a radial cross section of the torus and is identified by an angle (α). For a definition of the angle α, see Figure 2-4. The transducers in each figure are identified using the same numbering system as in Figures 3-2 and 3-3. Measured and calculated peak positive and peak negative pressures are plotted on separate polar graphs. For the measured data, the range of values for all the selected tests (i.e., Tests No. 2, 501, 801, 901, 1301, and 1601) is indicated by a bar for each transducer. This method of presentation was used (as opposed to "mean $\pm$ 1σ") so the multiplier needed for the prediction curve to bound all the data could be determined. This multiplier was determined to be 1.65 for the Monticello data. The bounding predictions are also shown in Figures 3-6 through 3-13.

3.3 1/4 SCALE T-QUENCHER TEST

The purpose of the 1/4 scale T-Quencher Test Program was to determine the sensitivity of shell pressures to variations in the following patameters:

a. Steam flow rate

b. Initial pipe and wetwell pressures

c. Length of discharge line

d. Diameter of discharge line

e. Water leg length

f. Submergence

g. Distance of quencher from the floor

h. Orientation of submerged portion of discharge line.

The ranges selected for these parameters (Table 3-7) bound the ranges encountered in all the Mark I plants to avoid any extrapolation beyond the range of tested parameters.

Scaling was performed according to scaling laws described in Reference 5 except for the scaling of the quencher, which was modified on the basis of preliminary test results. The reason for this change is discussed in Section 4. A summary of the scale factors is given in Table 3-8.

The various test conditions investigated are summarized in Table 3-9. Test 1 is the base case corresponding to Monticello cold pipe test conditions. The results of this test were used to confirm the validity of the scaling laws. The remaining tests in the test matrix were designed to provide the effects of various parameters on bubble and shell pressures.

1764 207

Each test was repeated at least four times to ensure repeatability and statistical significance of the variation of the dependent variables.

Geometric parameters of the 1/4 scale T-Quencher and pool are given in Table 3-10 and a summary of initial conditions in Table 3-11.

3.3.1 Comparison of Measured and Predicted Sensitivities

In order to demonstrate the capability of the model to correctly predict the effect of each parameter on the magnitude and frequency of the shell pressures, comparisons were made between the observed and the predicted trends for the following parameters (See Figures 3-16 through 3-41):

a. Steam flow rate

b. Initial pressure (wetwell and discharge line) 52-ft pipe length

c. Initial pressure (wetwell and discharge line) 26-ft pipe length

d. Initial pressure (wetwell and discharge line) 108-ft pipe length

e. Initial air volume 1 1/2-in. pipe, 3.7 psia pressure

f. Initial air volume 1 1/2-in. pipe, 11.25 psia pressure

g. Initial air volume 2 1/2-in. pipe, 3.7 psia pressure

h. Submergence

i. Distance from floor

j. Pipe diameter 52-ft pipe length

k. Pipe diameter 26-ft pipe length

l. Vertical water leg

m. Inclined water leg.

The locations of the pressure transducers are shown on Figures 3-14 and 3-15. In Figures 3-16 through 3-41, the measured peak overpressure is the maximum positive pressure recorded by any of the shell pressure transducers averaged over all four or more runs of a given test. Similarly, the peak underpressure is the maximum negative pressures recorded by any of the shell pressure transducers averaged over all the runs of a given test, and the measured frequency is the mean of the frequencies averaged over two or more cycles, whenever available, for all the runs of a given test. Test numbers are indicated on the graphs for reference to the test matrix. Plus and minus one standard deviation marks are shown for the measured data. The predictions for each test were obtained using averaged initial conditions. No multipliers were used for these predictions. The measured data are found in Reference 2 and in Appendix F.

As shown in Figures 3-16 through 3-41 and in Table 3-12, the model correctly predicts the effect of each of the parameters studied on shell pressure magnitude and frequency. Note that Tests 11, 15, 16, 17 and 19 were not used in sensitivity studies. These tests will be discussed in Section 4.

3.3.2 1/4 Scale Shell Pressure Comparisons

Shell pressure predictions for 1/4 scale tests were compared with the range of shell pressure measurements for each pressure transducer and each test, except for tests 17 and 19. These two tests were excluded because of their low submergence (outside the range of Mark I plants). For these two tests, both the interface pressures and the bubble pressures were overpredicted.

The same procedure used in comparing measured and predicted shell pressure for the Monticello test was also used in the 1/4 scale comparisons. The results are shown in Figures 3-42 through 3-83. The model predicts shell pressures with good accuracy and bounds all the data when the multiplier of 1.65 is used. The bounding predictions are not shown, but inspection can verify that increasing model predictions by 65% will bound the measured data in all cases. Comparisons of measured and predicted pressure distributions in the circumferential direction are shown in Figures 3-84 through 3-104.

3.3.3 Bubble Pressure and Frequency Comparisons

Bubble pressures were measured at two locations near the quencher arm where pressure transducers P19 and P20 were located (see Figures 3-14 and 3-15). The results of pressure and frequency comparisons are given in Table 3-13. The measured positive bubble pressure is the mean of the peak pressures measured by transducers P19 and P20 for all the runs of a given test. This is also true for the negative bubble pressure. Bubble frequency for each test is the mean of the bubble frequencies over two or more cycles, whenever available, of the four or more runs for that test. The standard deviation of the data is indicated in each case. In general, pressure magnitudes and frequencies are predicted with reasonable accuracy.

Table 3-1

SELECTED CASES FROM MONTICELLO TEST

	1	2	3	4
Actuation	SVA	CVA	CVA	SVA
Pipe Temp	CP	HP	HP	HP
Water Level	NWL	NWL	DWL	EWL
Valve Bay	A D	A D	A D	A D
Test Numbers	2/2	6/802	18/1303	31/2305
	3/501	8/902	21/1602	
	5/801	9/903	21/1603	
	7/901	10/904	21/1604	
	18/1301	11/905	21/1605	
	21/1601			

Terminology

SVA: Single Valve (First) Actuation

CVA: Single Valve (Subsequent) Consecutive Actuation

NWL: Normal Water Leg

DWL: Depressed Water Leg

EWL: Elevated Water Leg

CP: Cold Pipe

HP: Hot Pipe

1764 211

Table 3-2

INITIAL CONDITIONS*

Test Condition	Run No./ Test No.	Air Mass (lbm)	Pipe Pressure (psia)	Water Leg (ft)	Pool Temperature (°F)
	2/2	3.04	14.4	13.3	76
CP	3/501	2.89	14.4	13.3	76
NWL	5/801	2.78	14.5	13.3	77
SVA	7/901	2.86	15.1	13.4	75
	18/1301	3.03	14.7	13.3	72
	21/1601	2.87	14.7	13.3	72
	$\bar{x}$	2.91	14.6	13.3	74.7
	σ	0.10	0.27	0.04	2.16
	6/802	N/A	14.9	12.4	81
HP	8/902	N/A	15.5	12.3	79
NWL	9/903	N/A	15.8	11.6	79
CVA	10/904	N/A	15.6	12.1	81
	11/905	N/A	15.6	12.3	81
	$\bar{x}$	--	15.5	12.1	80.2
	σ	--	0.34	0.32	1.10
	18/1303	1.02	16.4	6.9	72
HP	21/1602	0.98	16.3	7.2	72
DWL	21/1603	1.09	16.0	8.8	72
CVA	21/1604	1.08	15.9	9.5	72
	21/1605	1.12	15.9	9.5	72
	$\bar{x}$	1.06	16.1	8.4	72
	σ	0.06	0.23	1.25	0
HP	31/2305	1.11	15.5	10.6	89

*From Reference 1.

1764 212

Table 3-3

MONTICELLO BUBBLE PRESSURES (psid)*

Test Condition	Run No./ Test No.	P8	P9	P10	P11
	2/2				
CP	3/501				
NWL	5/801				**
SVA	7/901				
	18/1301				
	21/1601				
	$\bar{x}$				
	σ				
	AVG				
	6/802				
HP	8/902				
NWL	9/903				
CVA	10/904				
	11/905				
	$\bar{x}$				
	σ				
	AVG				
HP	18/1305				
DWL	21/1602				
CVA	21/1603				
	21/1604				
	21/1605				
	$\bar{x}$				
	σ				
	AVG				
HP	31/2305				

*From Reference 1.

** Proprietary information has been deleted.

1764 213

Table 3-4

MONTICELLO TORUS AND T-QUENCHER GEOMETRIES

Parameter	Values	
Pipe Area per Quencher	765.1 ft^2	
Pool Depth	11.2 ft	
Distance from Floor	4.67 ft	
Torus Major Radius	49.0 ft	
Quencher Arm Length from $\mathbb{Q}$	9.415 ft	
Cross-sectional Area of One Quencher Arm	0.706 ft^2	
Radius of One Quencher Hole	ft	**
Length of the 1st Field of Holes	ft	
Length of the 2nd Field of Holes	ft	
Length of the 3rd Field of Holes	ft	
Length of the 4th Field of Holes	ft	
Total Area of 1st Hole Pattern	ft^2	
Total Area of 2nd Hole Pattern	ft^2	
Total Area of 3rd Hole Pattern	ft^2	
Total Area of 4th Hole Pattern	ft^2	
Number of Quencher Arms	2	
Number of Bubbles after Coalescence	4	

*Dummy Number

**Proprietary information has been deleted.

Table 3-5

MAXIMUM INTERFACE PRESSURES AND WATER CLEARING TIMES OBTAINED FROM WATER CLEARING TRANSIENT ANALYSIS

Test Condition	Maximum Interface Pressure (psia)	Time Water Clears (sec)
CP, NWL	220	0.201
HP, NWL	280	0.208
HP, DWL	264	0.194
HP, EWL	303	0.201

Table 3-6

COMPARISON OF MEASURED* AND PREDICTED BUBBLE PRESSURES AND FREQUENCIES

Test Condition	Bubble Pressure P_B^+ (psid)		Bubble Pressure P_B^- (psid)		Frequency f (Hz)	
	Measured ±σ	Calculated	Measured ±σ	Calculated ±σ**	Measured**	Calculated
CP, NWL	5.55 ± 1.81	6.12	-5.35 ± 1.25	-4.23	7.3 ± 1.10	7.2
HP, NWL	3.11 ± 1.20	3.61	-3.80 ± 1.34	-3.41	10.98 ± 1.62	10.3
HP, DWL	2.50 ± 0.93	3.68	-3.02 ± 0.87	-3.33	13.0 ± 1.95	10.5
HP, EWL	3.42 ± 0.63	3.82	-2.97 ± 0.44	-3.74	11.2 ± 1.68	10.2

*Reference 1

**The frequency ranges given bound the data for 2nd cycle oscillation because maximum pressures usually occur during this cycle.

Table 3-7

RANGE OF PARAMETERS STUDIED IN THE 1/4 SCALE TEST PROGRAM

Parameter	Units	Range (1/4 Scale)	Corresponding Full-Scale Range
Steam Flow Rate	lbm/sec	0.8-2.5	102.4-320.0
Initial Pipe Pressure	psia	2.45-11.25	9.8-45.0
Initial Wetwell Pressure	psia	3.7-11.25	14.8-45.0
Discharge Pipe Cross-Sectional Area	ft^2	0.014-0.029	0.53-1.10
Discharge Pipe Air Length	ft	26-108	44.5-185.0
Water Leg Length	ft	1.65-6.25	6.6-25.0
Submergence	ft	1.0-3.38	4.0-13.5
Distance from Floor	ft	0.7-1.2	2.8-4.8

1764 217

Table 3-8

COMPARISON OF MONTICELLO AND 1/4 SCALE GEOMETRIES USING S/RV SCALING MODEL

Parameter	Scaling Law	Monticello CP, NWL	1/4 Scale Base Case	Monticello 1/4 Scale	Scaling Requirement
Steam flow rate (lbm/sec)	$\lambda_x^{3.5}$	200.0	1.55	129.03	128.0
Distance from floor (ft)	λ_x	4.67	1.2	3.892	4.0
SR/V line air length (ft)	$\lambda_x^{0.5}\lambda_T^{0.5}$	88.67	52	1.705	1.712
SR/V line X-section area (ft^2)	$\lambda_x^{2.5}/\lambda_T^{0.5}$	0.5273	0.01414	37.291	37.387
Water leg length (ft)	λ_x	13.3	3.38	3.935	4.0
Gas/pipe pressure (psia)	λ_x	14.6	3.7	3.946	4.0
Wetwell pressure (psia)	λ_x	14.6	3.7	3.946	4.0
Quencher hole area (ft^2)	λ_x^2				16.0
Quencher arm area (ft^2)	λ_x^2	0.706	0.04588	15.388	16.0
Quencher arm length from quencher C_L (ft)	λ_x	9.415	2.39	3.939	4.0
Quencher submergence (ft)	λ_x	6.53	1.65	3.958	4.0
Torus minor radius (ft)	λ_x	18.83	3.45	4.009	4.0

* $$\lambda_x = \frac{(\text{Quencher Submergence})_{\text{Model}}}{(\text{Quencher Submergence})_{\text{Full scale}}} = 0.25$$

$$\lambda_T = \frac{(\text{Absolute Temperature of Discharge Line})_{\text{Model}}}{(\text{Absolute Temperature of Discharge Line})_{\text{Full Scale}}} = 1.365$$

** Proprietary Information has been deleted.

Table 3-9

1/4 SCALE TEST MATRIX

Test Number	Submergence (ft)	Distance from Floor (ft)	Steam Flow Rate (lbm/sec)	Pipe Air Length (ft)	Pipe Air Diameter (in)	Water Leg Length (ft)	Wetwell/ Pipe Pressure (psia)
1	1.65	1.2	1.55	52	1-1/2	3.38	3.7
2	1.65	1.2	0.8	52	1-1/2	3.38	3.7
3	1.65	1.2	2.5	52	1-1/2	3.38	3.7
4	1.65	1.2	1.55	52	1-1/2	3.38	11.25
4A	1.65	1.2	1.55	52	1-1/2	3.38	7.7
5	1.65	1.2	1.55	26	1-1/2	3.38	3.7
6	1.65	1.2	1.55	26	1-1/2	3.38	11.25
7	1.65	1.2	1.55	108	1-1/2	3.38	3.7
8	1.65	1.2	1.55	108	1-1/2	3.38	11.25
9	1.65	0.7	1.55	52	1-1/2	3.38	3.7
10	1.65	1.2	1.55	52	2-1/2	3.38	3.7
11	1.65	1.2	1.55	52	1-1/2	6.25	3.7
12	1.65	1.2	1.55	26	2-1/2	3.38	3.7
13	2.80	1.2	1.55	52	1-1/2	3.38	3.7
14	1.65	1.2	1.55	52	1-1/2	1.65	3.7
15	1.65	1.2	1.55	51.25	1-1/2	6.25	3.7/2.4
16	1.65	1.2	1.55	48.1	1-1/2	3.38	3.7
17	1.0	1.2	1.55	48.1	1-1/2	2.5	3.7
18	1.65	1.2	1.55	51.25	1-1/2	6.25	5.0/3.7
19	1.0	1.2	1.55	51.25	1-1/2	3.38	4.0/3.7
20	3.38	1.2	1.55	52	1-1/2	3.38	3.7

Table 3-10

1/4 SCALE TORUS AND T-QUENCHER GEOMETRIES

Parameter	Values	
Pool Area per Quencher	190.44 ft^2	
Pool Depth	2.85, 4.0 ft	
Distance from Floor	1.2, 0.7 ft	
Torus Major Radius	12.25 ft	
Quencher Arm Length from Quencher L	2.39 ft	
Cross-sectional area of One Quencher Arm	0.04588 ft^2	
Radius of One Quencher Hole	ft	**
Length of the 1st Field of Holes	ft	
Length of the 2nd Field of Holes	ft	
Length of the 3rd Field of Holes	ft	
Length of the 4th Field of Holes	ft	
Total Area of 1st Hole Pattern	ft^2	
Total Area of 2nd Hole Pattern	ft^2	
Total Area of 3rd Hole Pattern	ft^2	
Total Area of 4th Hole Pattern	ft^2	
Number of Quencher Arms	2	
Number of Bubbles	4	
Number of Bubbles After Coalescence	4	

*Dummy Number

**Proprietary information has been deleted.

1764 220

Table 3-11

AVERAGE 1/4 SCALE TEST INITIAL CONDITIONS

Test Number	Air Mass (lbm)	Pipe Pressure (psia)	Wetwell Pressure (psia)	Initial Pipe Temperature (°F)	Pipe Temperature (°F)	Pool Depth (ft)	Air Volume (ft^3)
1	0.0098	3.67	3.67	295.69	79.0	2.85	0.7480
2	0.0098	3.67	3.67	296.87	84.33	2.85	0.7480
3	0.0099	3.695	3.70	294.78	85.0	2.85	0.7480
4	0.0301	11.24	11.24	295.32	79.0	2.85	0.7480
4A	0.0213	7.69	7.69	296.10	81.0	2.85	0.7480
5	0.0052	3.67	3.67	270.15	82.0	2.85	0.3803
6	0.0155	11.24	11.24	271.39	78.0	2.85	0.3803
7	0.0198	3.68	3.68	313.45	82.0	2.85	1.54
8	0.0606	11.21	11.21	309.66	76.0	2.85	1.54
9	0.0101	3.72	3.72	280.73	78.0	2.35	0.7480
10	0.0210	3.73	3.73	274.86	78.0	2.85	1.5308
11	0.0098	3.73	3.73	298.83	79.0	2.85	0.7356
12	0.0102	3.69	3.69	289.45	77.0	2.85	0.7654
13	0.0103	3.70	3.70	258.24	77.0	4.00	0.7448
14	0.0105	3.70	3.79	255.60	78.0	2.85	0.7480
15	0.0063	2.45	3.69	290.67	81.0	2.85	0.7176
16	0.0104	3.72	3.72	303.70	81.6	2.84	0.7897
17	0.0108	3.73	3.70	298.60	83.5	2.08	0.8165
18	0.0106	3.78	4.94	297.60	80.2	2.84	0.7904
19	0.0102	3.66	4.02	303.20	75.8	2.08	0.7897
20	0.0098	3.70	3.70	294.60	69.8	4.55	0.7381

Table 3-12

COMPARISON OF 1/4 SCALE TEST MEASURED AND PREDICTED PEAK SHELL PRESSURES AND FREQUENCIES

Test Case	P^{+}_{max} (psid)		P^{-}_{max} (psid)		Frequency f (Hz)	
	Measured ±σ	Predicted	Measured ±σ	Predicted	Measured ±σ	Predicted
1	1.01 ± 0.14	1.07	-0.82 ± 0.09	-0.88	15.47 ± 0.15	15.8
2	0.57 ± 0.11	0.67	-0.66 ± 0.08	-0.60	16.3 ± 0.42	15.6
3	1.65 ± 0.28	1.81	-1.18 ± 0.05	-1.32	15.63 ± 0.65	15.1
4	0.85 ± 0.09	1.09	-1.36 ± 0.15	-1.28	26.94 ± 0.42	26.0
4A	0.83 ± 0.22	1.05	-1.14 ± 0.11	-1.16	24.4 ± 1.14	22.1
5	1.18 ± 0.09	1.12	-0.95 ± 0.06	-0.89	20.17 ± 0.73	19.4
6	1.00 ± 0.18	1.10	-1.12 ± 0.18	-1.22	31.93 ± 1.71	32.6
7	1.41 ± 0.12	1.43	-1.27 ± 0.01	-1.20	12.20 ± 0.33	11.8
8	2.33 ± 0.14	2.30	-2.29 ± 0.09	-2.02	19.90 ± 0.70	20.2
9	1.03 ± 0.20	1.38	-1.03 ± 0.13	-1.13	15.10 ± 0.57	15.4
10	1.51 ± 0.17	1.59	-1.19 ± 0.06	-1.29	12.55 ± 0.33	11.8
12	1.01 ± 0.13	1.21	-0.80 ± 0.10	-0.98	15.43 ± 0.36	15.7
13	0.80 ± 0.15	0.95	-0.65 ± 0.09	-0.84	16.07 ± 0.40	17.1
14	1.84 ± 0.16	1.74	-1.41 ± 0.12	-1.28	14.35 ± 0.43	15.5
16	0.69 ± 0.17	1.05	-0.64 ± 0.08	-0.86	15.21 ± 0.40	15.5
18	0.93 ± 0.12	0.77	-0.90 ± 0.06	-0.84	17.08 ± 0.54	19.7
20	0.71 ± 0.22	0.96	-0.73 ± 0.24	-0.89	15.67 ± 0.58	18.6

Table 3-13

COMPARISON OF 1/4 SCALE MEASURED AND PREDICTED BUBBLE PRESSURES AND FREQUENCIES

Test Case	Bubble Pressure P_B^+ (psid)		Bubble Pressure P_B^- (psid)		Frequency f (Hz)	
	Measured ±σ	Predicted	Measured ±σ	Predicted	Measured ±σ	Predicted
1	1.55 ± 0.67	1.60	-1.17 ± 0.27	-1.11	15.47 ± 0.15	15.8
2	1.08 ± 0.24	0.98	-1.04 ± 0.18	-0.79	16.3 ±0.42	15.6
3	2.05 ± 0.55	2.75	-1.42 ± 0.09	-1.55	15.63 ± 0.65	15.1
4	1.03 ± 0.30	1.56	-2.03 ± 0.33	-1.78	26.94 ± 0.42	26.0
4A	1.41 ± 0.53	1.50	-1.59 ± 0.24	-1.56	24.4 ± 1.14	22.1
5	2.06 ± 0.93	2.10	-1.31 ± 0.28	-1.32	20.17 ± 0.73	19.4
6	1.52 ± 0.31	1.91	-1.63 ± 0.29	-2.04	31.93 ± 1.71	32.6
7	1.70 ± 0.26	1.68	-1.46 ± 0.12	-1.17	12.20 ± 0.33	11.8
8	2.60 ± 0.45	2.67	-2.58 ± 0.27	-2.10	19.90 ± 0.70	20.2
9	1.18 ± 0.37	1.71	-1.08 ± 0.07	-1.16	15.10 ± 0.57	15.4
10	1.66 ± 0.36	1.84	-1.39 ± 0.10	-1.25	12.55 ± 0.33	11.8
11	0.77 ± 0.53	1.23	-0.65 ± 0.24	-1.07	14.52 ± 0.54	16.4
12	1.62 ± 0.33	1.83	-1.14 ± 0.18	-1.21	15.43 ± 0.36	15.7
13	1.18 ± 0.37	1.46	-0.95 ± 0.21	-1.11	16.07 ± 0.40	17.1
14	2.63 ± 0.46	2.70	-1.63 ± 0.07	-1.54	14.35 ± 0.43	15.5
15	1.57 ± 0.46	1.05	-1.21 ± 0.23	-1.01	17.71 ± 0.74	18.4
16	1.38 ± 0.72	1.53	-0.87 ± 0.10	-1.08	15.21 ± 0.40	15.5
17	0.77 ± 0.32	2.31	-0.92 ± 0.21	-1.35	16.51 ± 0.63	15.0
18	1.65 ± 0.53	1.22	-1.37 ± 0.22	-1.20	17.08 ± 0.54	19.7
19	1.15 ± 0.35	1.78	-0.95 ± 0.19	-1.19	18.59 ± 0.69	16.7
20	1.35 ± 0.58	1.55	-1.14 ± 0.20	-1.24	15.67 ± 0.58	18.6

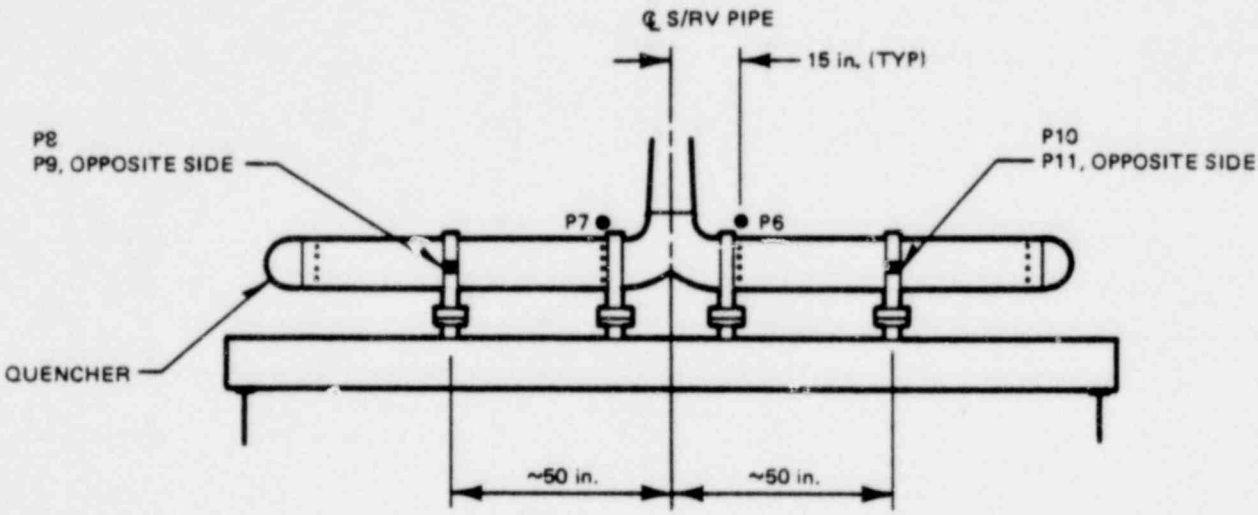

Figure 3-1. Bubble Pressure Sensors Locations for Monticello Test

1764 224

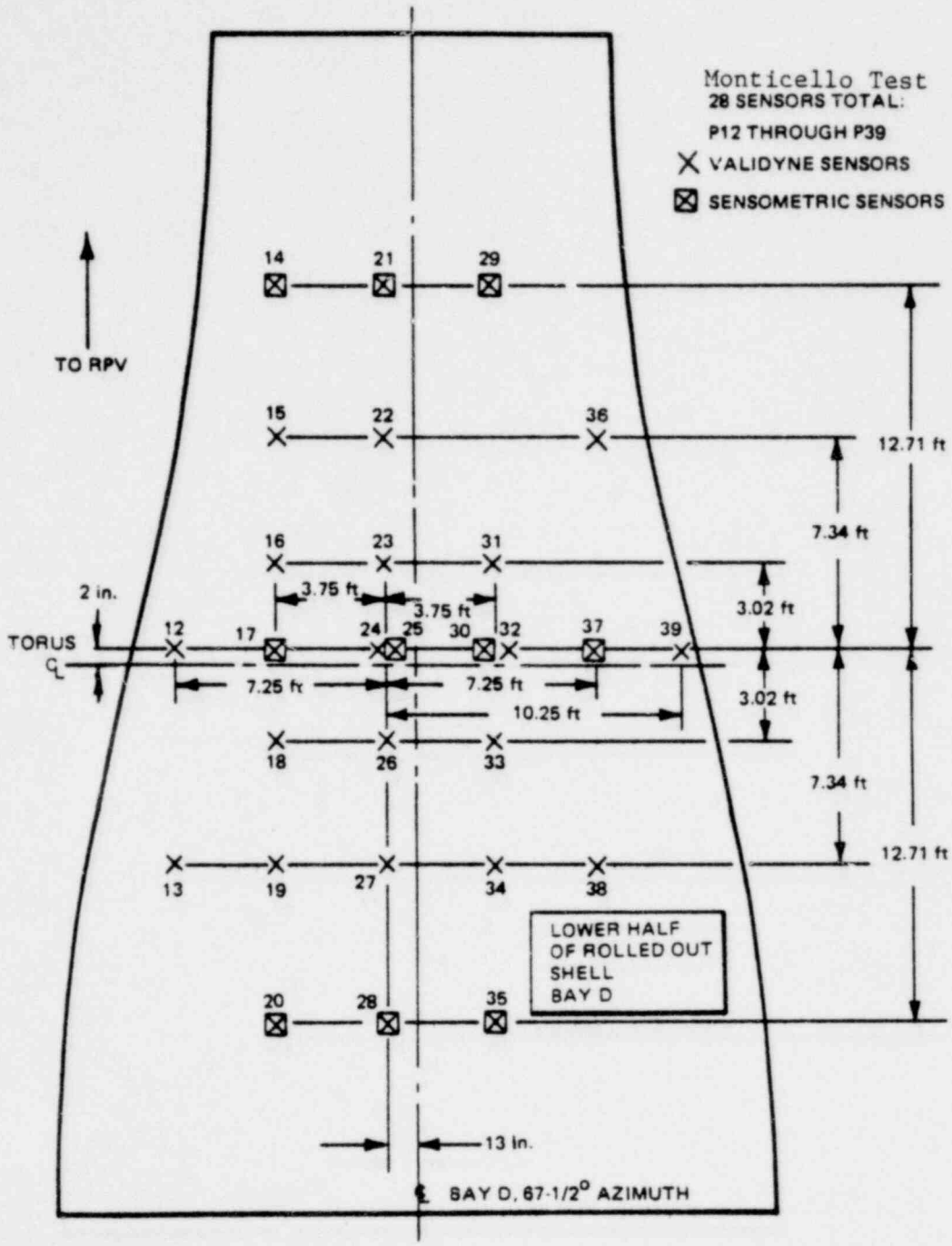

Figure 3-2. Pressure Transducer Location - Half-Shell Layout of Bay D

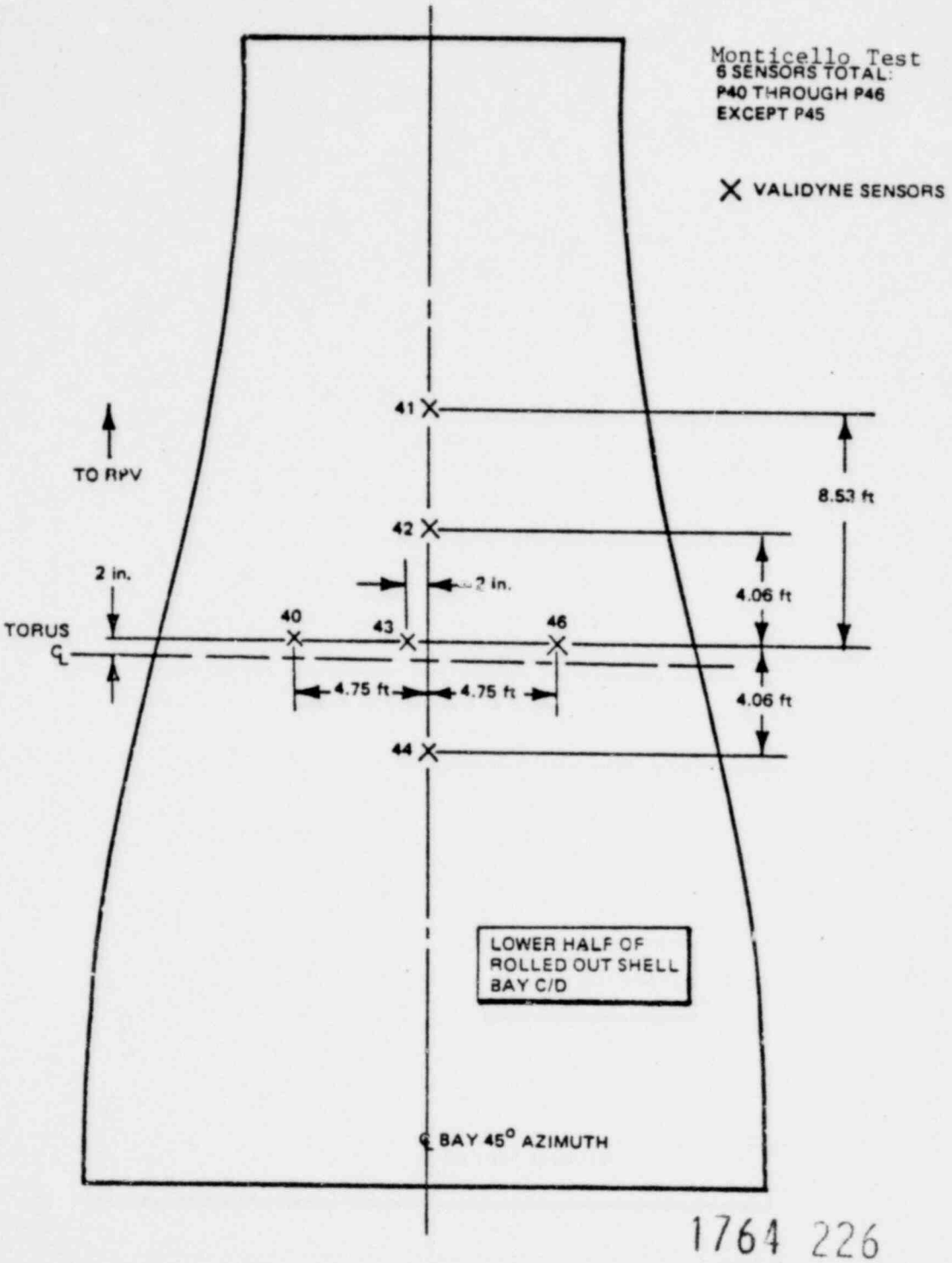

Figure 3-3. Pressure Transducer Location - Half-Shell Layout of Bay C/D

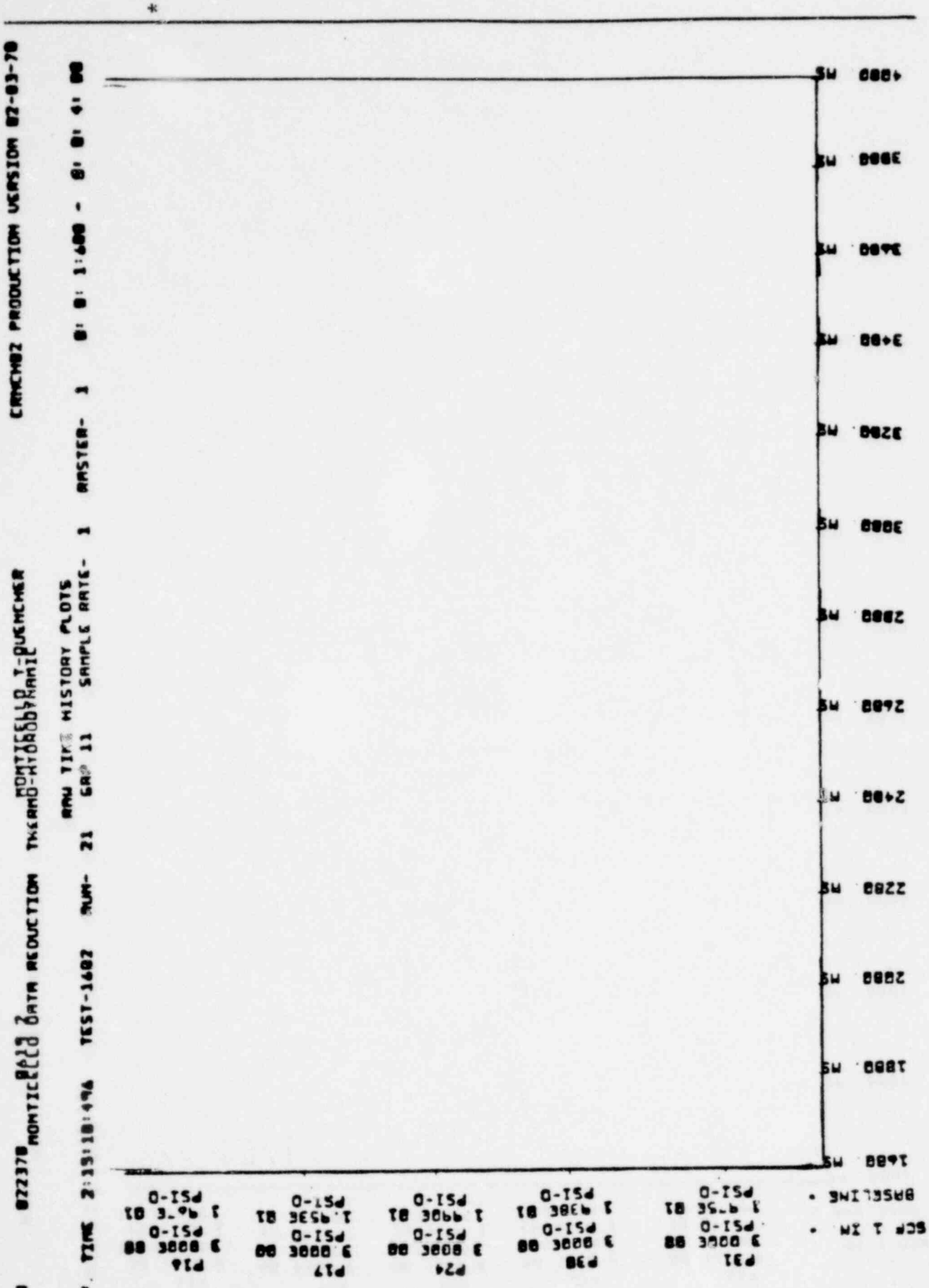

Figure 3-4. Typical Monticello Wall Pressure Traces

*Proprietary information has been deleted.

1764 227

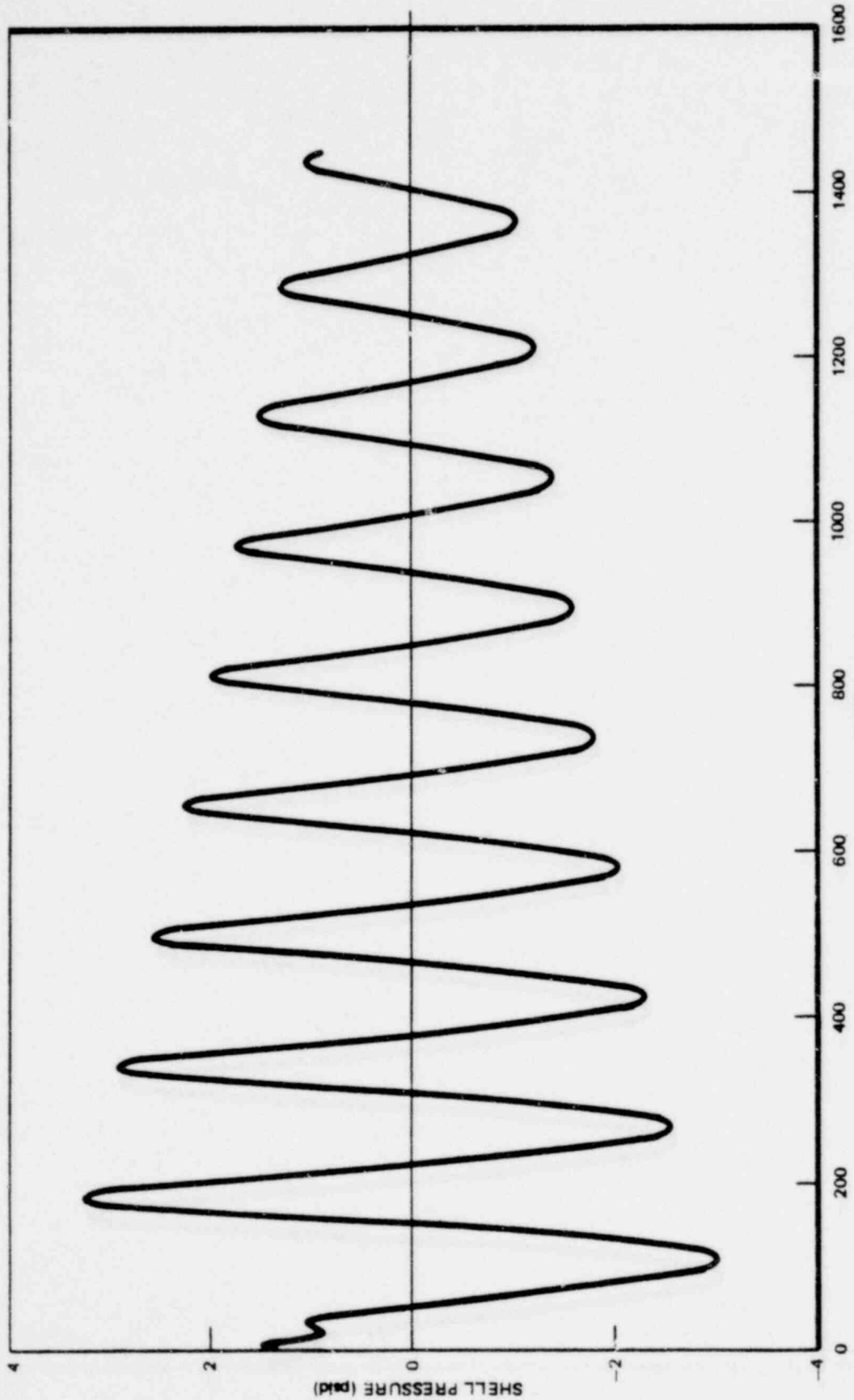

Figure 3-5. Typical Shell Pressure Time History Plot

1764 228

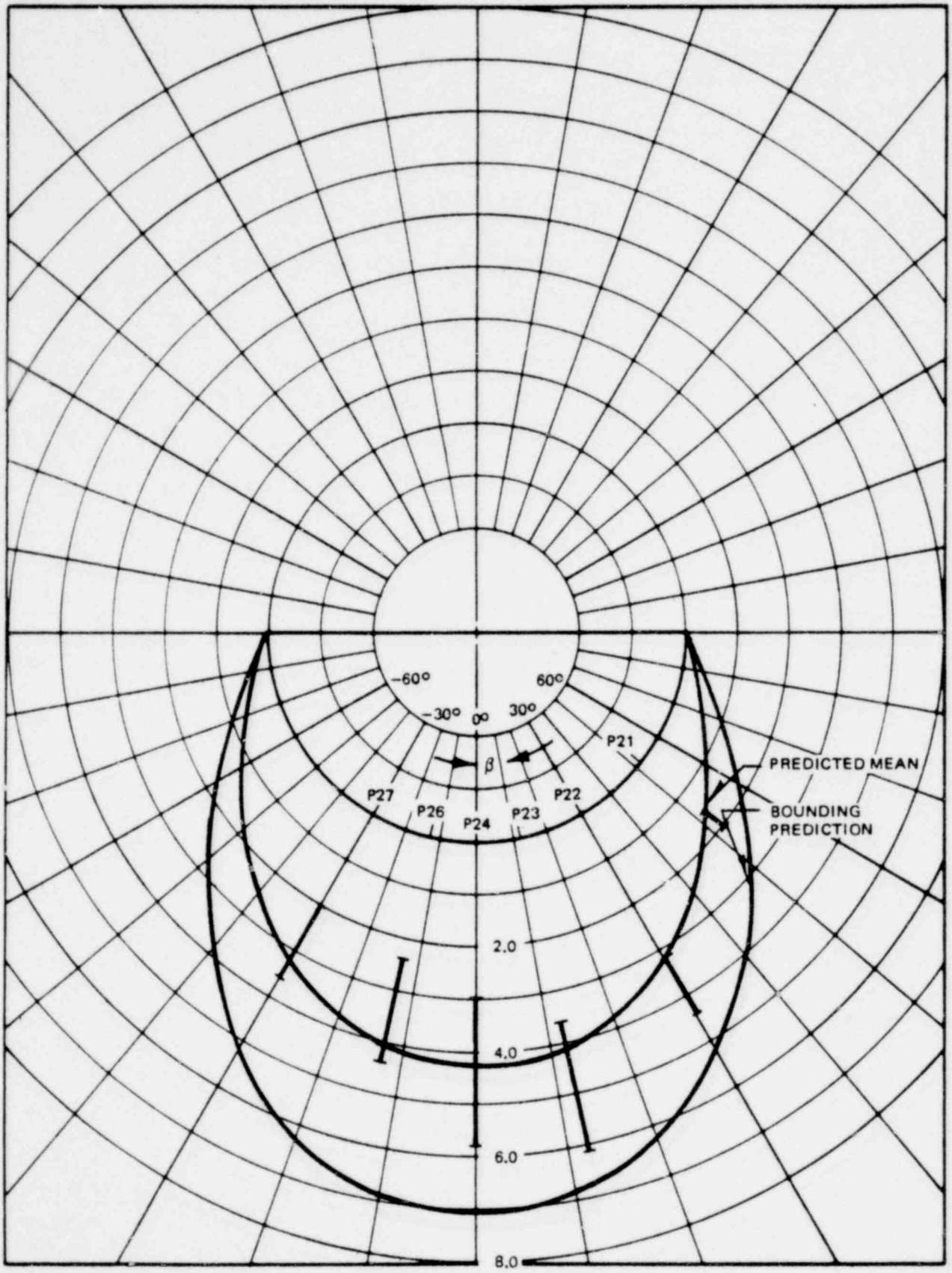

Figure 3-6. Peak Positive Pressure Distribution for Monticello CP, NWL @ α = 0 Radians

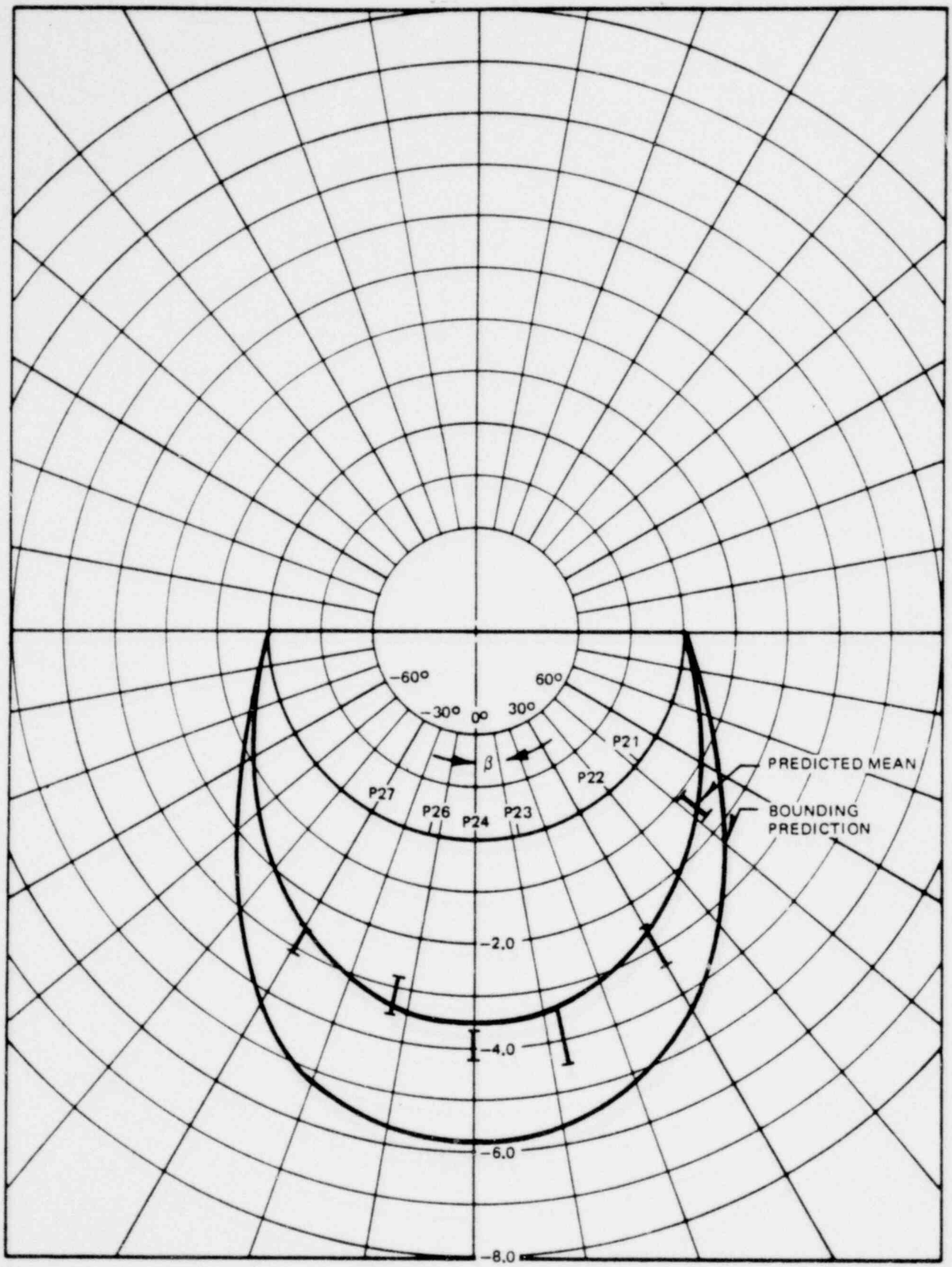

Figure 3-7. Peak Positive Pressure Distribution for Monticello CP, NWL @ α = 0

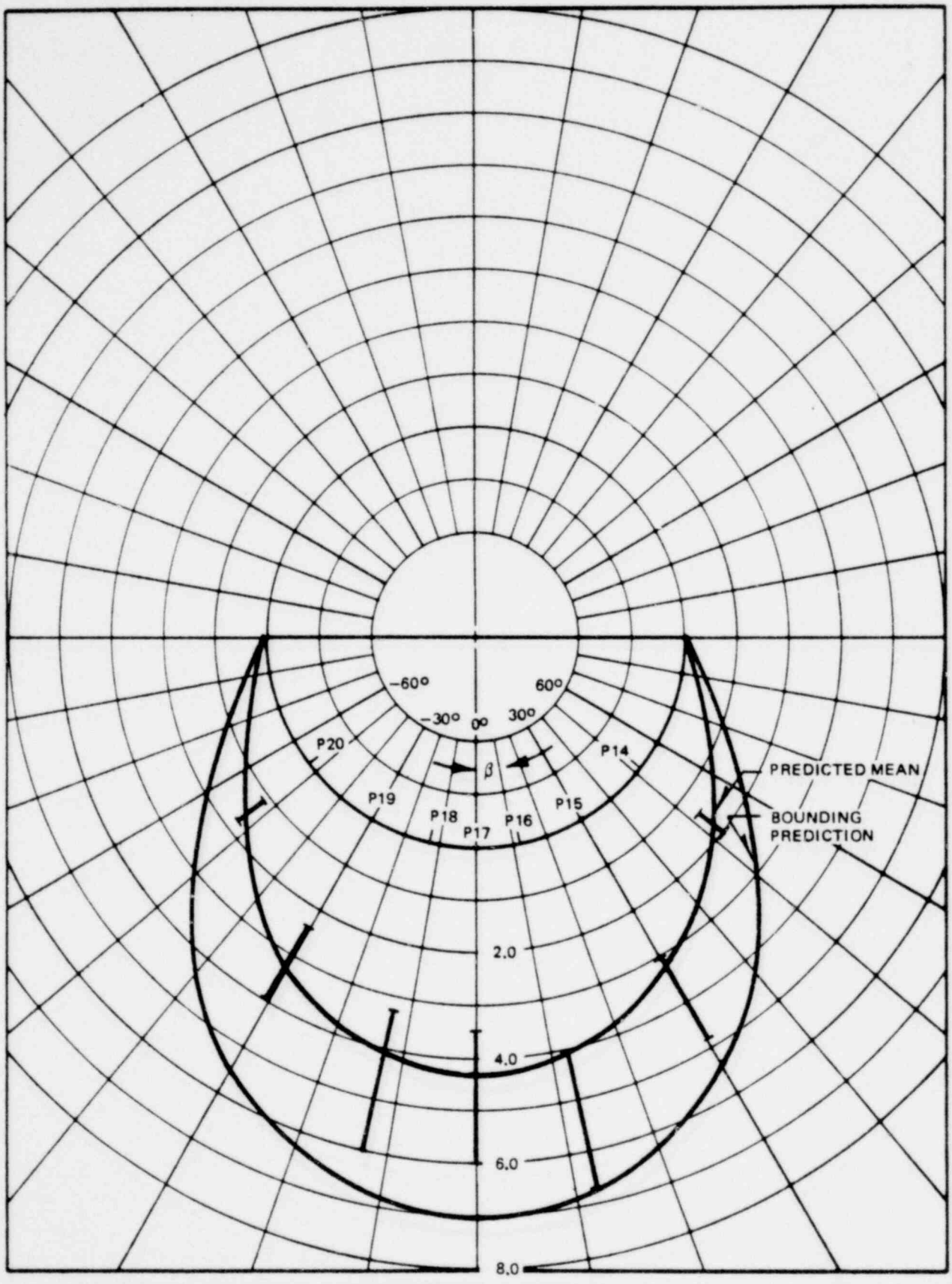

Figure 3-8. Peak Positive Pressure Distribution for Monticello CP, NWL @ α = 0.0765

1764 231

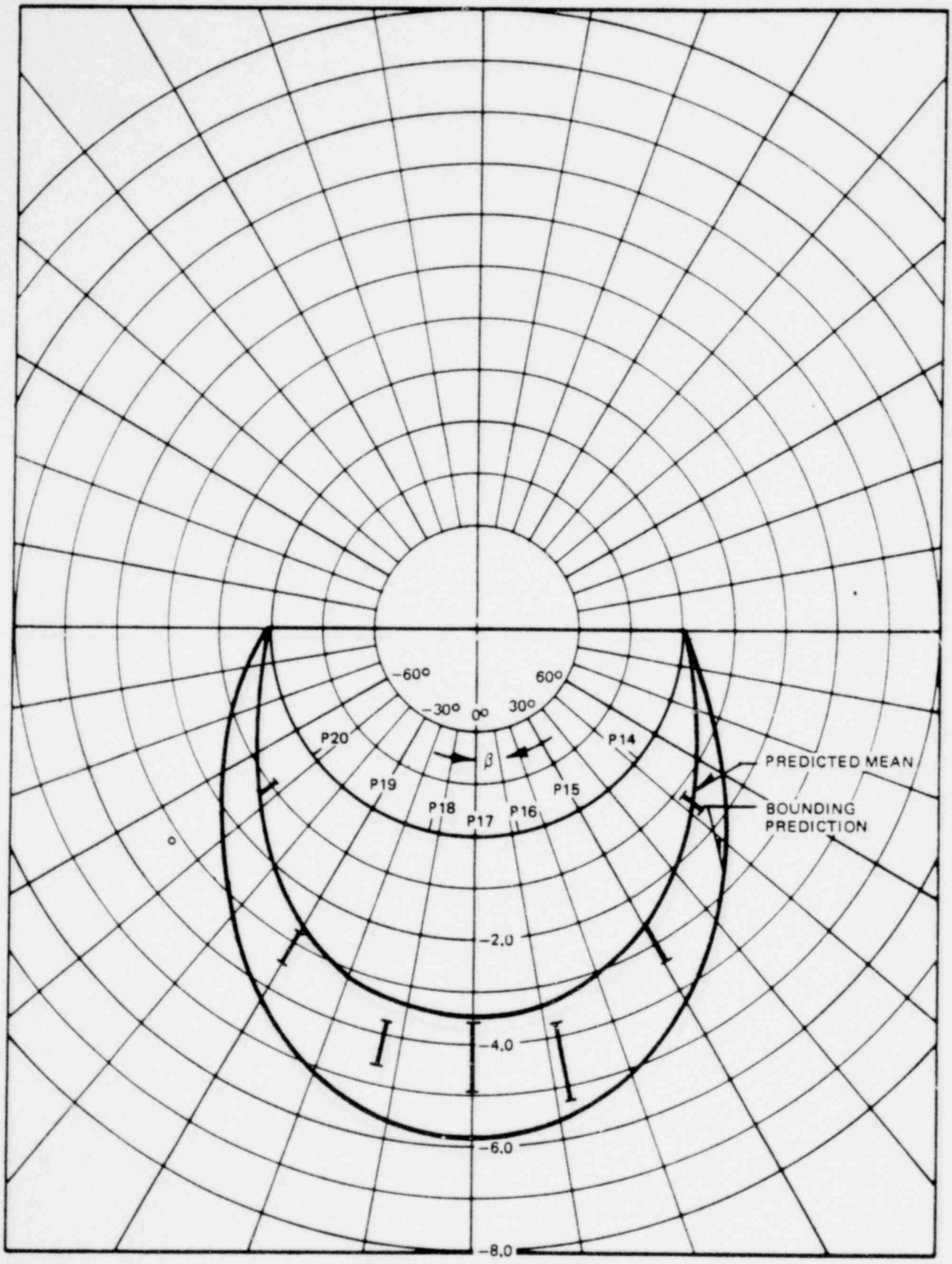

Figure 3-9. Peak Negative Pressure Distribution for Monticello CP, NWL @ α = 0.0765

1764 232

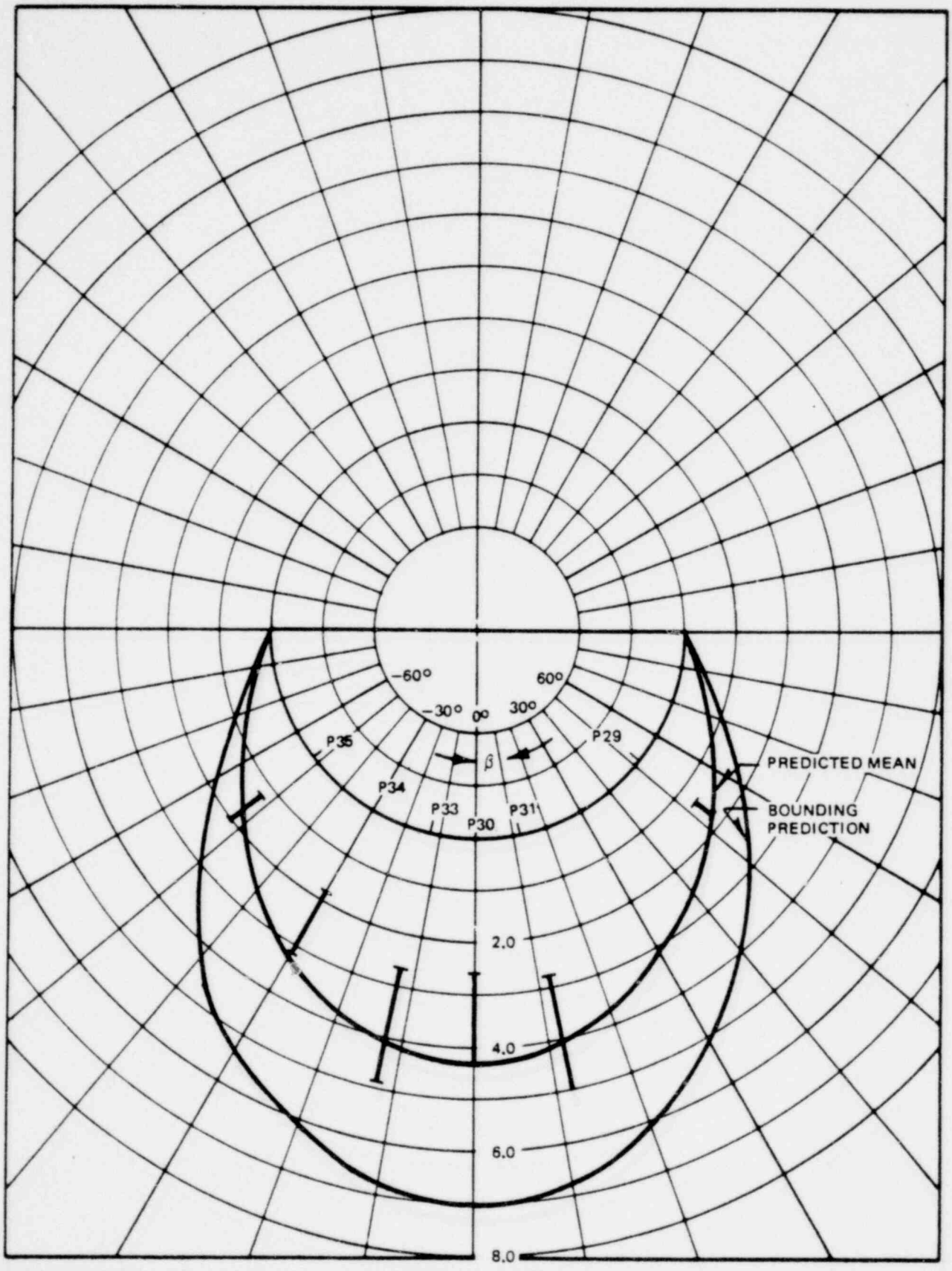

Figure 3-10. Peak Positive Pressure Distribution for Monticello CP, NWL @ α = 0.0765

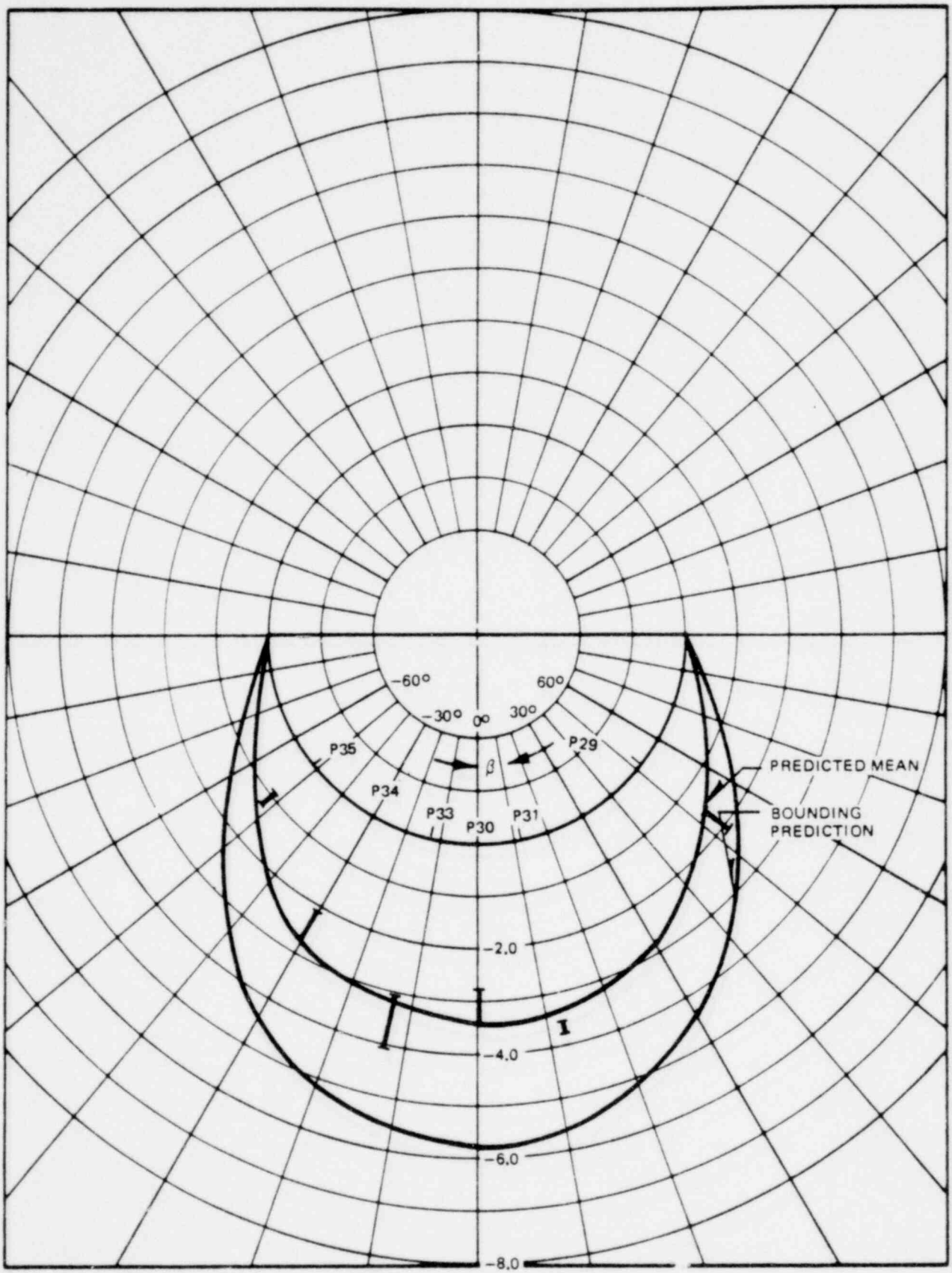

Figure 3-11. Peak Negative Pressure Distribution for Monticello CP, NWL @ α = 0.0765

1764 234

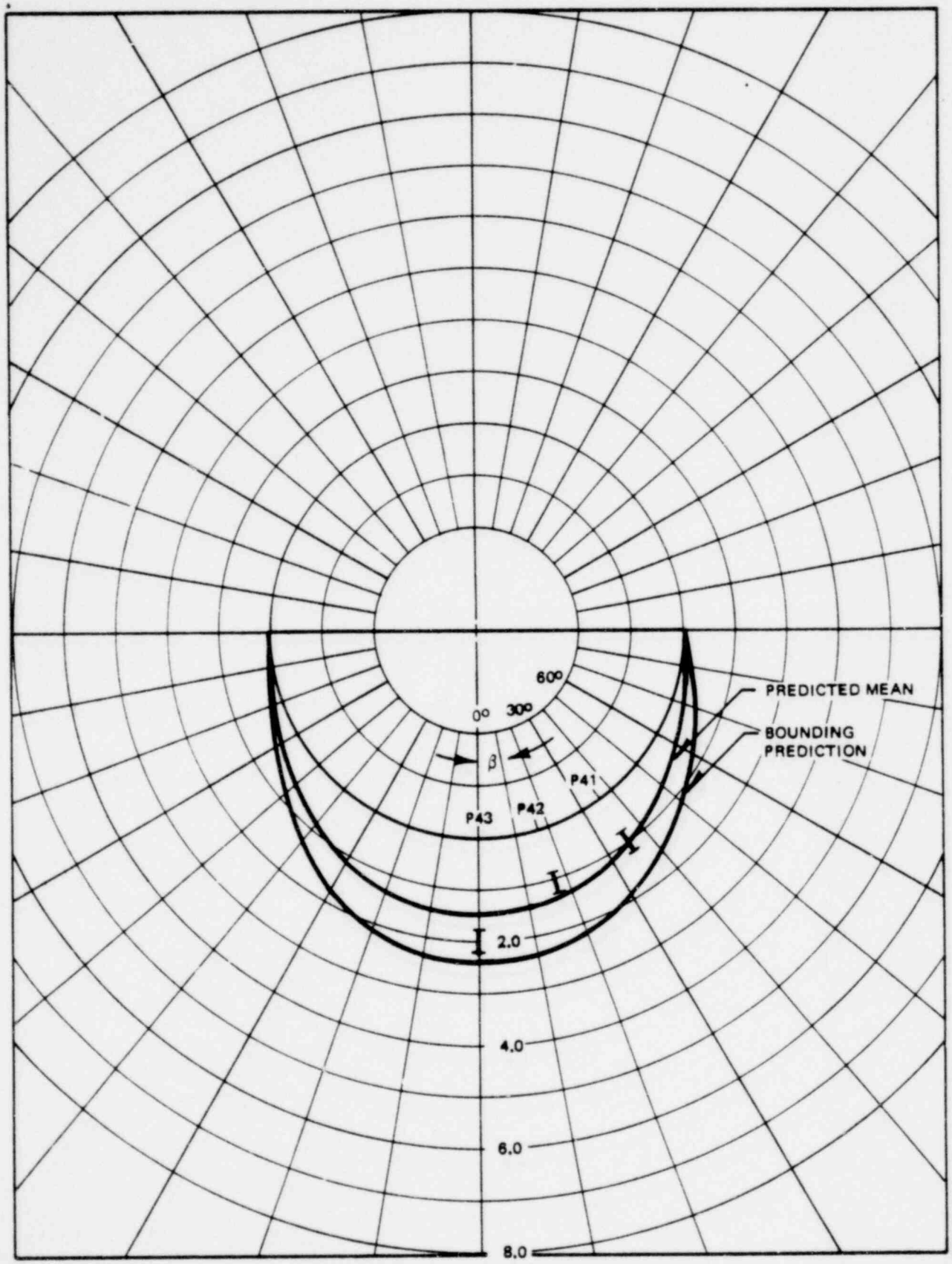

Figure 3-12. Peak Positive Pressure Distribution for Monticello CP, NWL @ α = 0.422

1764 235

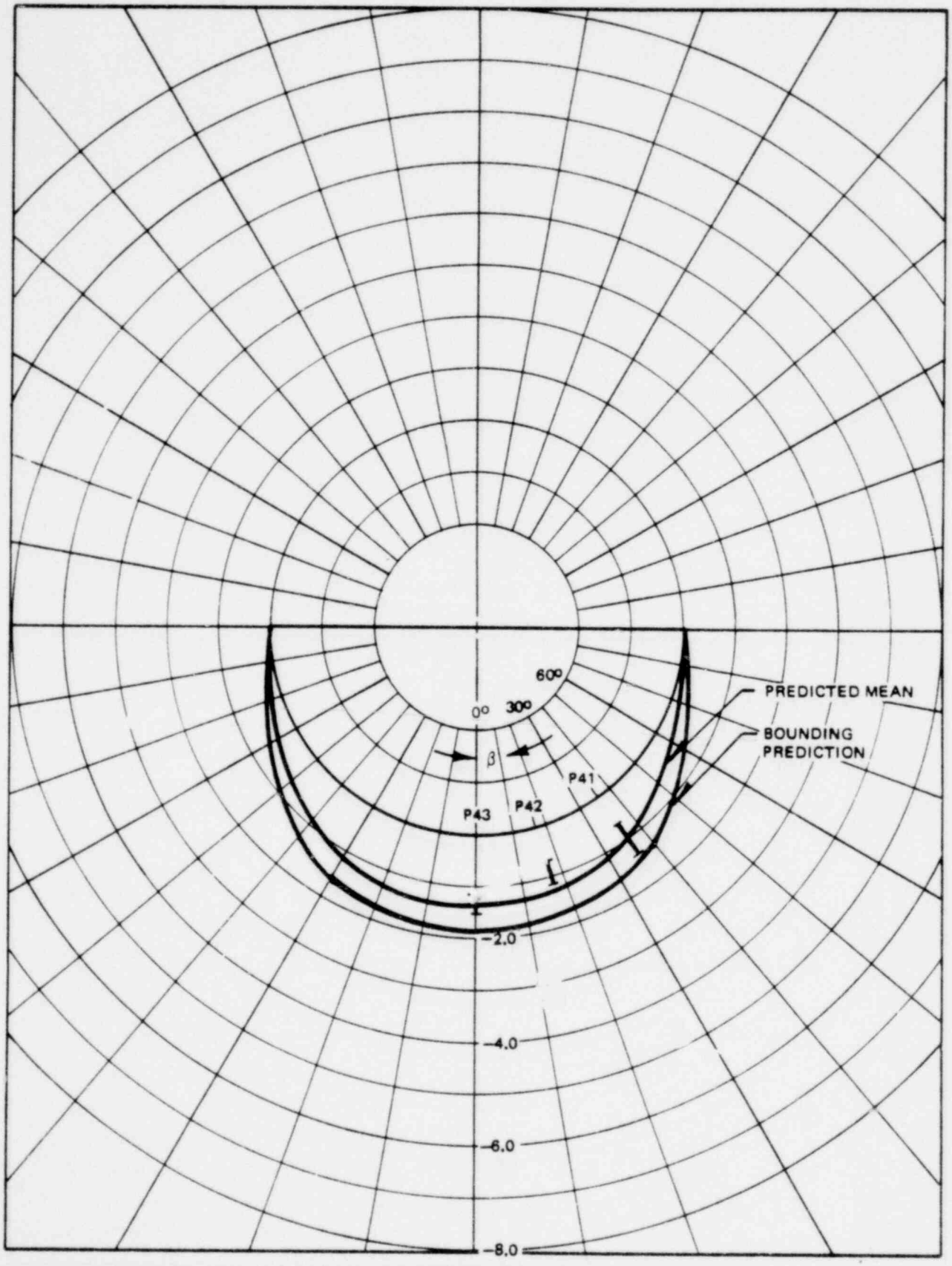

Figure 3-13. Peak Negative Pressure Distribution for Monticello CP, NWL @ α = 0.422

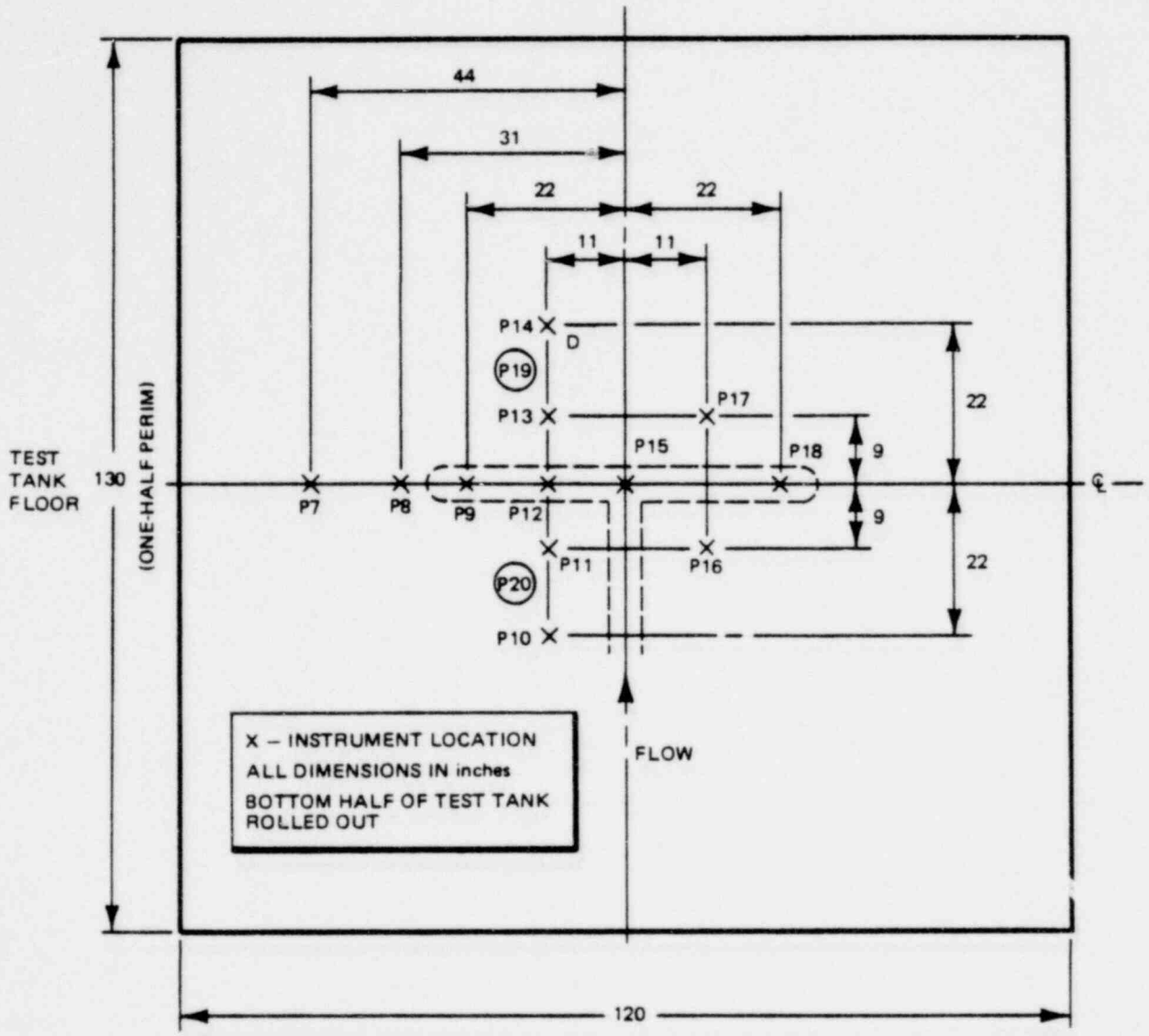

Figure 3-14. Location of 1/4 Scale Test Pressure Transducers

1764 237

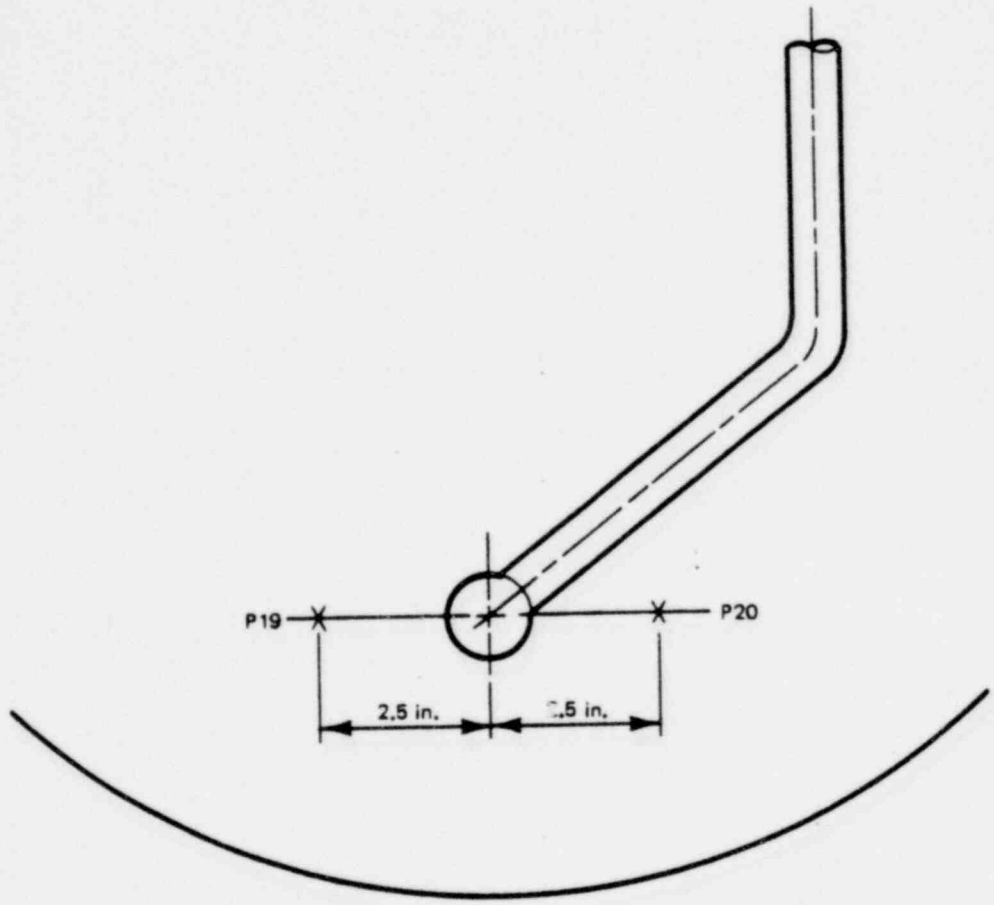

Figure 3-15. Location of 1/4 Scale Test Pressure Transducers P19 and P20

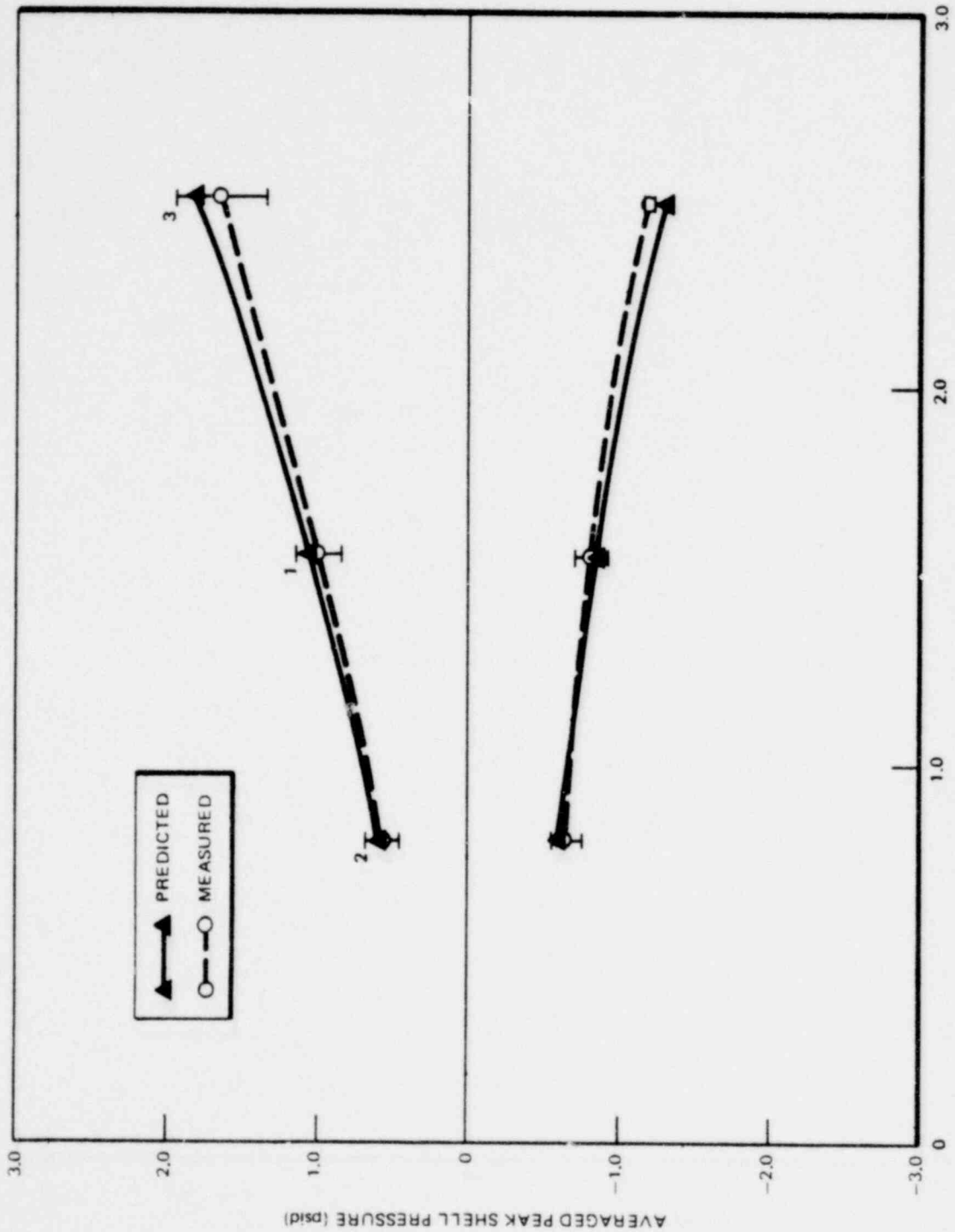

Figure 3-16. Effect of Steam Flow Rate on Maximum Shell Pressure

1764 239

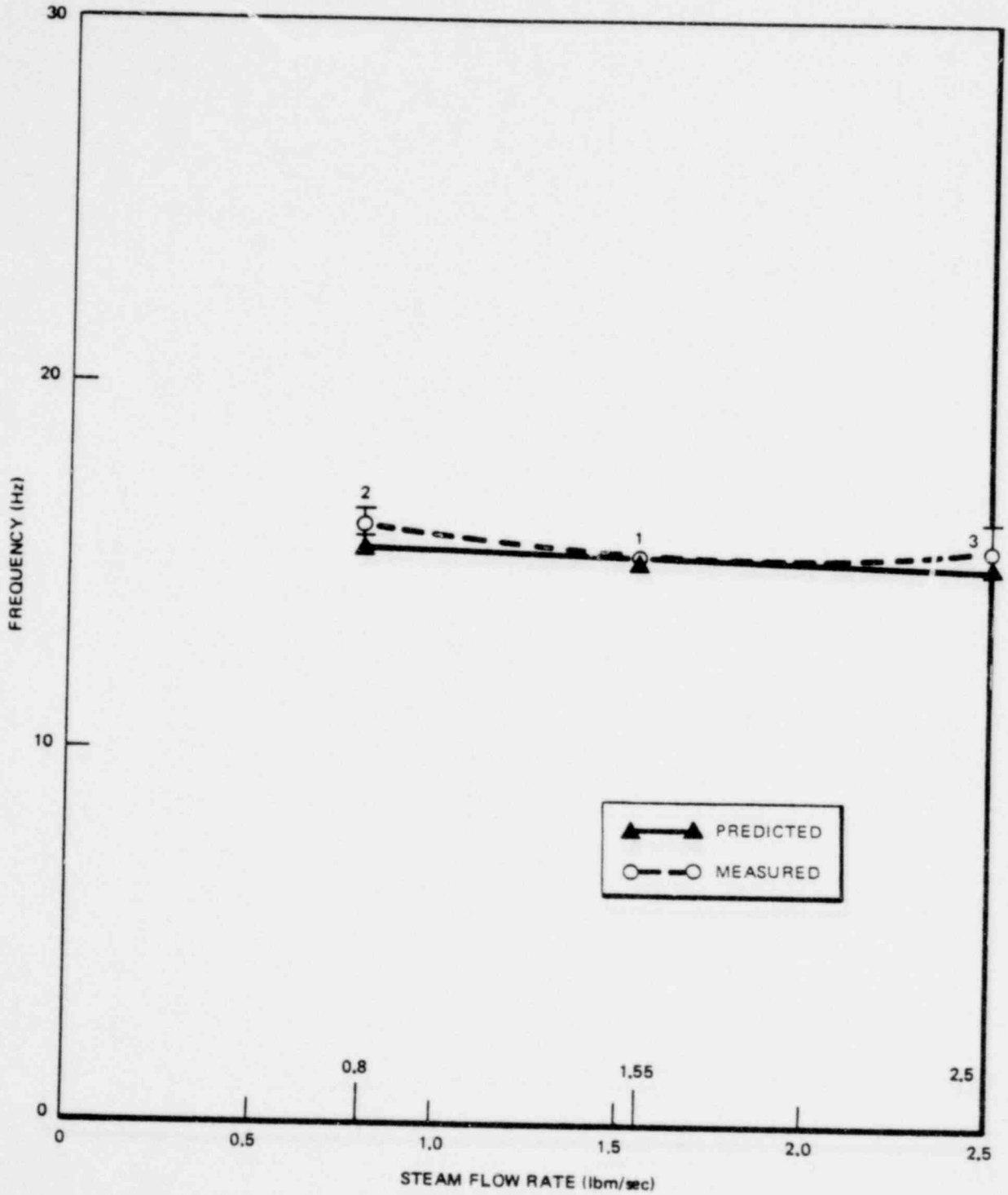

Figure 3-17. Effect of Steam Flow Rate on Frequency for Pipe Air Length of 52 Ft

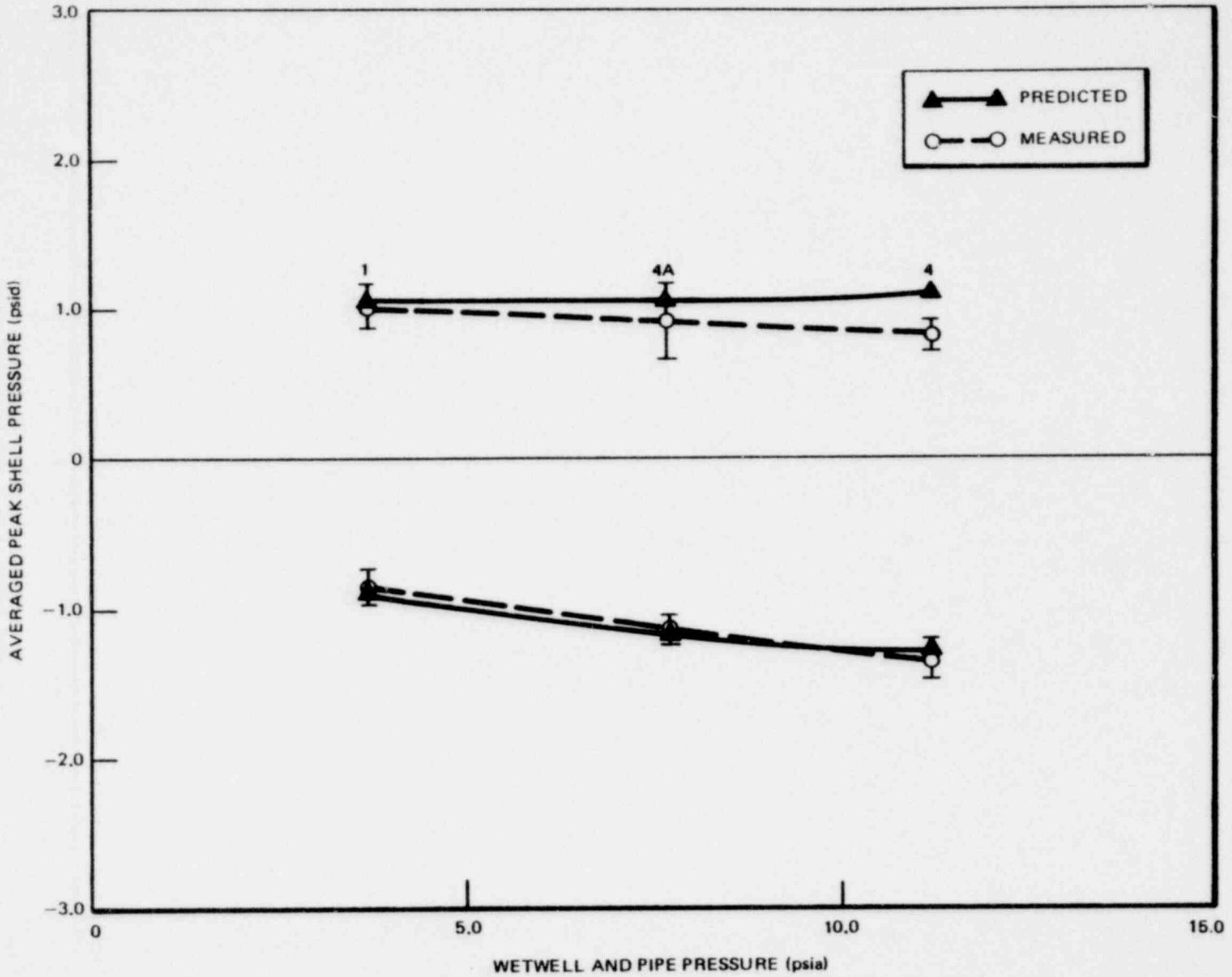

Figure 3-18. Effect of Wetwell and Pipe Pressures on Maximum Shell Pressure for Pipe Air Length of 52 Ft

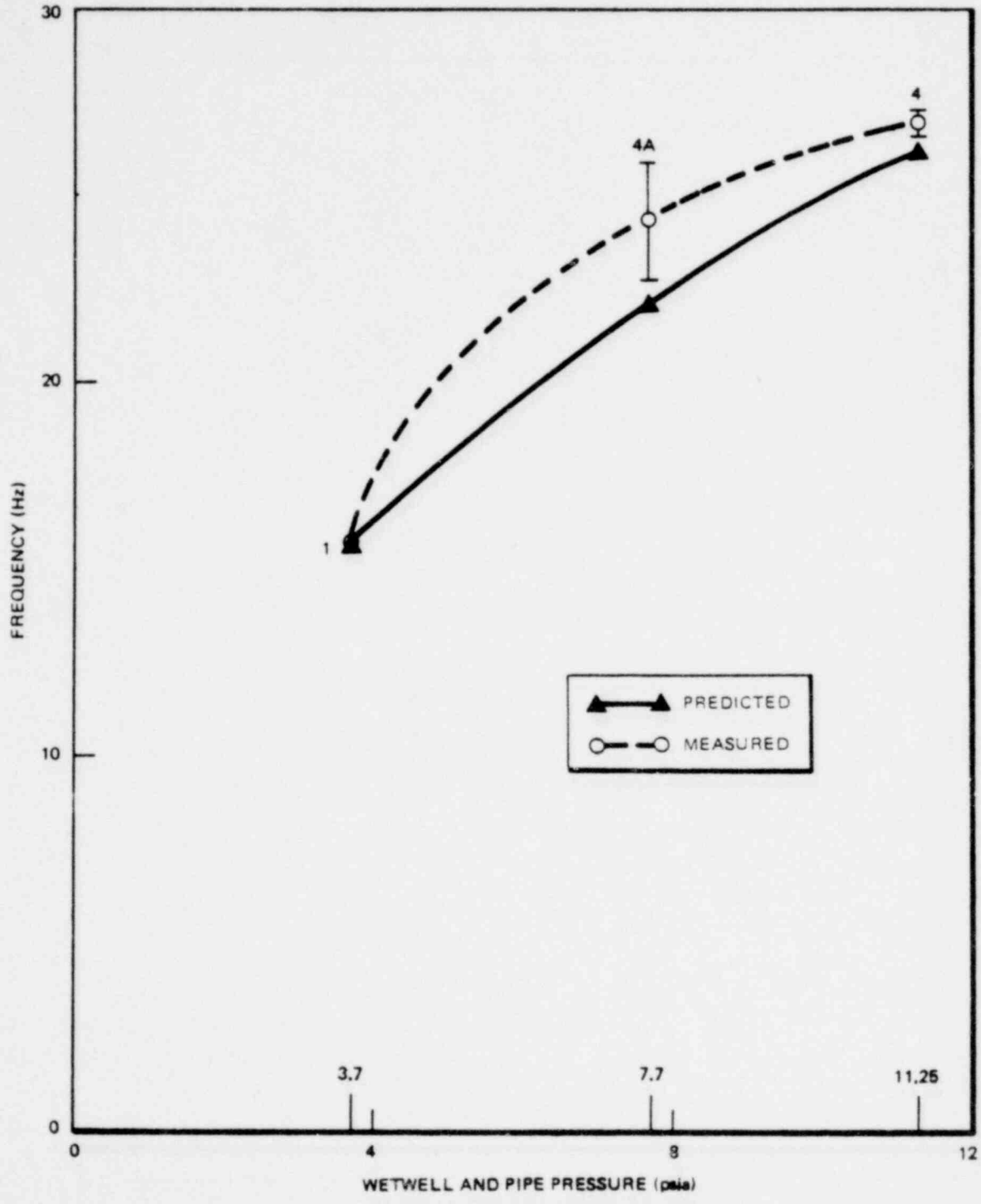

Figure 3-19. Effect of Wetwell and Pipe Pressures on Frequency for Pipe Air Length of 52 Ft

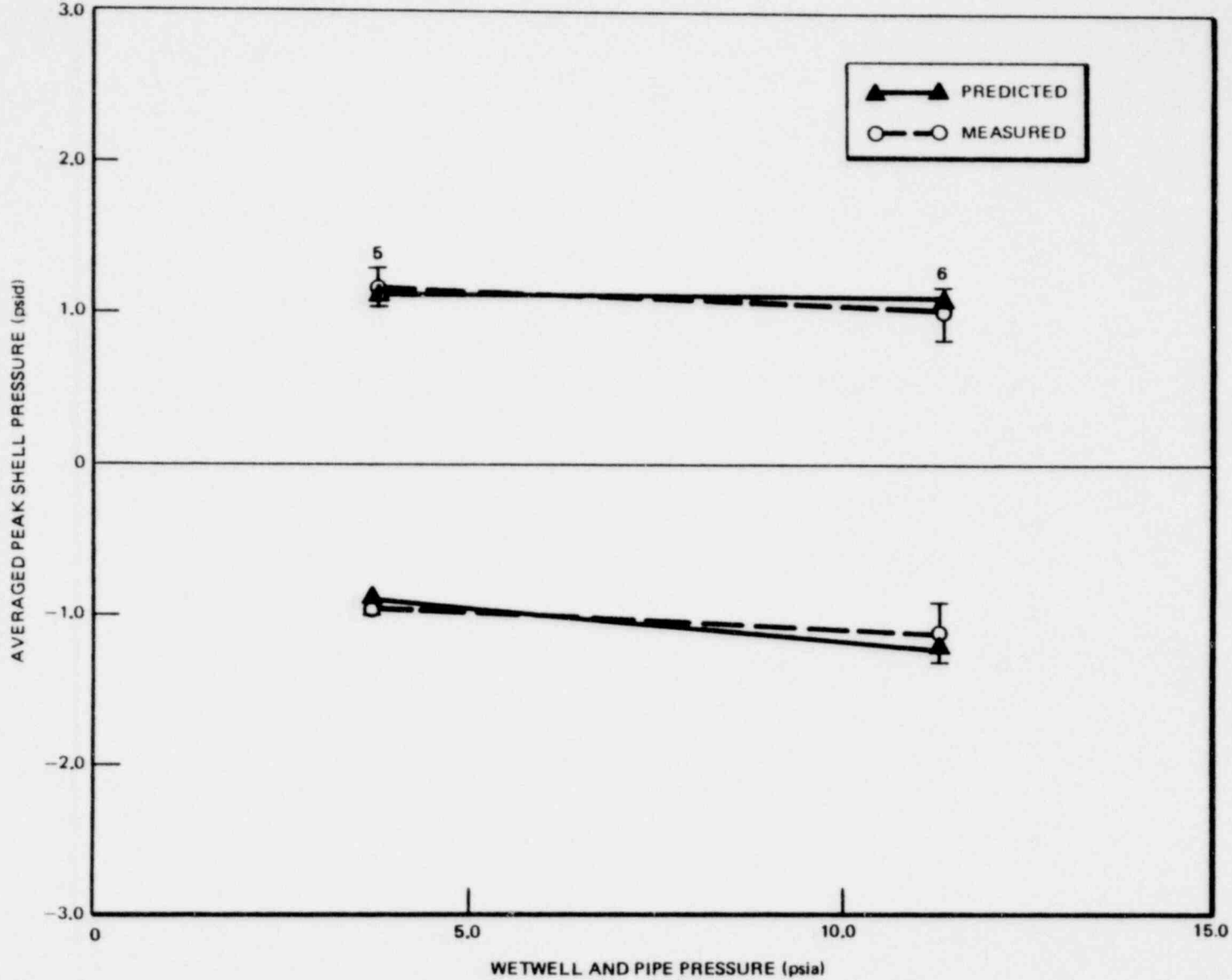

Figure 3-20. Effect of Wetwell and Pipe Pressures on Maximum Shell Pressures for Pipe Air Length of 26 Ft

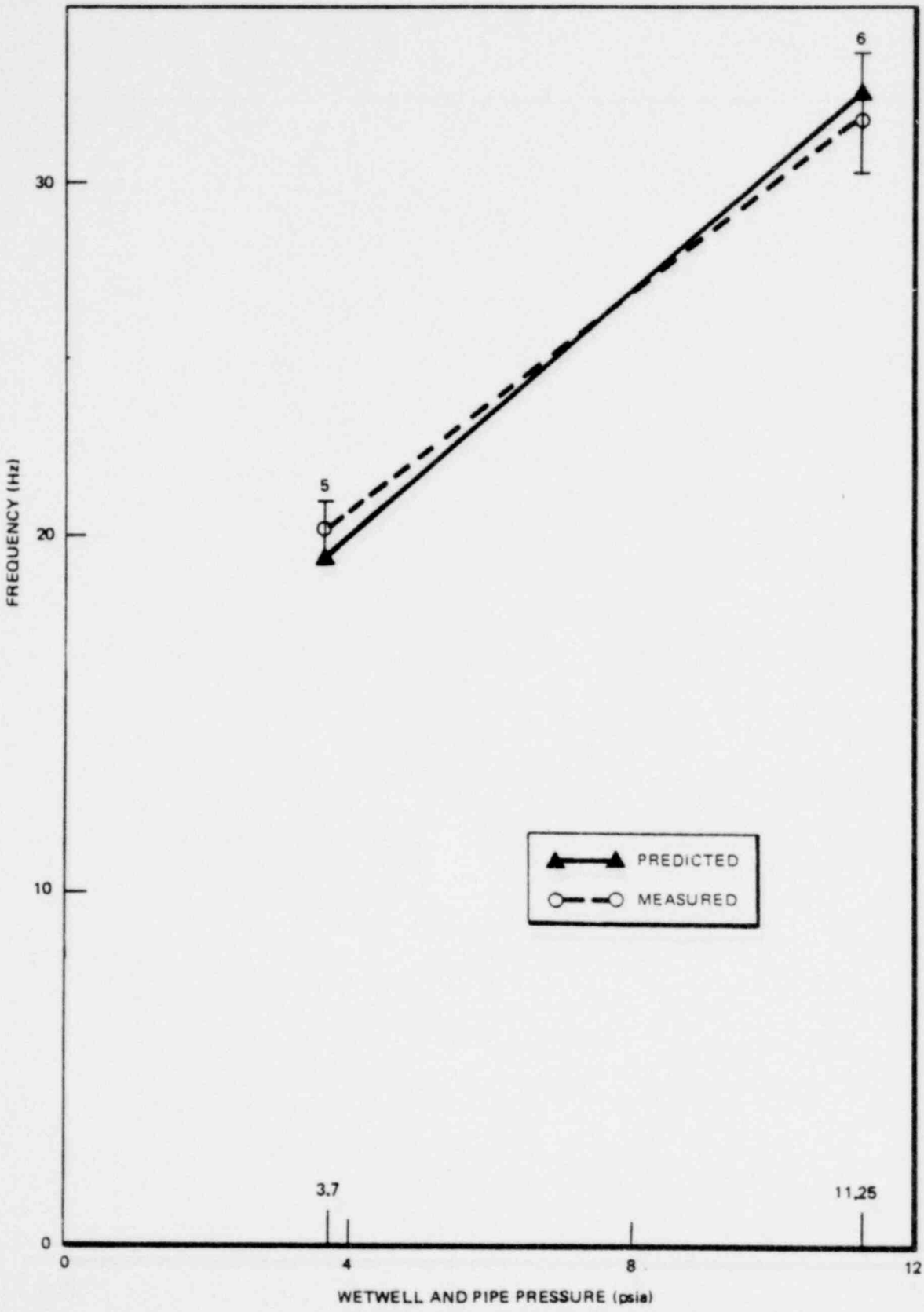

Figure 3-21. Effect of Wetwell and Pipe Pressures on Frequency for Pipe Air Length of 26 Ft

1764 244

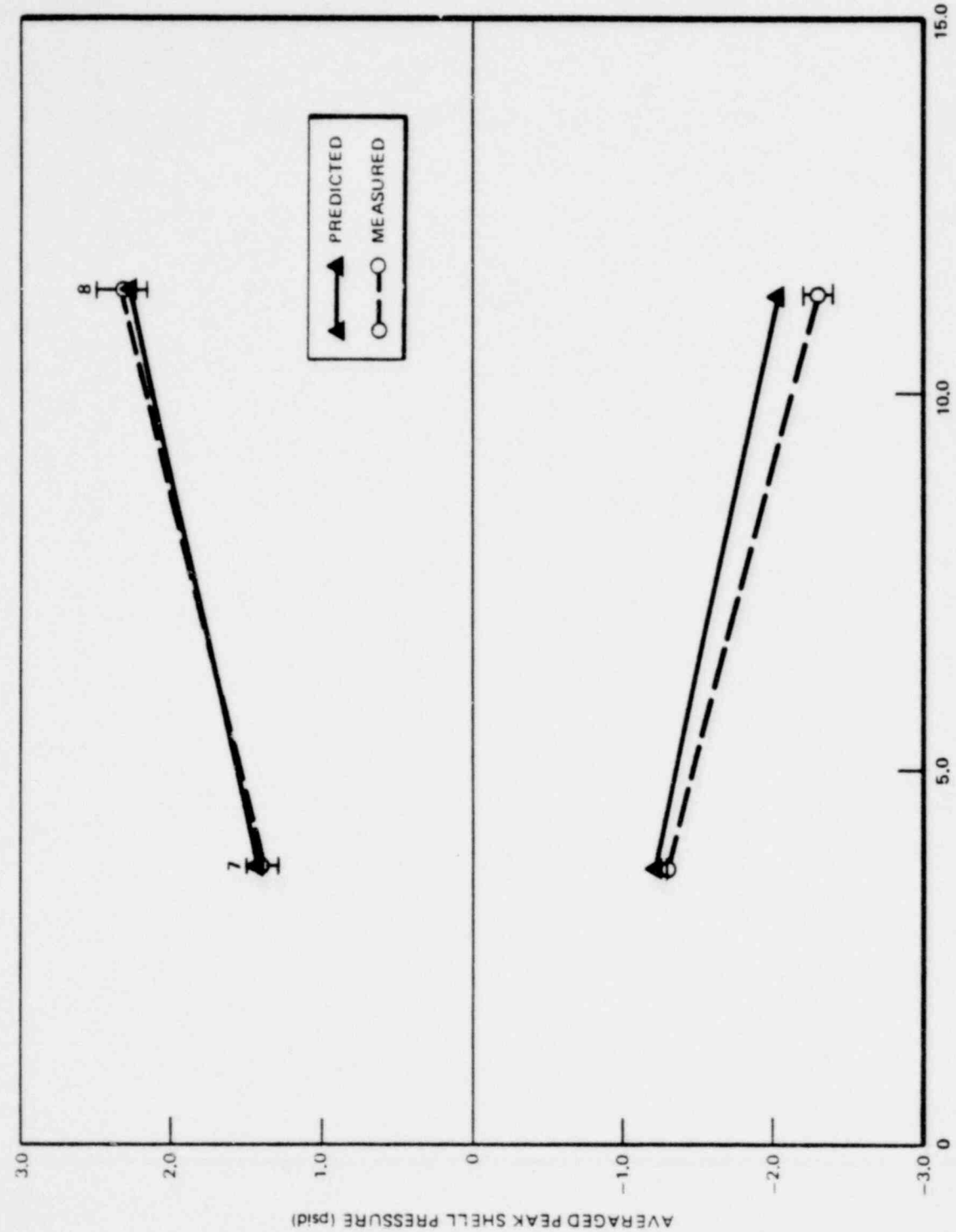

Figure 3-22. Effect of Wetwell and Pipe Pressures on Maximum Shell Pressures for Pipe Air Length of 108 Ft

1764 245

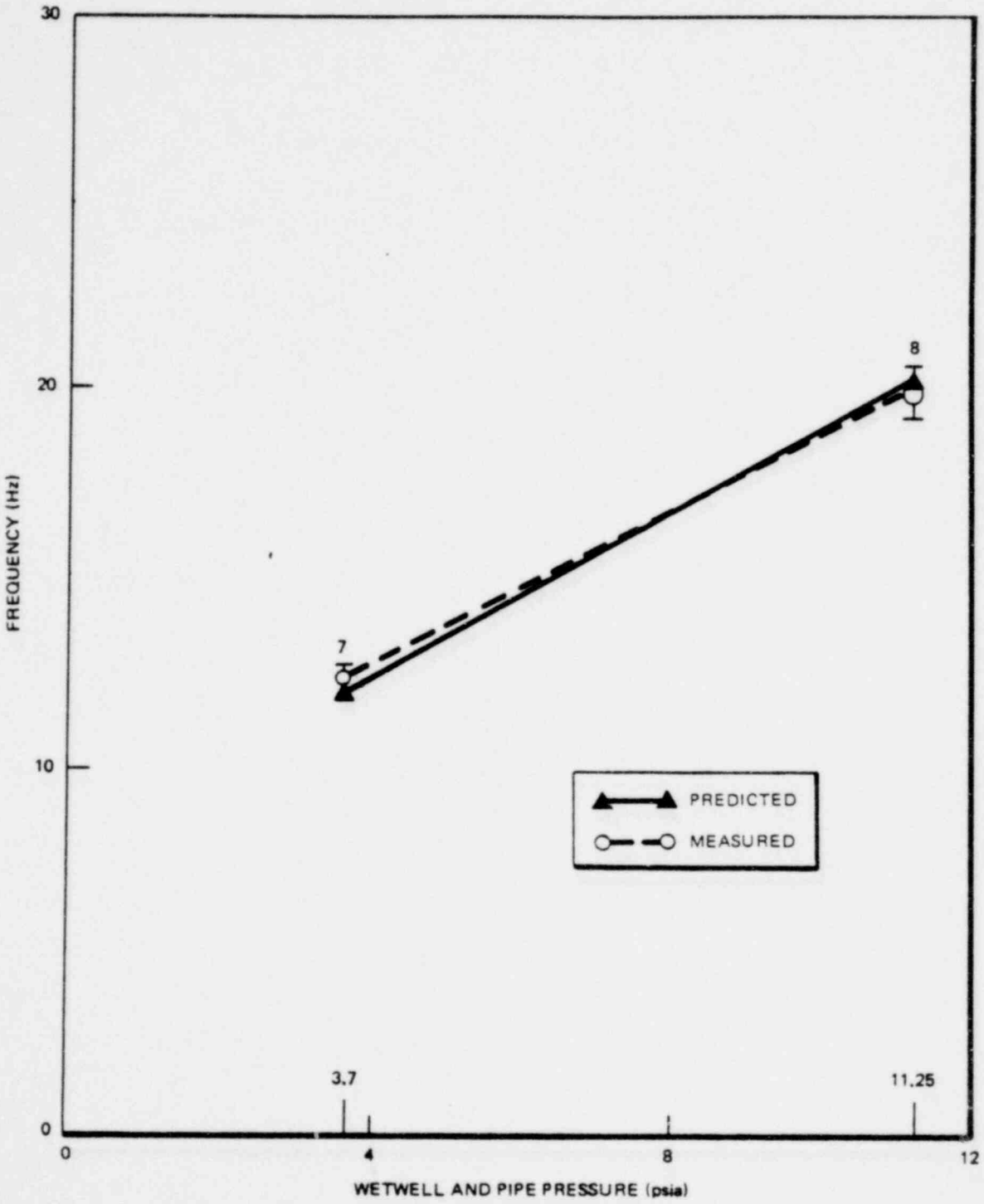

Figure 3-23. Effect of Wetwell and Pipe Pressures on Frequency for Pipe Air Length of 108 Ft

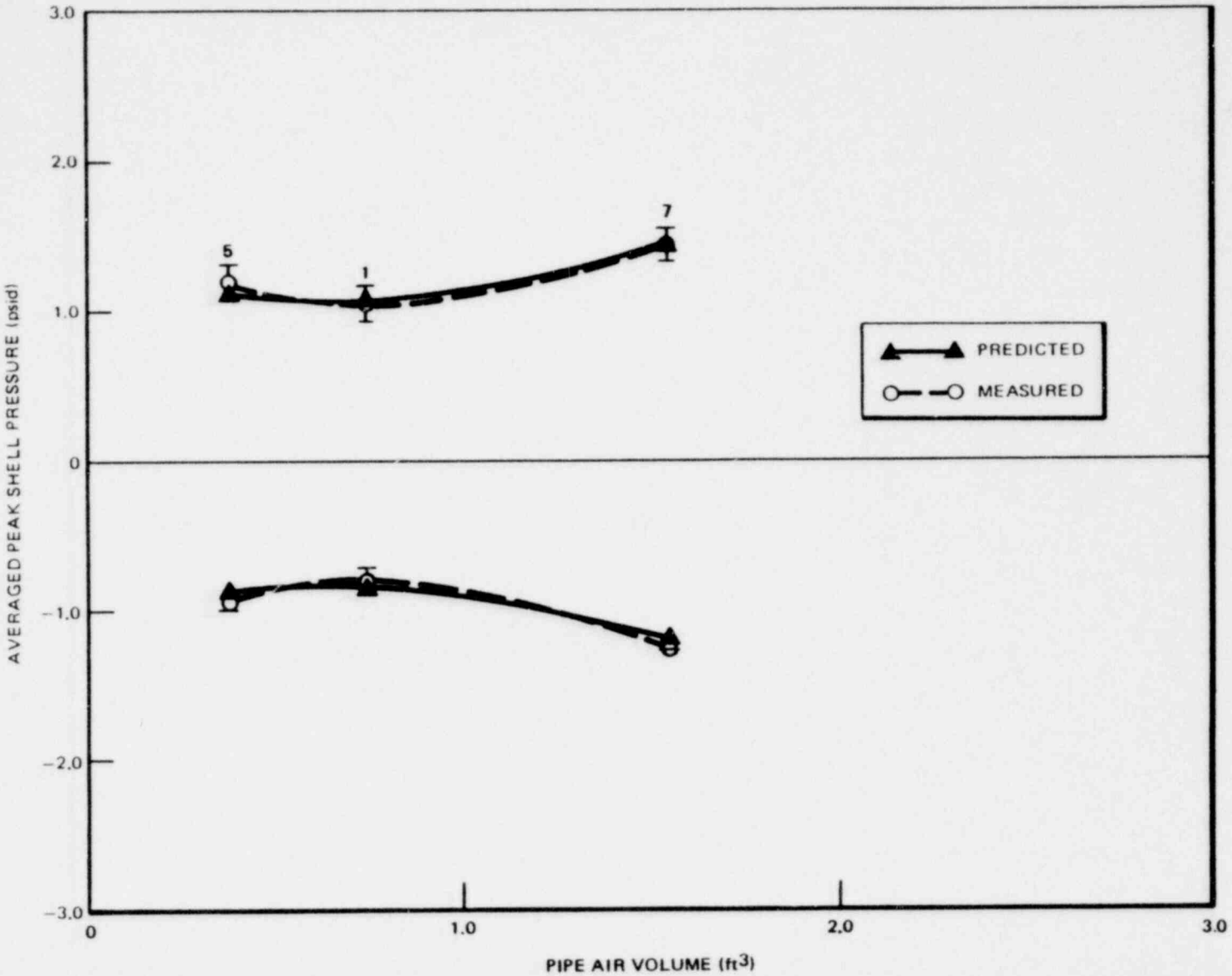

Figure 3-24. Effect of Pipe Air Volume on Maximum Shell Pressure for Initial Pipe and Wetwell Pressure of 3.7 psia

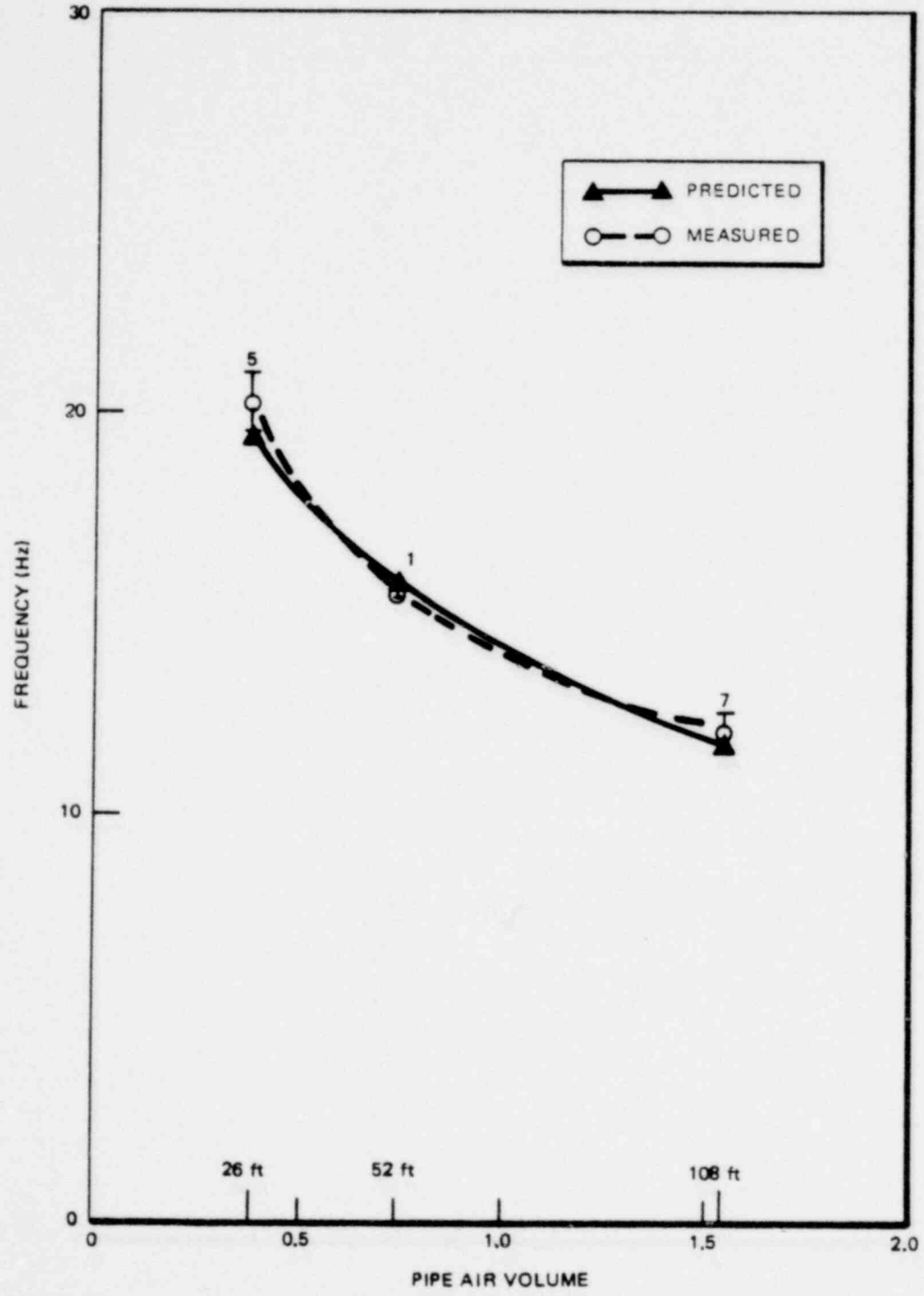

Figure 3-25. Effect of Pipe Air Volume on Frequency for Initial Pipe and Wetwell Pressure of 3.7 psia

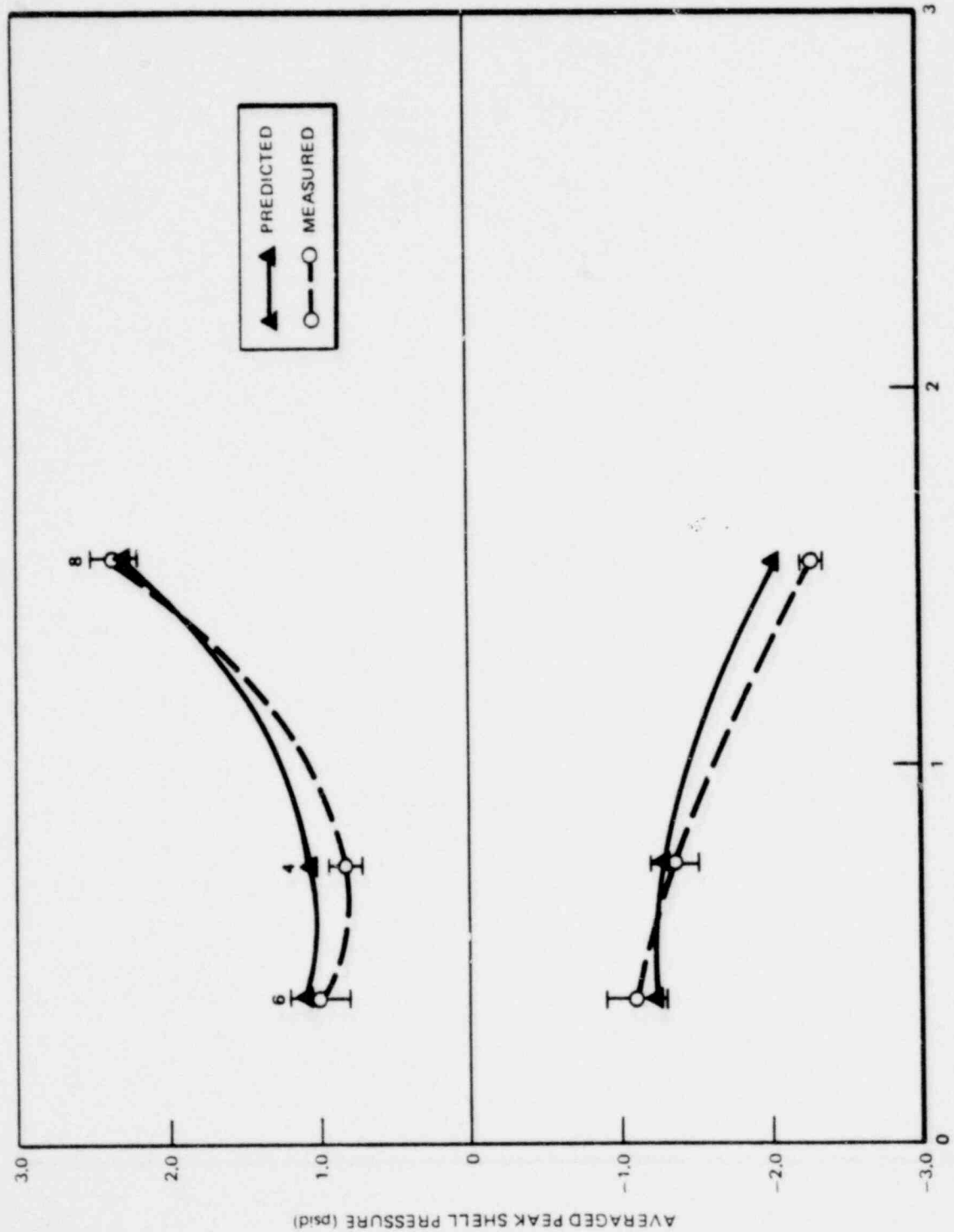

Figure 3-26. Effect of Pipe Air Volume on Maximum Shell Pressure for Initial Pipe and Wetwell Pressures of 11.25 psia

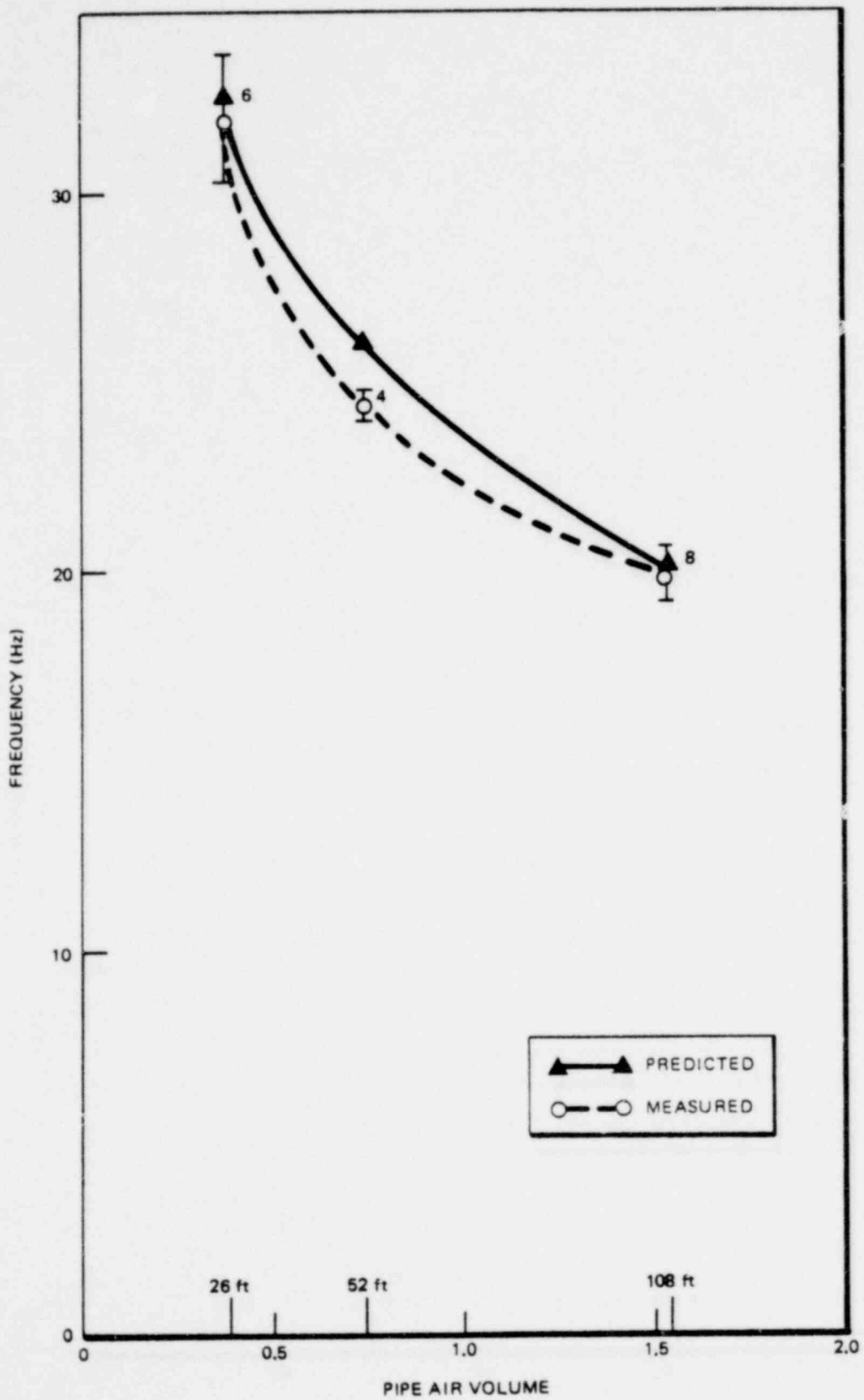

Figure 3-27. Effect of Pipe Air Volume on Frequency for Initial Pipe and Wetwell Pressures of 11.25 psia

1764 250

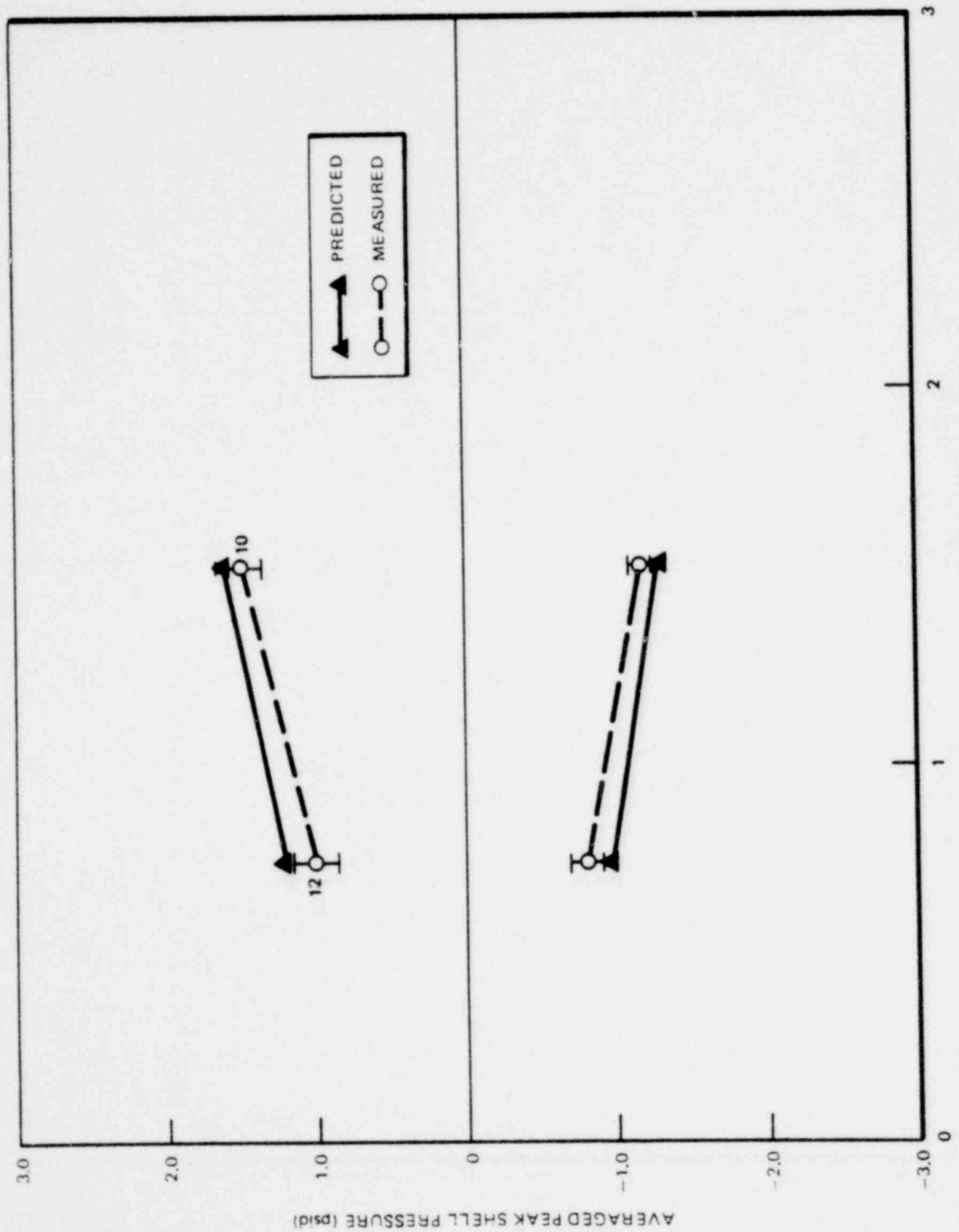

Figure 3-28. Effect of Pipe Air Volume on Maximum Shell Pressures for 2-1/2-inch Pipe Diameter

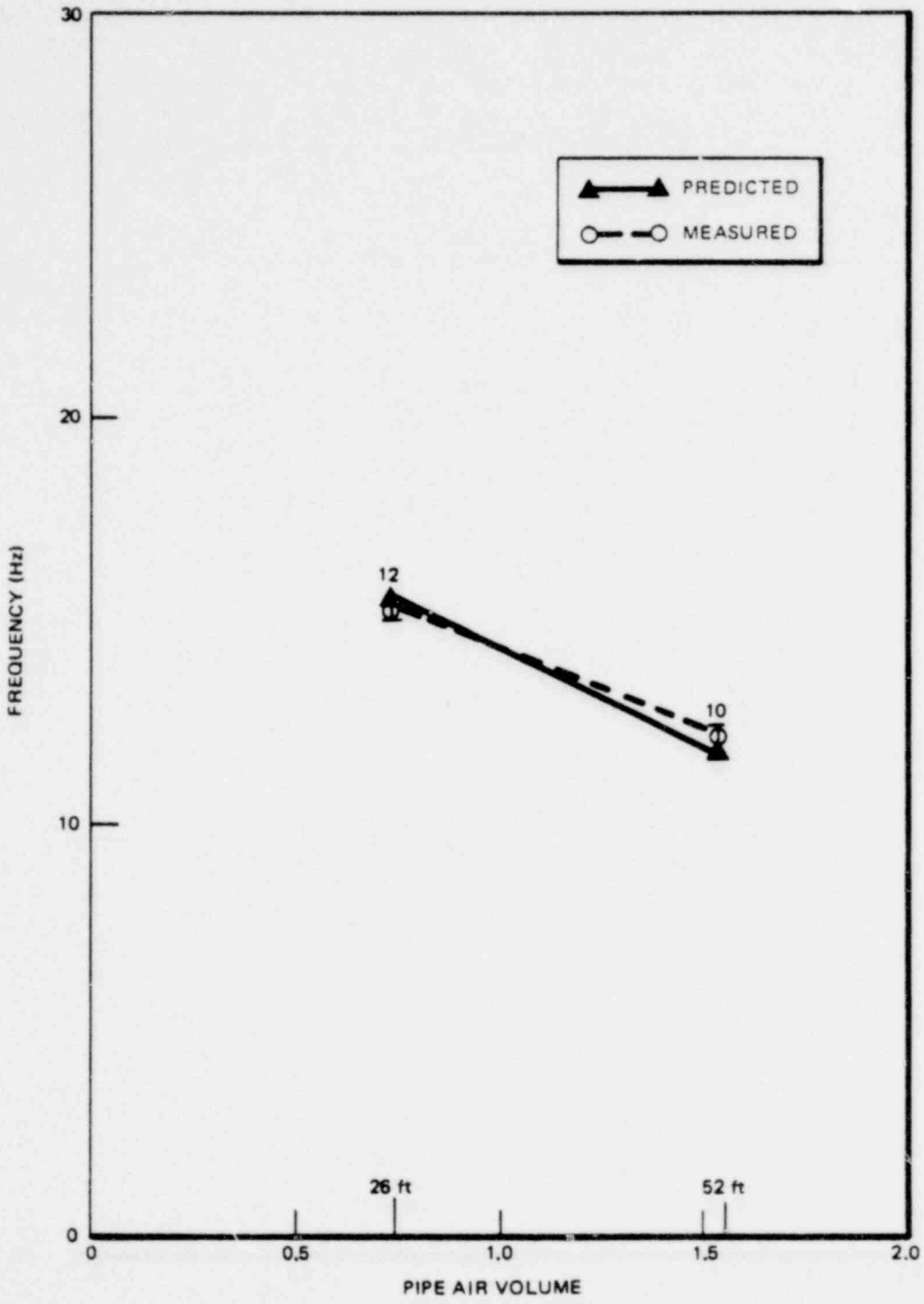

Figure 3-29. Effect of Pipe Air Volume on Frequency for 2-1/2-Inch Pipe Diameter

1764 252

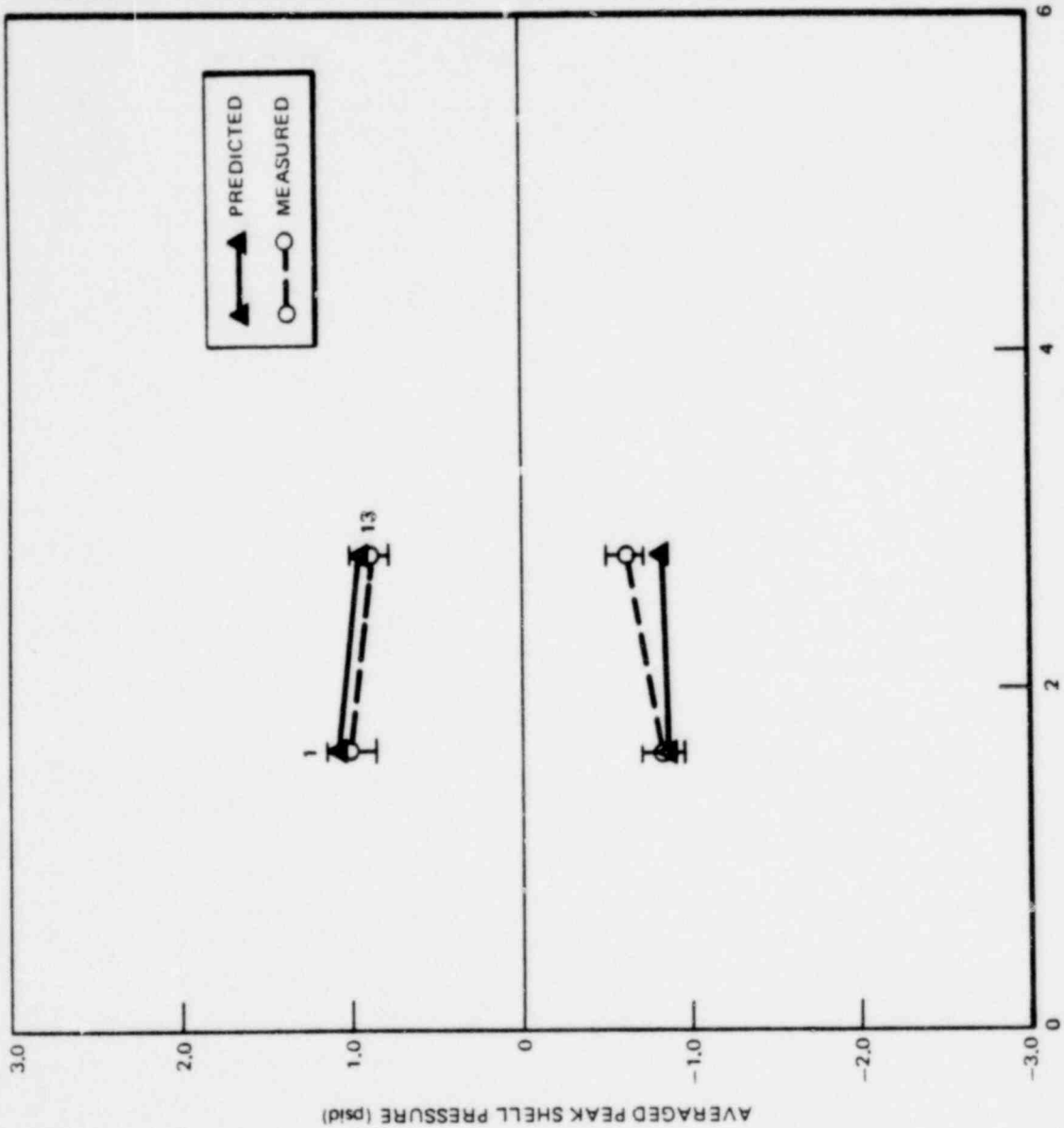

Figure 3-30. Effect of Submergence on Maximum Shell Pressures

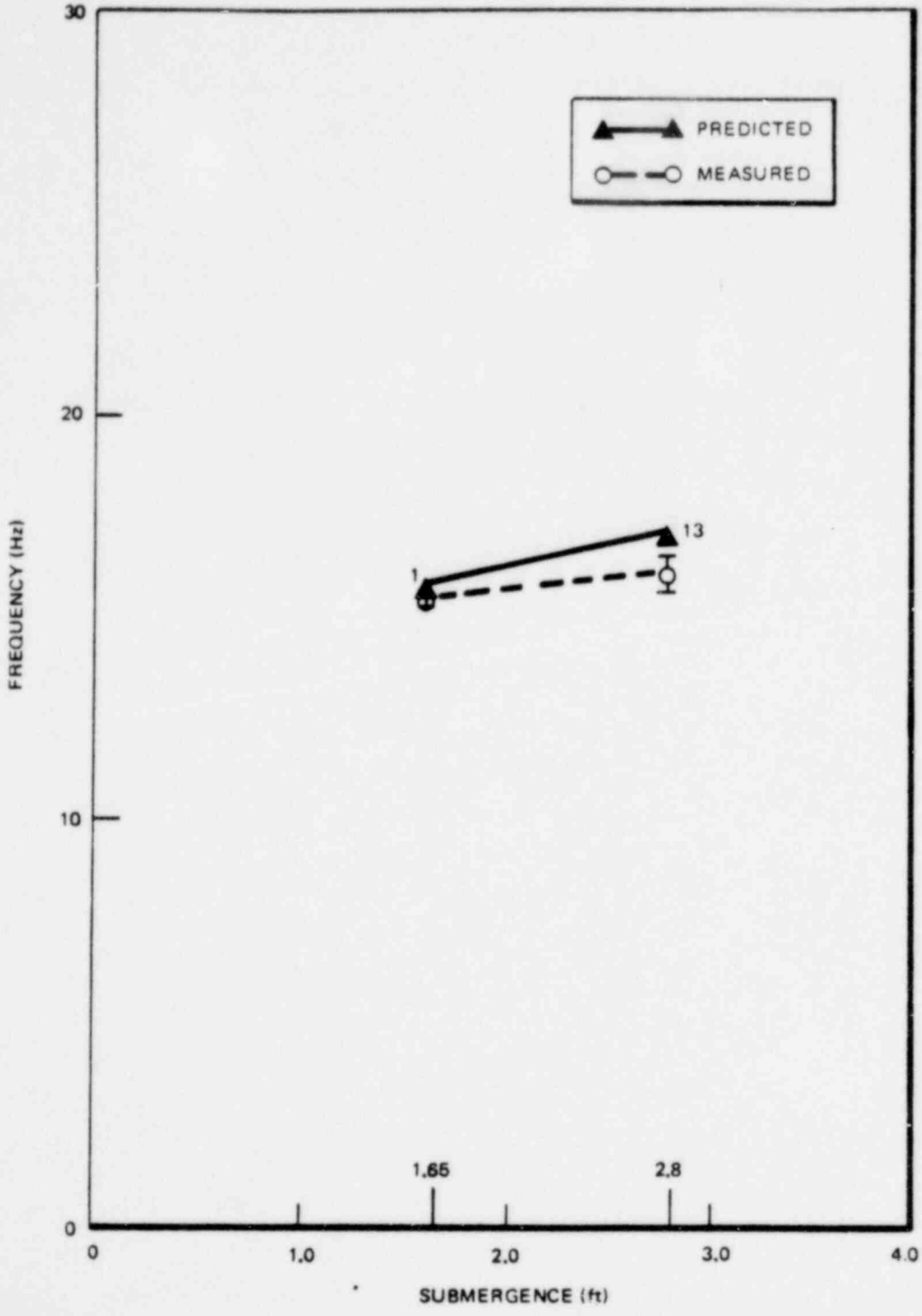

Figure 3-31. Effect of Submergence on Frequency

1764 254

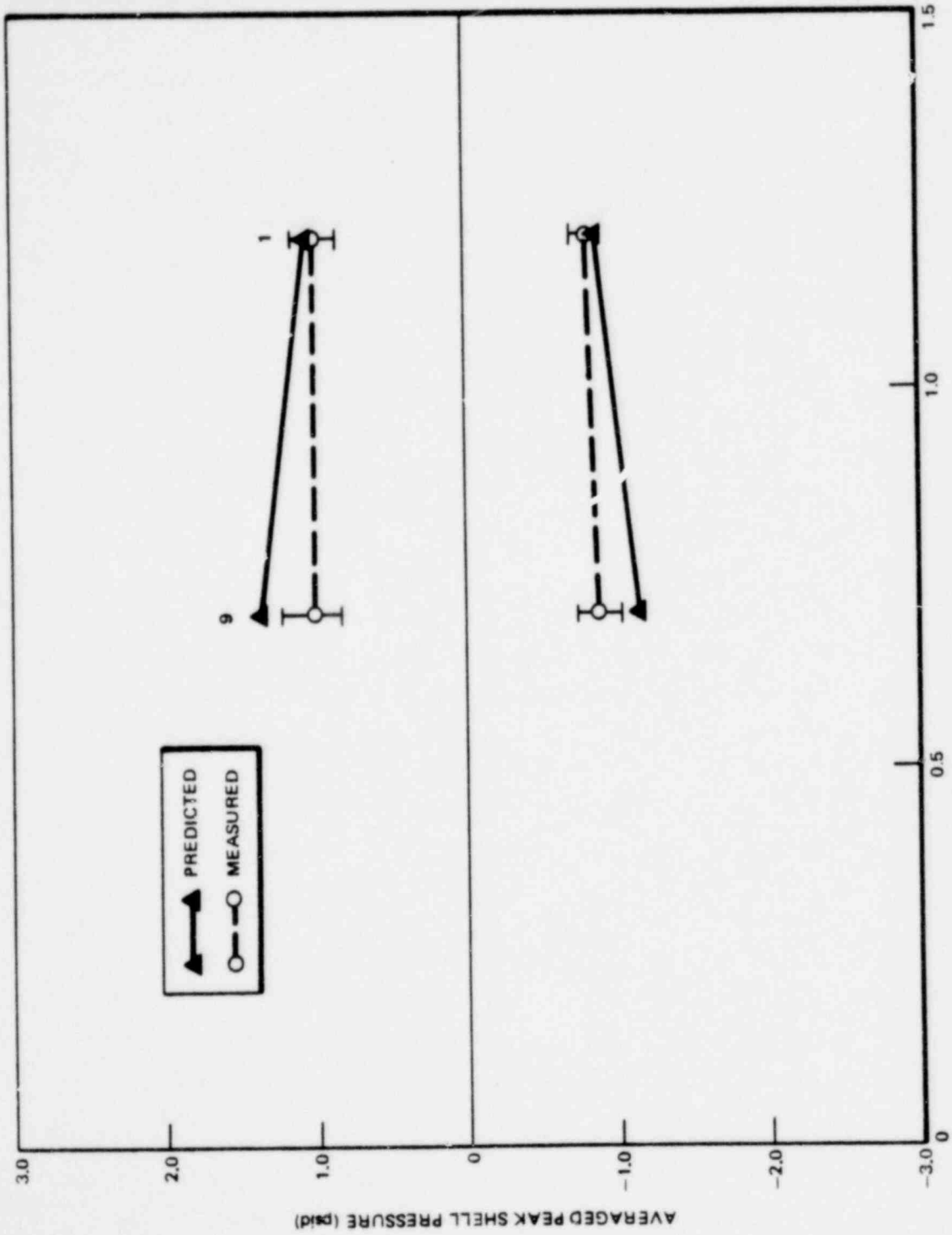

Figure 3-32. Effect of Distance from Floor on Maximum Shell Pressure

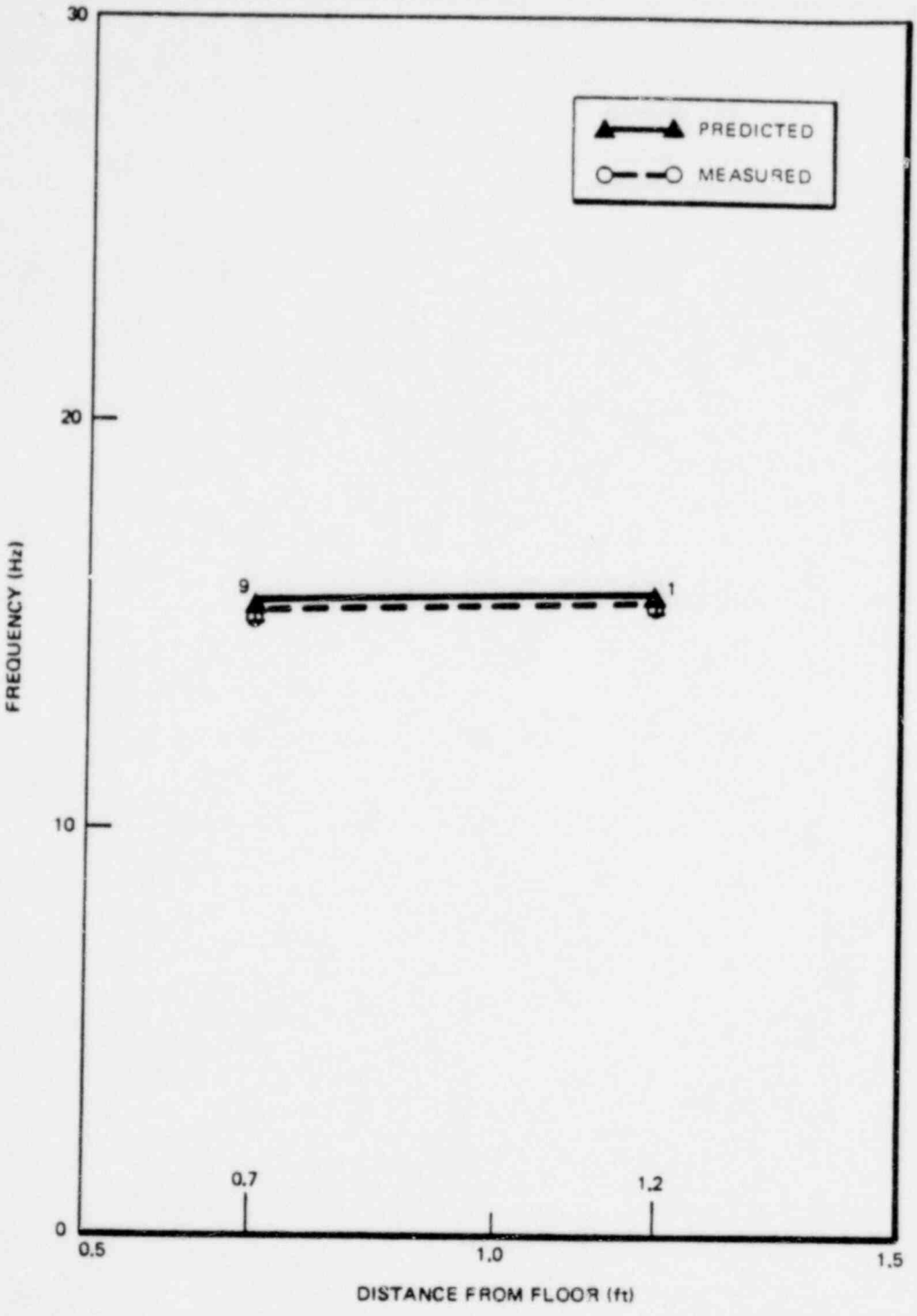

Figure 3-33. Effect of Distance from Floor on Frequency

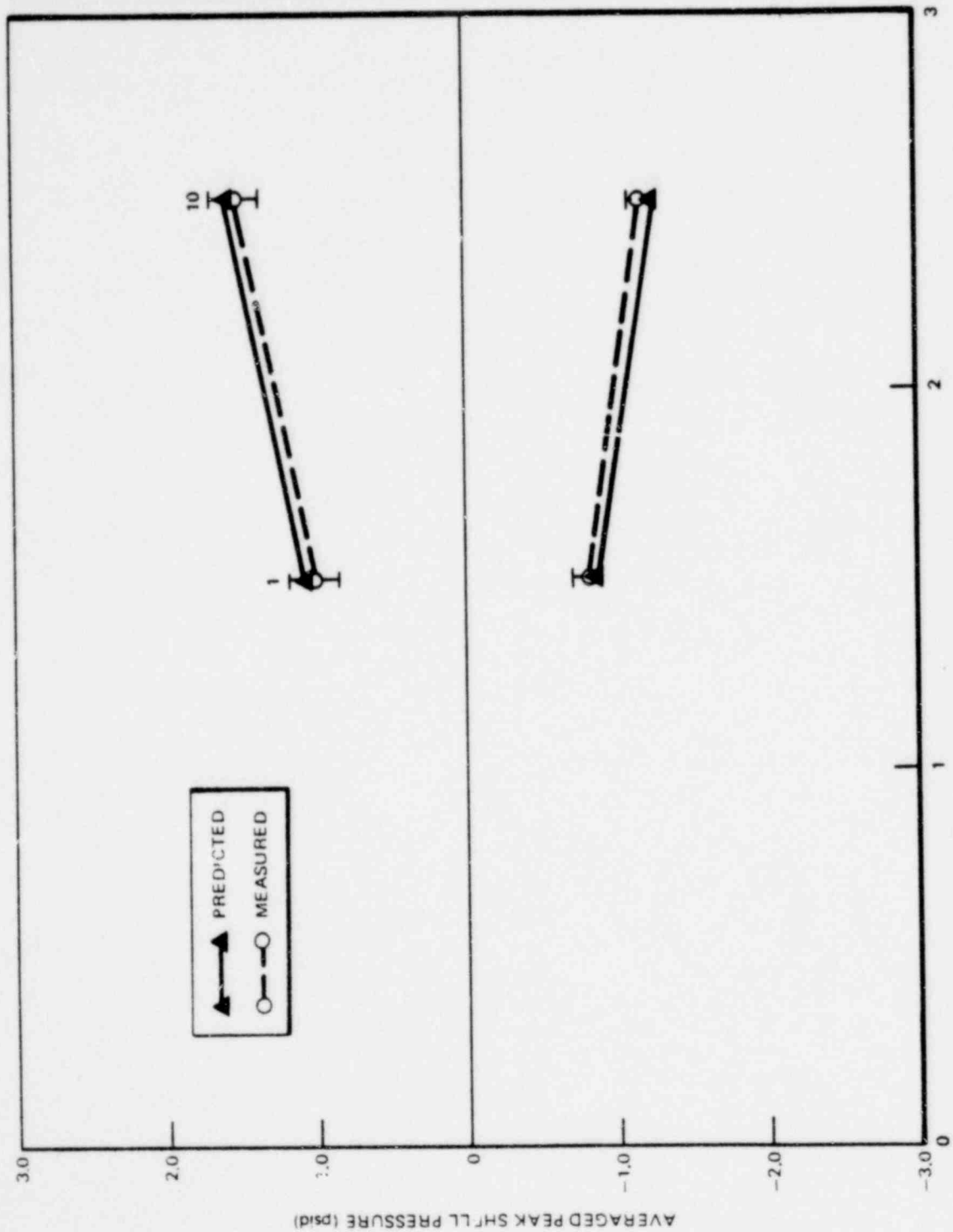

Figure 3-34. Effect of Pipe Diameter on Maximum Shell Pressure for Pipe Air Length of 52 Ft

1764 257

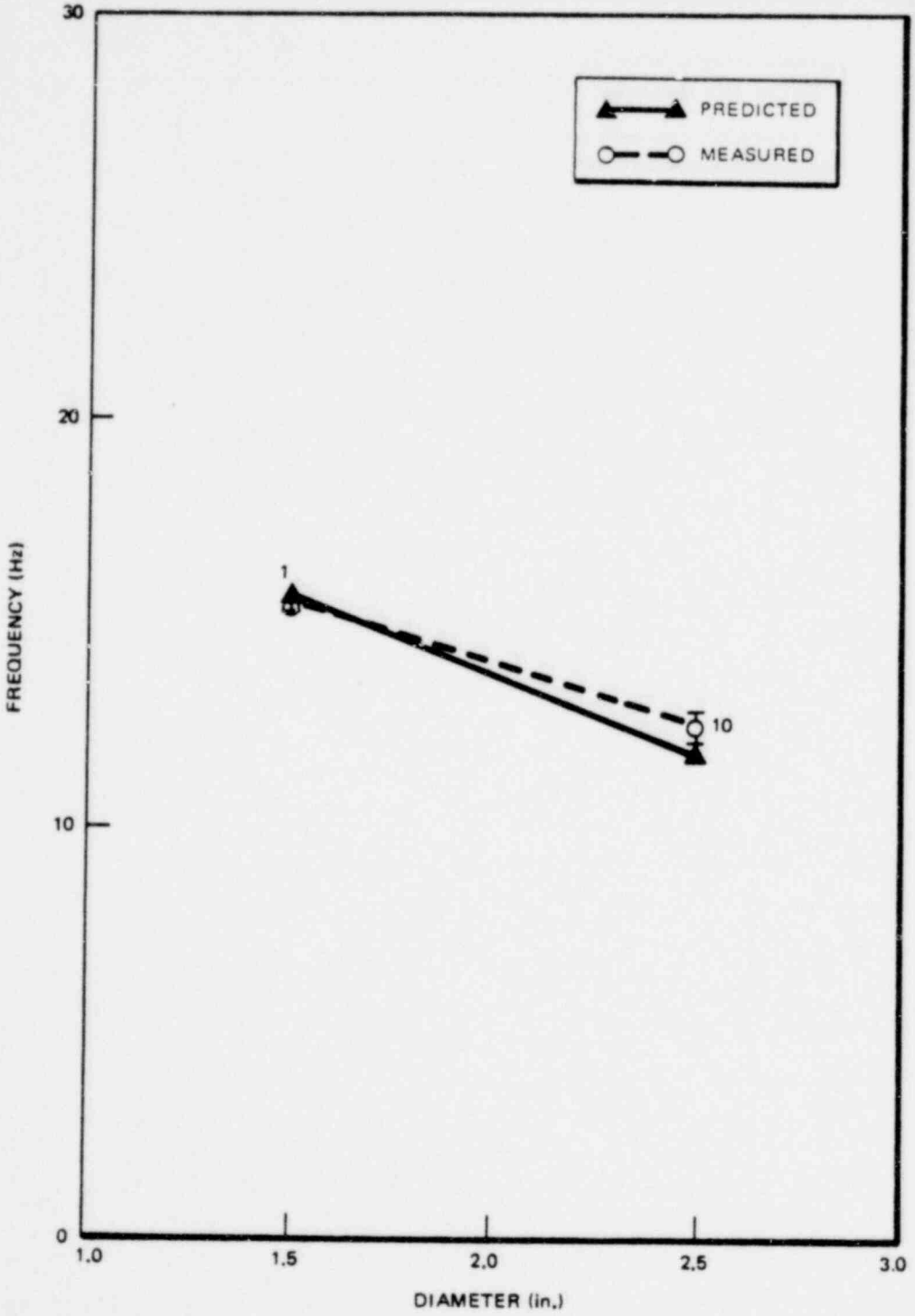

Figure 3-35. Effect of Pipe Diameter on Frequency for Pipe Air Length of 52 Ft

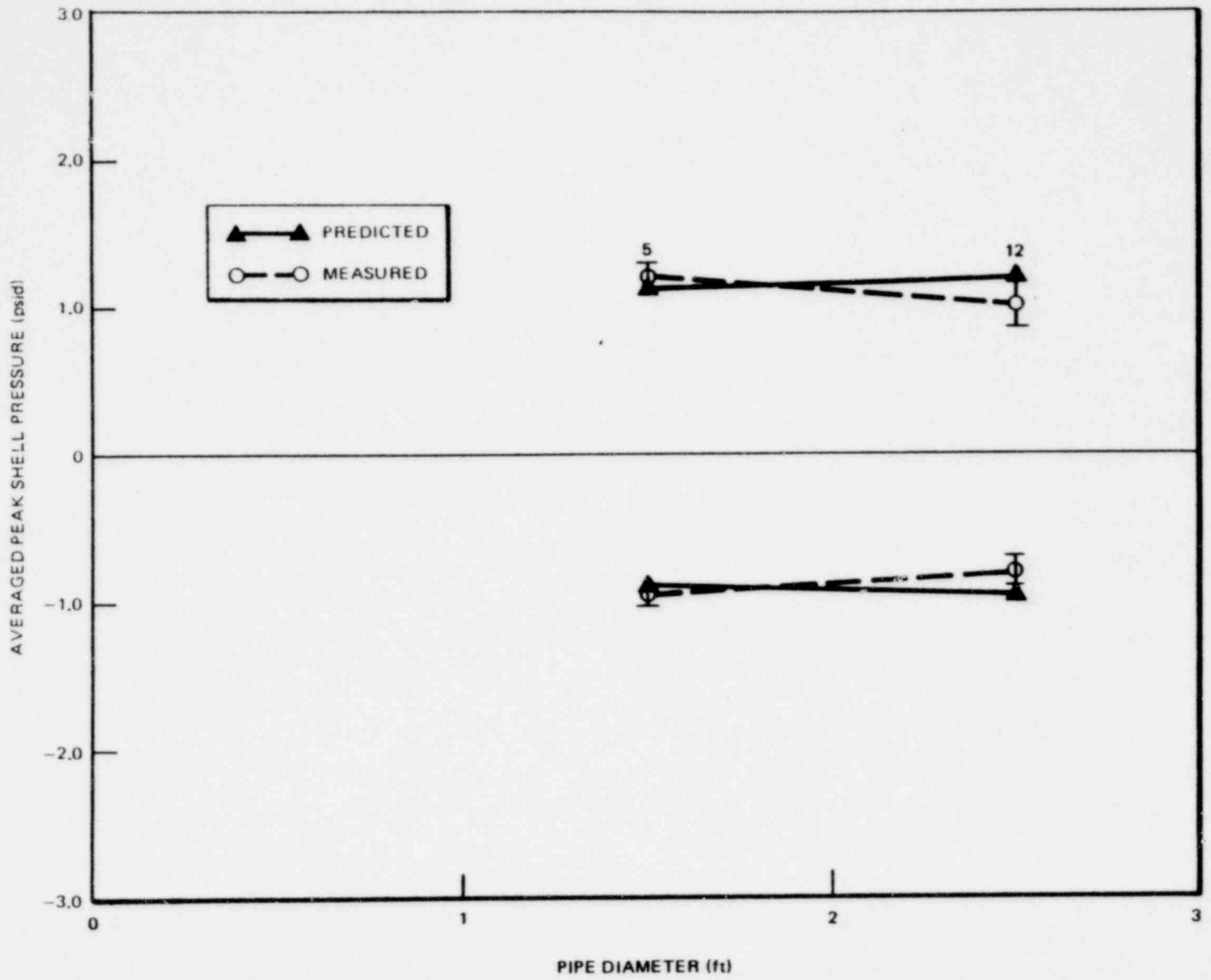

Figure 3-36. Effect of Pipe Diameter on Maximum Shell Pressure for Pipe Air Length of 26 Ft

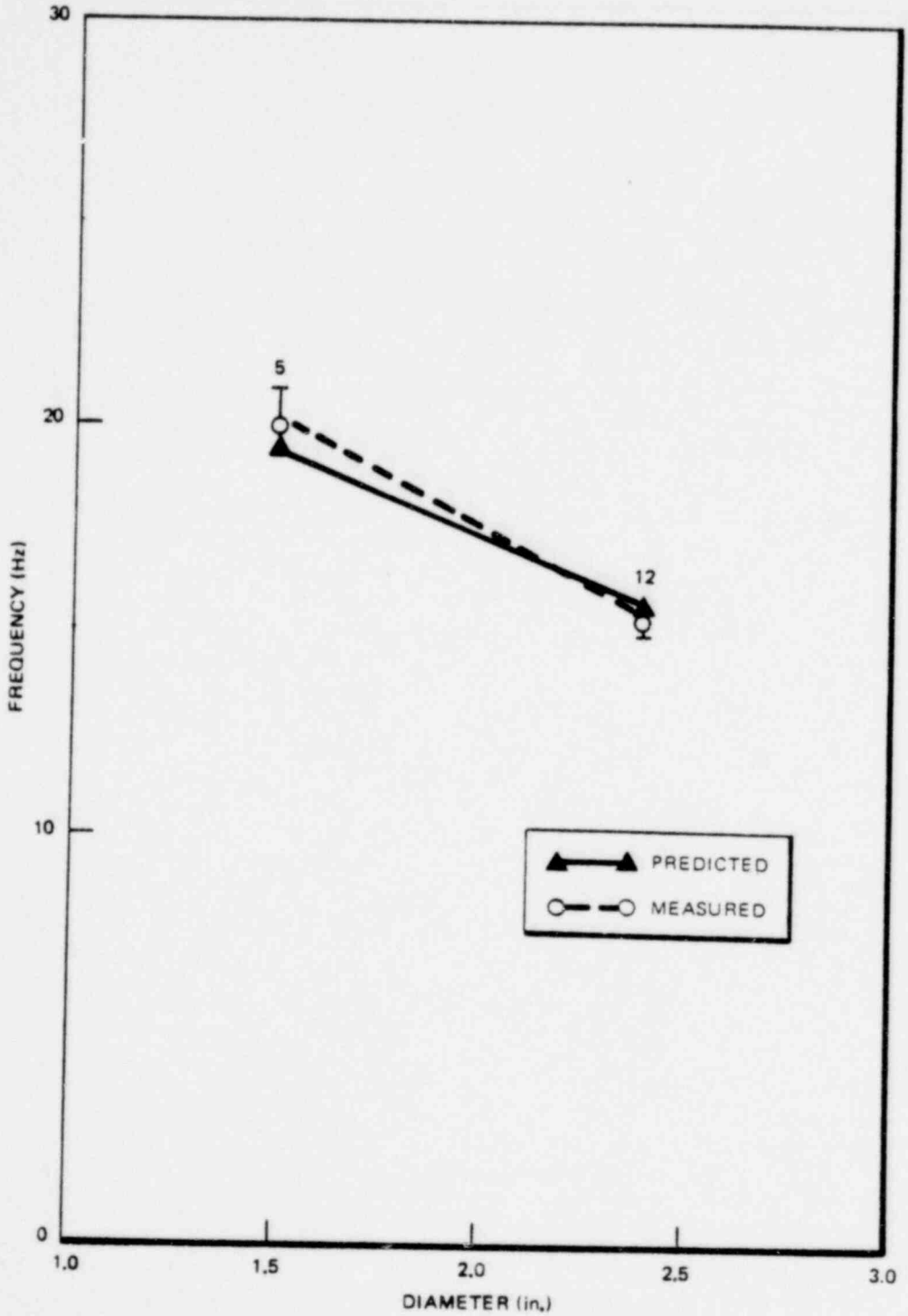

Figure 3-37. Effect of Pipe Diameter on Frequency for Pipe Air Length of 26 Ft

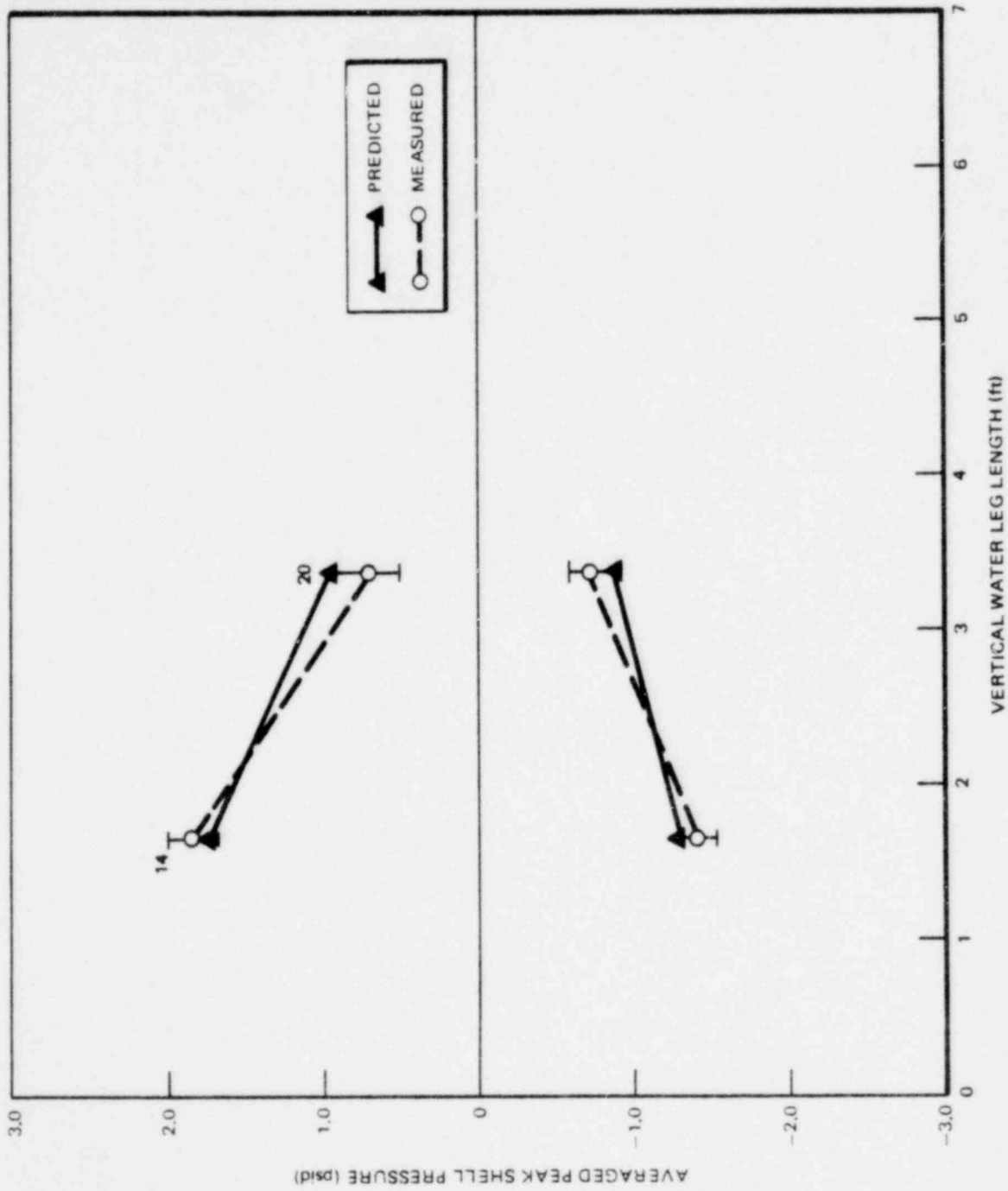

Figure 3-38. Effect of Vertical Water Leg Length on Maximum Shell Pressure

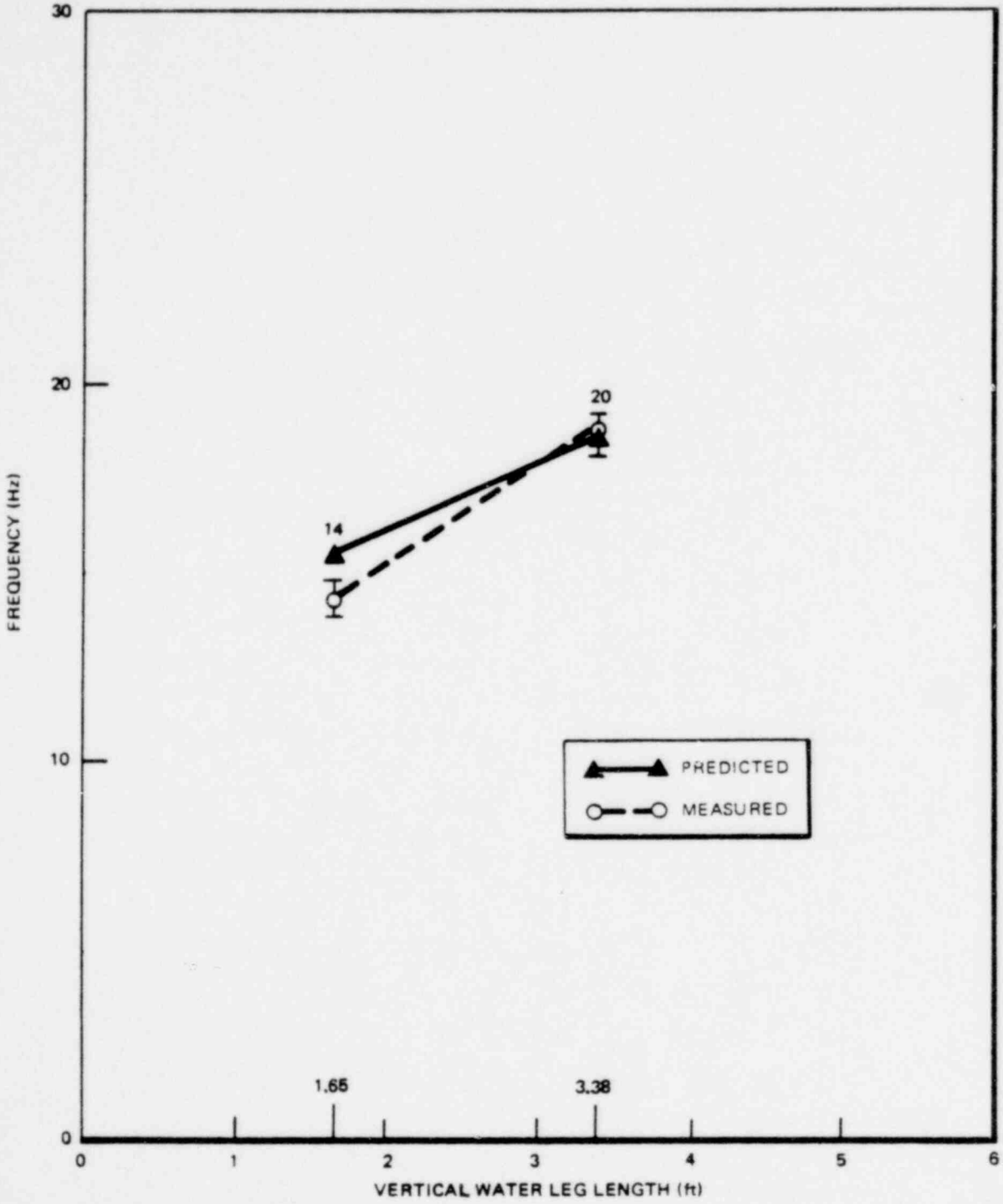

Figure 3-39. Effect of Vertical Water Leg Length on Frequency

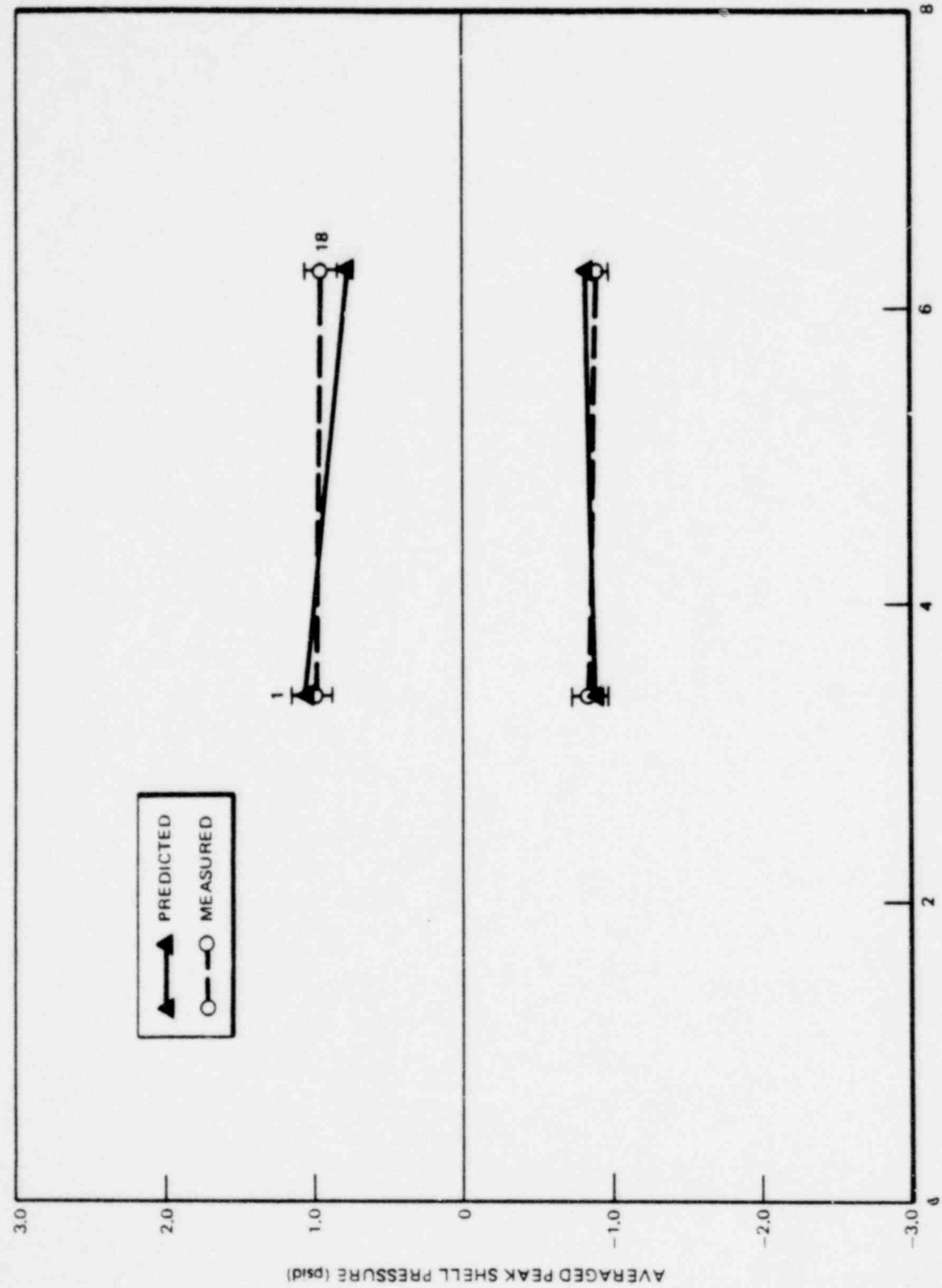

Figure 3-40. Effect of Inclined Water Leg Length on Maximum Shell Pressure

1764 263

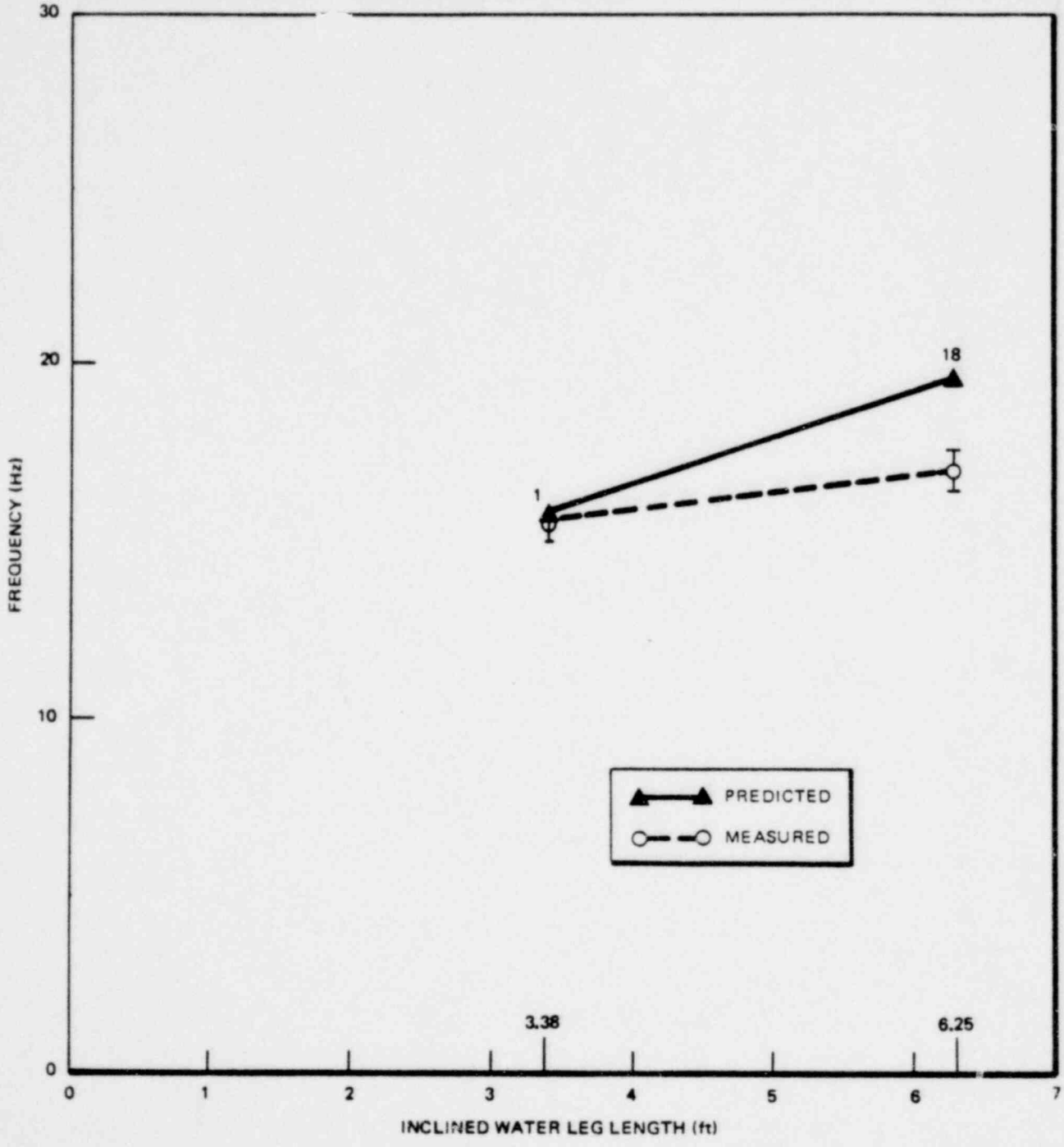

Figure 3-41. Effect of Inclined Water Leg Length on Frequency

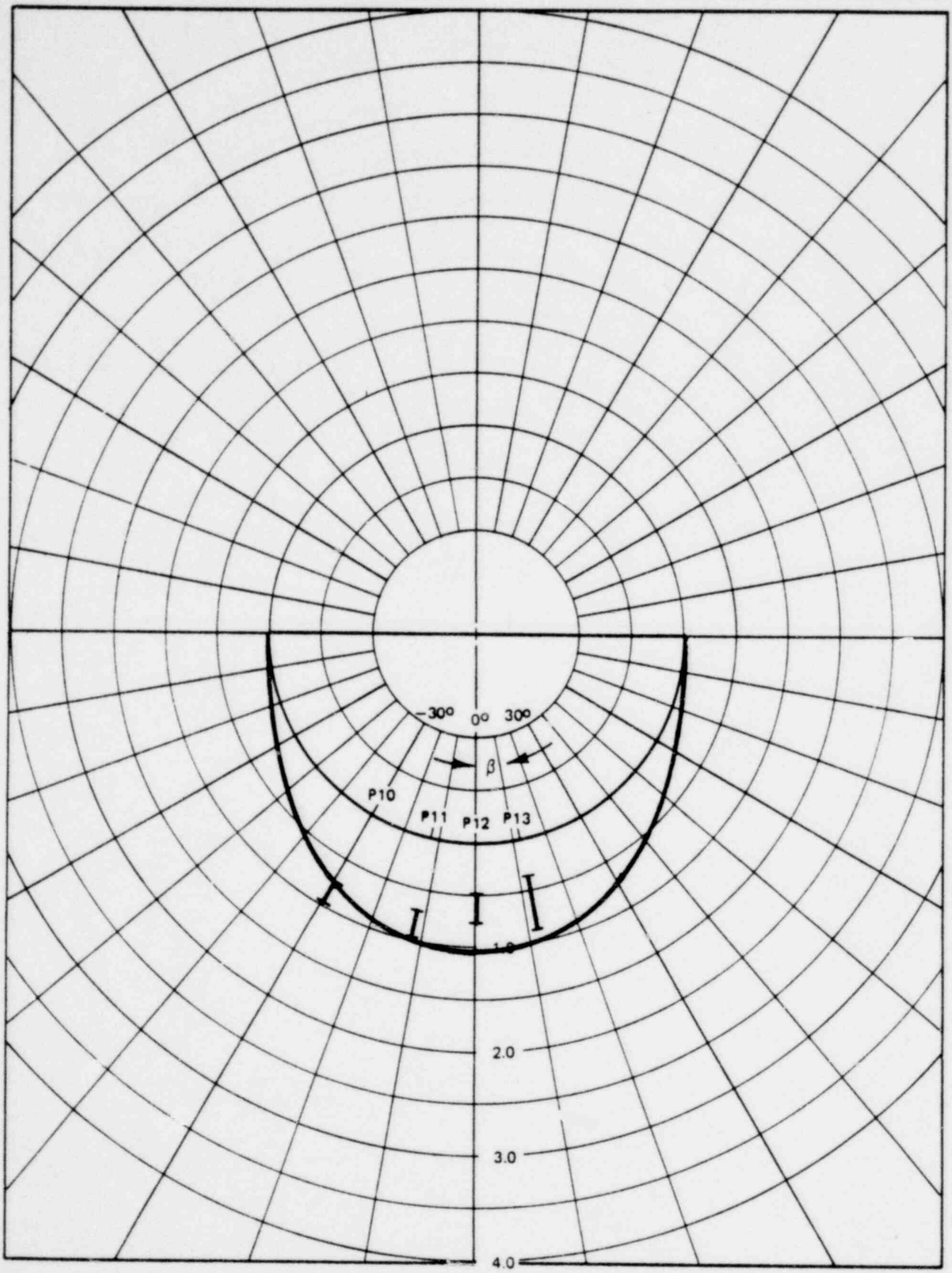

Figure 3-42. Peak Positive Pressure Distribution for 1/4 Scale Test Case 1 @ α = 0.0748

1764 265

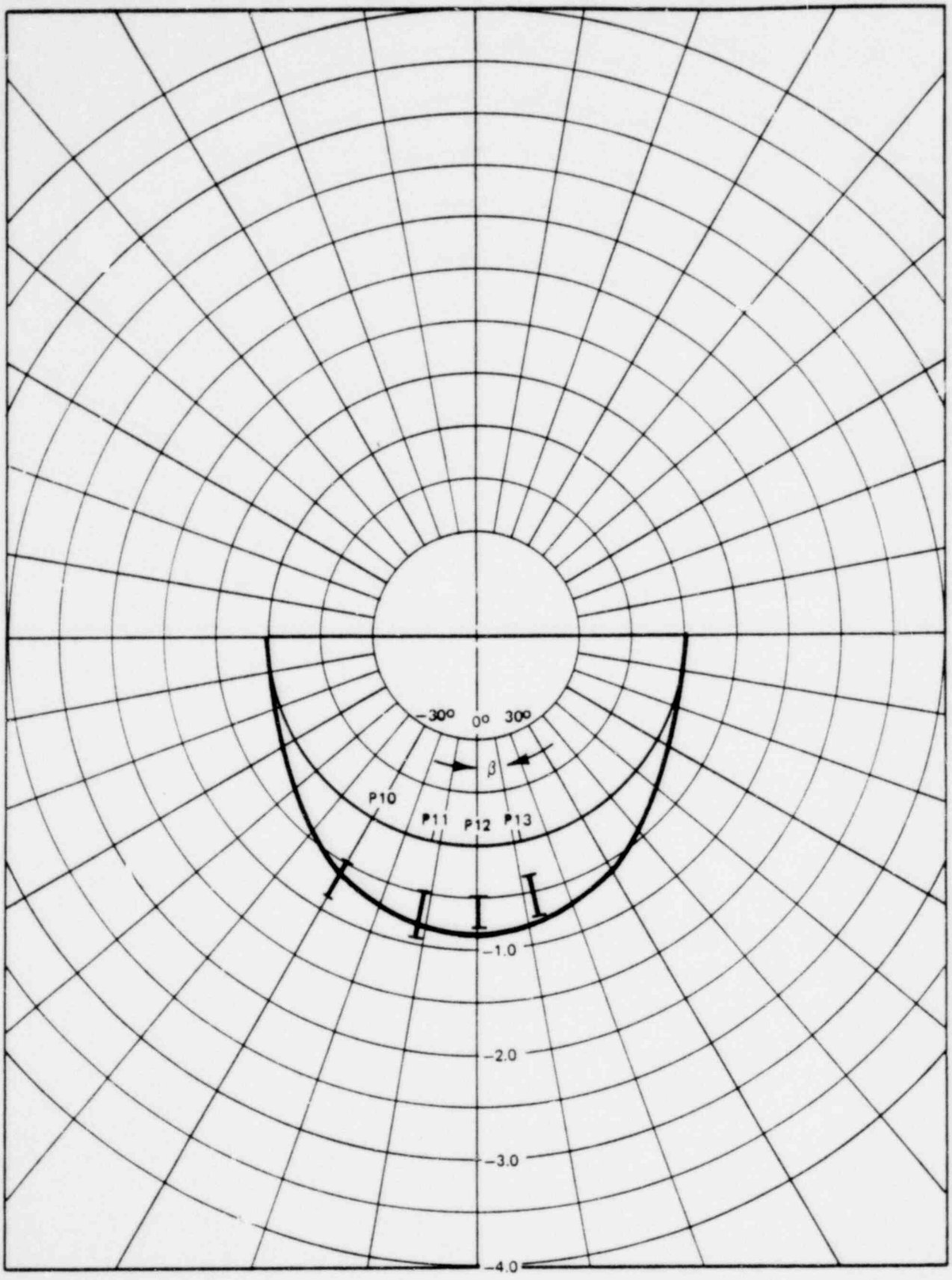

Figure 3-43. Peak Negative Pressure Distribution for 1/4 Scale Test Case 1 @ α = 0.0748

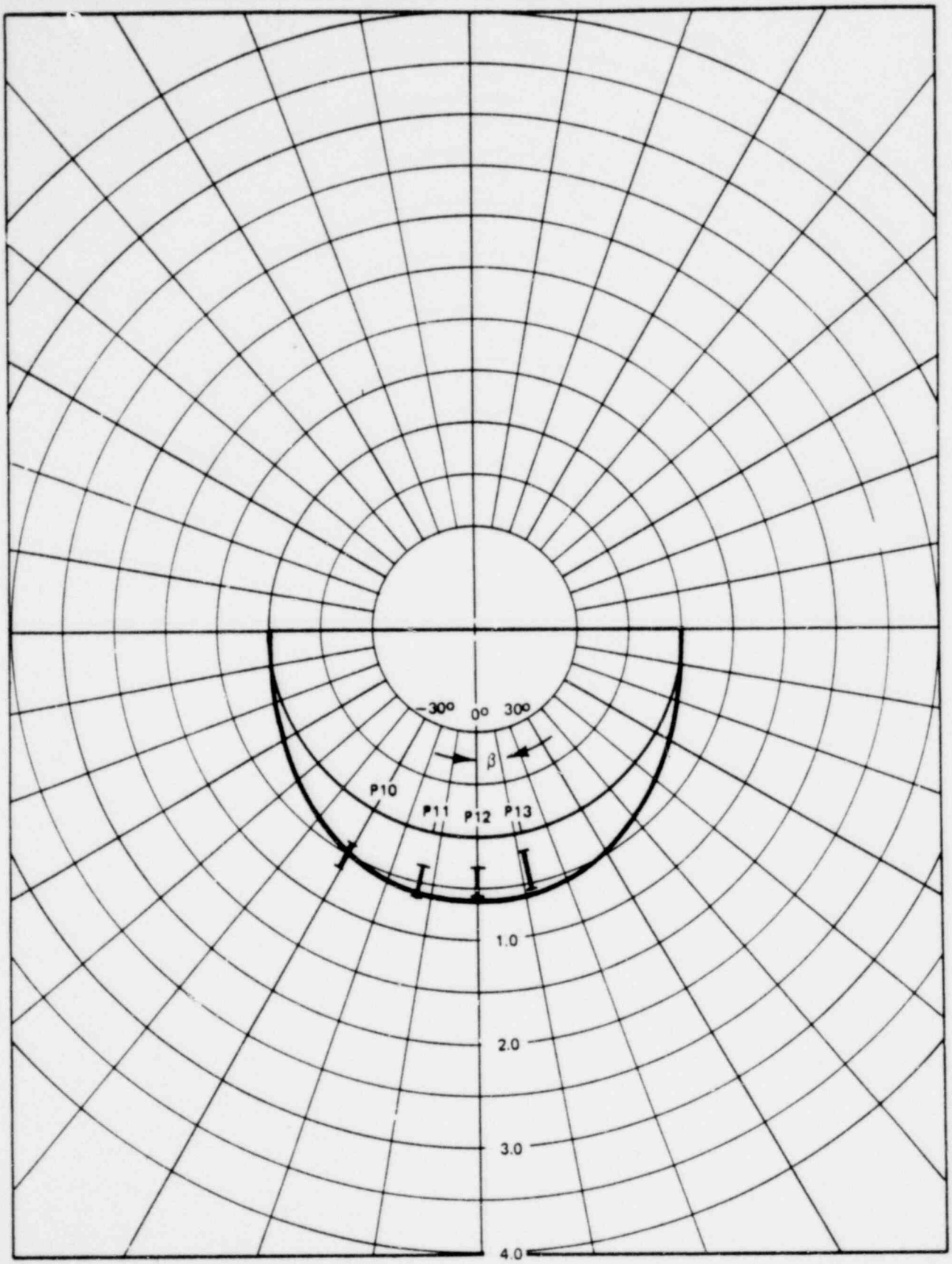

Figure 3-44. Peak Positive Pressure Distribution for 1/4 Scale Test Case 2 @ α = 0.0748

1764 267

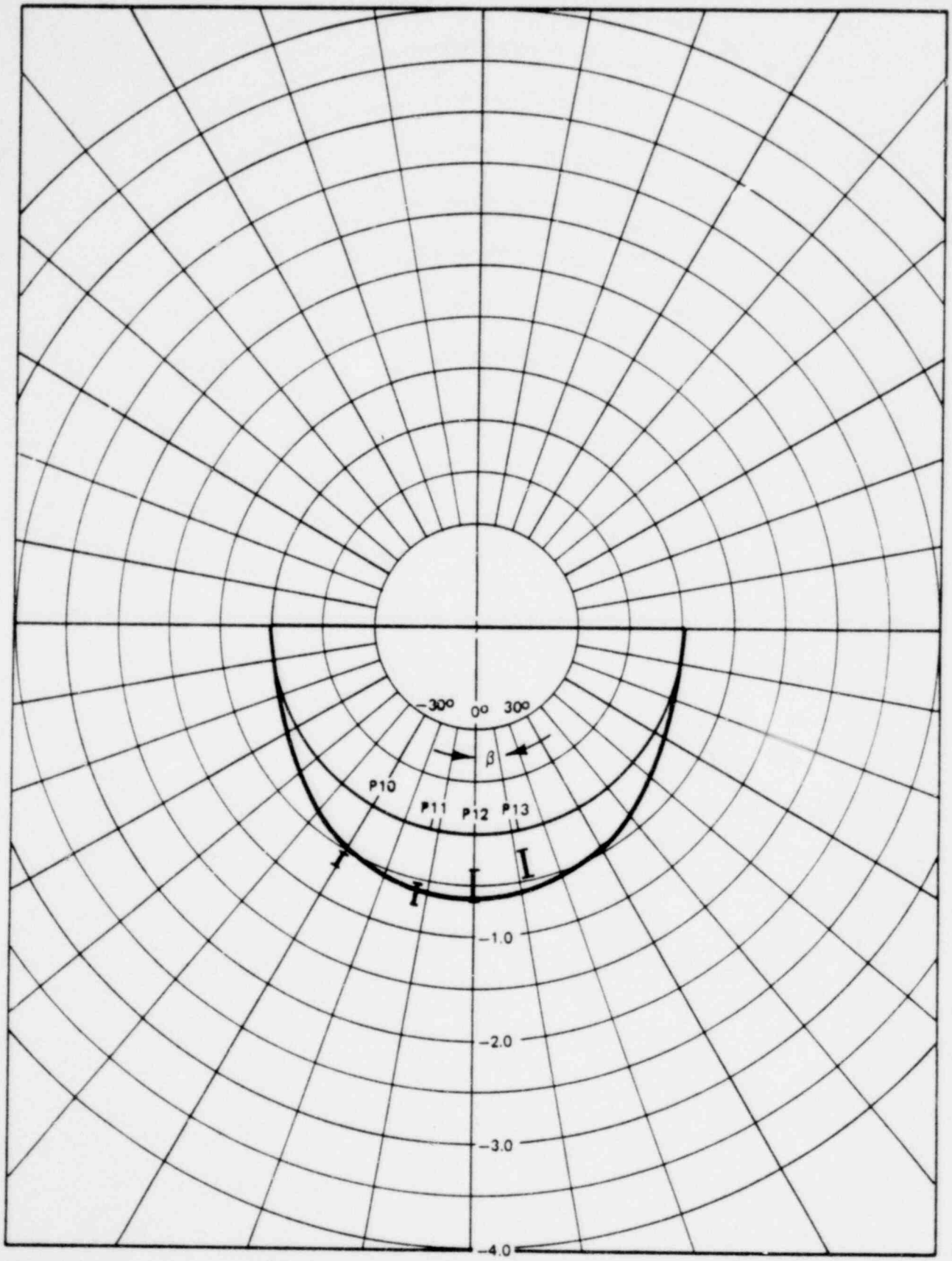

Figure 3-45. Peak Negative Pressure Distribution for 1/4 Scale Test Case 2 @ α = 0.0748

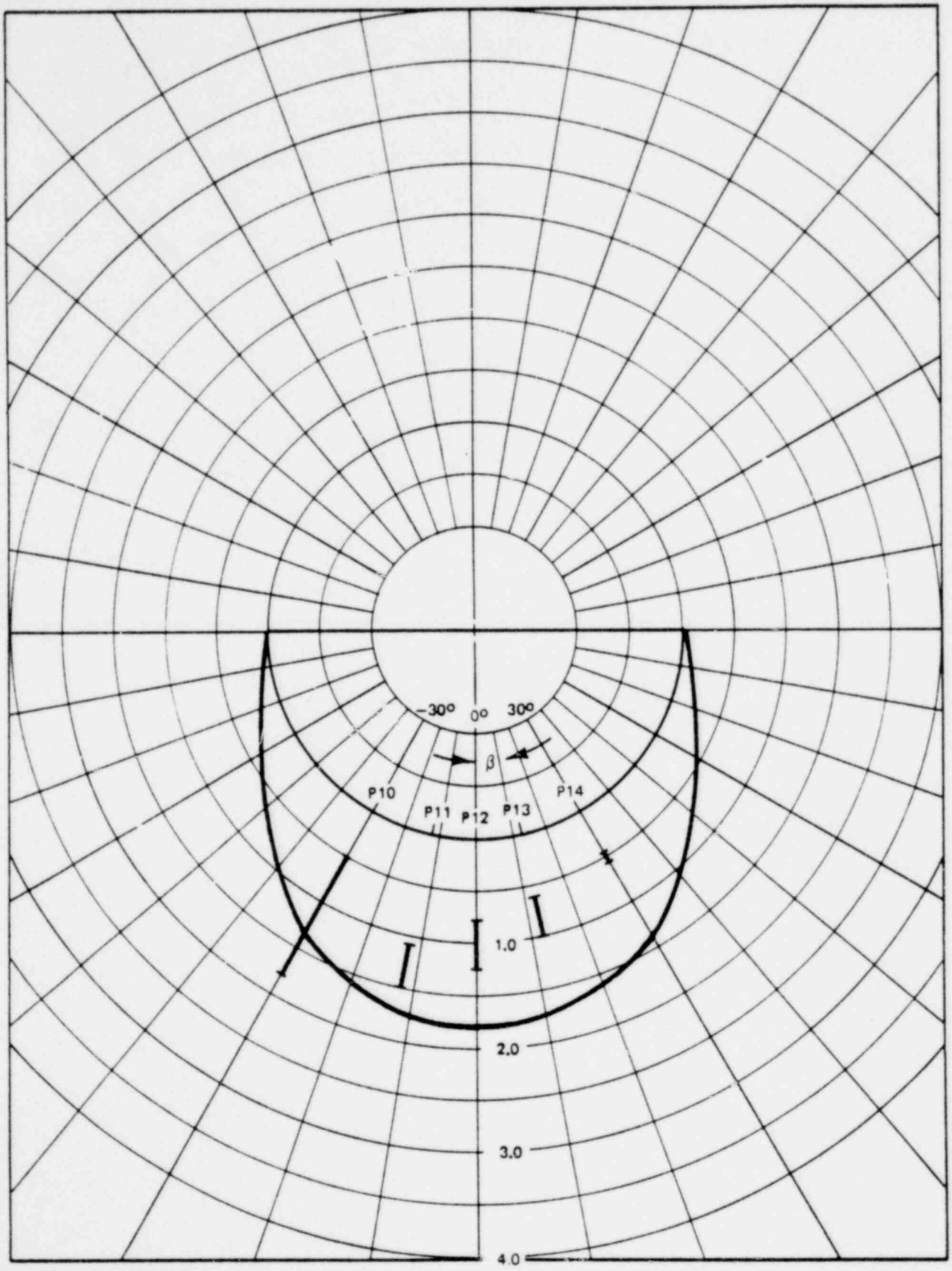

Figure 3-46. Peak Positive Pressure Distribution for 1/4 Scale Test Case 3 @ α = 0.0748

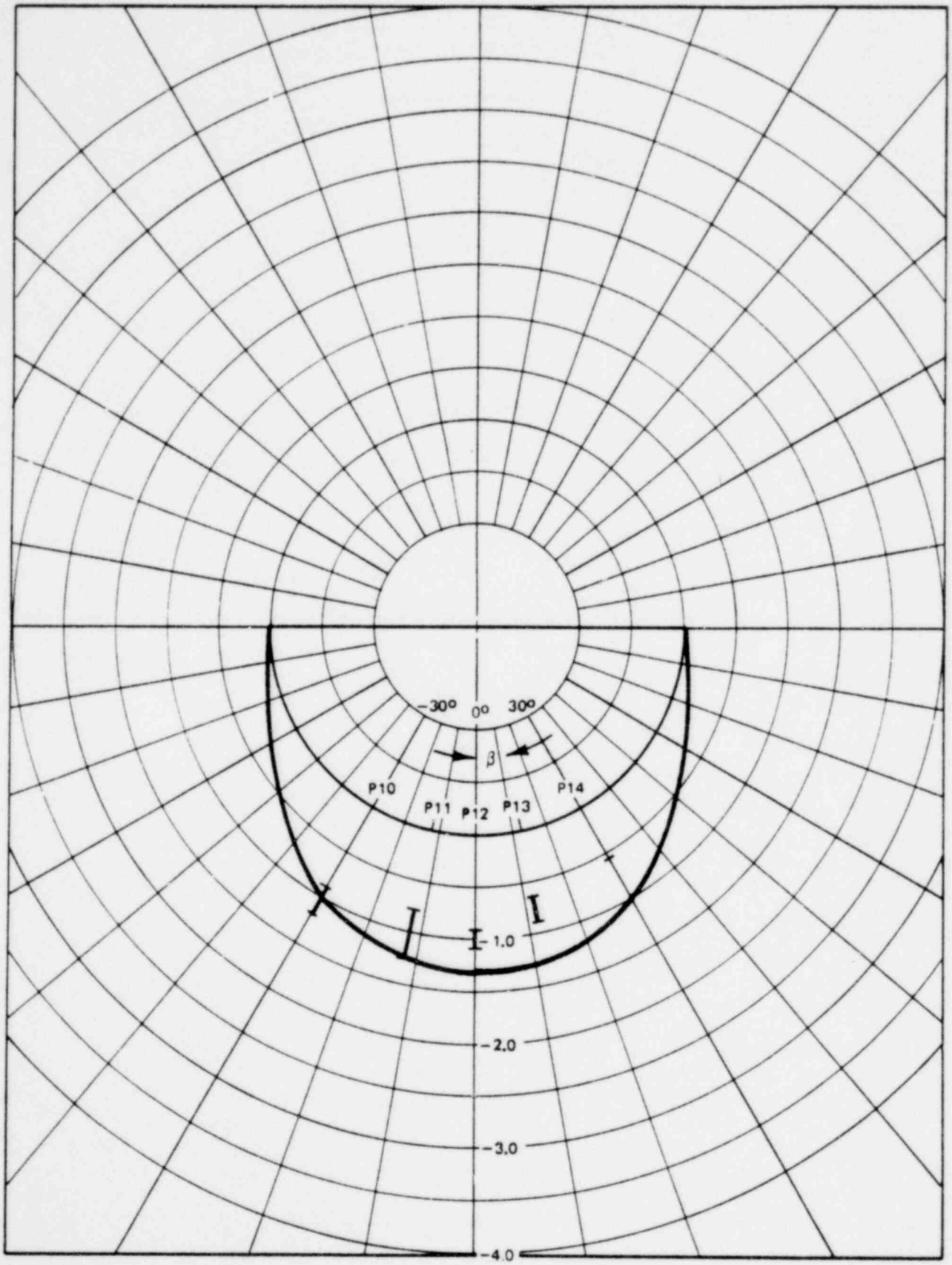

Figure 3-47. Peak Negative Pressure Distribution for 1/4 Scale Test Case 3 @ α= 0.0748

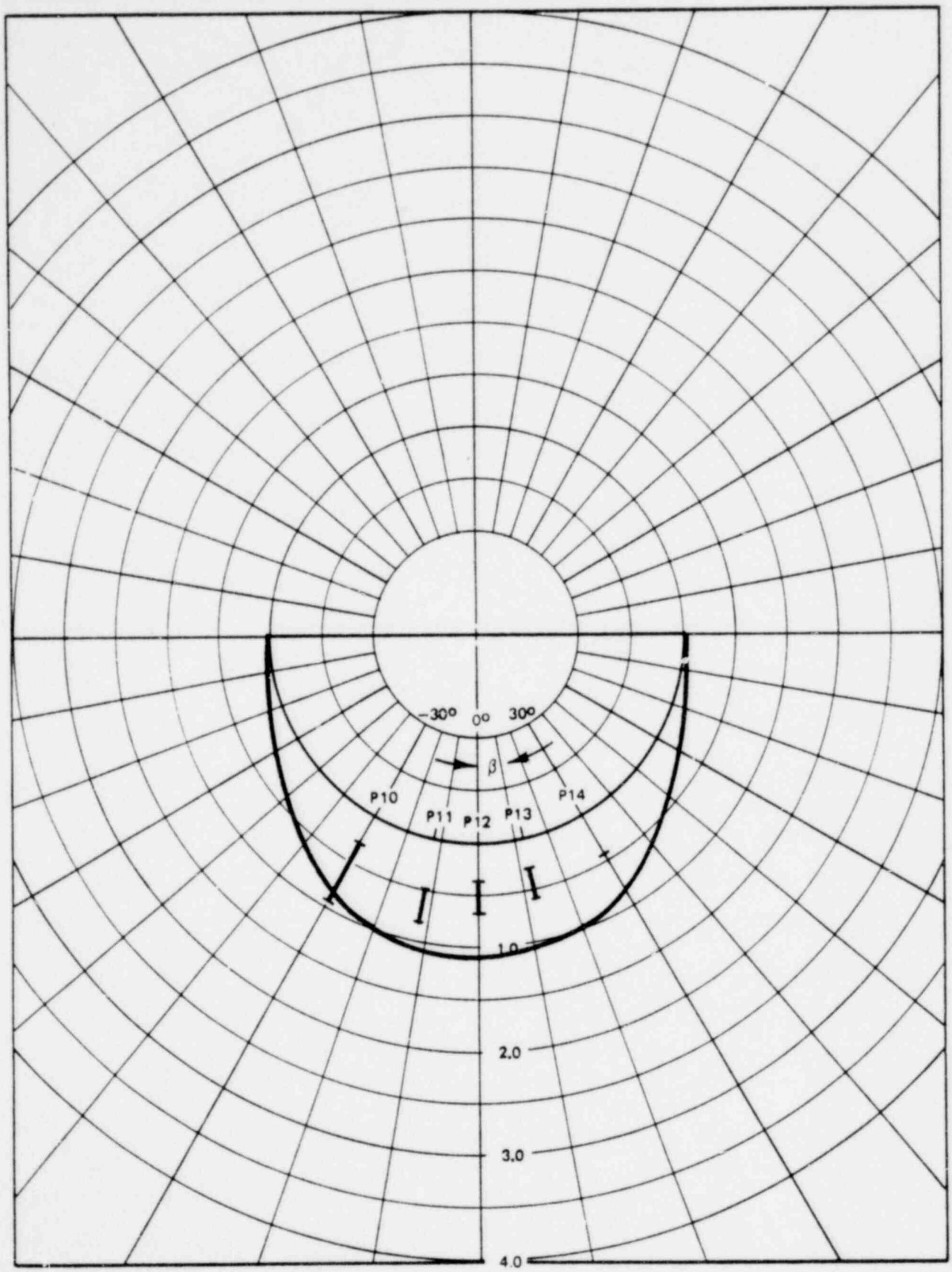

Figure 3-48. Peak Positive Pressure Distribution for 1/4 Scale Test Case 4 @ α = 0.0748

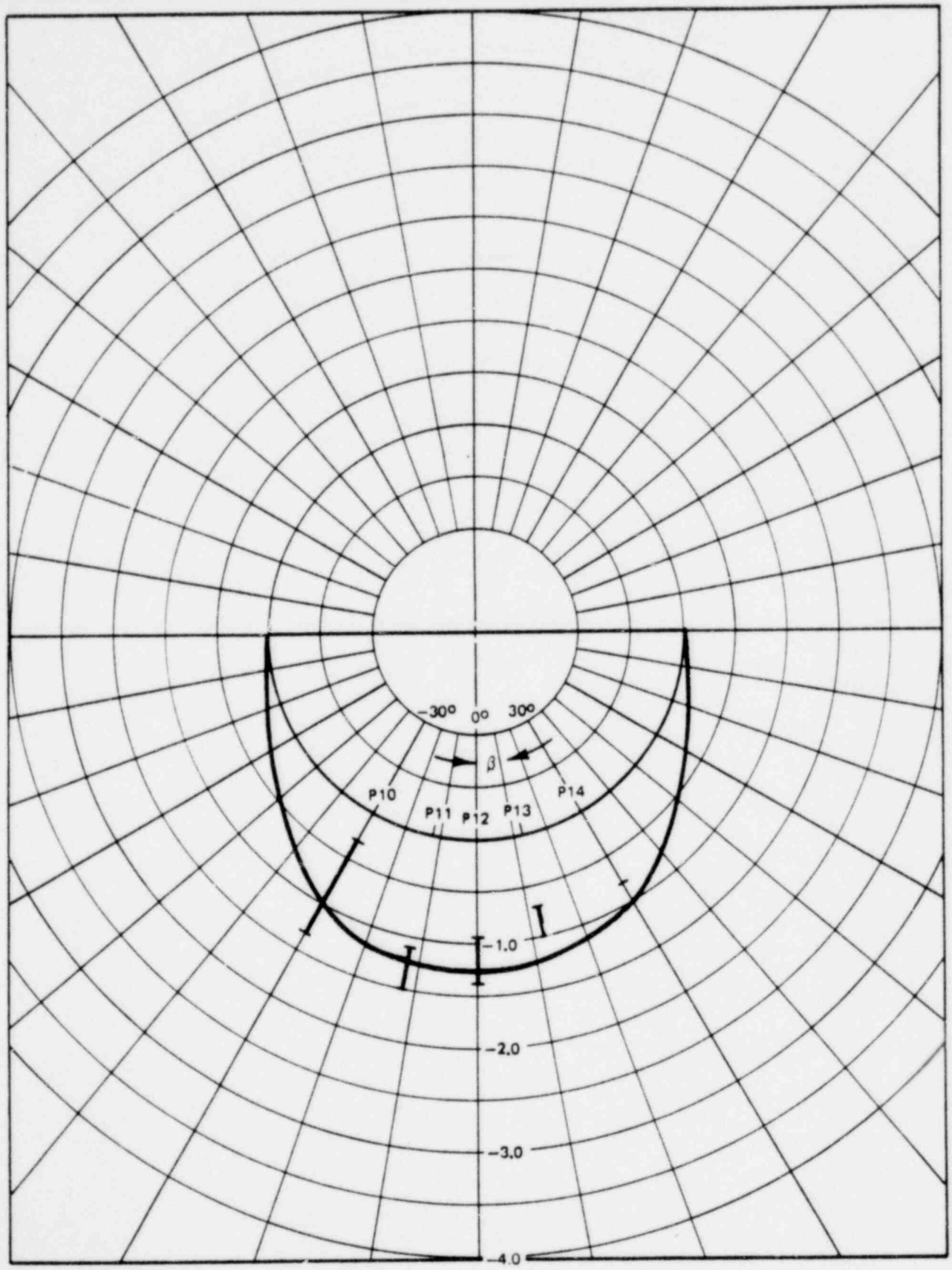

Figure 3-49. Peak Negative Pressure Distribution for 1/4 Scale Test Case 4 @ α = 0.0748

1764 272

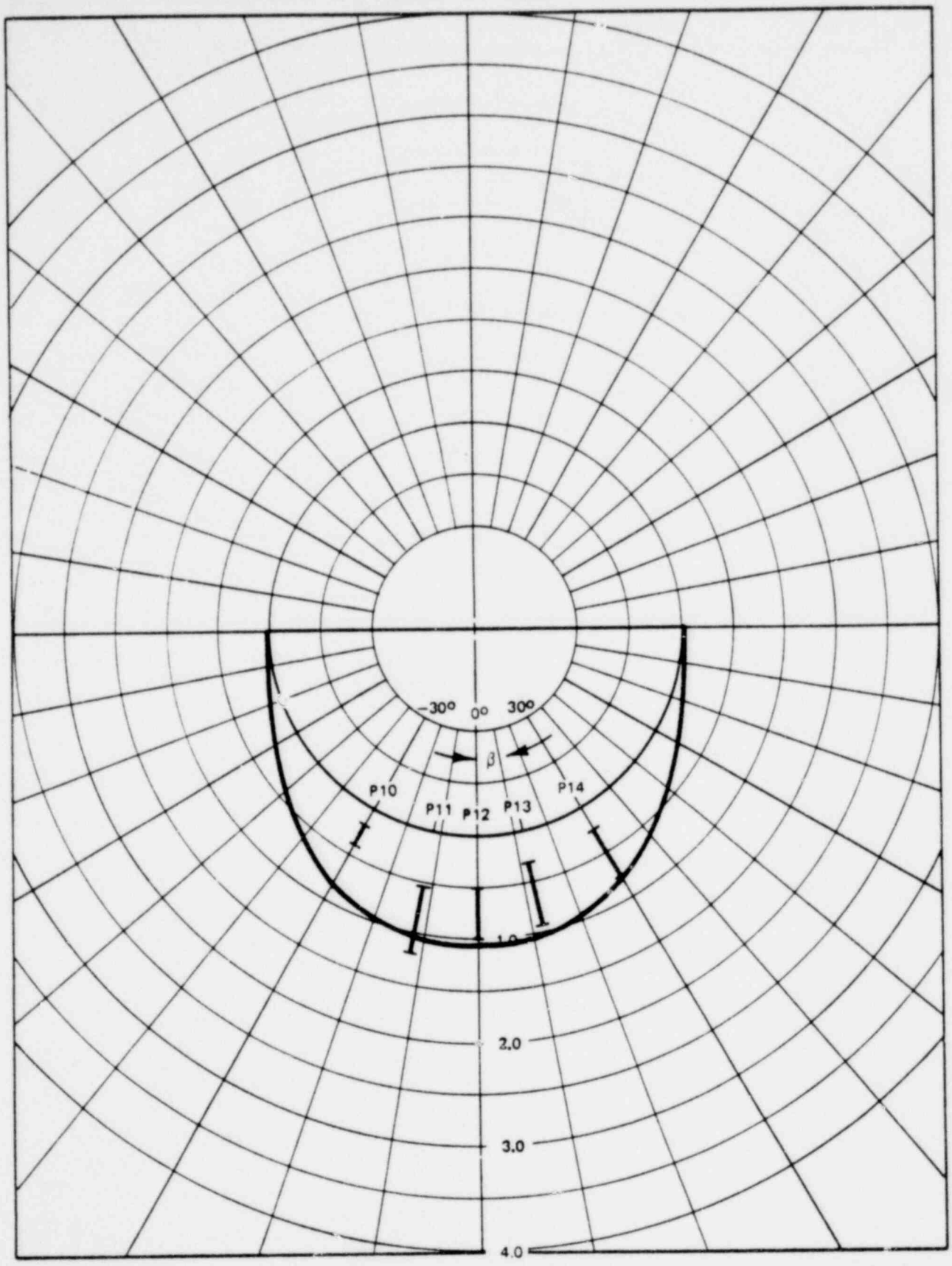

Figure 3-50. Peak Positive Pressure Distribution for 1/4 Scale Test Case 4A @ α = 0.0748

1764 273

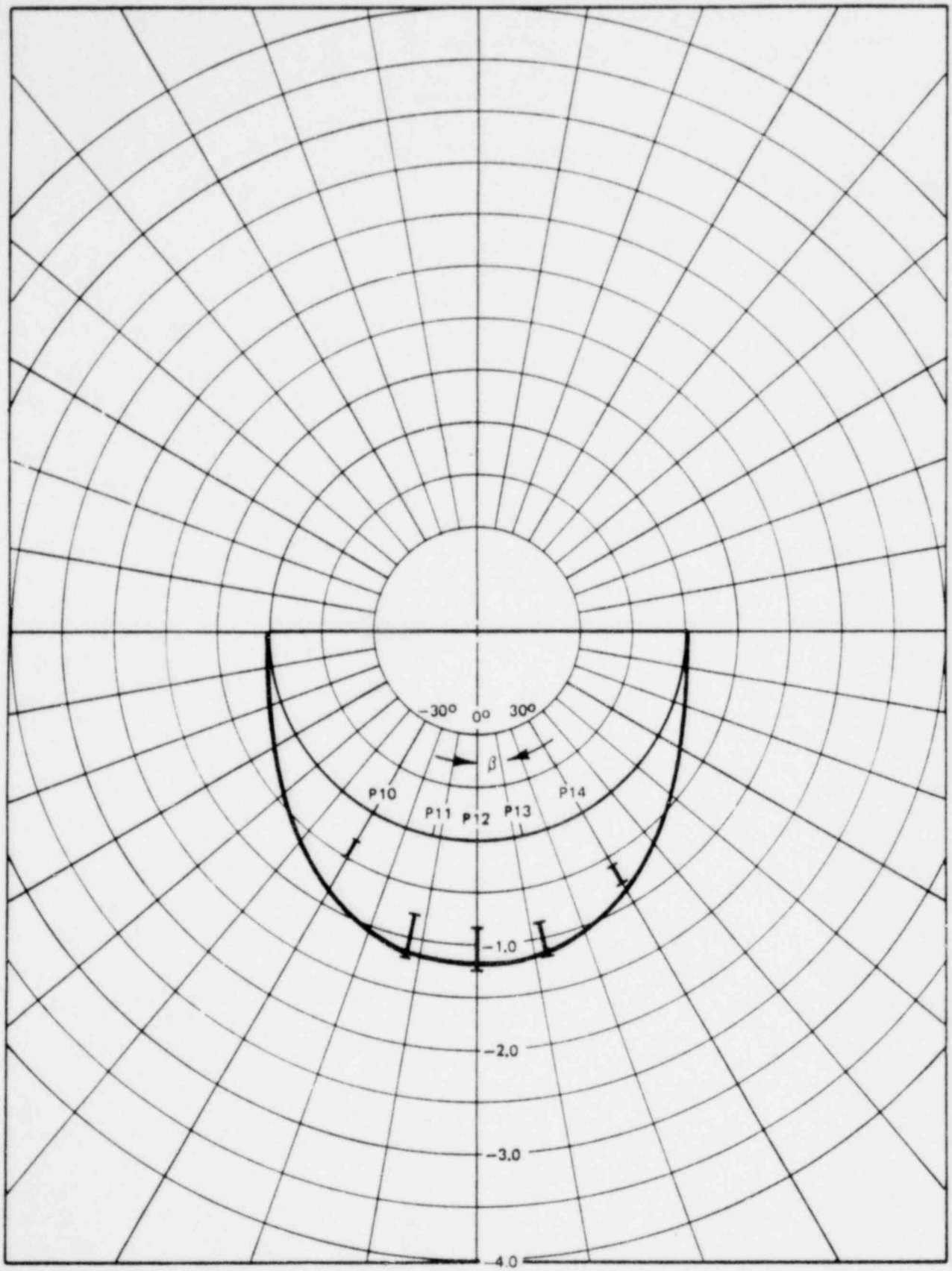

Figure 3-51. Peak Negative Pressure Distribution for 1/4 Scale Test Case 4A @ α = 0.0748

1764 274

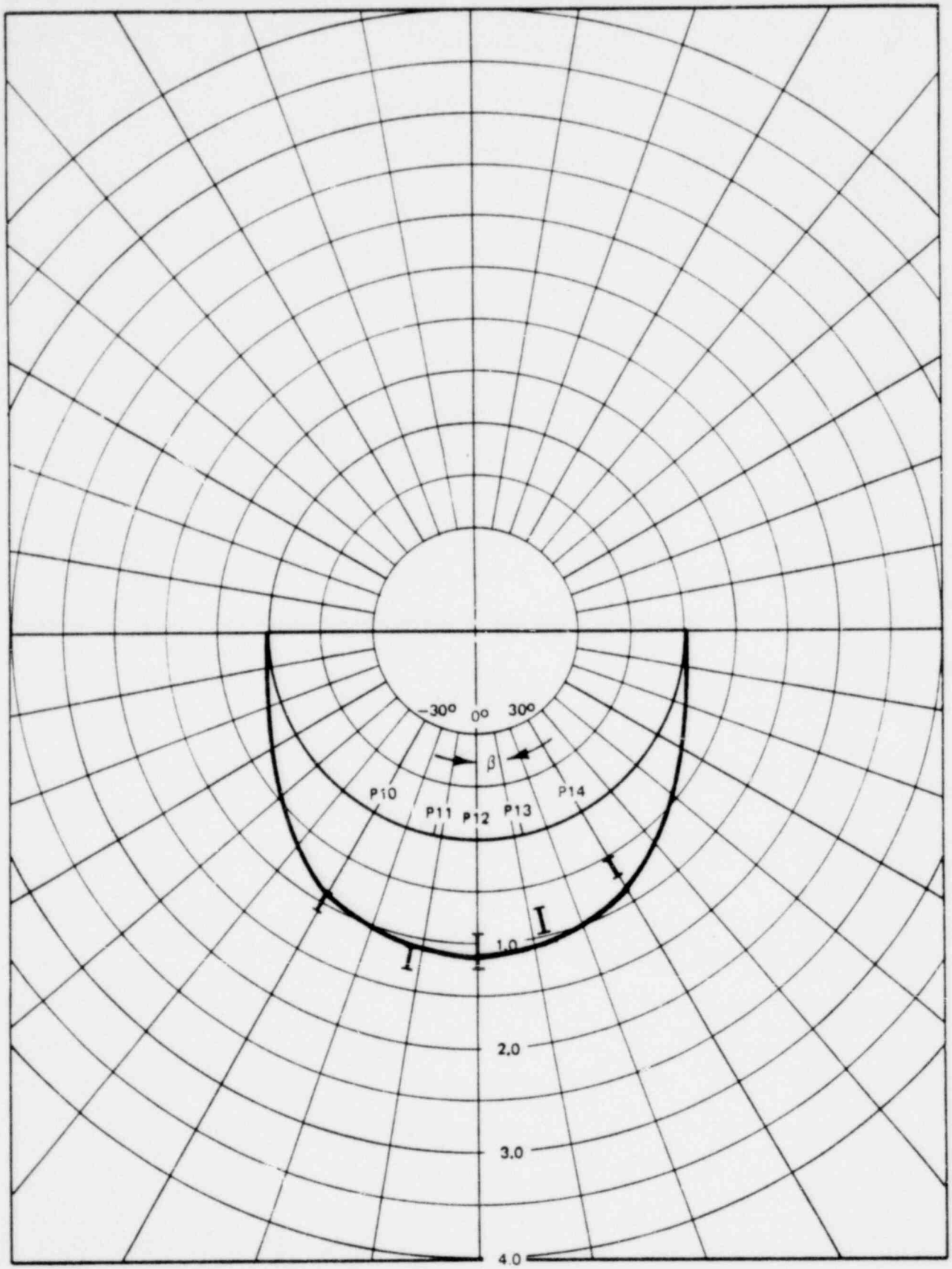

Figure 3-52. Peak Positive Pressure Distribution for 1/4 Scale Test Case 5 @ α = 0.0748

1764 275

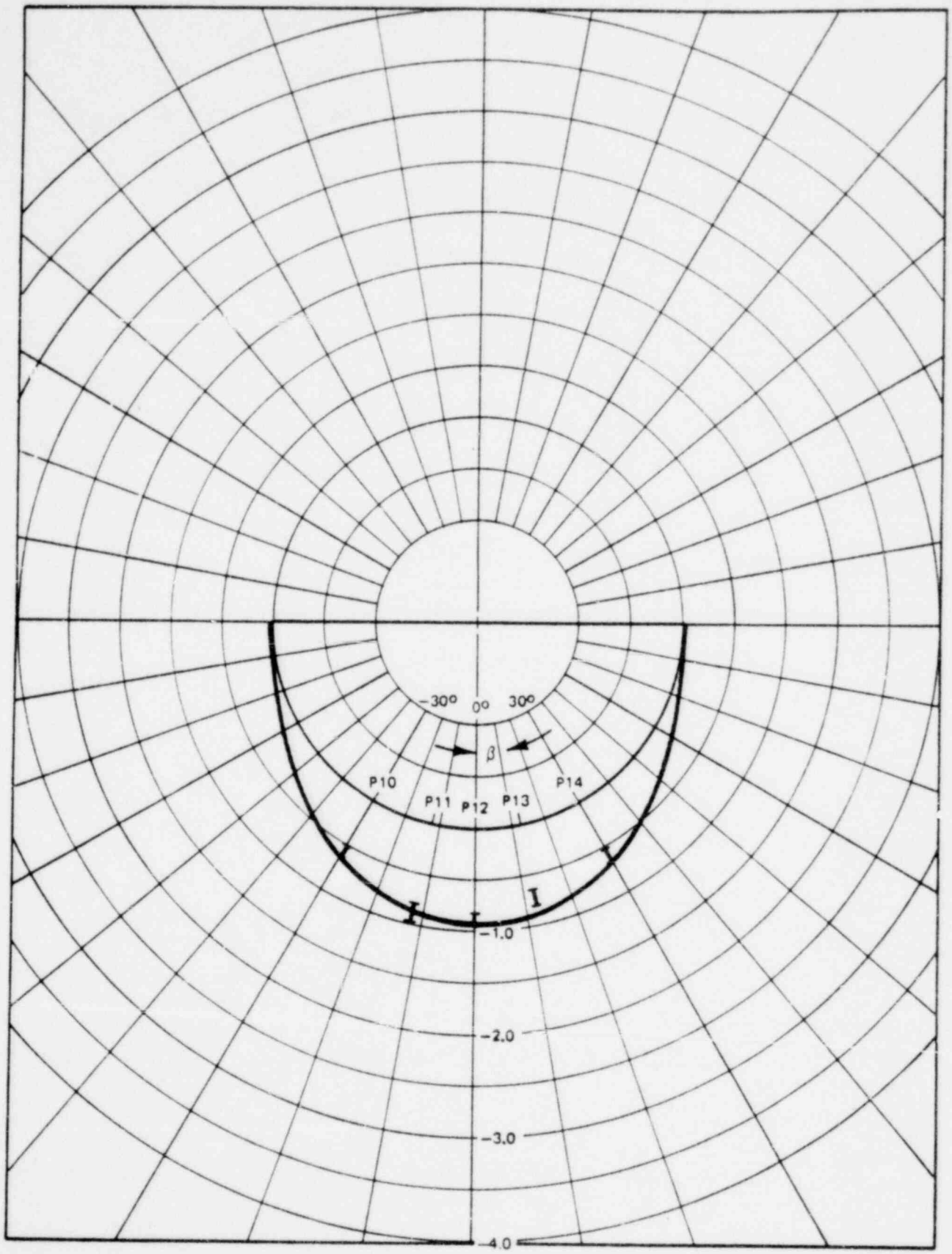

Figure 3-53. Peak Negative Pressure Distribution for 1/4 Scale Test Case 5 @ α = 0.0748

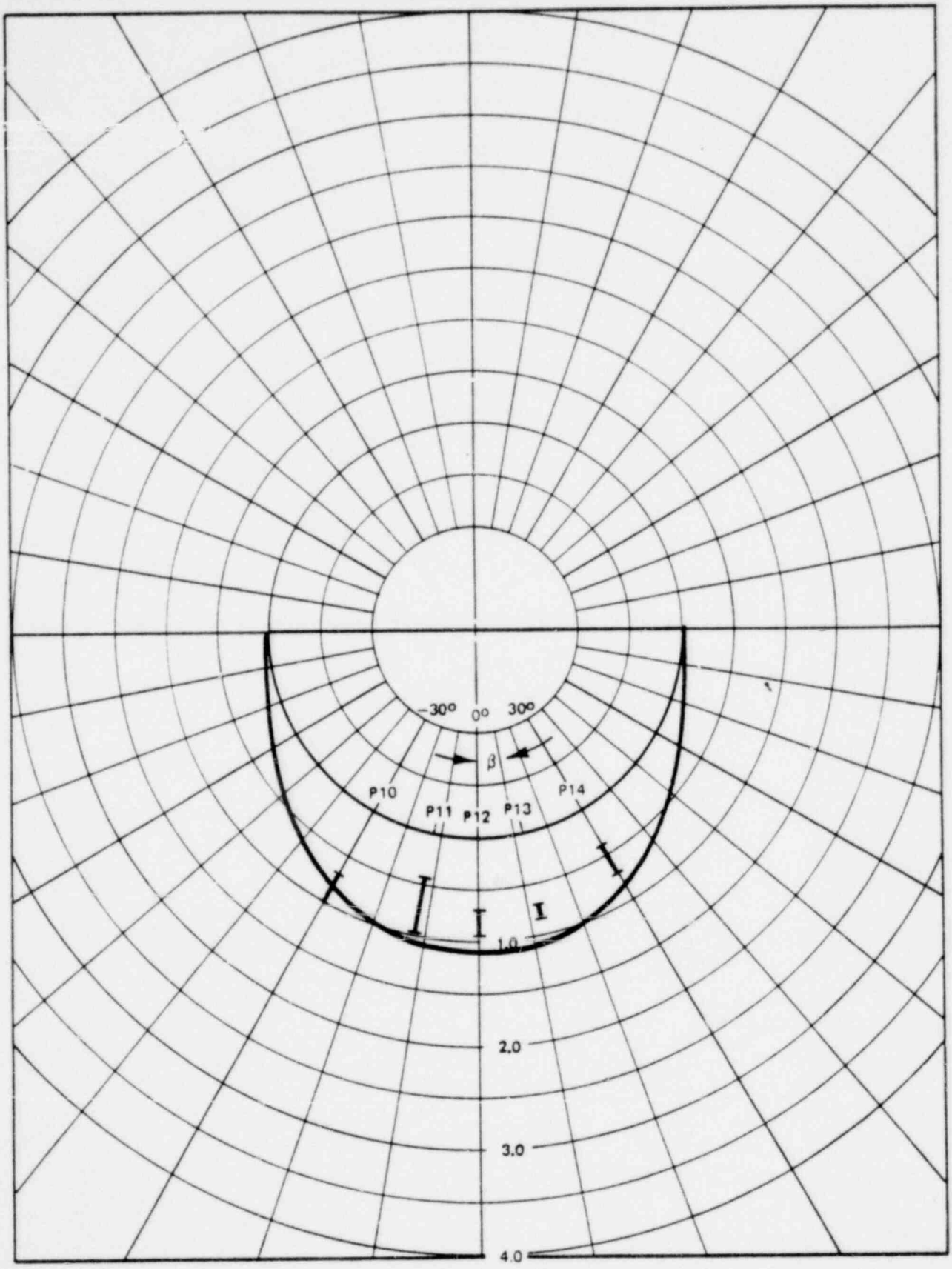

Figure 3-54. Peak Positive Pressure Distribution for 1/4 Scale Test Cases 6 and 6A @ α = 0.0748

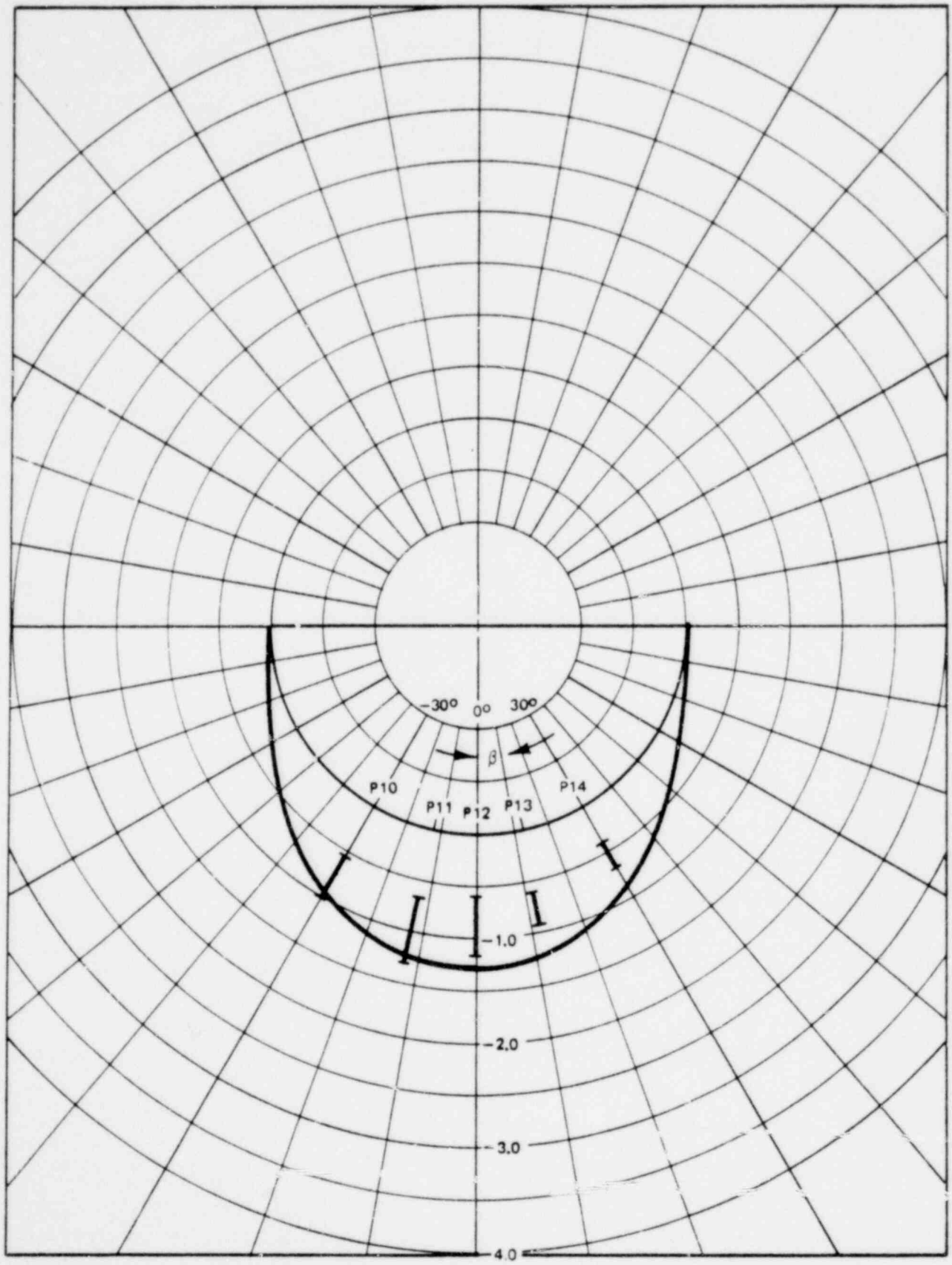

Figure 3-55. Peak Positive Pressure Distribution for 1/4 Scale Test Cases 6 and 6A @ α = 0.0748

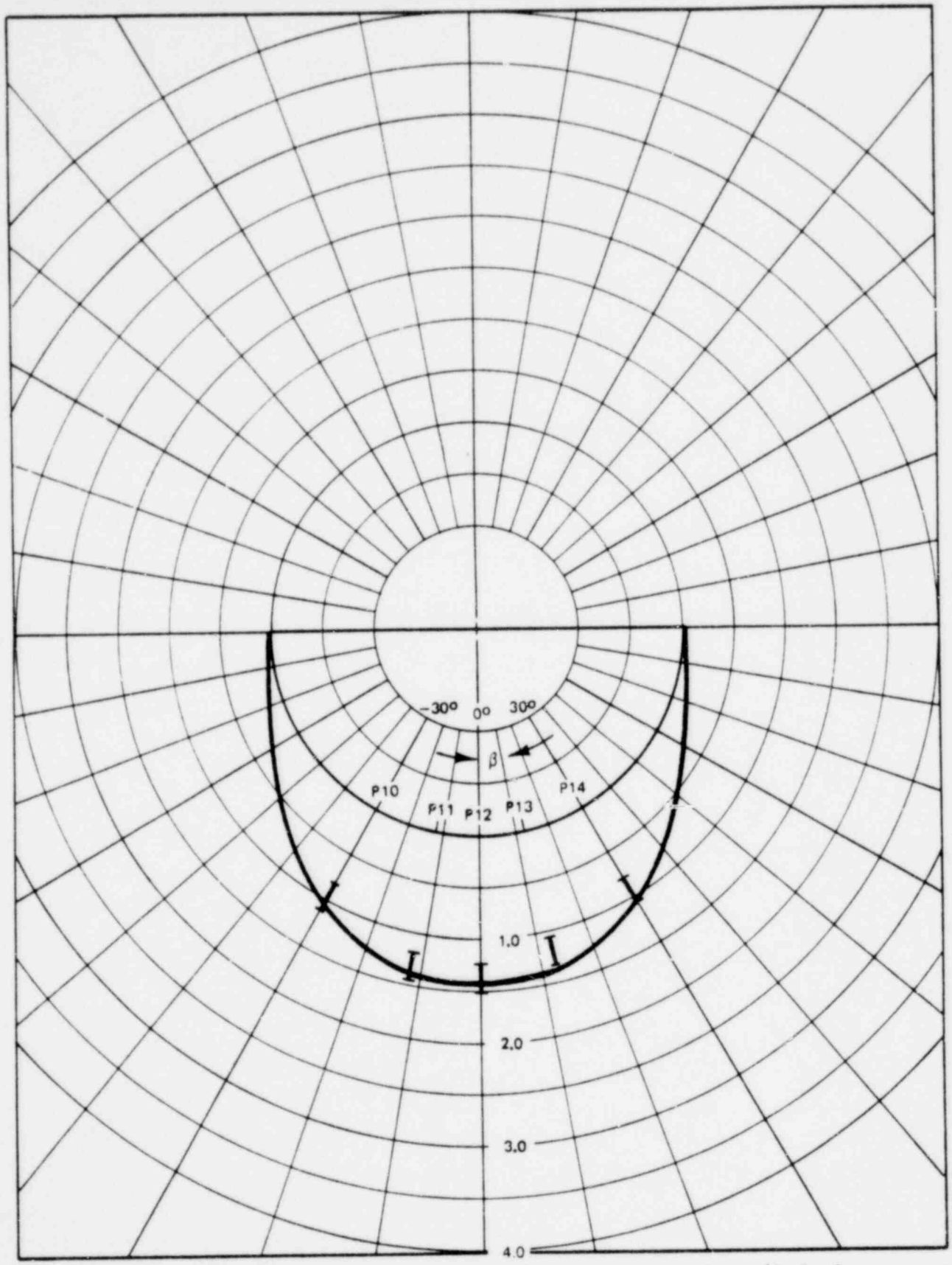

Figure 3-56. Peak Positive Pressure Distribution for 1/4 Scale Test Case 7 @ α = 0.0748

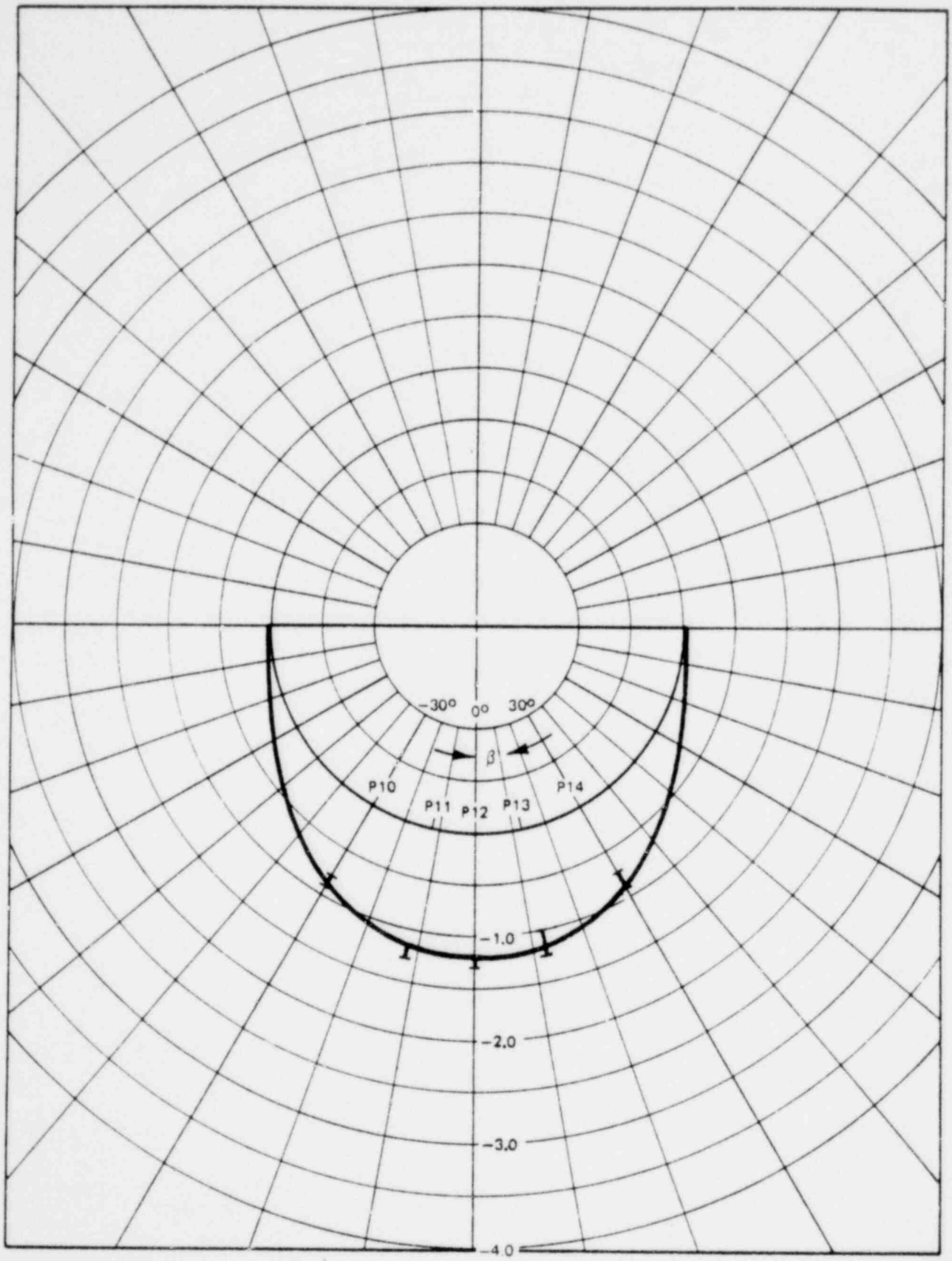

Figure 3-57. Peak Negative Pressure Distribution for 1/4 Scale Test Case 7 @ α = 0.0748

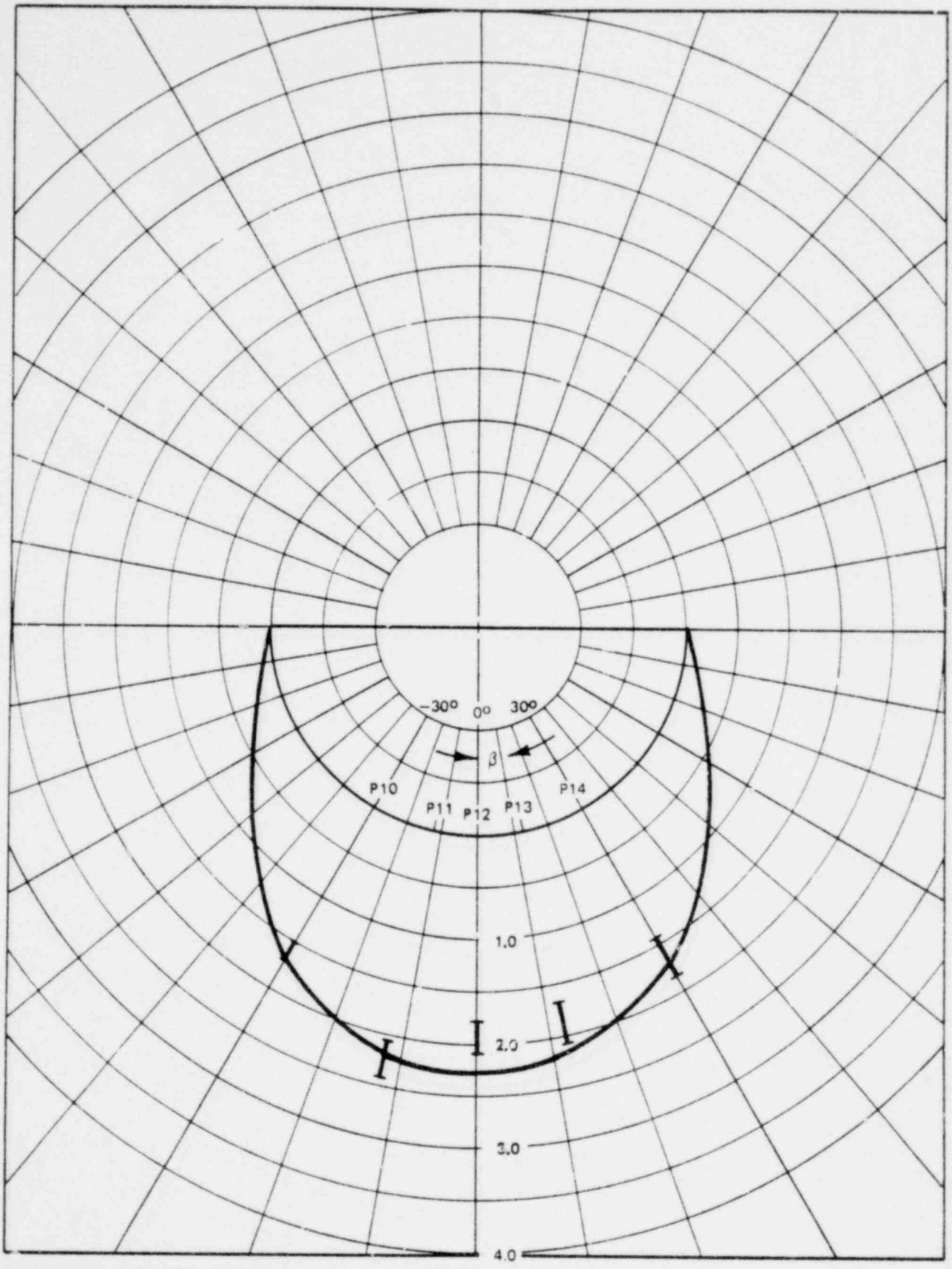

Figure 3-58. Peak Positive Pressure Distribution for 1/4 Scale Test Case 8 @ α = 0.0748

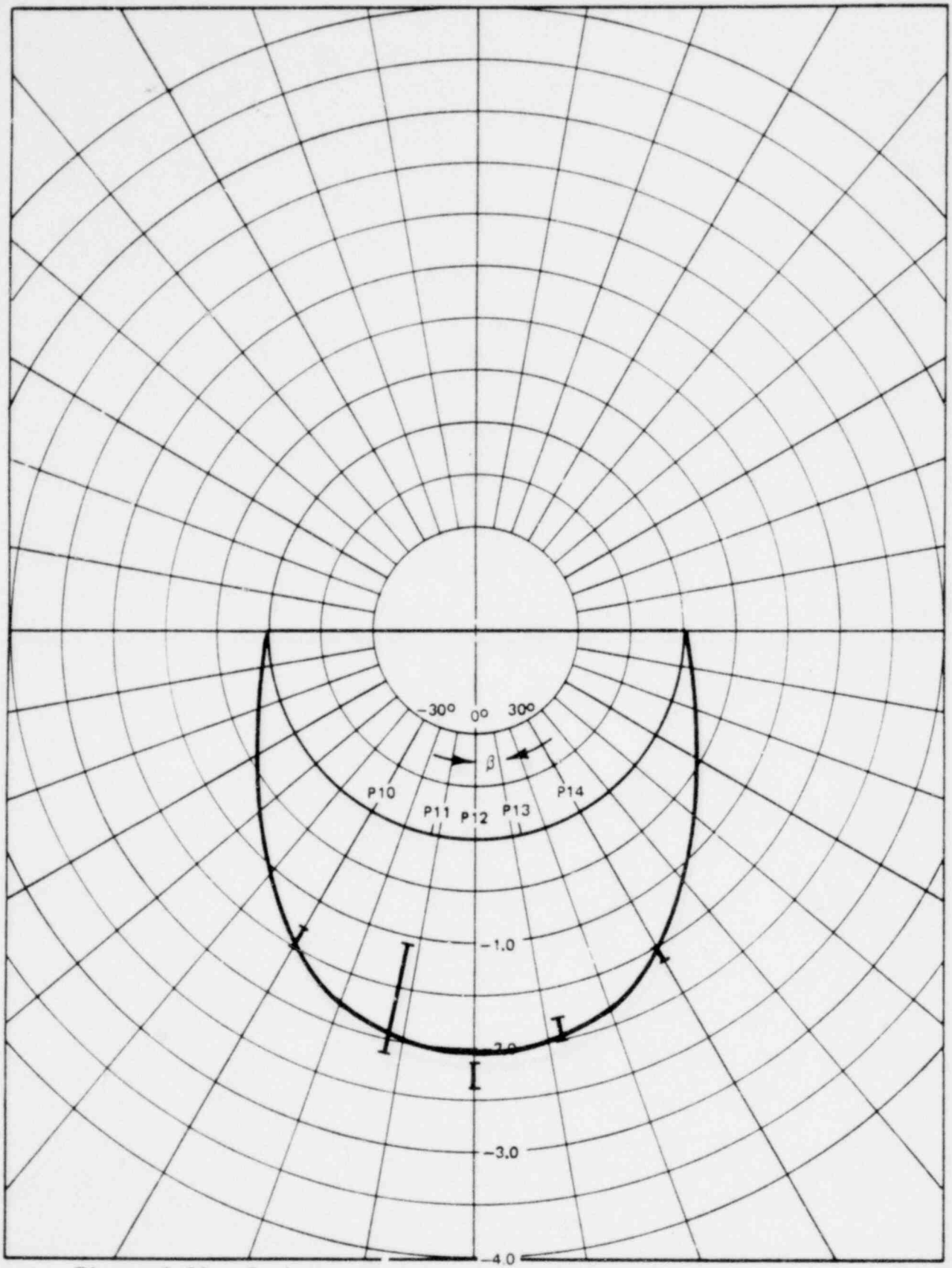

Figure 3-59. Peak Negative Pressure Distribution for 1/4 Scale Test Case 8 @ α = 0.0748

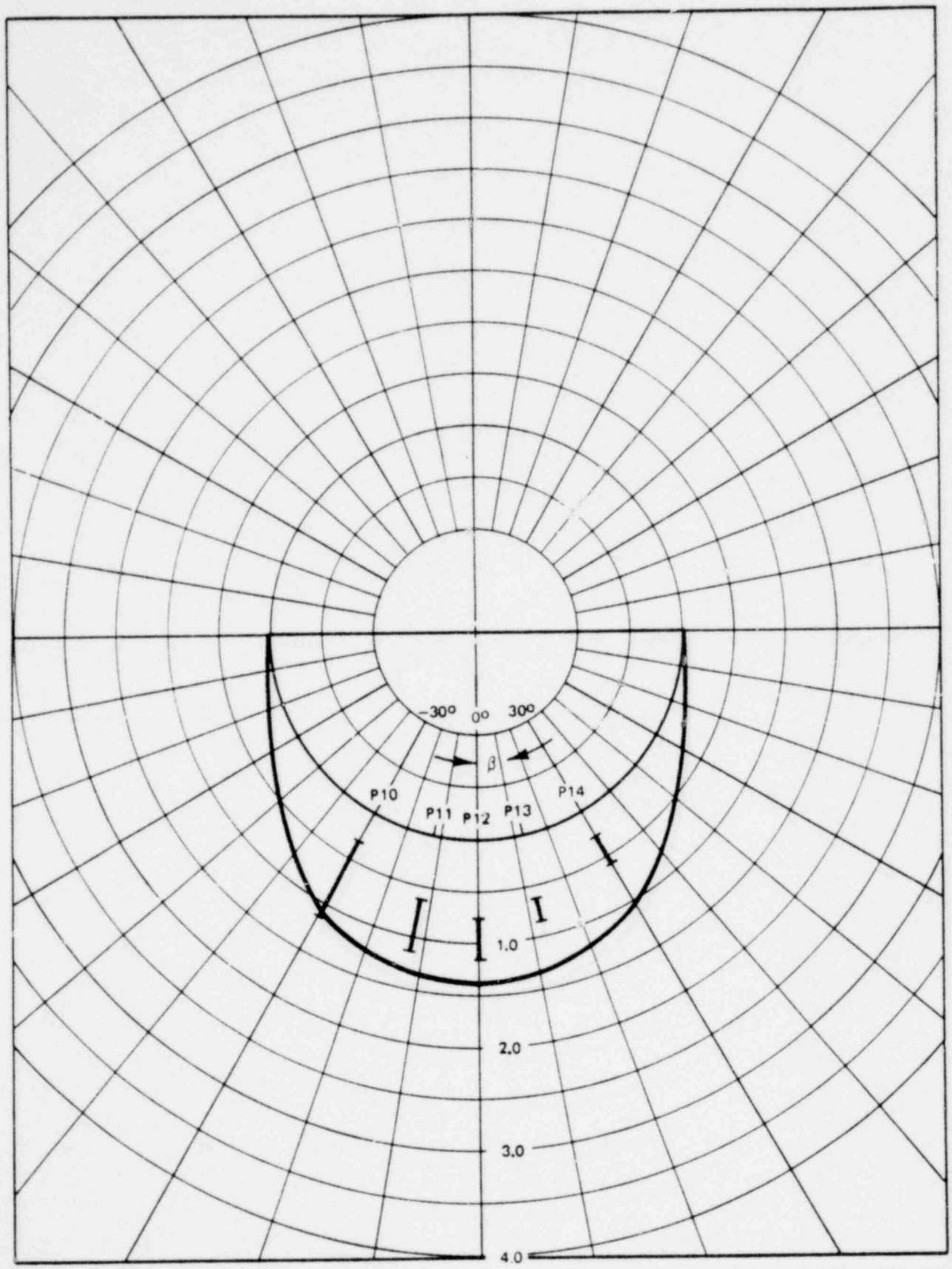

Figure 3-60. Peak Positive Pressure Distribution for 1/4 Scale Test Cases 9 and 9A @ α = 0.0748

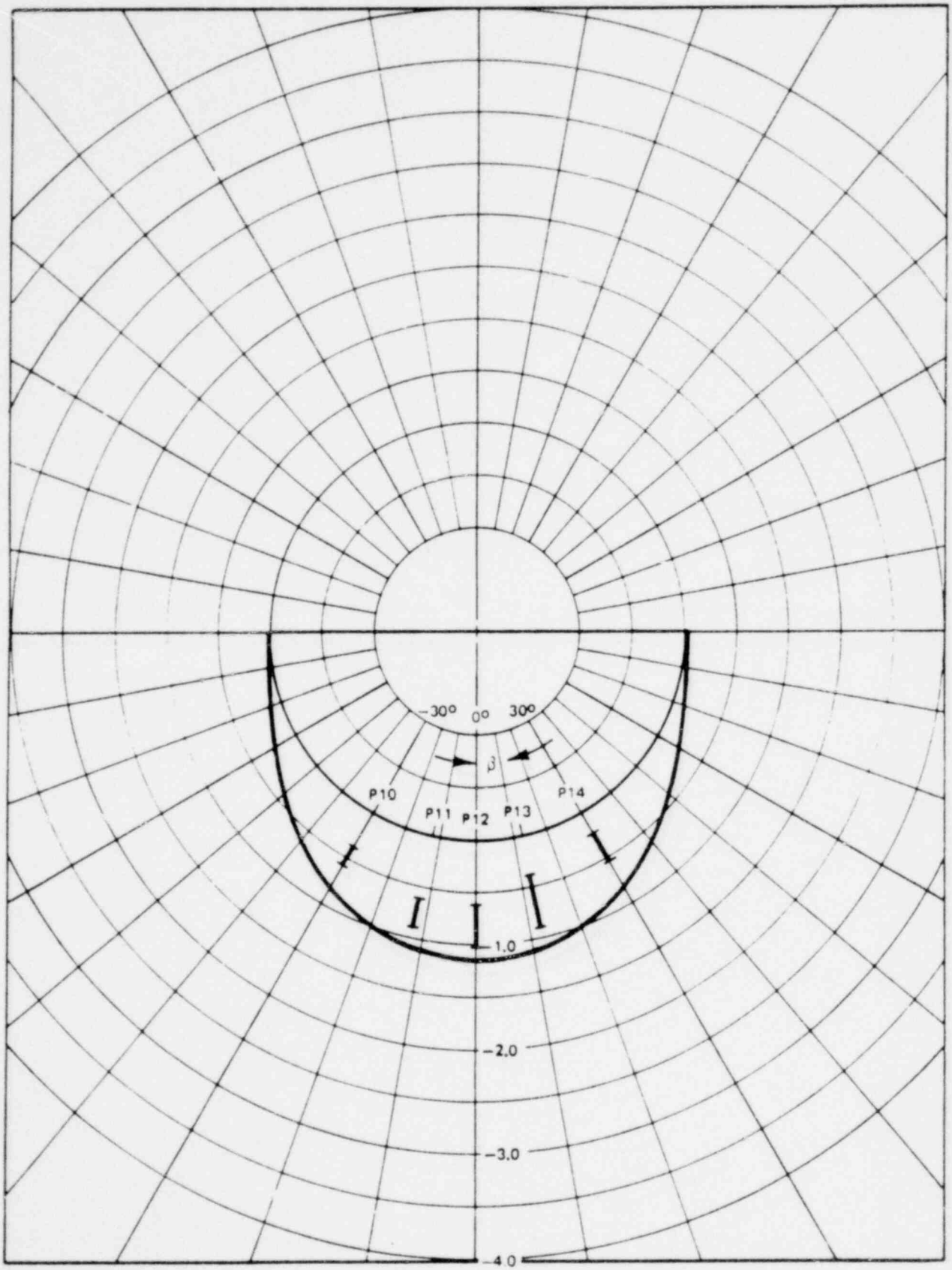

Figure 3-61. Peak Negative Pressure Distribution for 1/4 Scale Test Cases 9 and 9A @ α = 0.0748

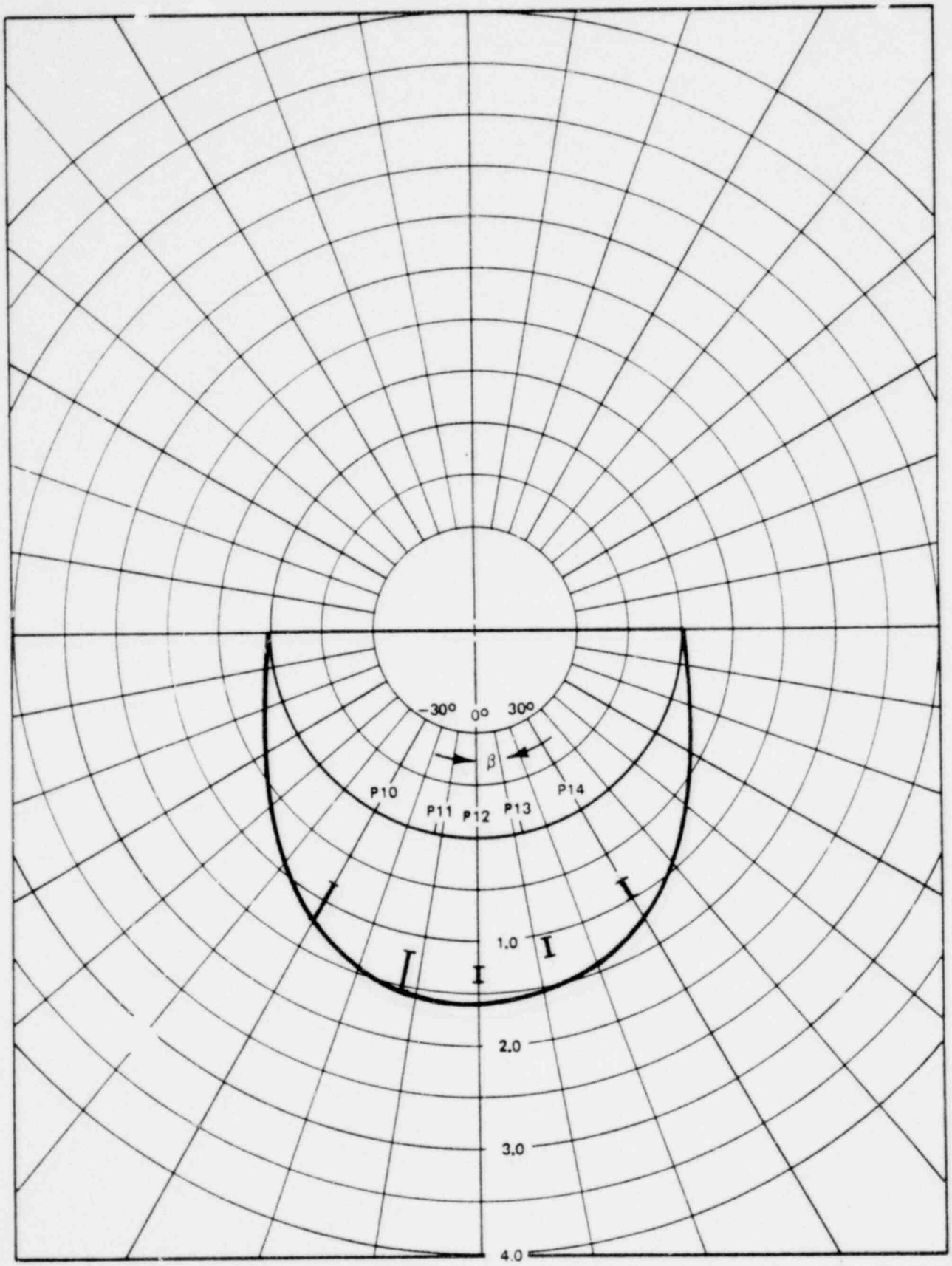

Figure 3-62. Peak Positive Pressure Distribution for 1/4 Scale Test Case 10 @ α = 0.0748

1764 285

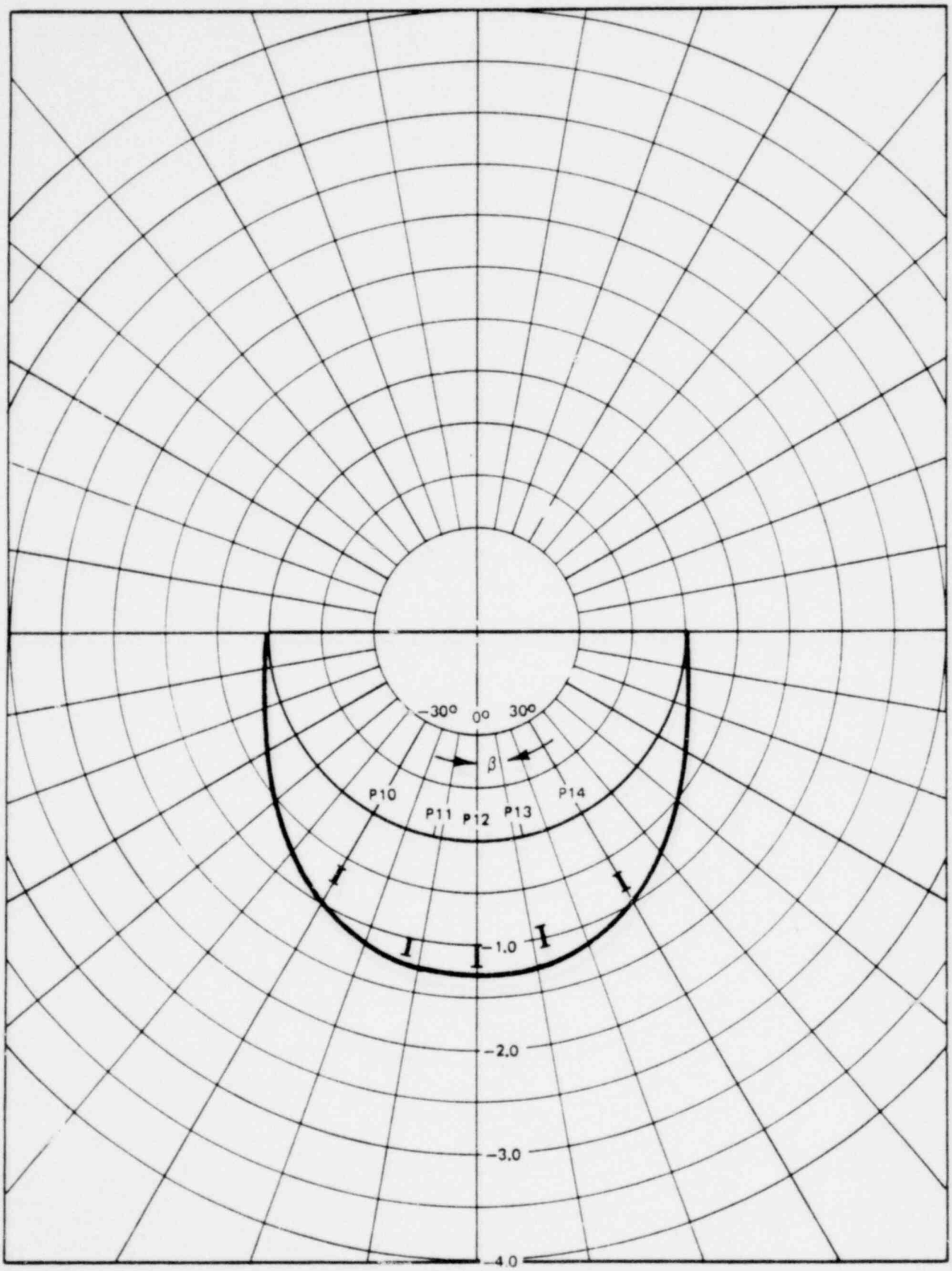

Figure 3-63. Peak Negative Pressure Distribution For 1/4 Scale Test Case 10 @ α = 0.0748

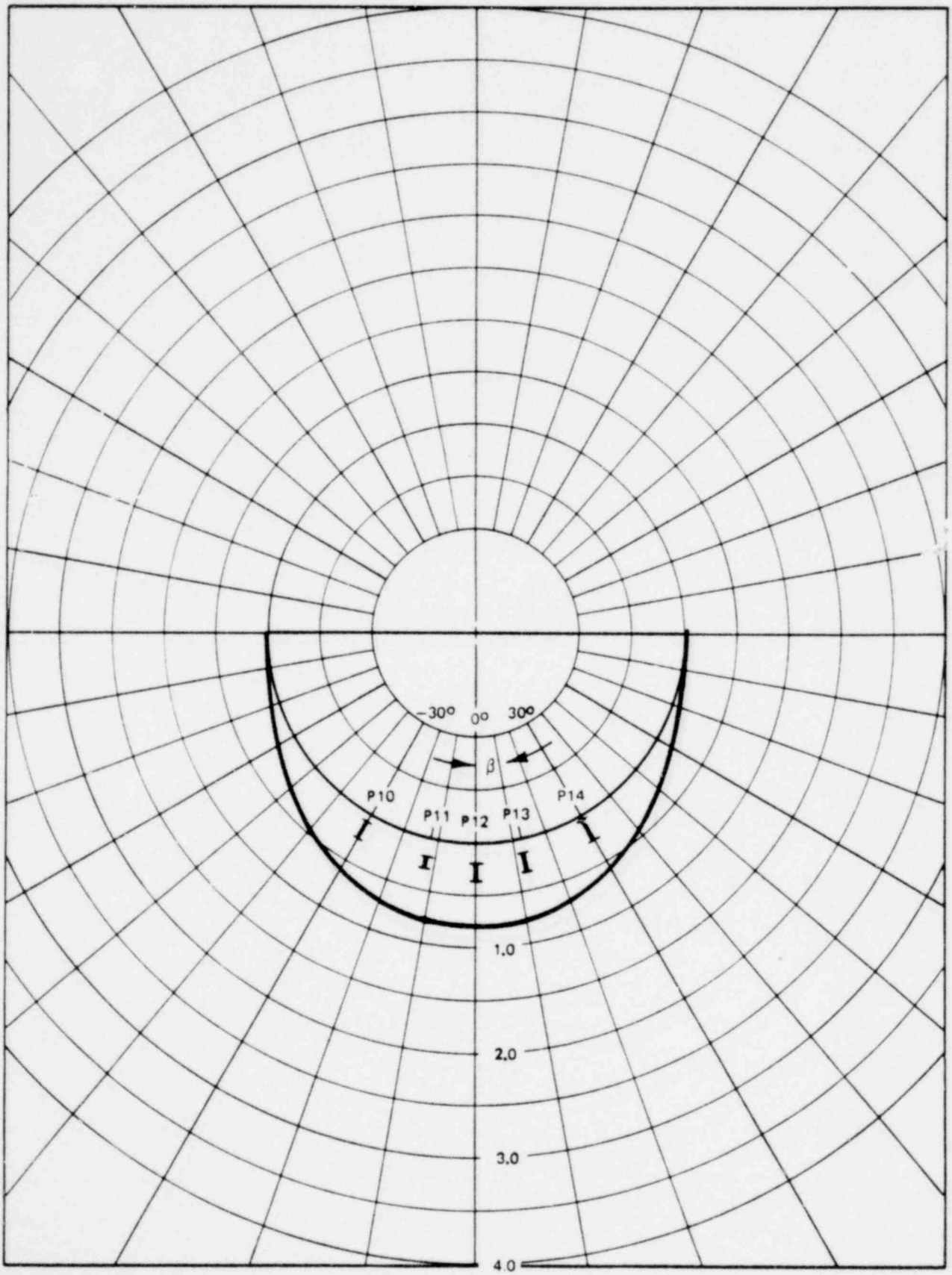

Figure 3-64. Peak Positive Pressure Distribution For 1/4 Scale Test Case 11 @ α = 0.748

1764 287

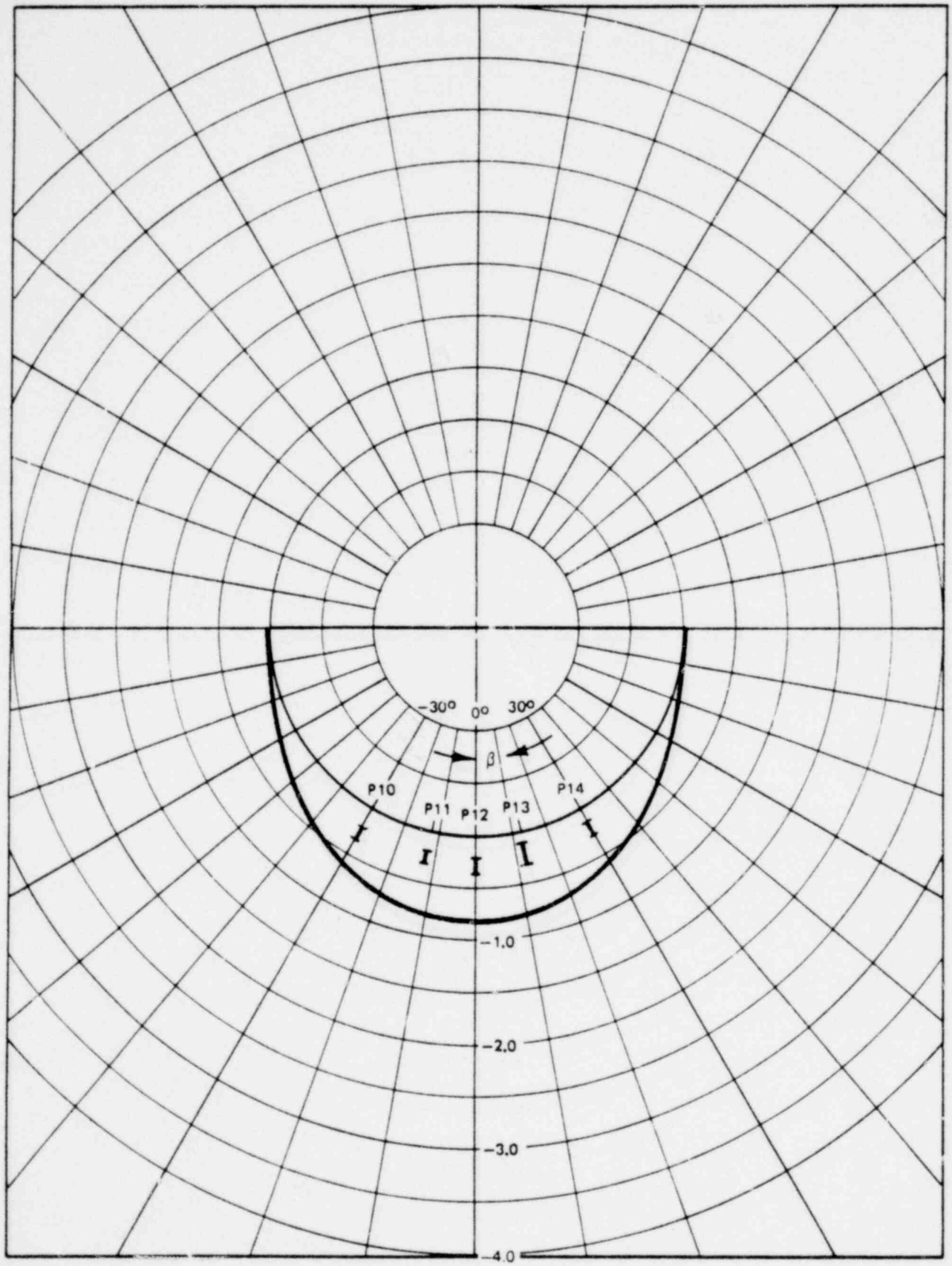

Figure 3-65. Peak Negative Pressure Distribution For 1/4 Scale Test Case 11 @ α = 0.0748

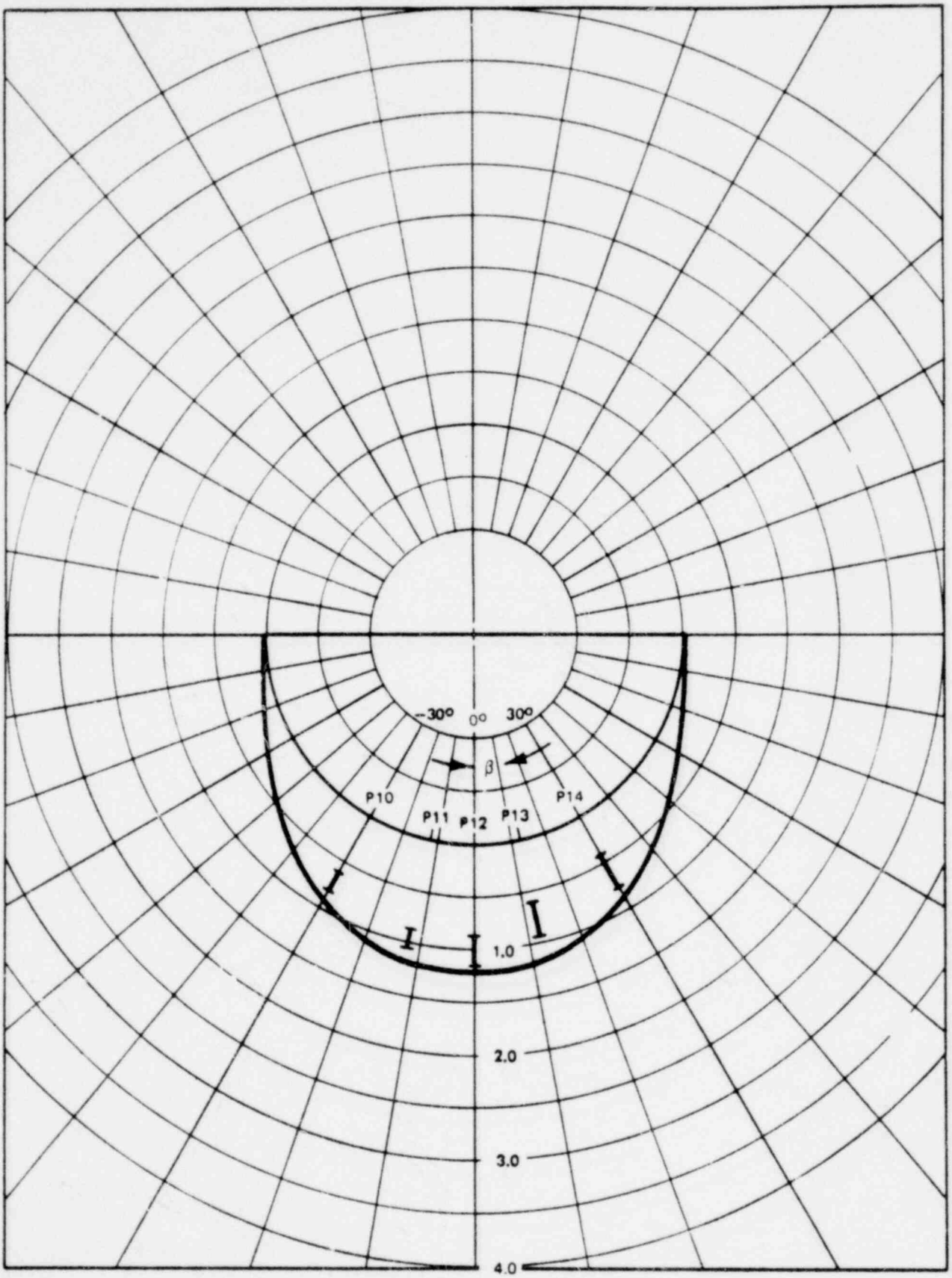

Figure 3-66. Peak Positive Pressure Distribution For 1/4 Scale Test Case 12 @ α = 0.0748

1764 289

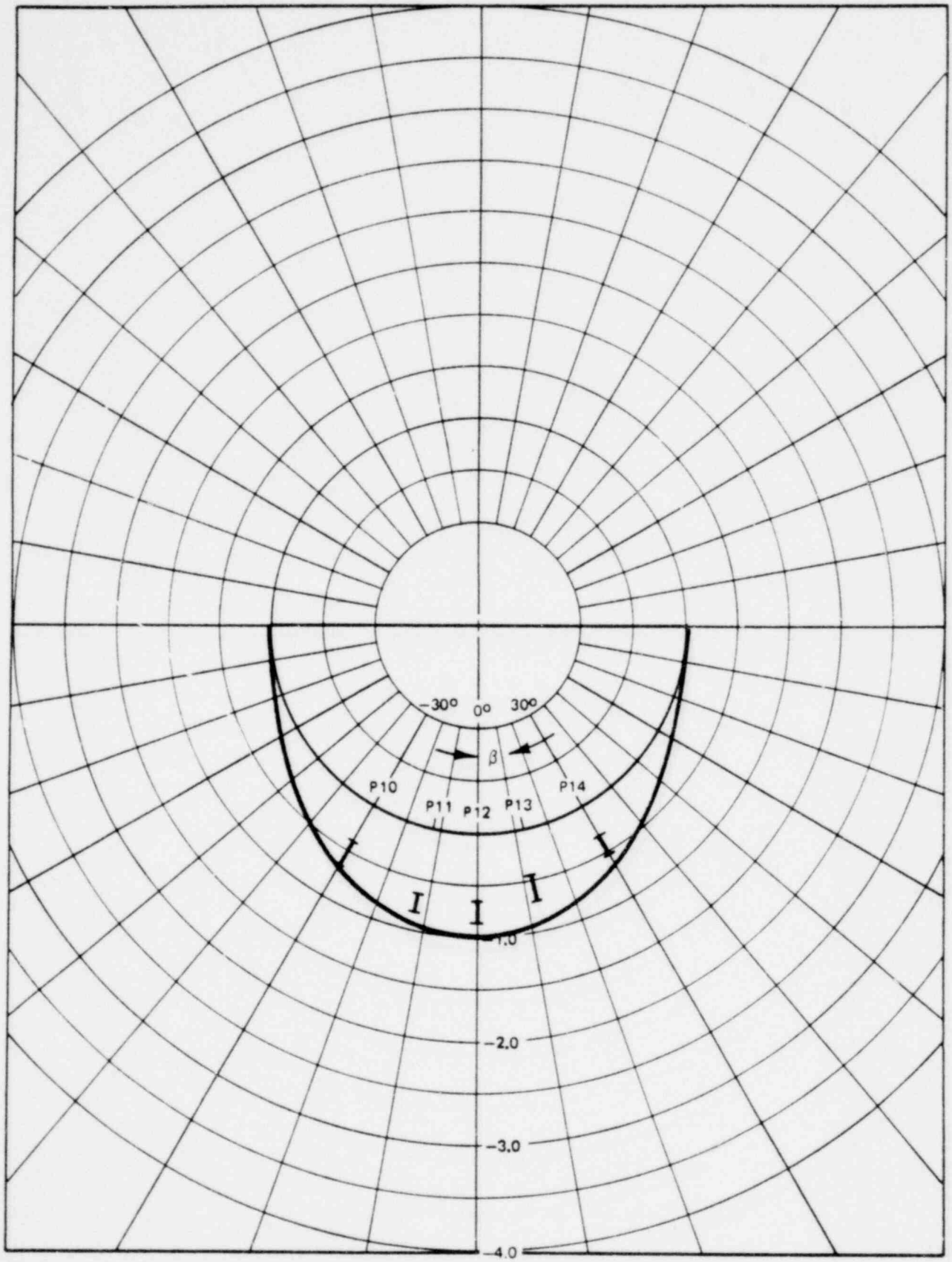

Figure 3-67. Peak Negative Pressure Distribution For 1/4 Scale Test Case 12 @ α = 0.0748

1764 290

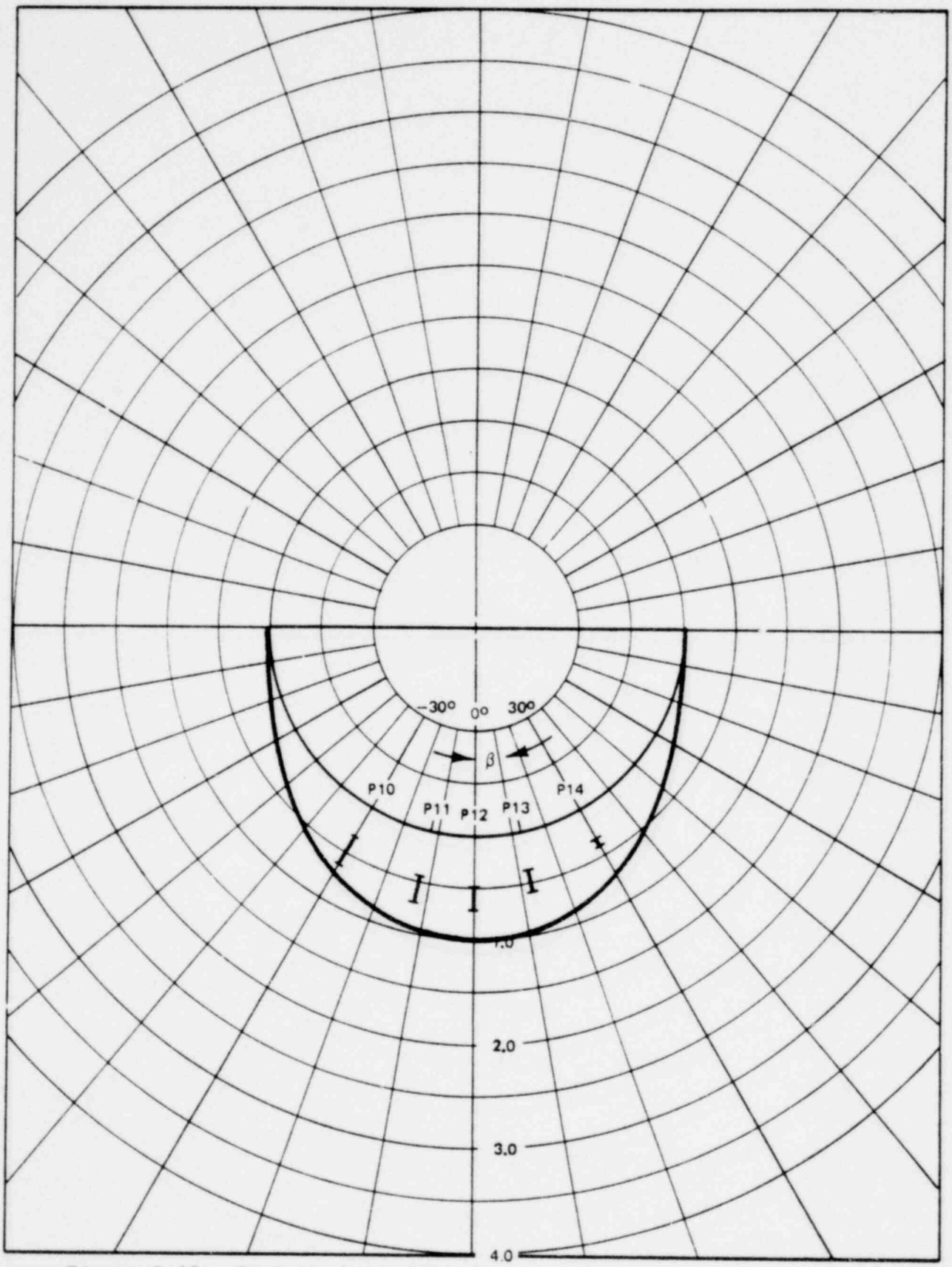

Figure 3-68. Peak Positive Pressure Distribution For 1/4 Scale Test Case 13 @ α = 0.0748

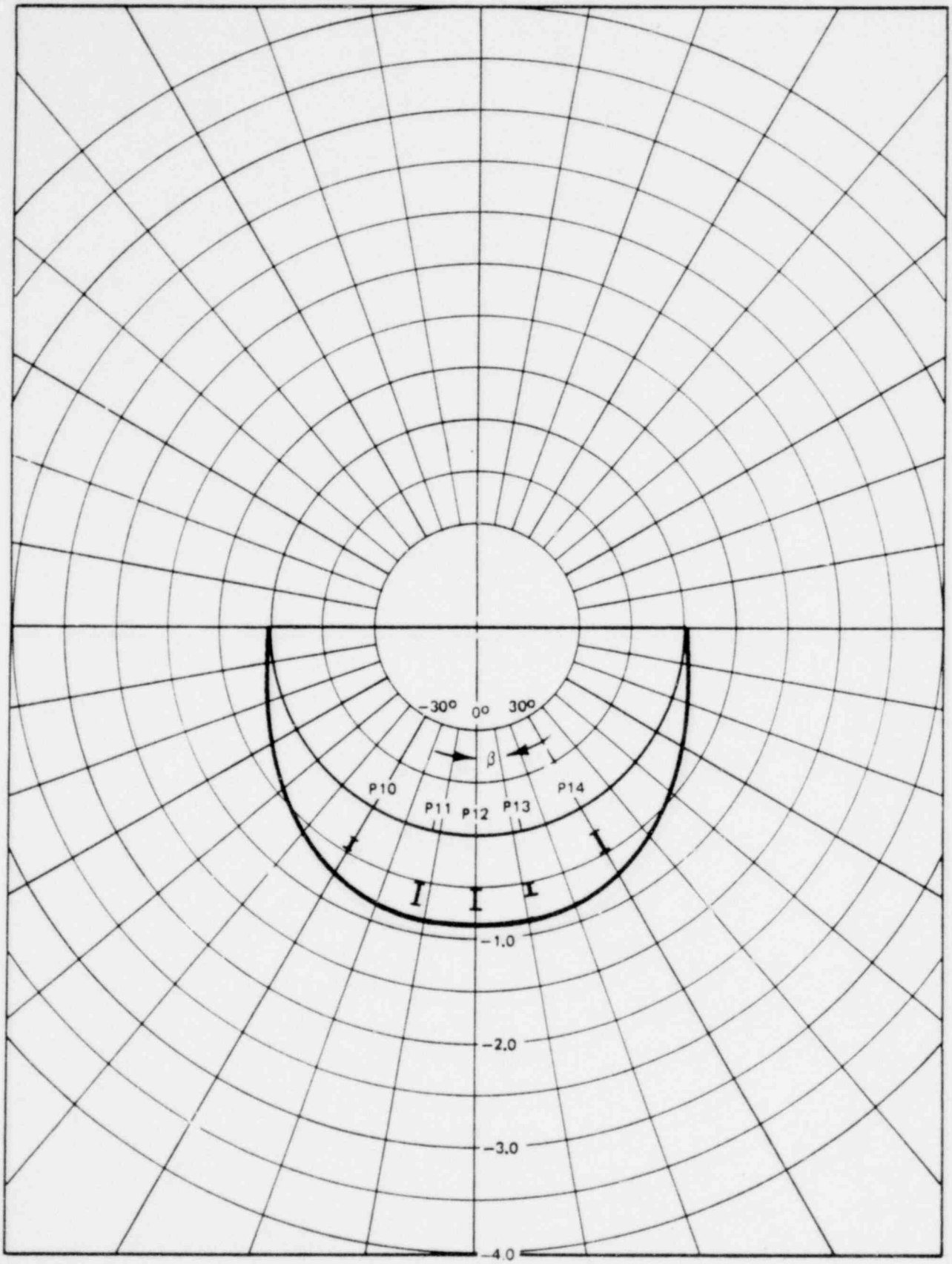

Figure 3-69. Peak Negative Pressure Distribution For 1/4 Scale Case 13 @ α = 0.0748

1764 292

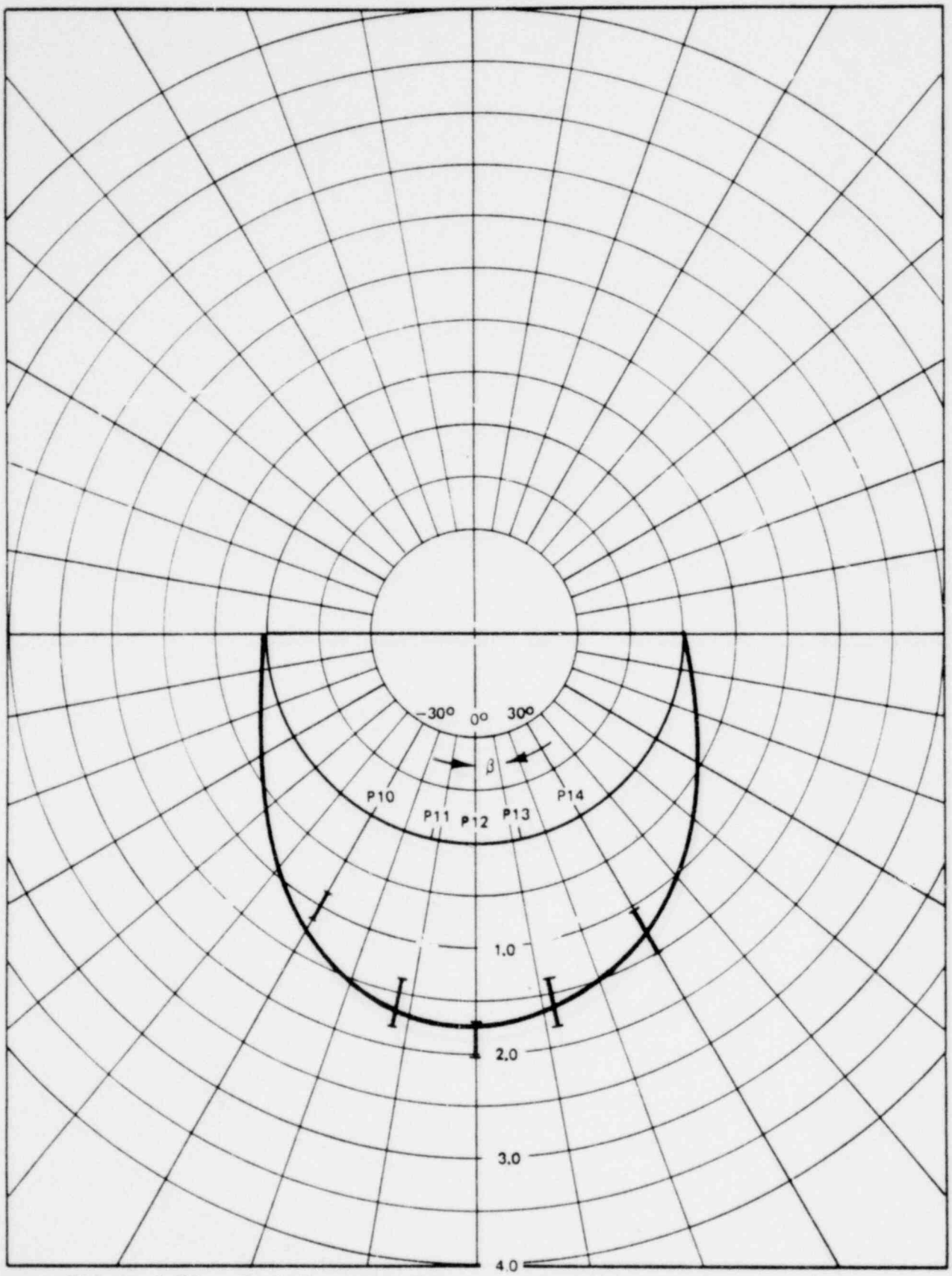

Figure 3-70. Peak Positive Pressure Distribution For 1/4 Scale Test Case 14 @ α = 0.0748

1764 293

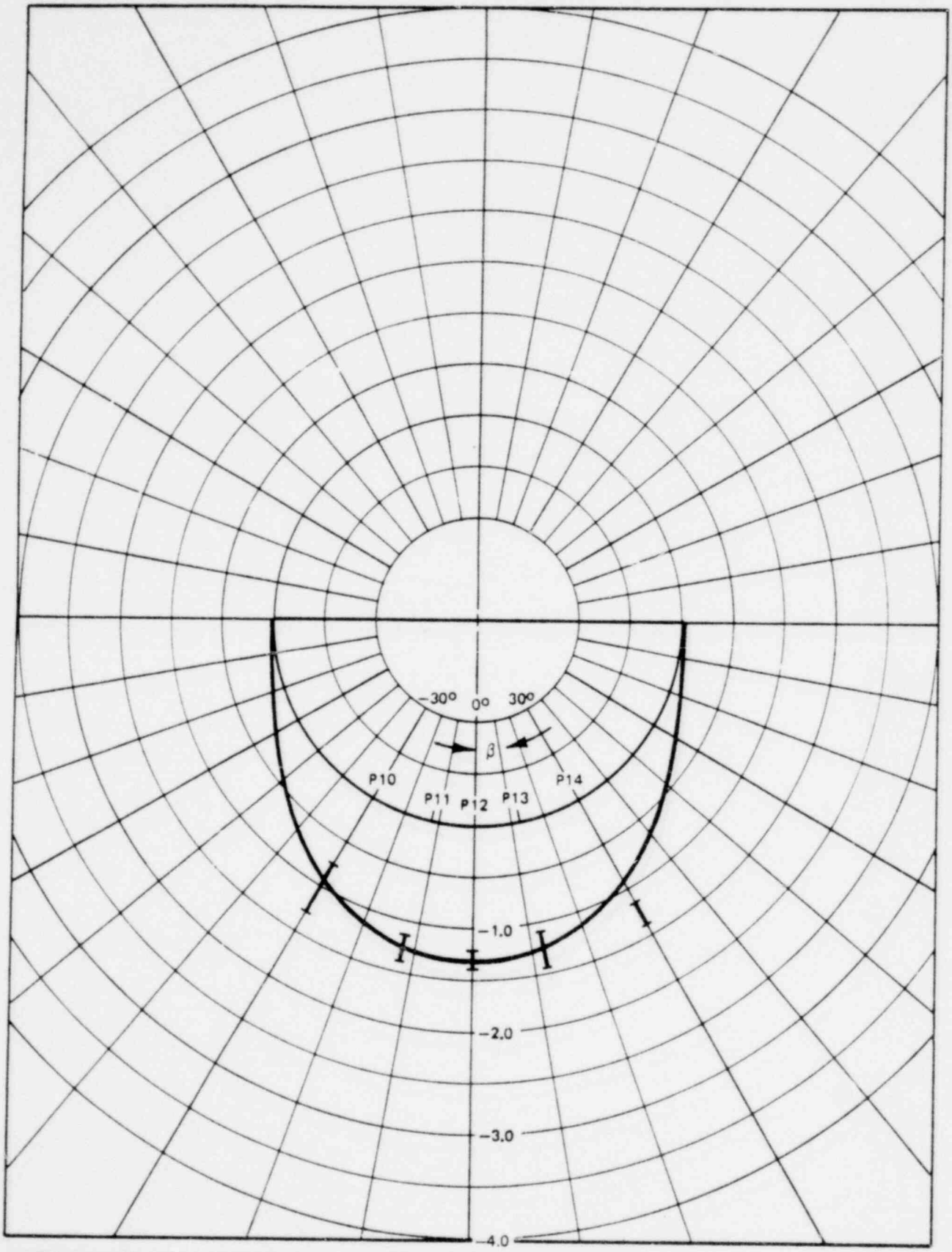

Figure 3-71. Peak Negative Pressure Distribution For 1/4 Scale Test Case 14 @ α = 0.0748

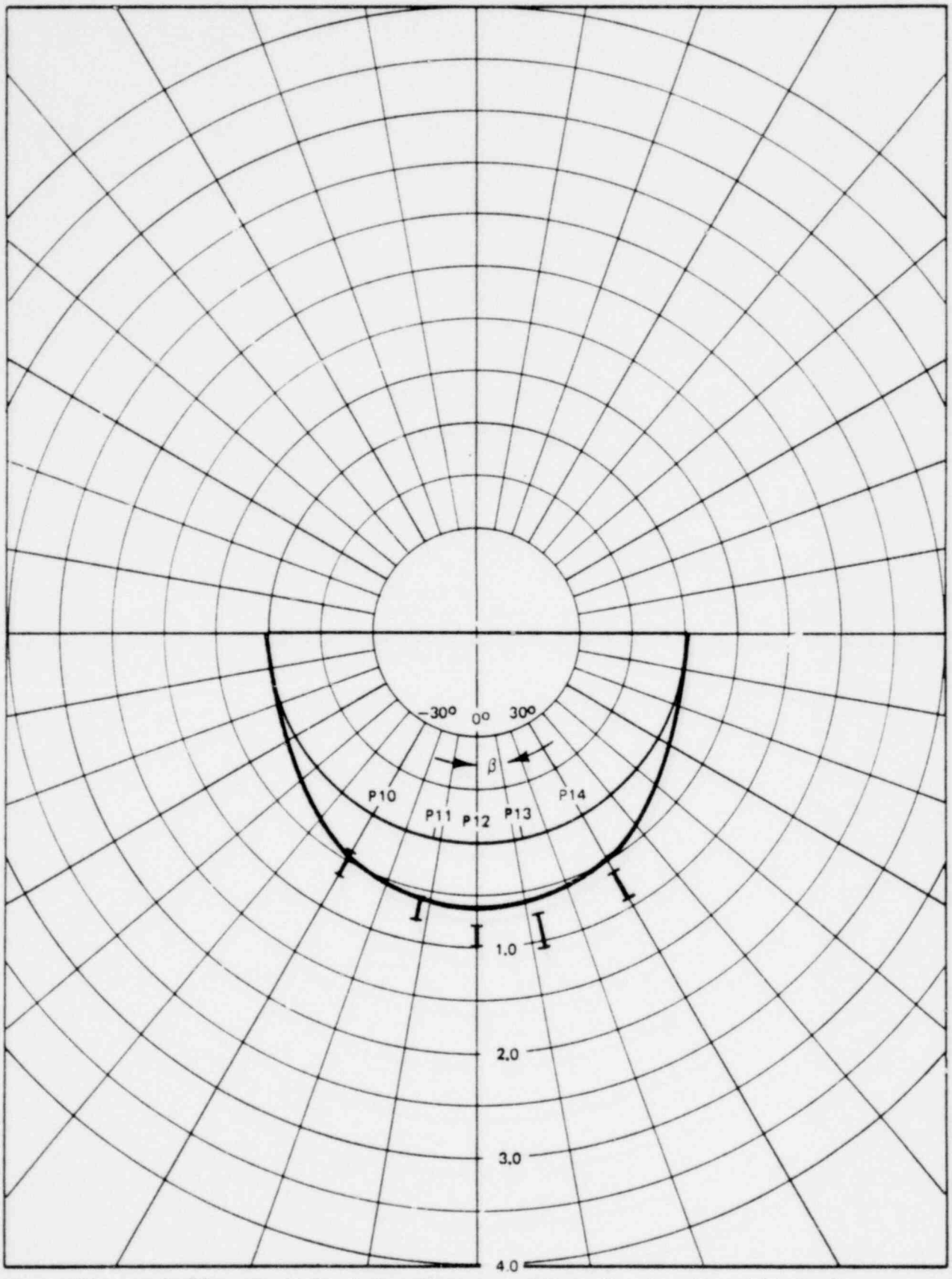

Figure 3-72. Peak Positive Pressure Distribution For 1/4 Scale Test Case 15 @ α = 0.0748

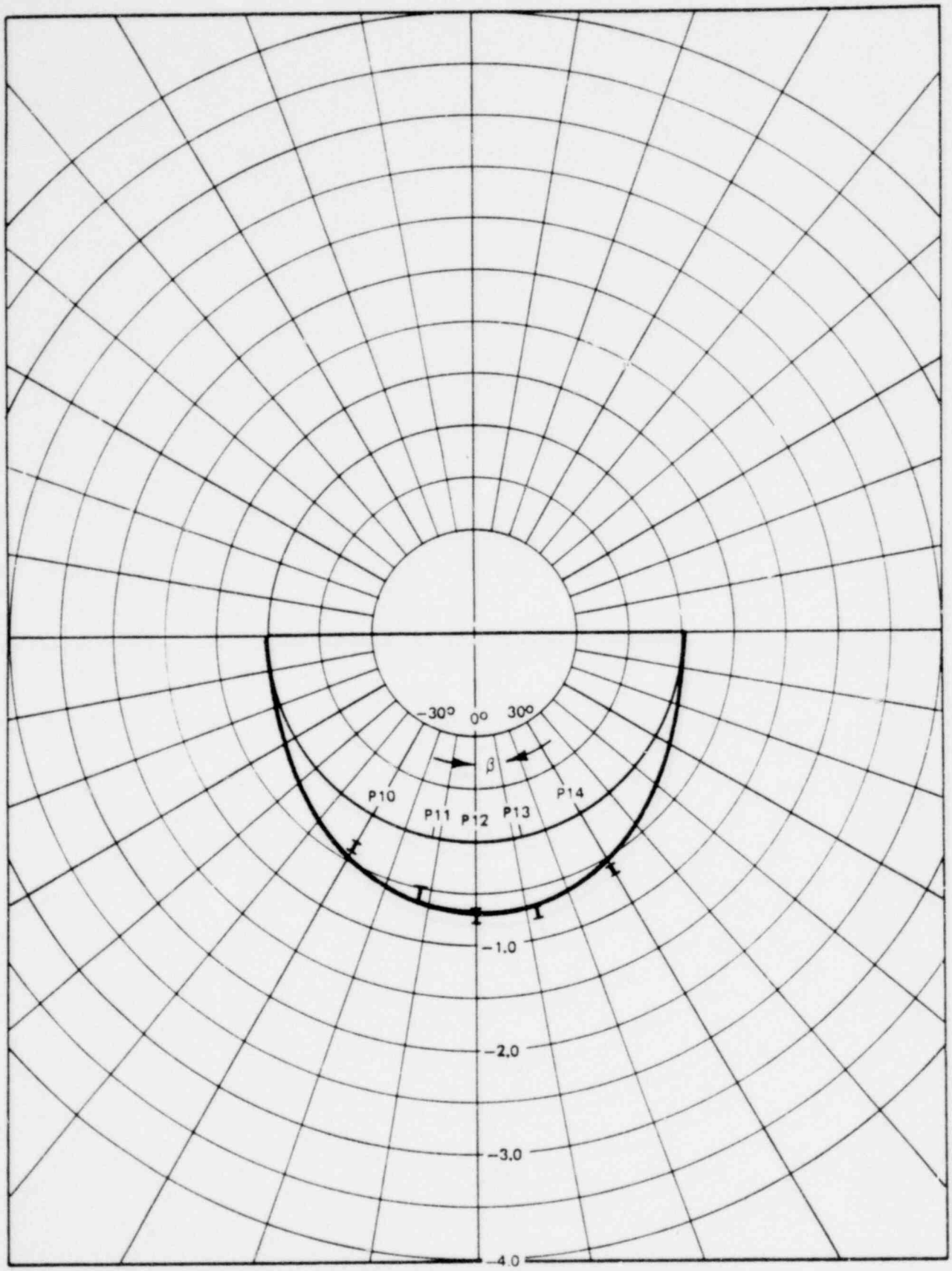

Figure 3-73. Peak Negative Pressure Distribution For 1/4 Scale Test Case 15 @ α = 0.0748

1764 296

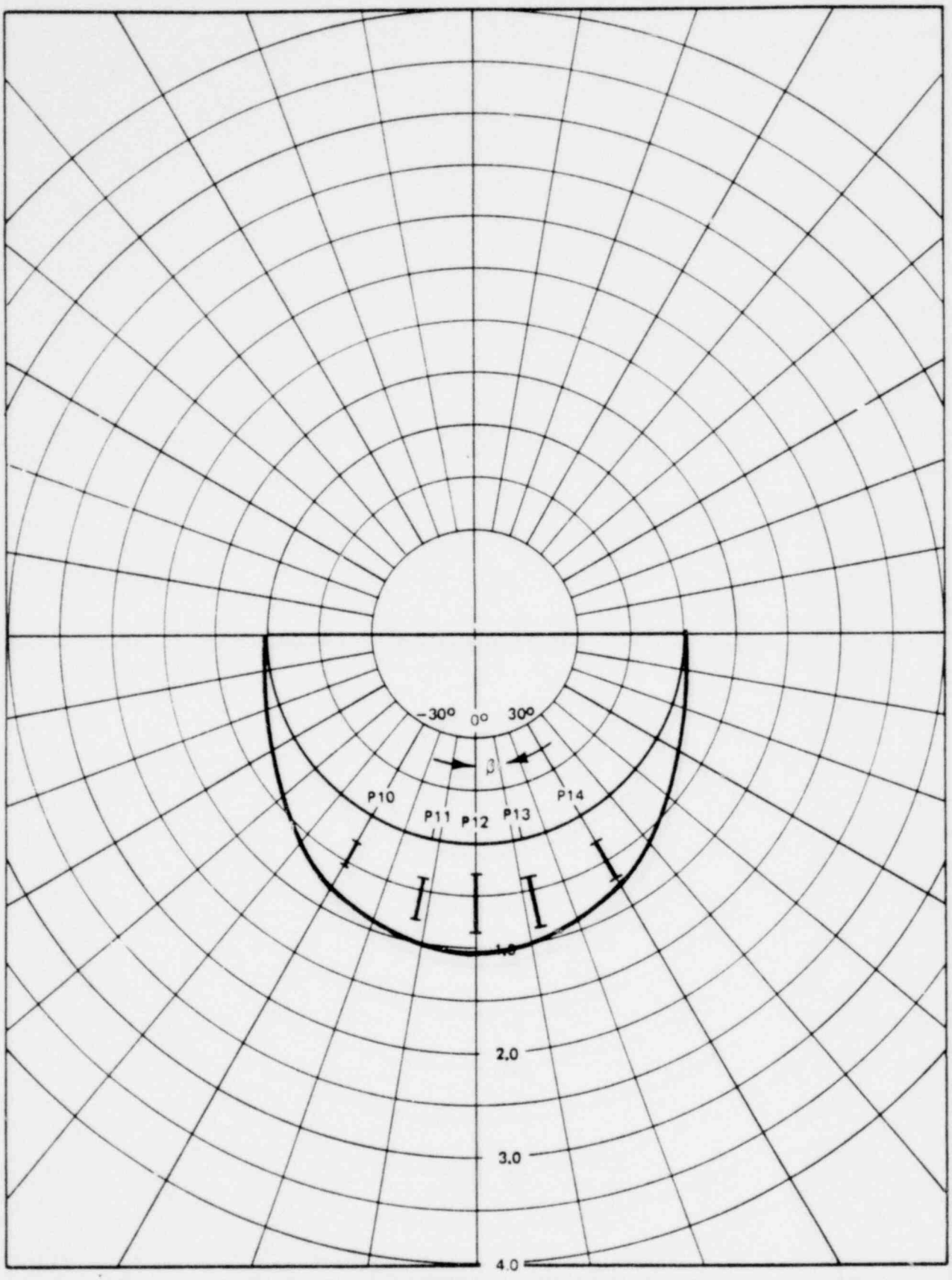

Figure 3-74. Peak Positive Pressure Distribution For 1/4 Scale Test Case 16 @ α = 0.748

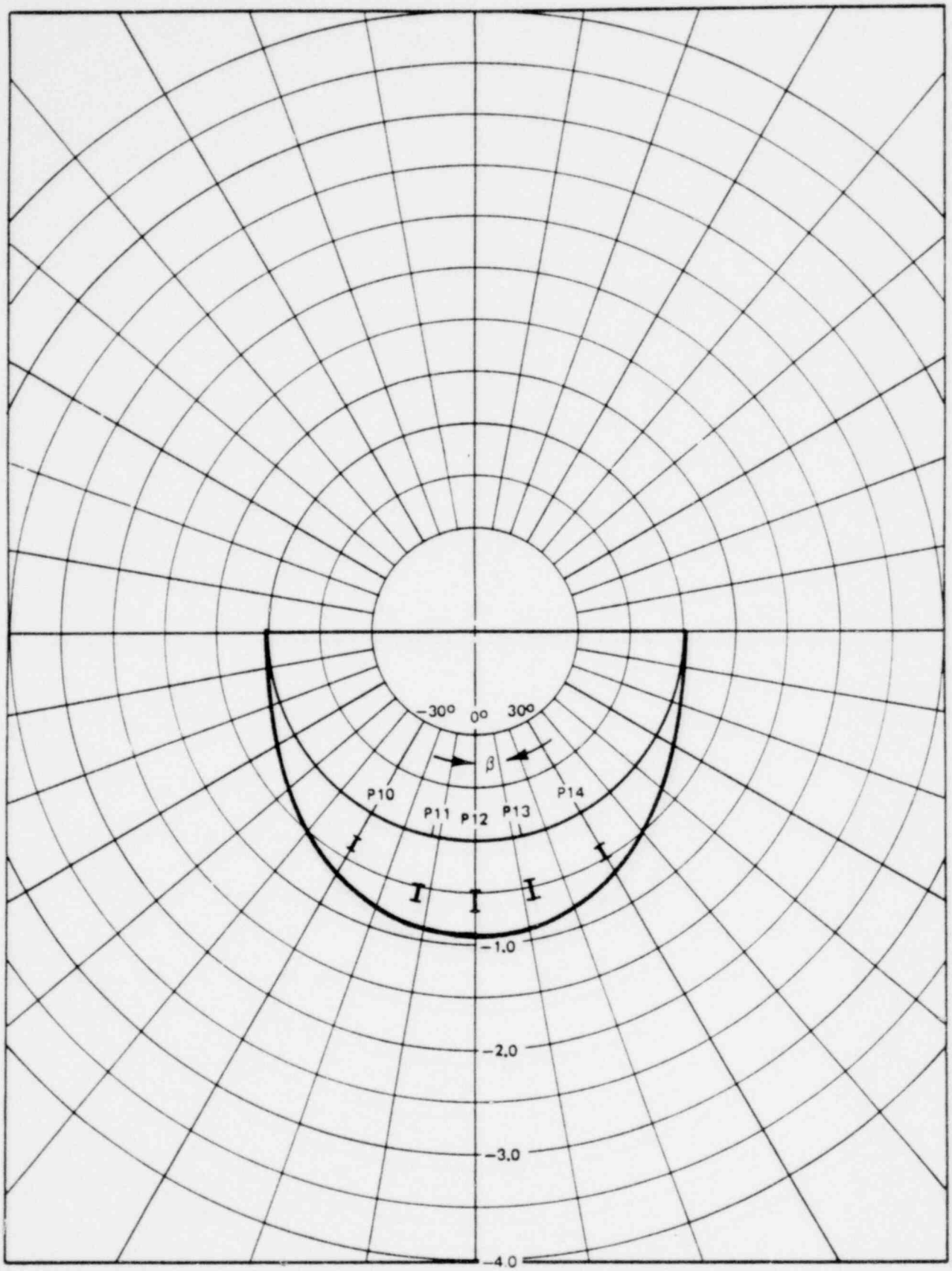

Figure 3-75. Peak Negative Pressure Distribution For 1/4 Scale Test Case 16 @ α = 0.0748

1764 298

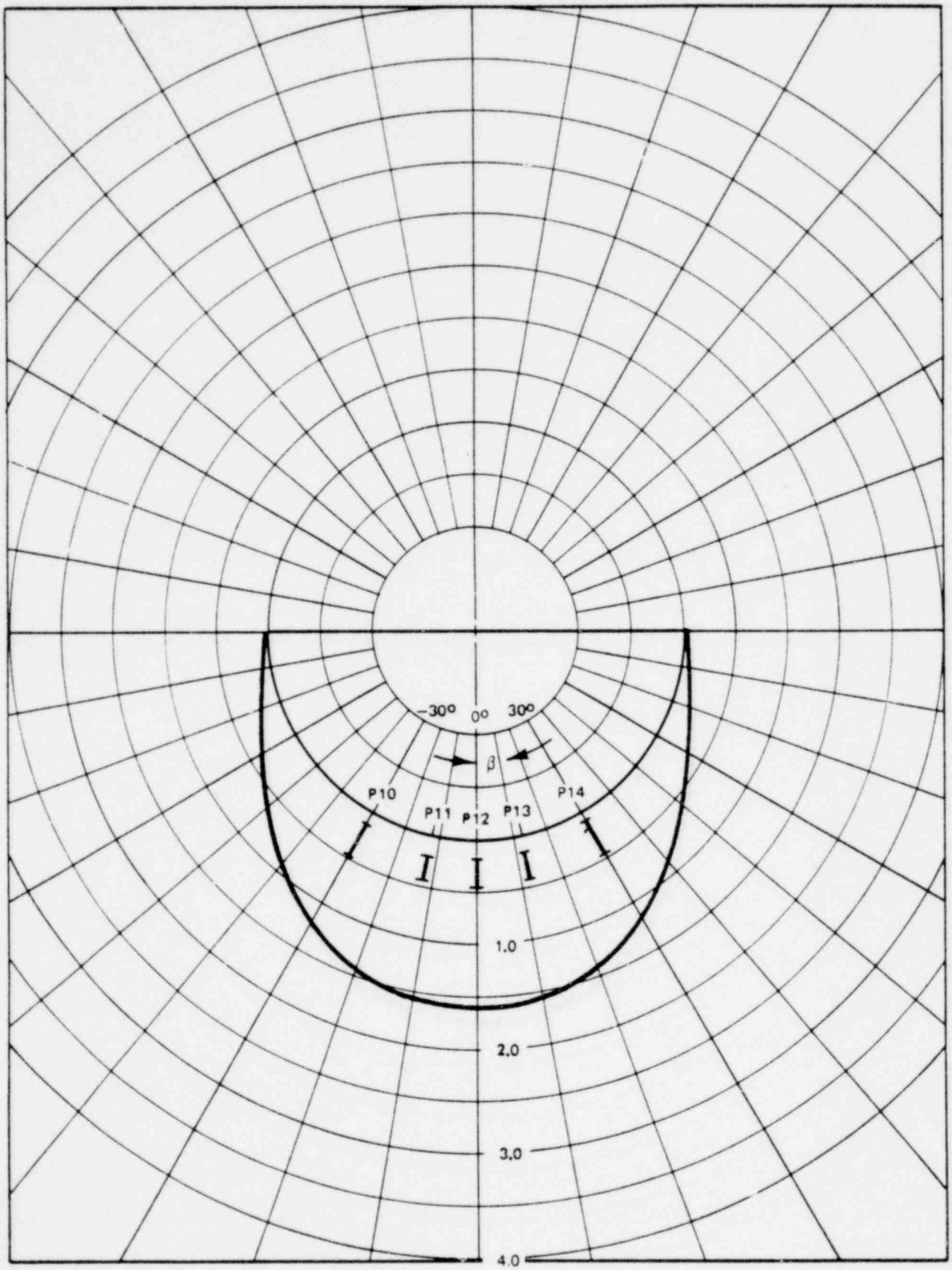

Figure 3-76. Peak Positive Pressure Distribution For 1/4 Scale Test Case 17 @ α = 0.0748

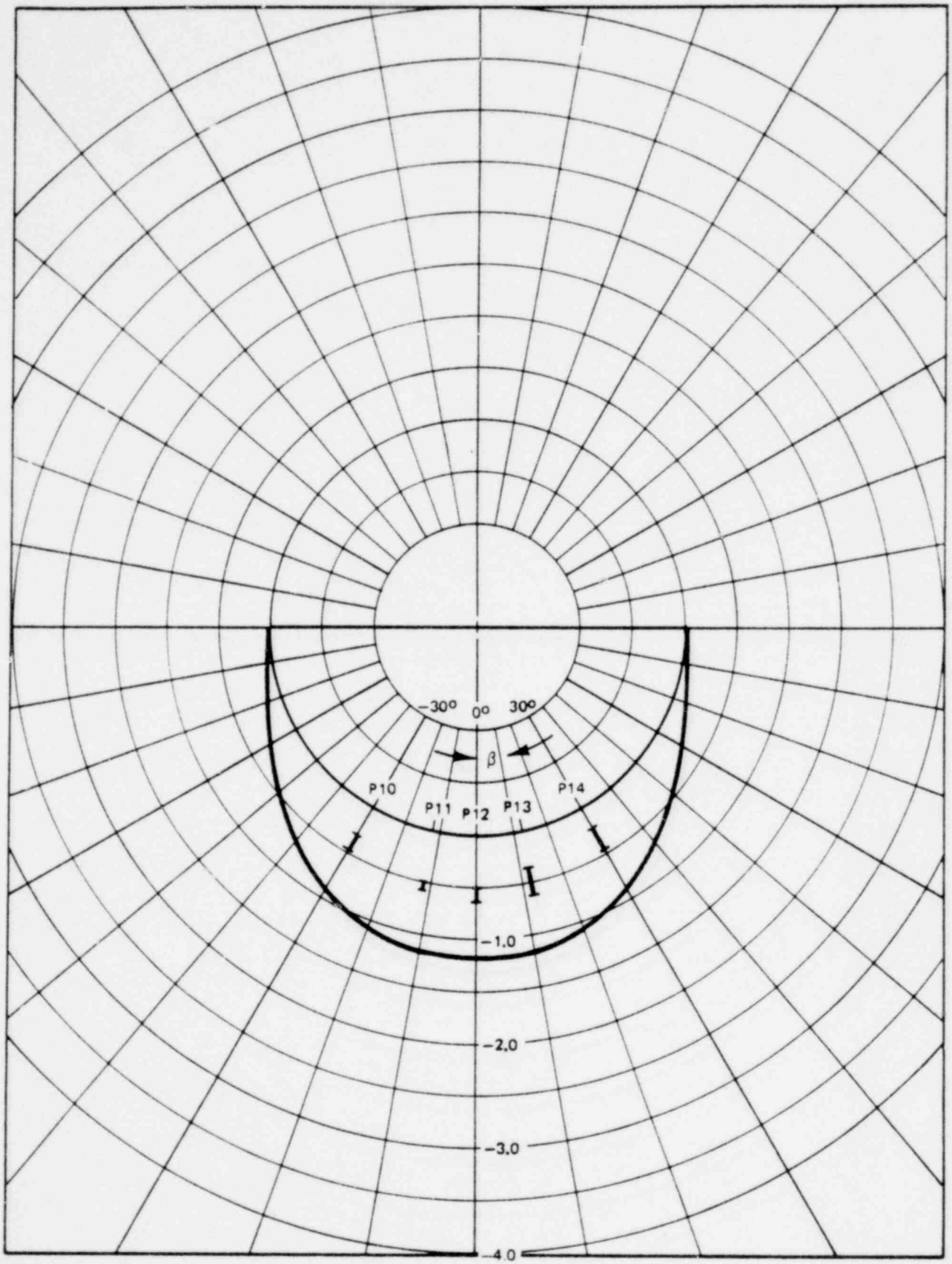

Figure 3-77. Peak Negative Pressure Distribution For 1/4 Scale Test 17 @ α = 0.0748

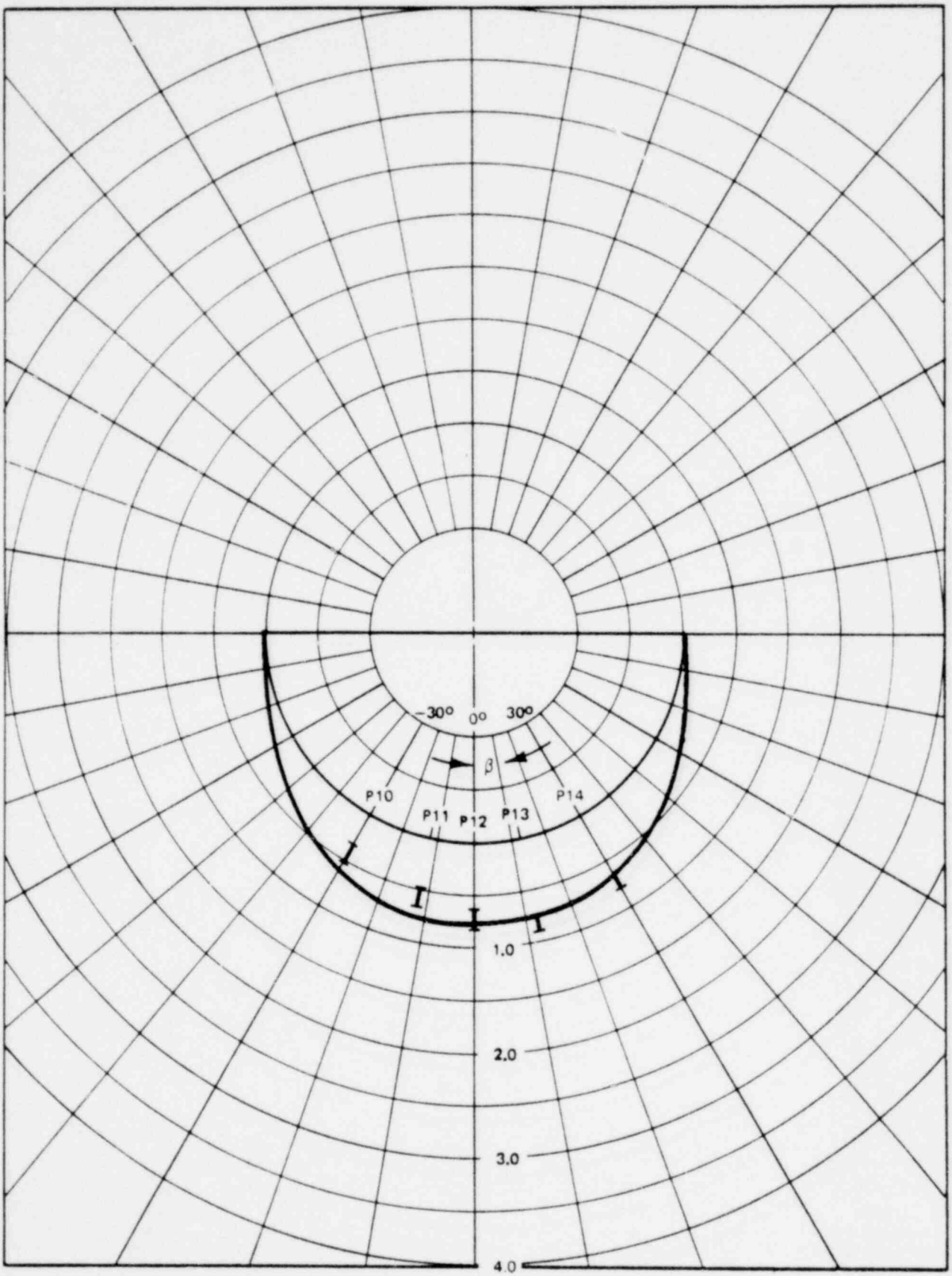

Figure 3-78. Peak Positive Pressure Distribution For 1/4 Scale Test Case 18 @ α = 0.0748

1764 301

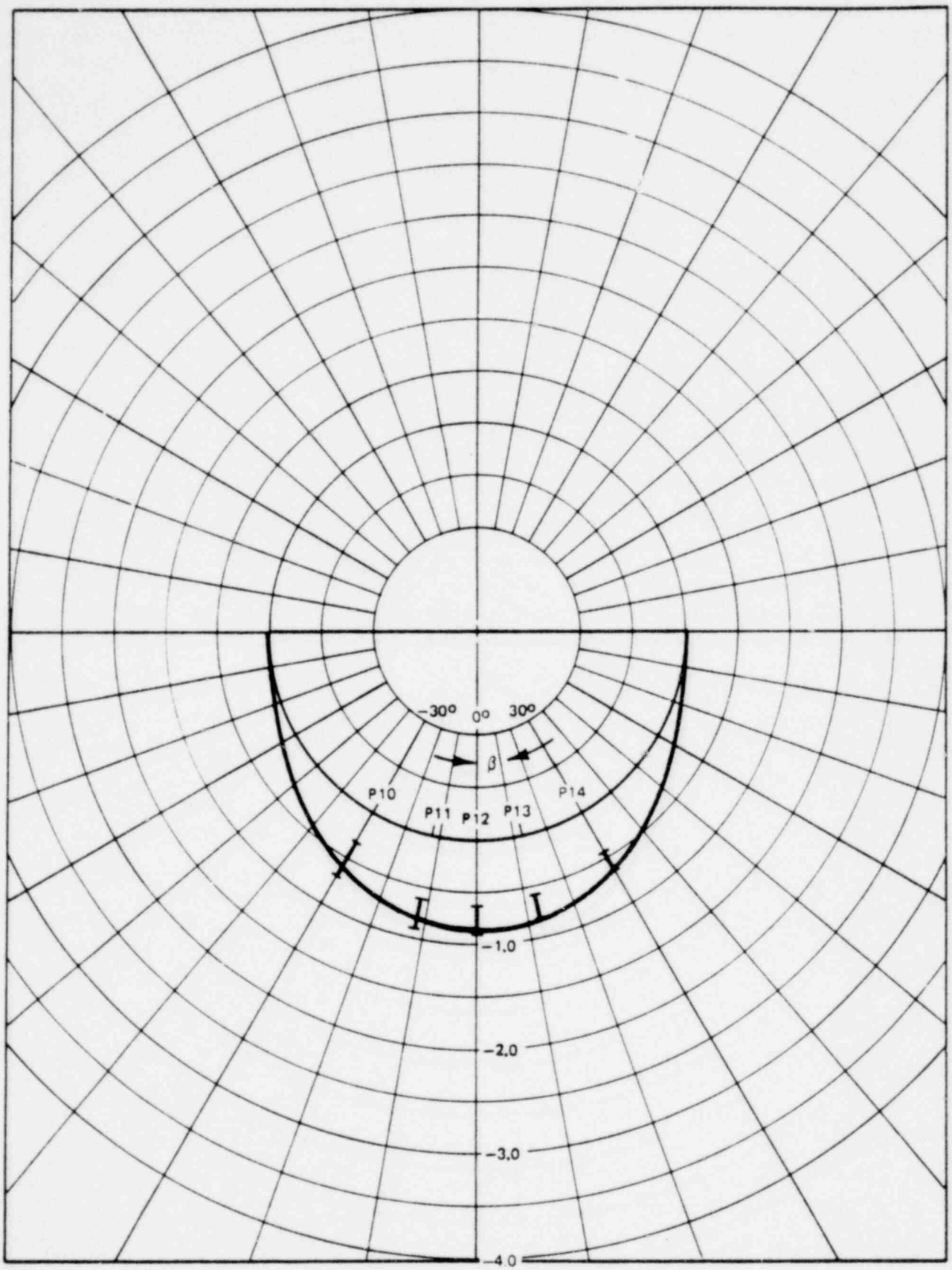

Figure 3-79. Peak Negative Pressure Distribution For 1/4 Scale Test Case 18 @ α = 0.0748

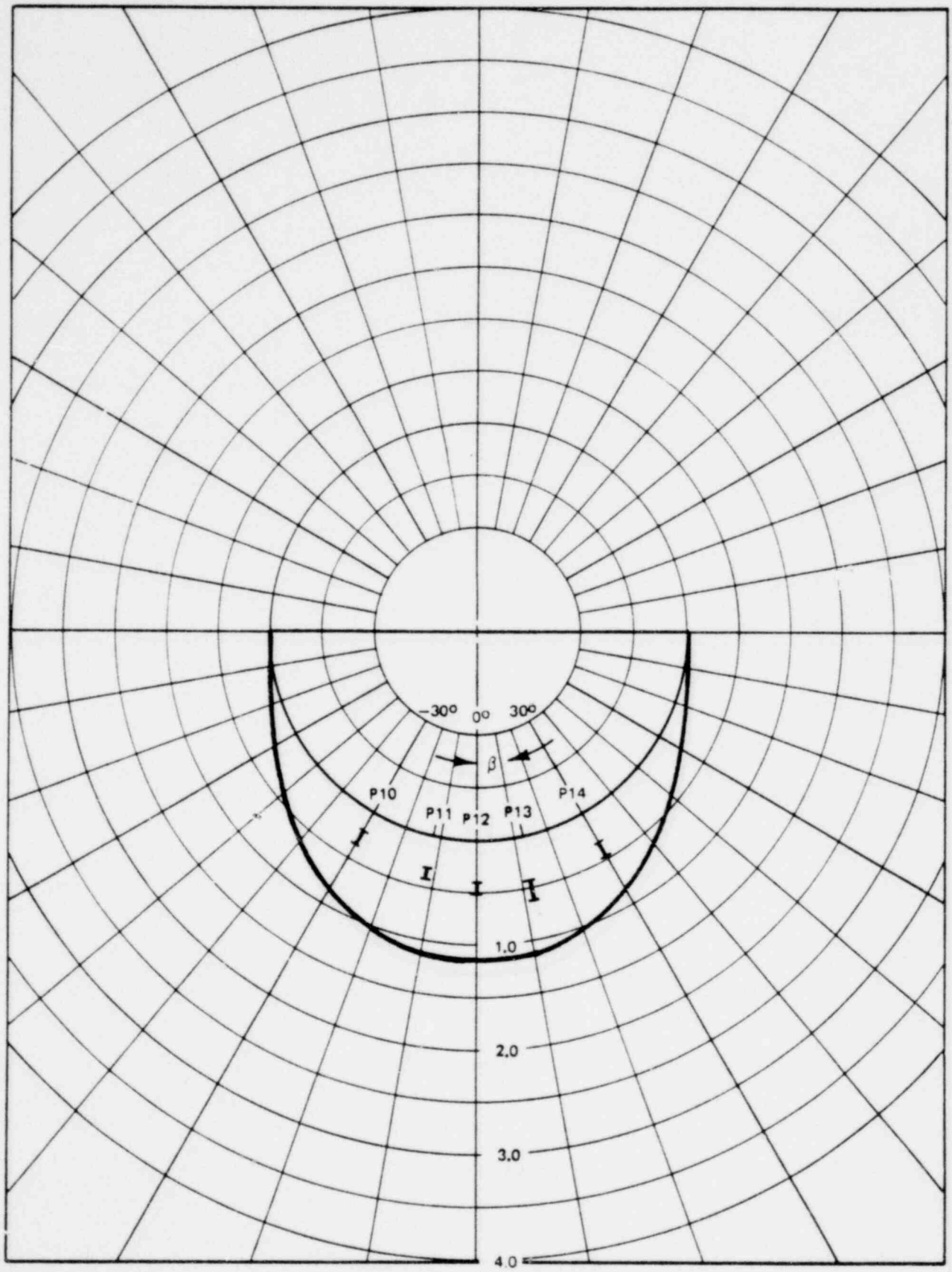

Figure 3-80. Peak Positive Pressure Distribution For 1/4 Scale Test Case 19 @ α = 0.0748

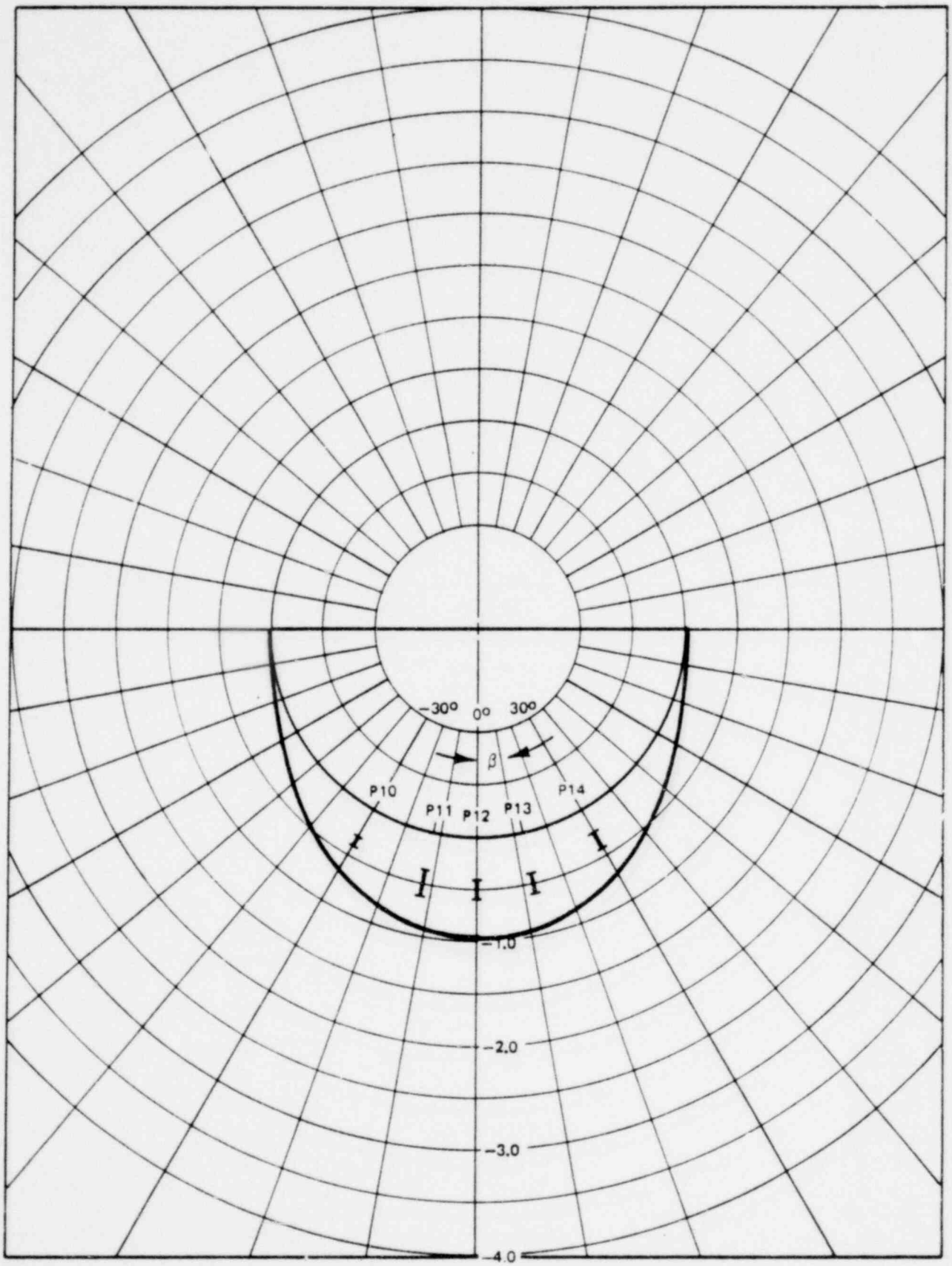

Figure 3-81. Peak Negative Pressure Distribution For 1/4 Scale Test Case 19 @ α = 0.0748

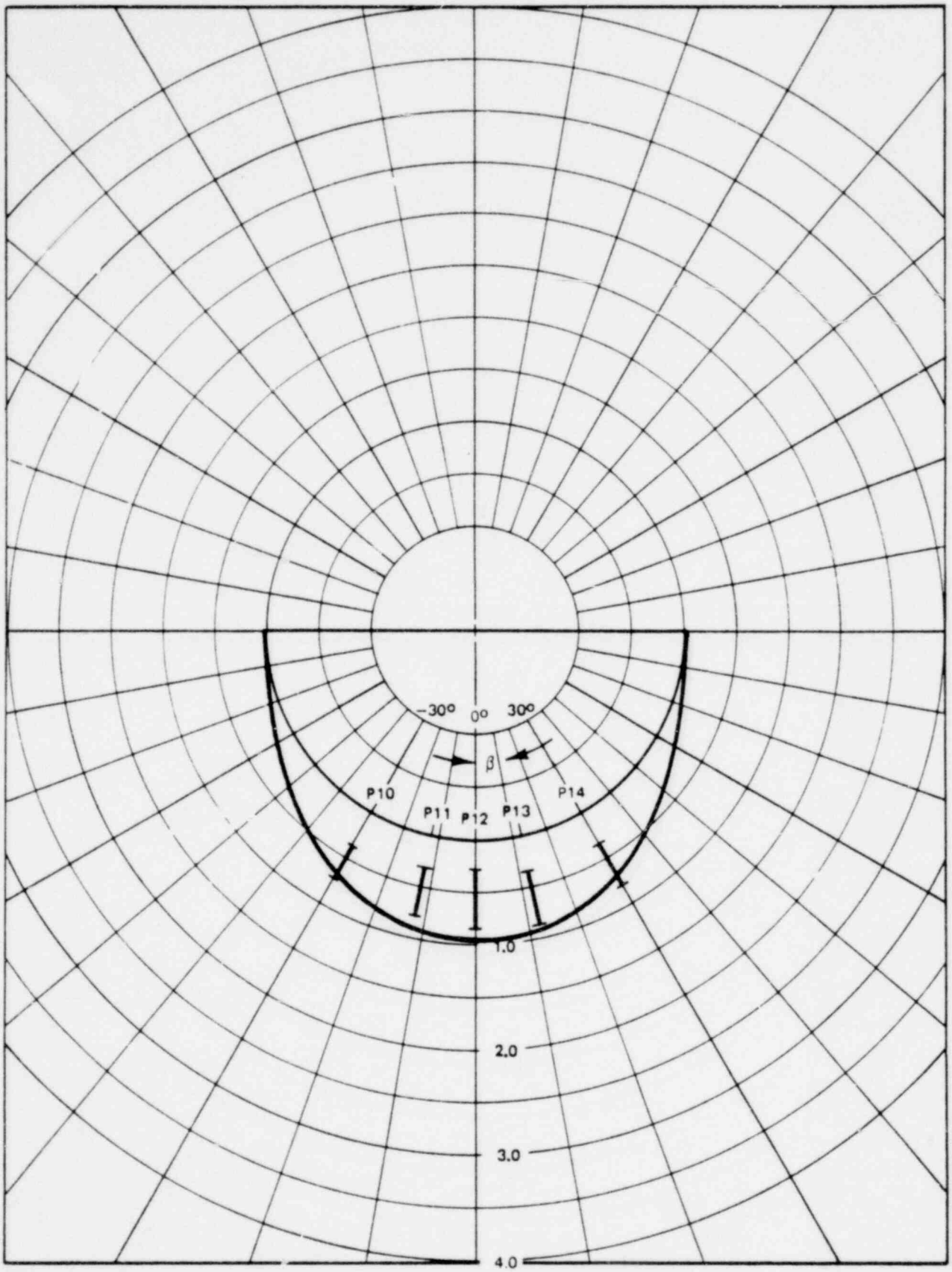

Figure 3-82. Peak Positive Pressure Distribution For 1/4 Scale Test Case 20 @ α = 0.0748

1764 505

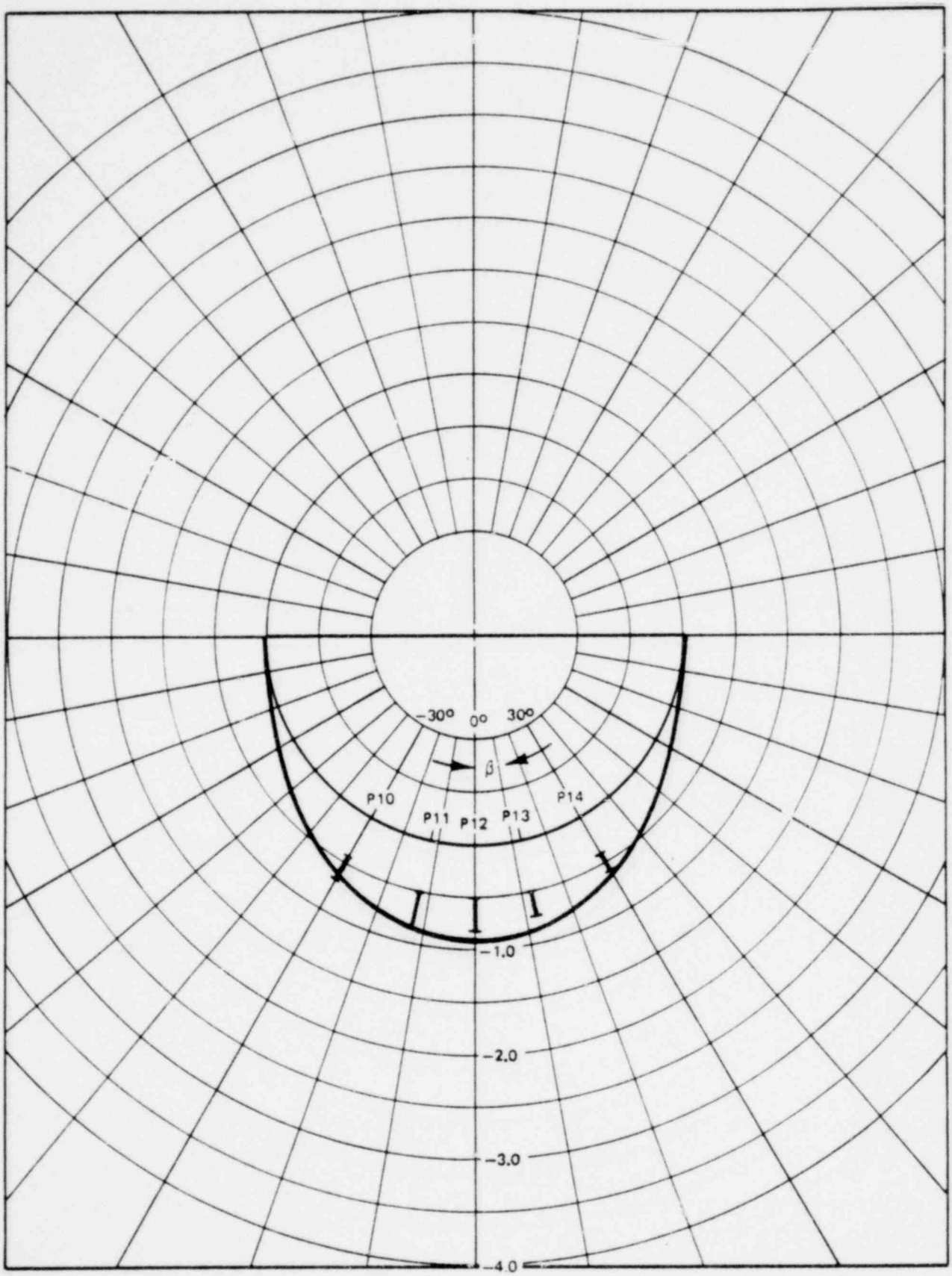

Figure 3-83. Peak Negative Pressure Distribution For 1/4 Scale Test Case 20 @ α = 0.0748

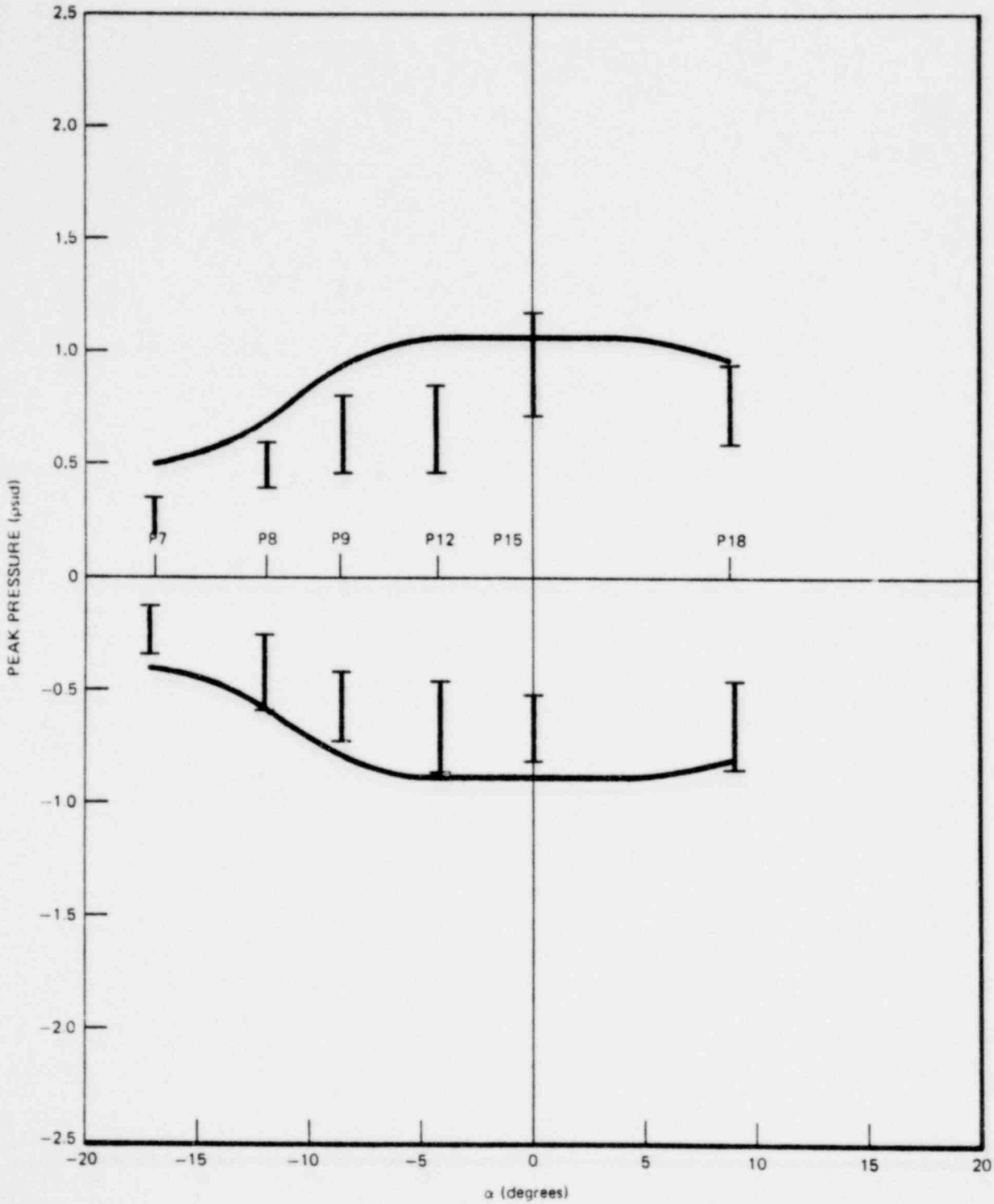

Figure 3-84. Peak Pressure Distribution For 1/4 Scale Test Case 1 @ β = 0.0

1764 307

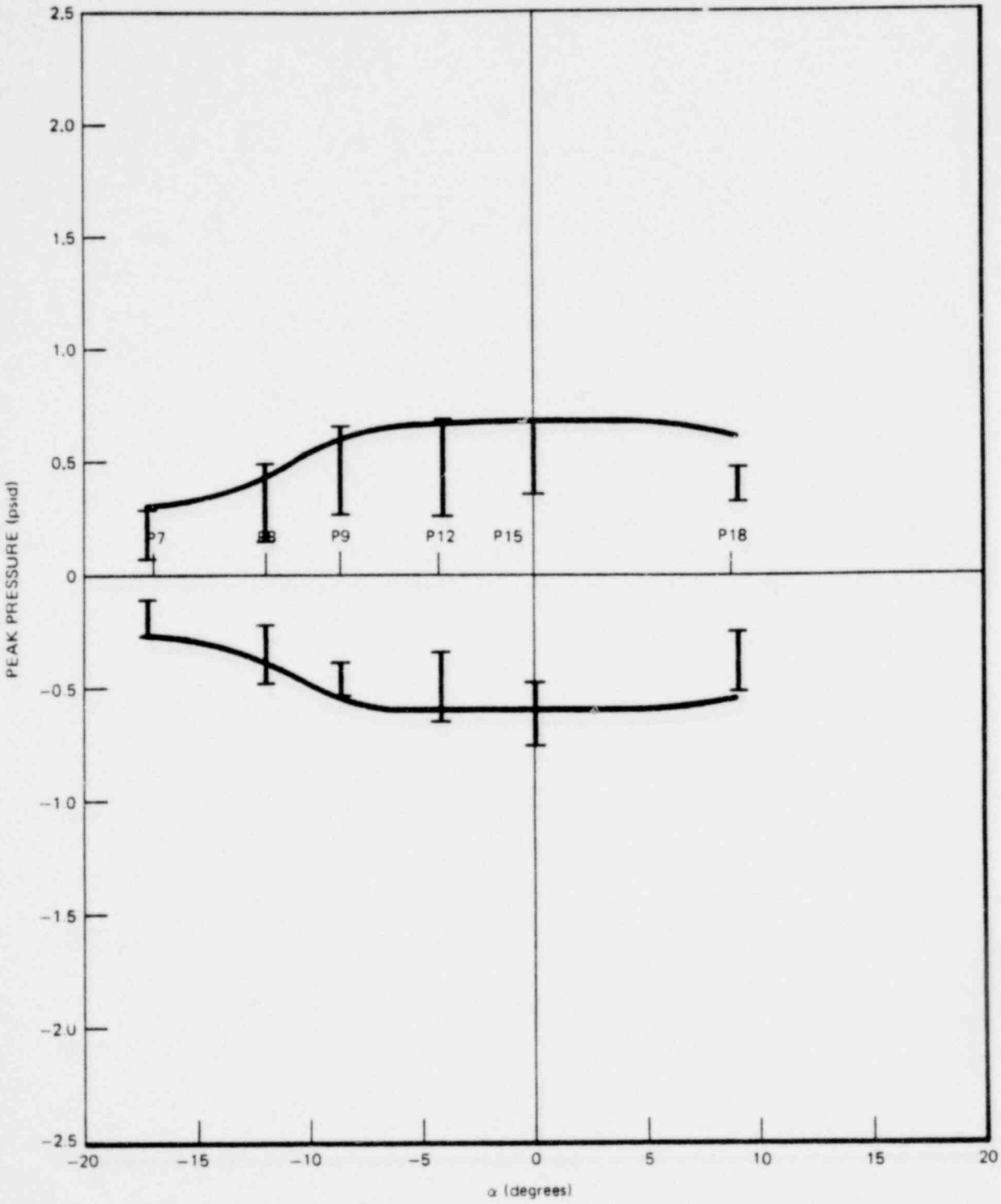

Figure 3-85. Peak Pressure Distribution For 1/4 Scale Test Case 2 @ β = 0.0

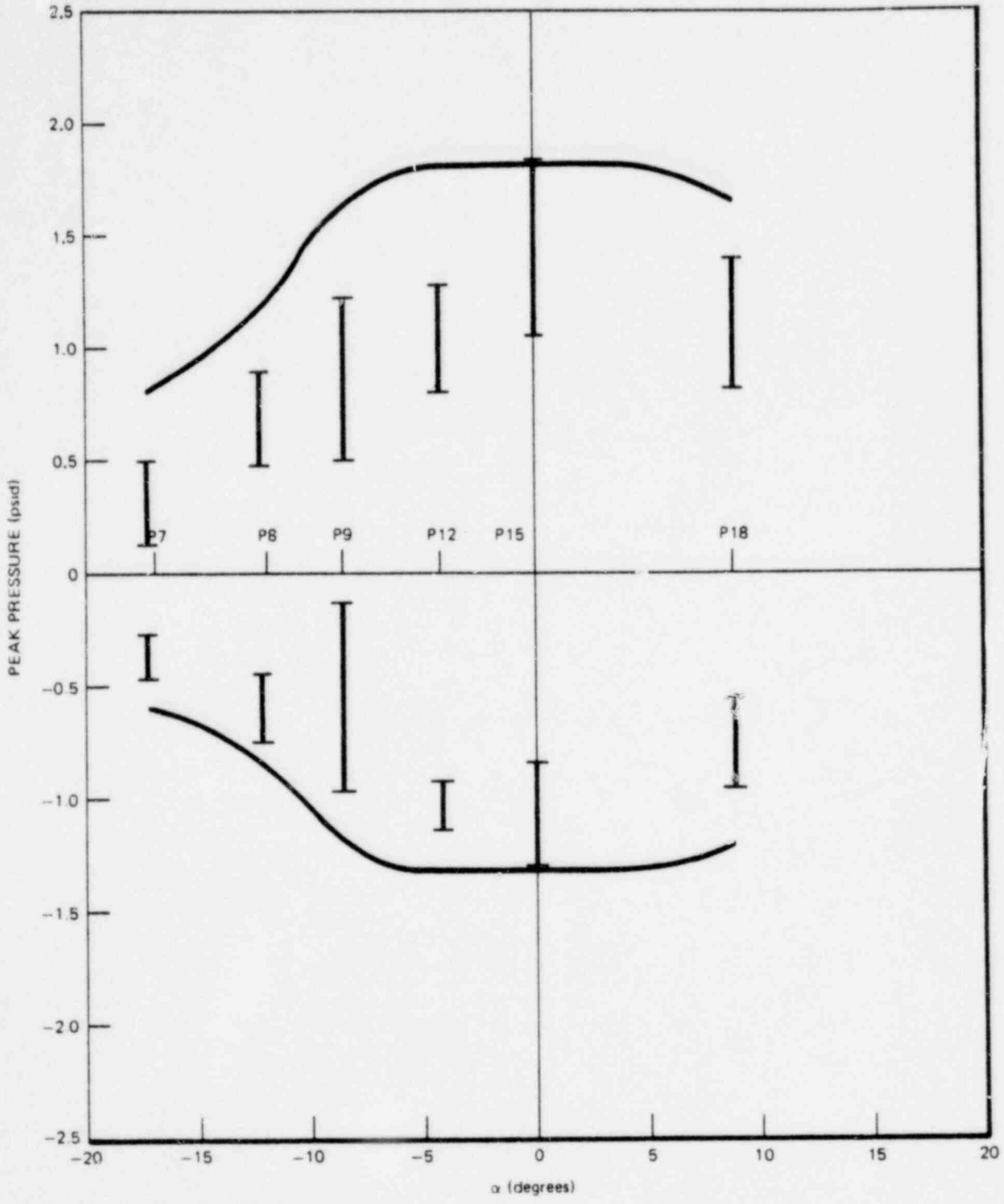

Figure 3-86. Peak Pressure Distribution For 1/4 Scale Test Case 3 @ β = 0.0

1764 309

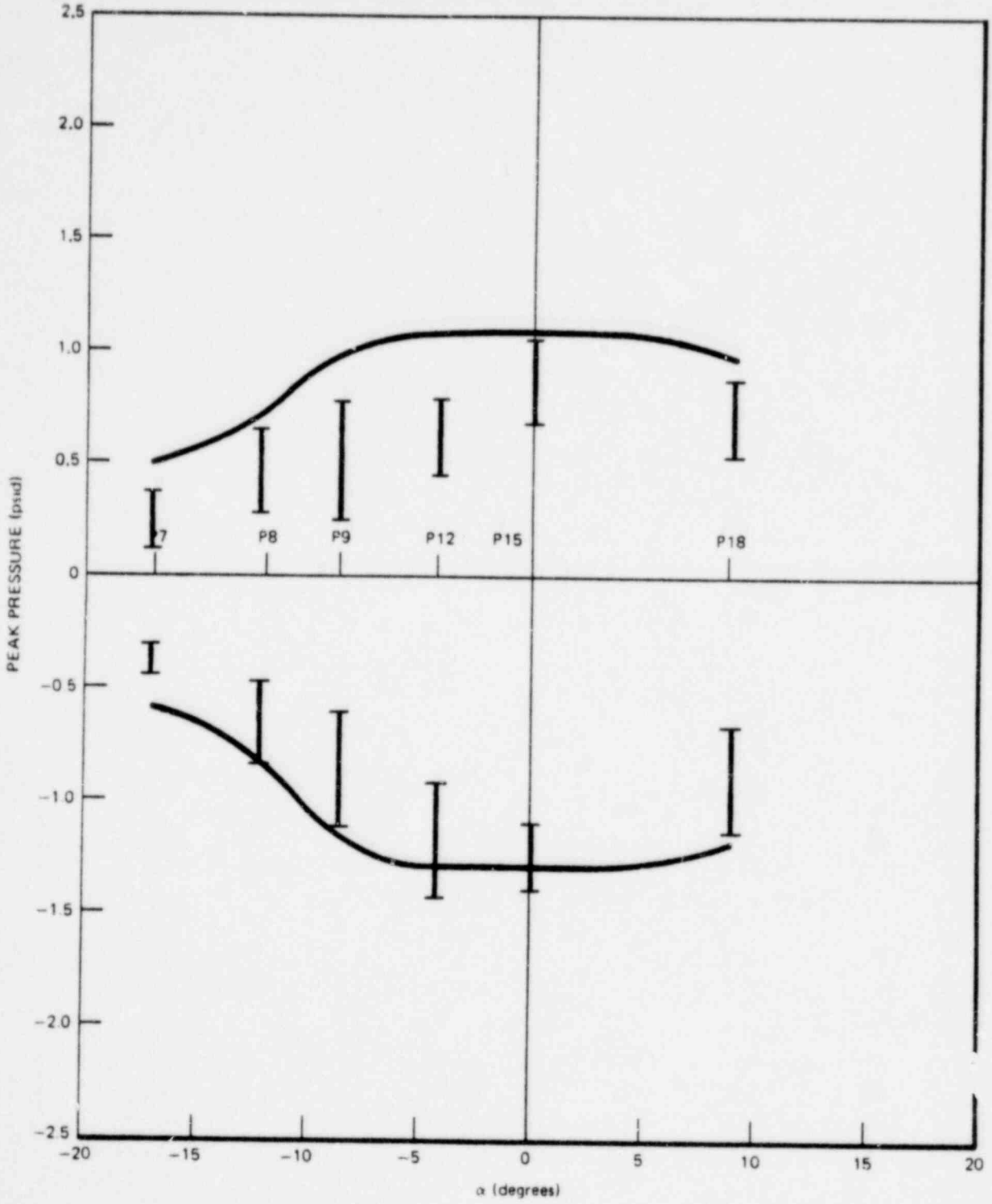

Figure 3-87. Peak Pressure Distribution For 1/4 Scale Test Case 4 @ β = 0.0

1764 310

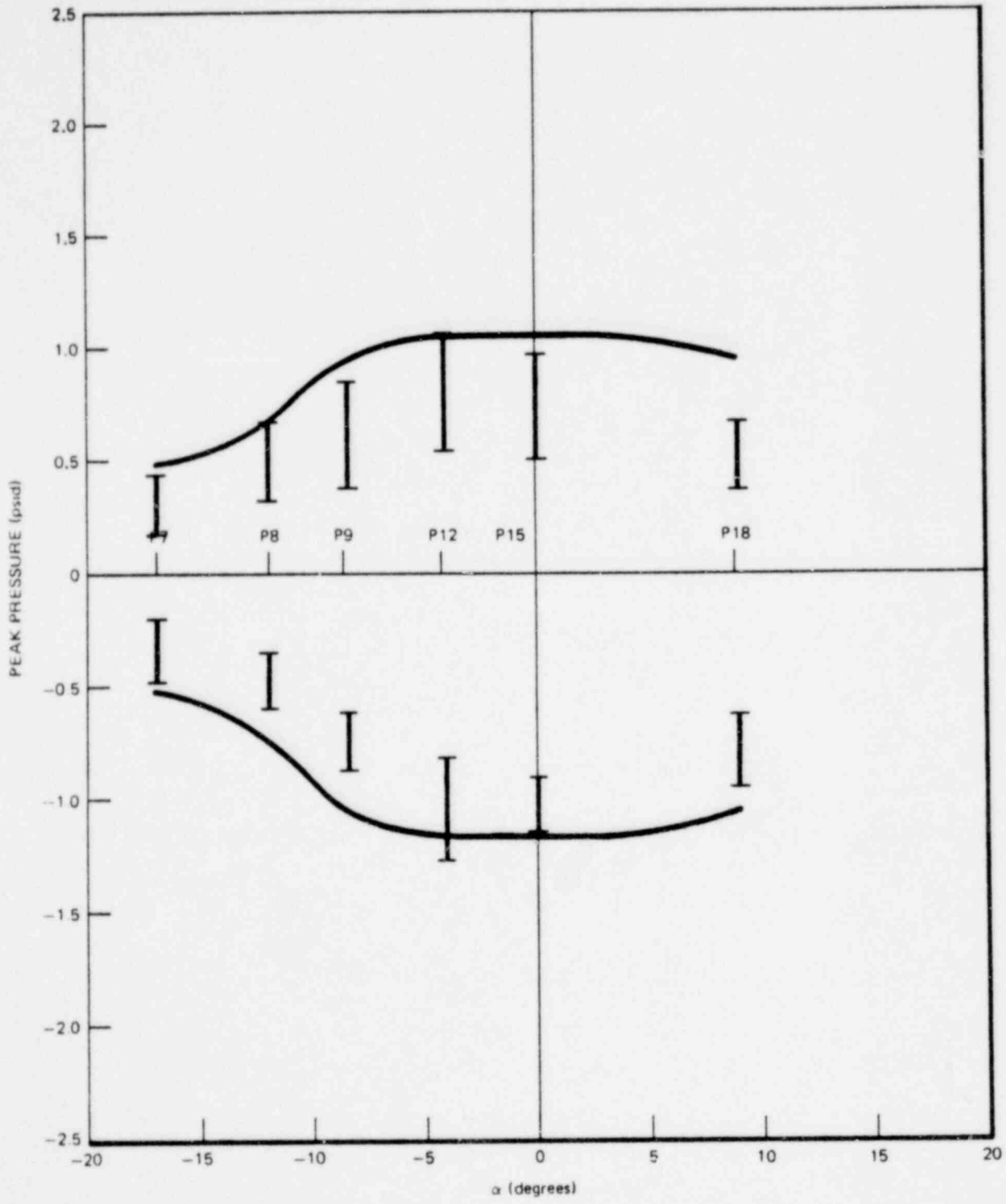

Figure 3-88. Peak Pressure Distribution For 1/4 Scale Test Case 4A @ β = 0.0

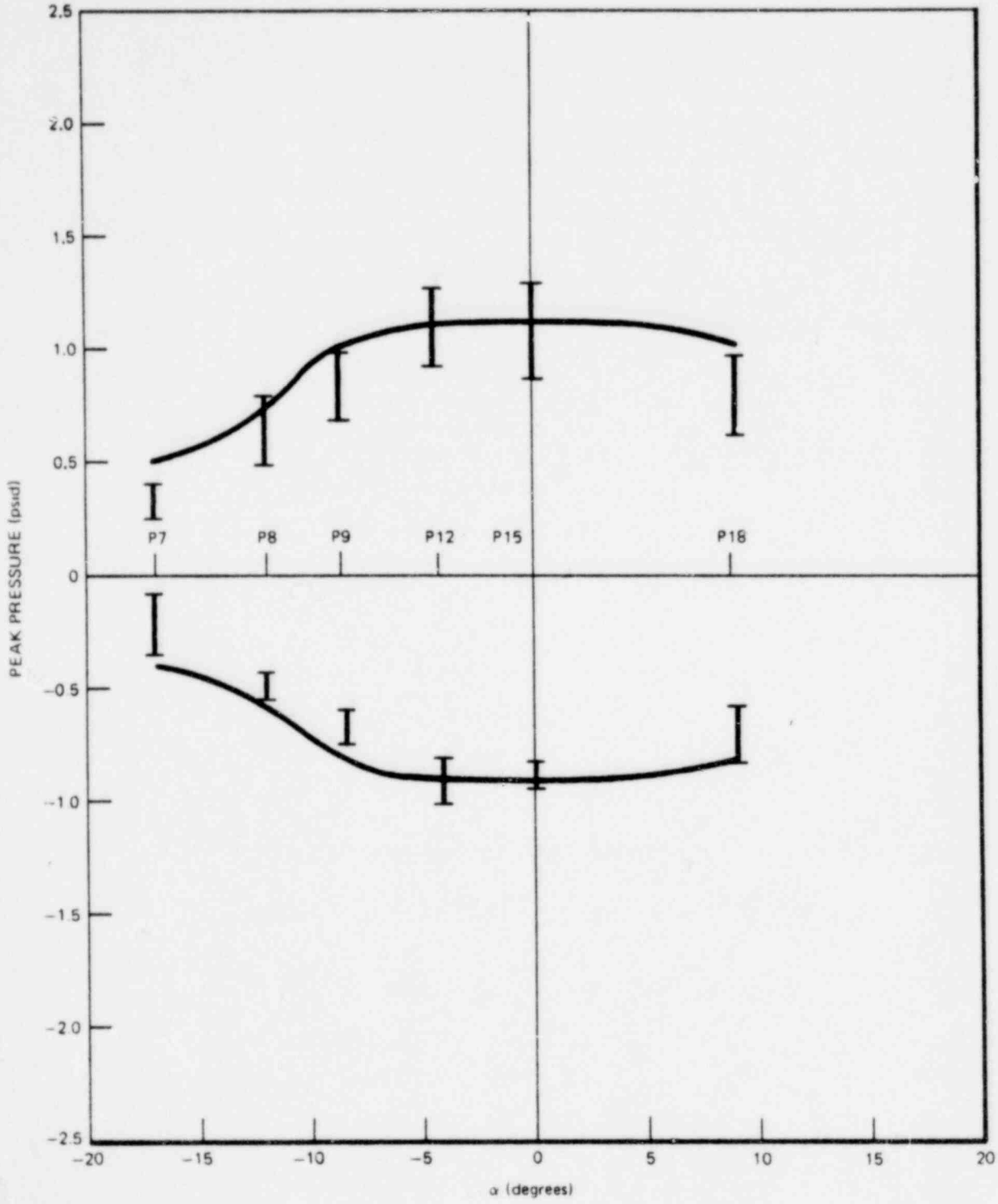

Figure 3-89. Peak Pressure Distribution For 1/4 Scale Test Case 5 @ β = 0.0

1764 312

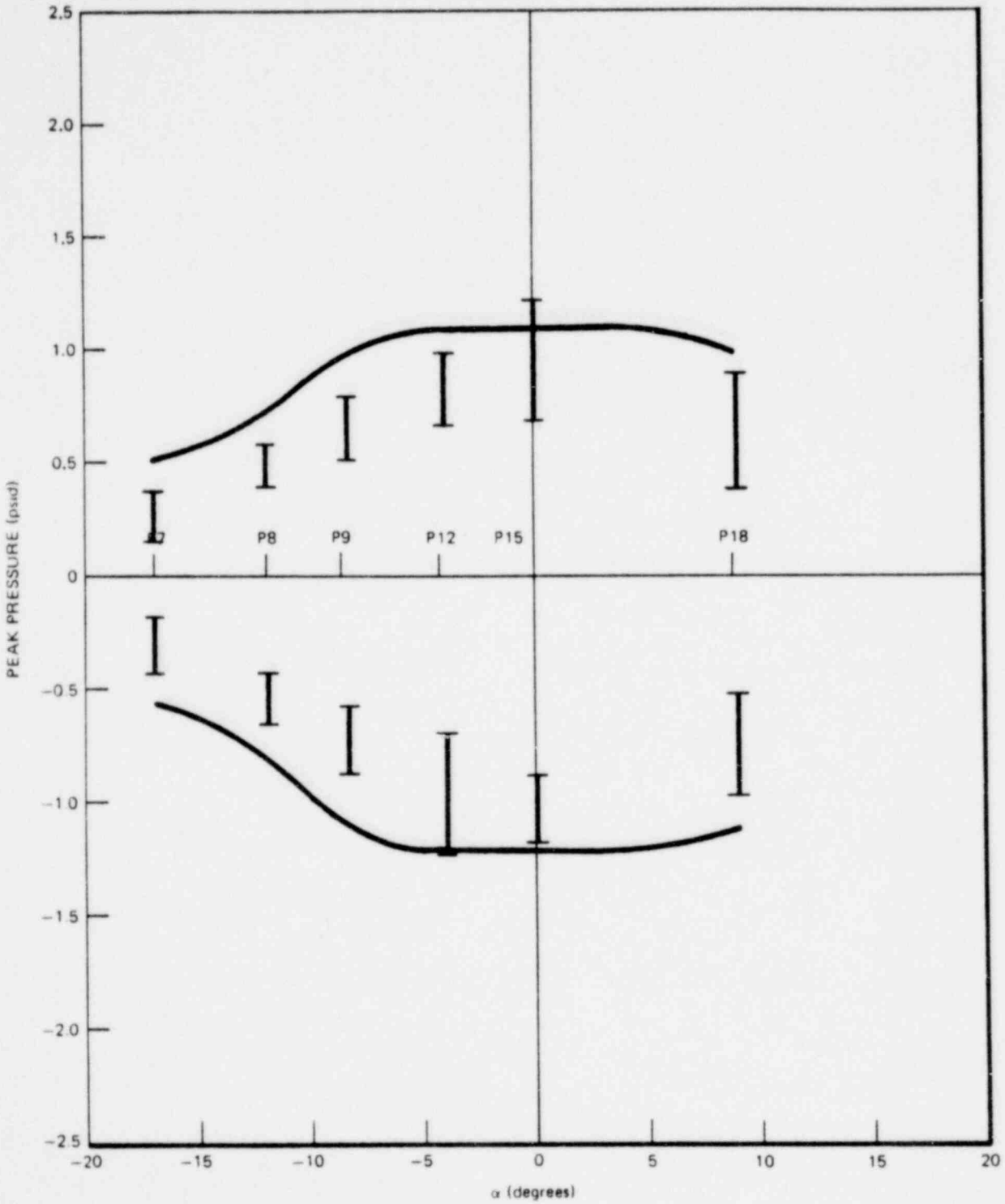

Figure 3-90. Peak Pressure Distribution For 1/4 Scale Test Case 6 and 6 A @ β = 0.0

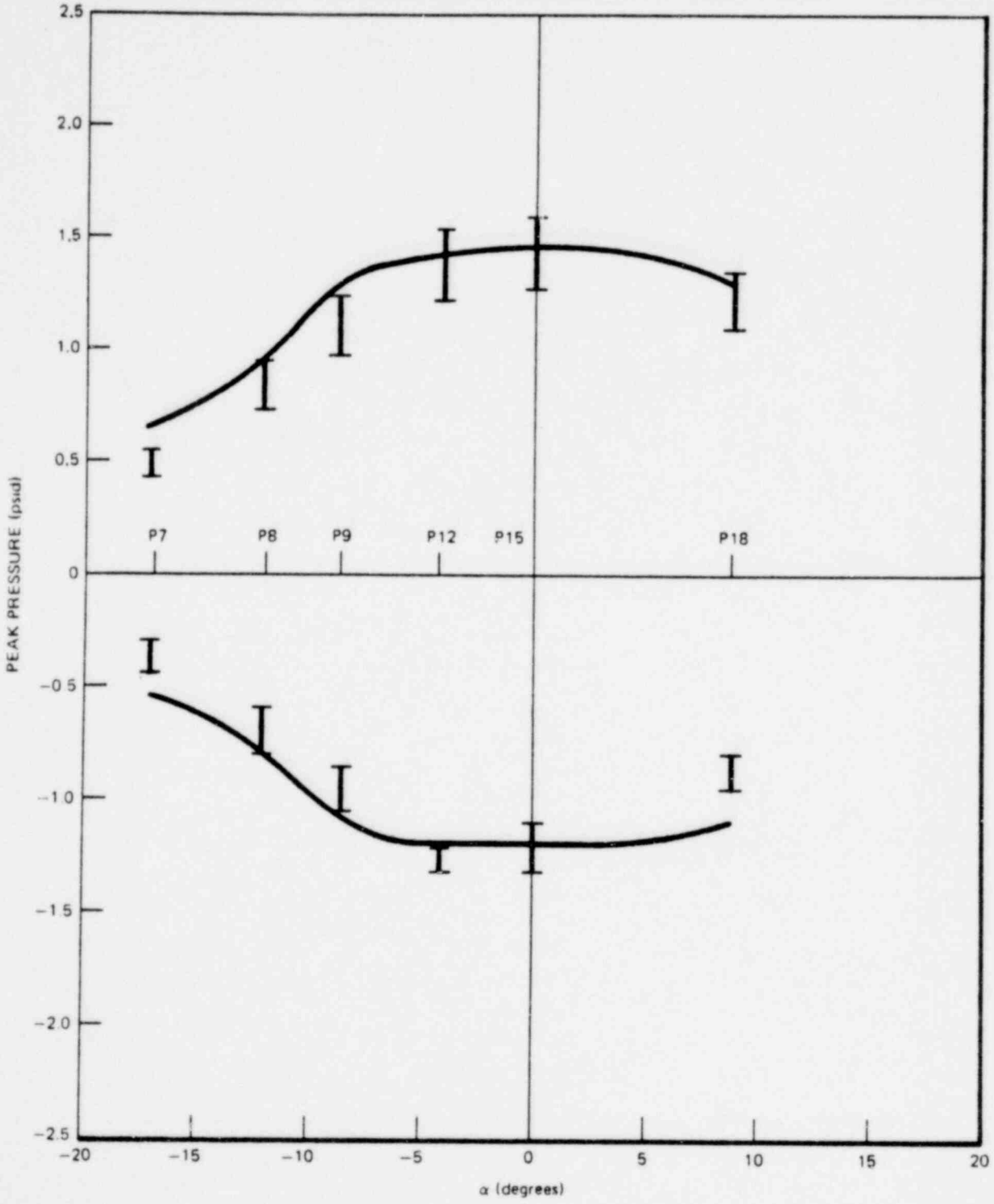

Figure 3-91. Peak Pressure Distribtuion For 1/4 Scale Test Case 7 @ β = 0.0

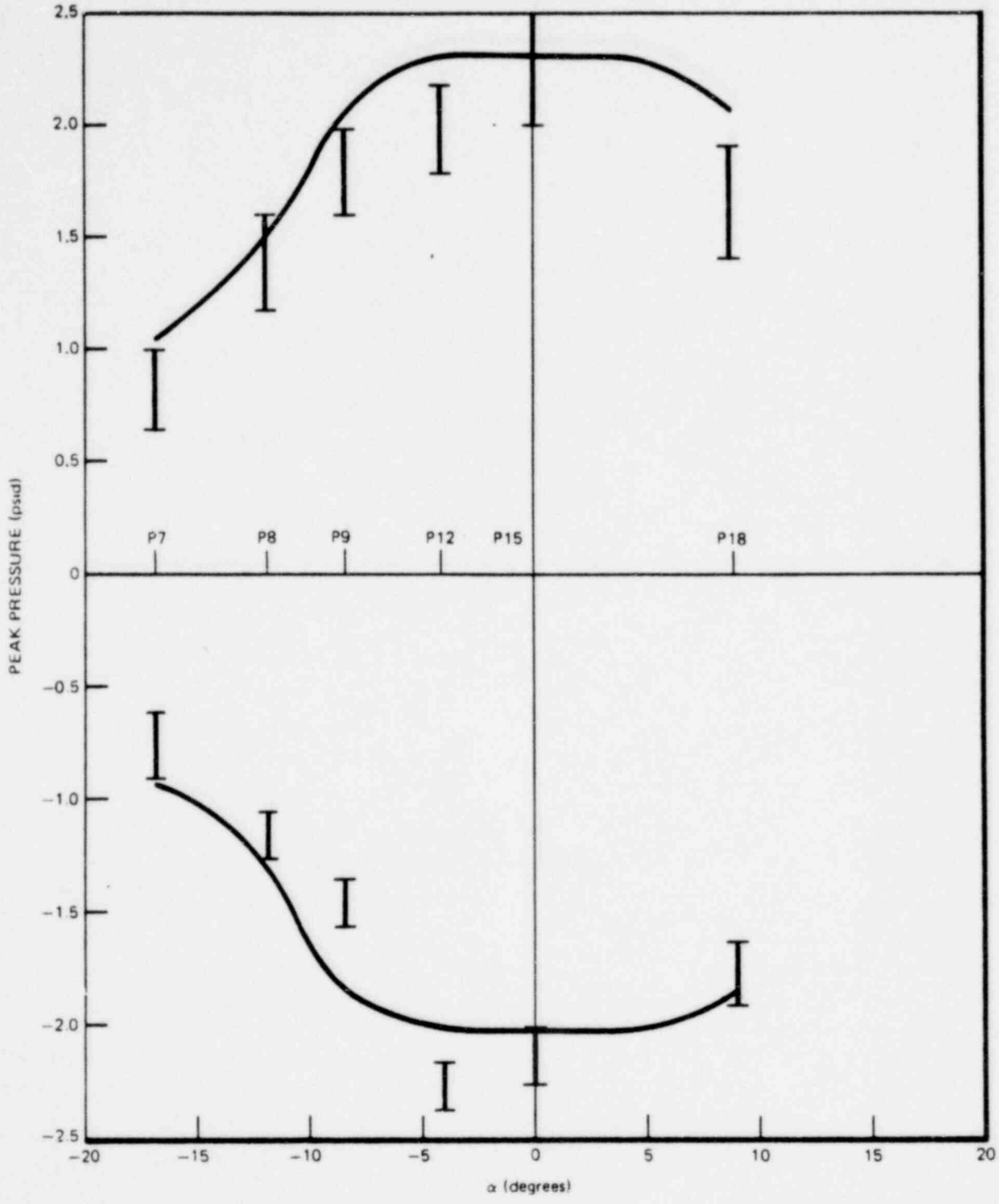

Figure 3-92. Peak Pressure Distribution For 1/4 Scale Test Case 8 @ β = 0.0

1764 315

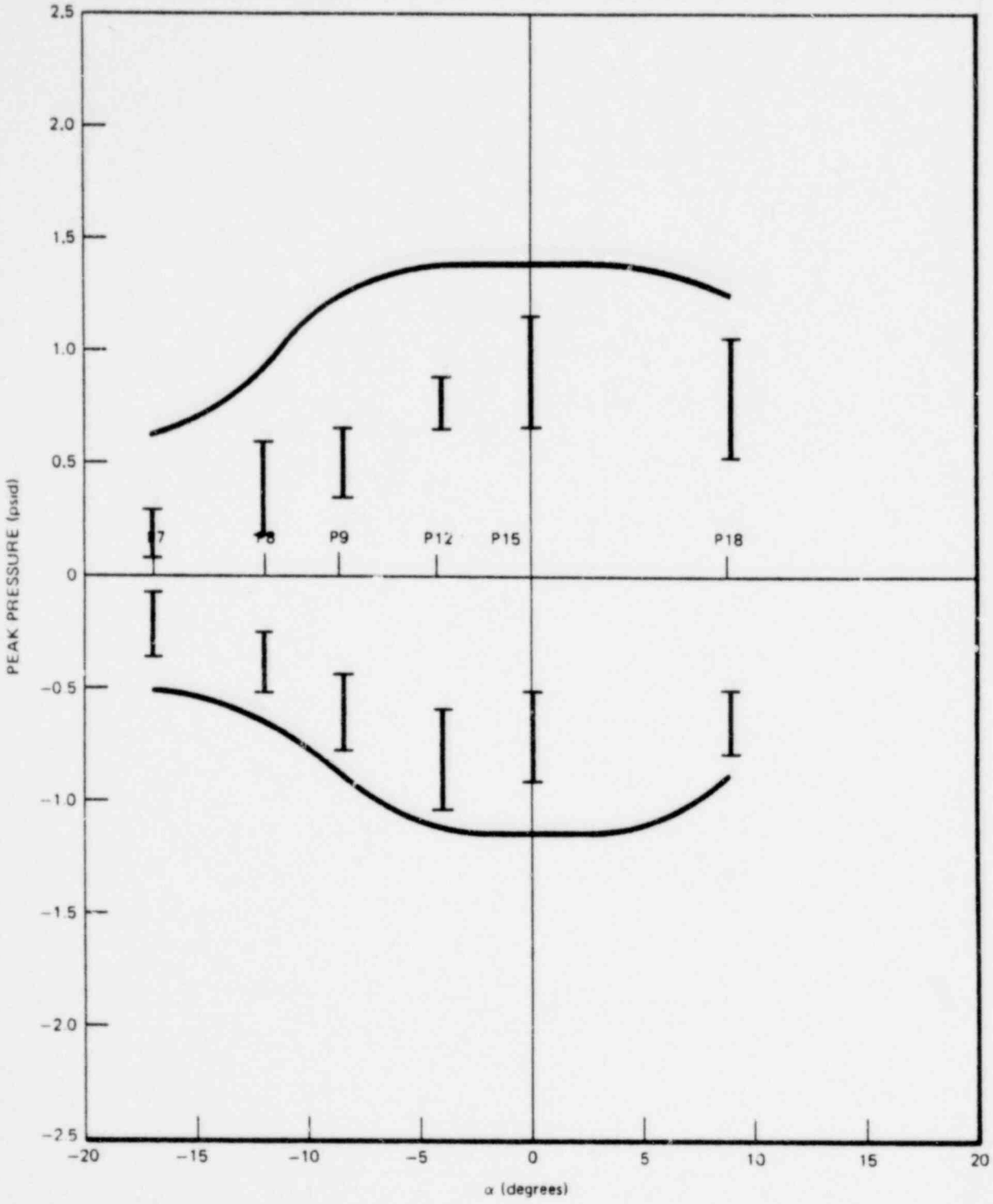

Figure 3-93. Peak Pressure Distribution For 1/4 Scale Test Cases 9 and 9A @ β = 0.0

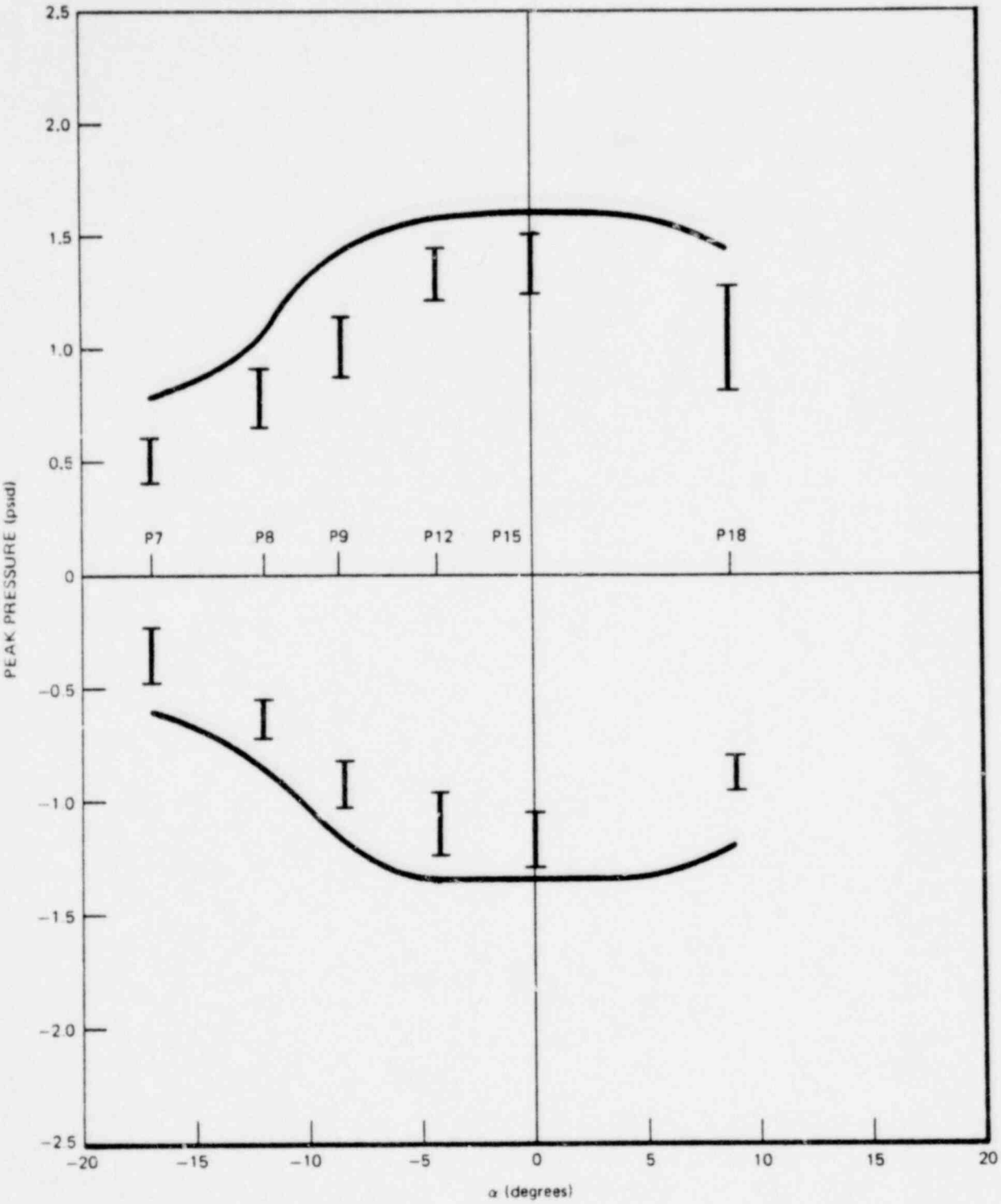

Figure 3-94. Peak Pressure Distribution For 1/4 Scale Test Case 10 @ β = 0.0

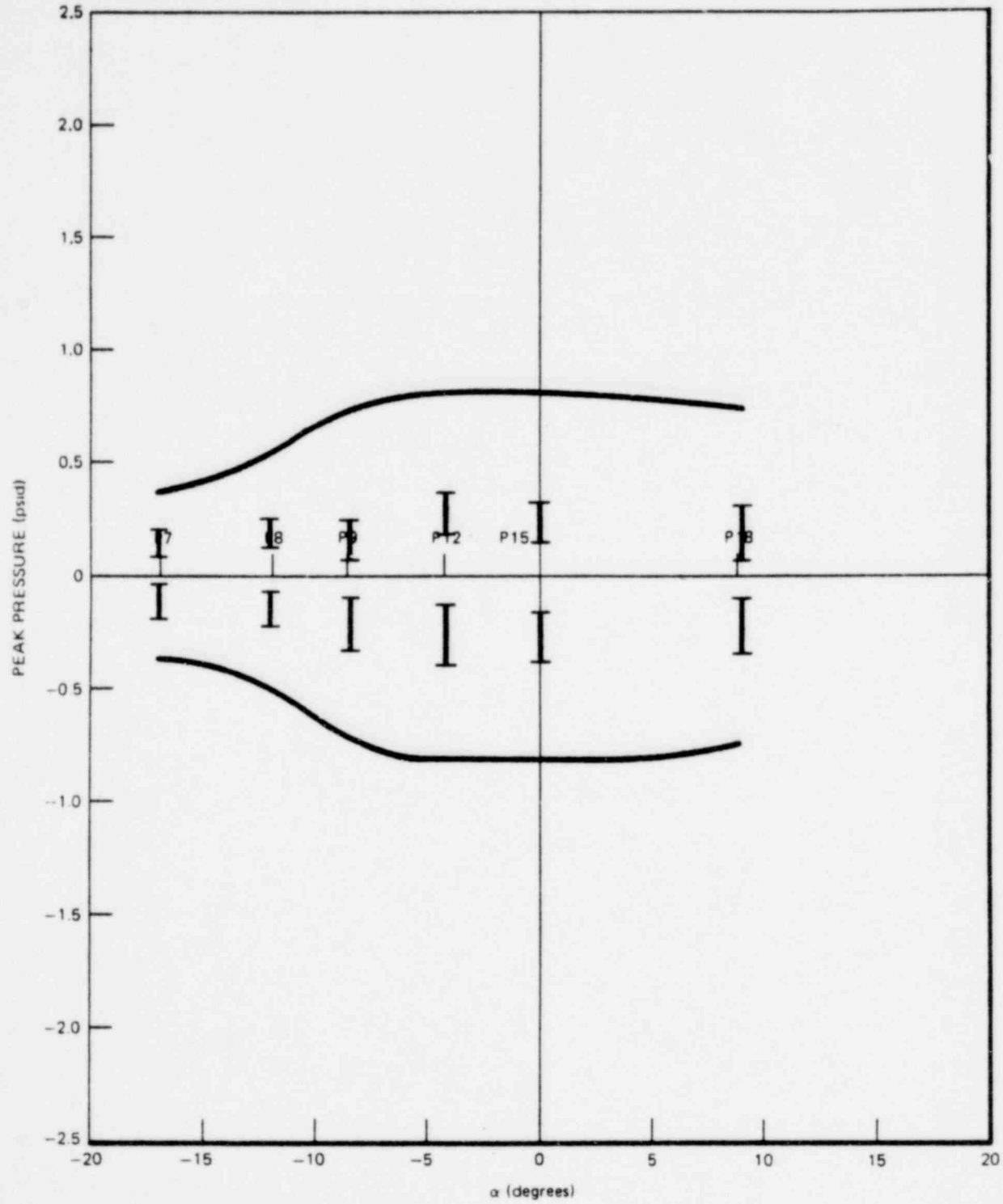

Figure 3-95. Peak Pressure Distribtuion For 1/4 Scale Test 11 @ β = 0.0

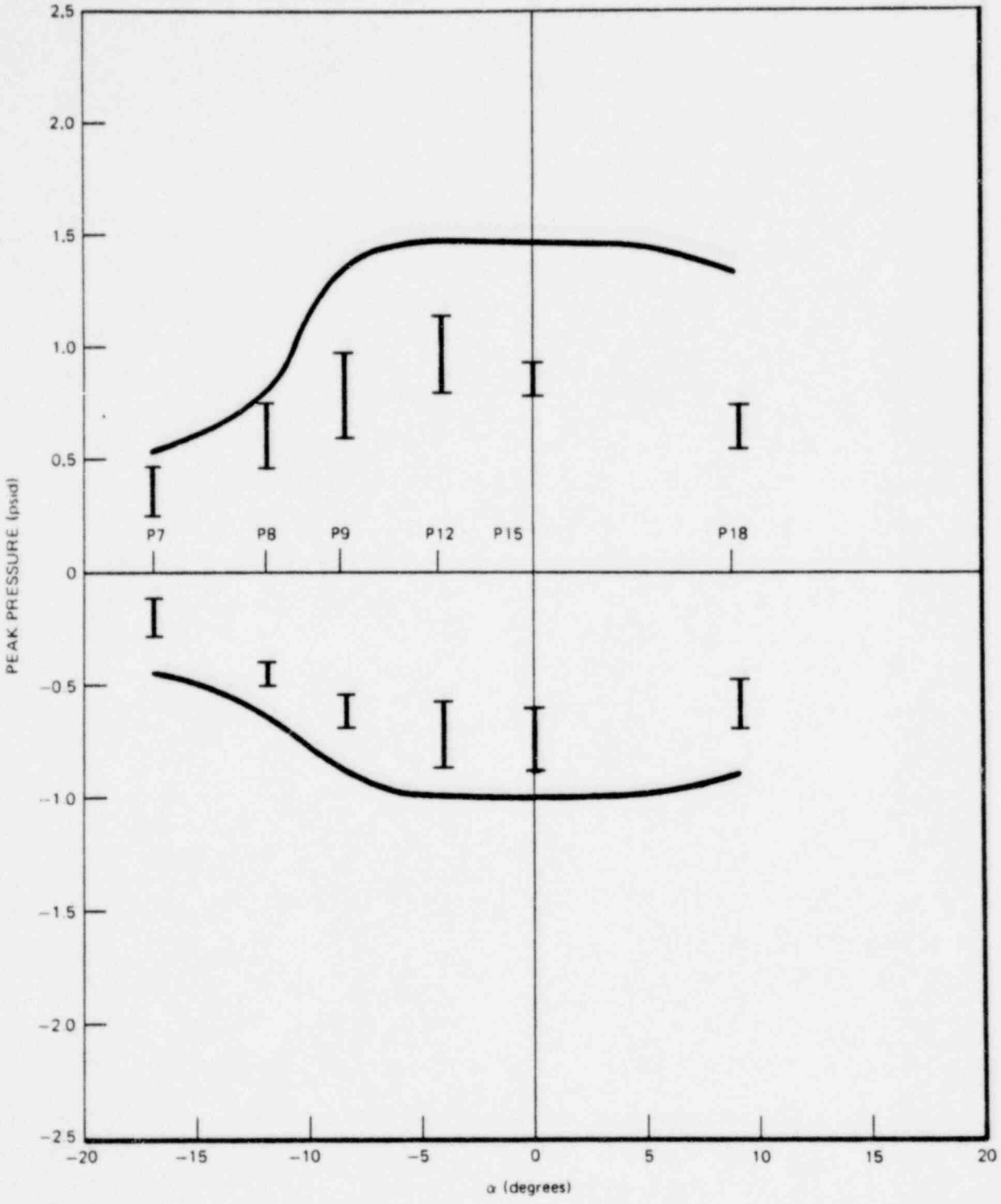

Figure 3-96. Peak Pressure Distribution For 1/4 Scale Test 12 @ β = 0.0

1764 319

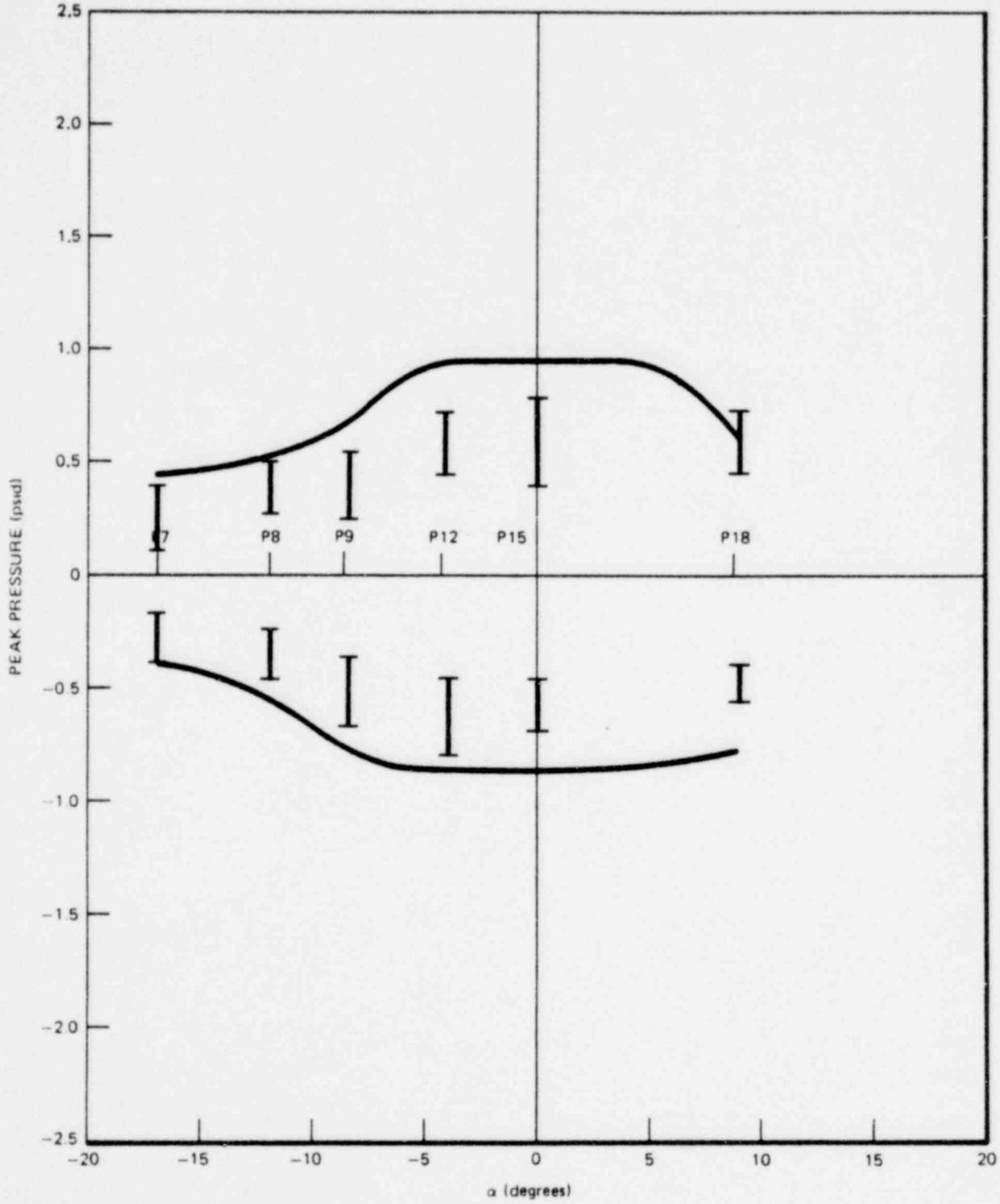

Figure 3-97. Peak Pressure Distribution For 1/4 Scale Test 13 @ β = 0.0

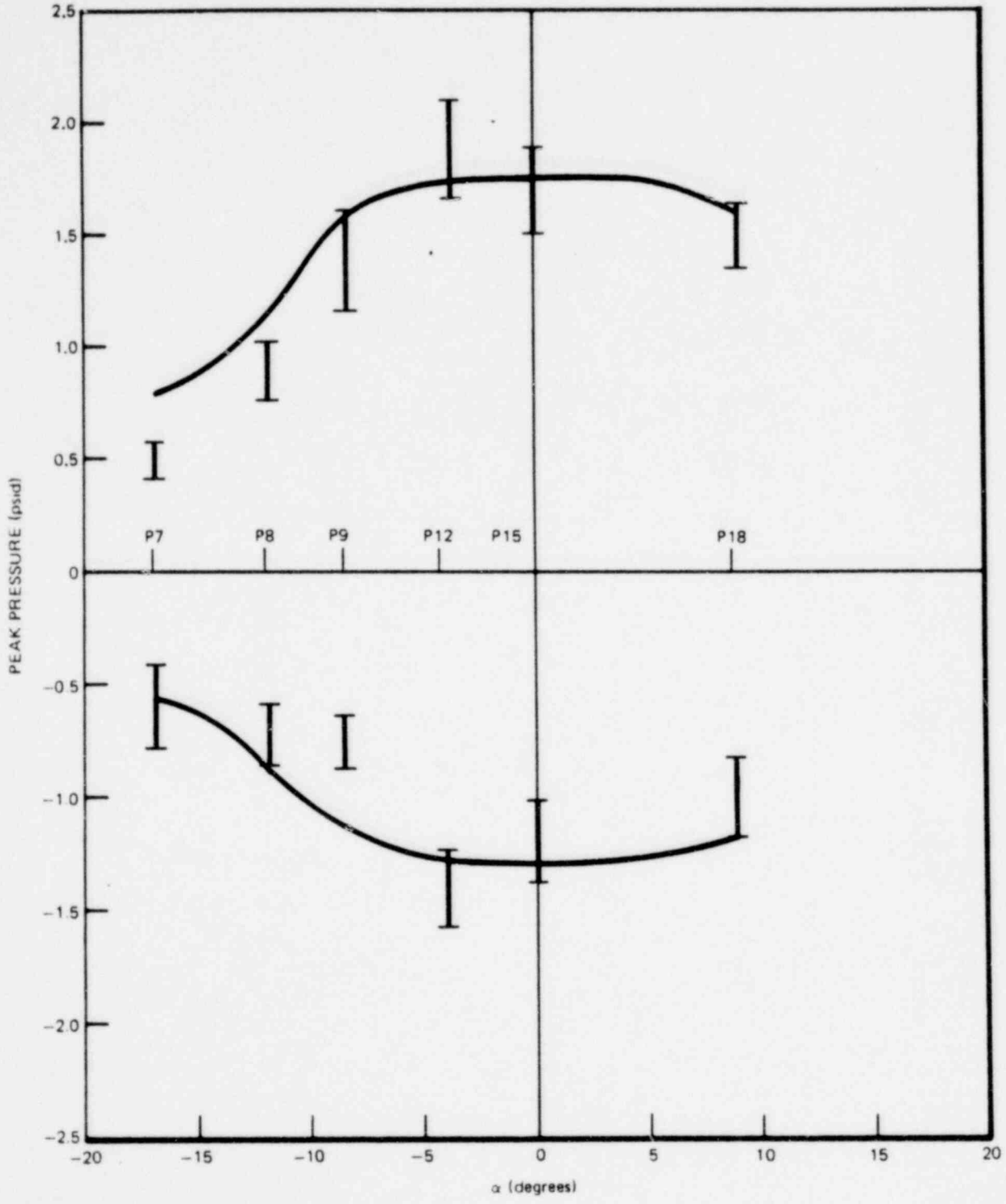

Figure 3-98. Peak Pressure Distribution For 1/4 Scale Test Case 14 @ β = 0.0

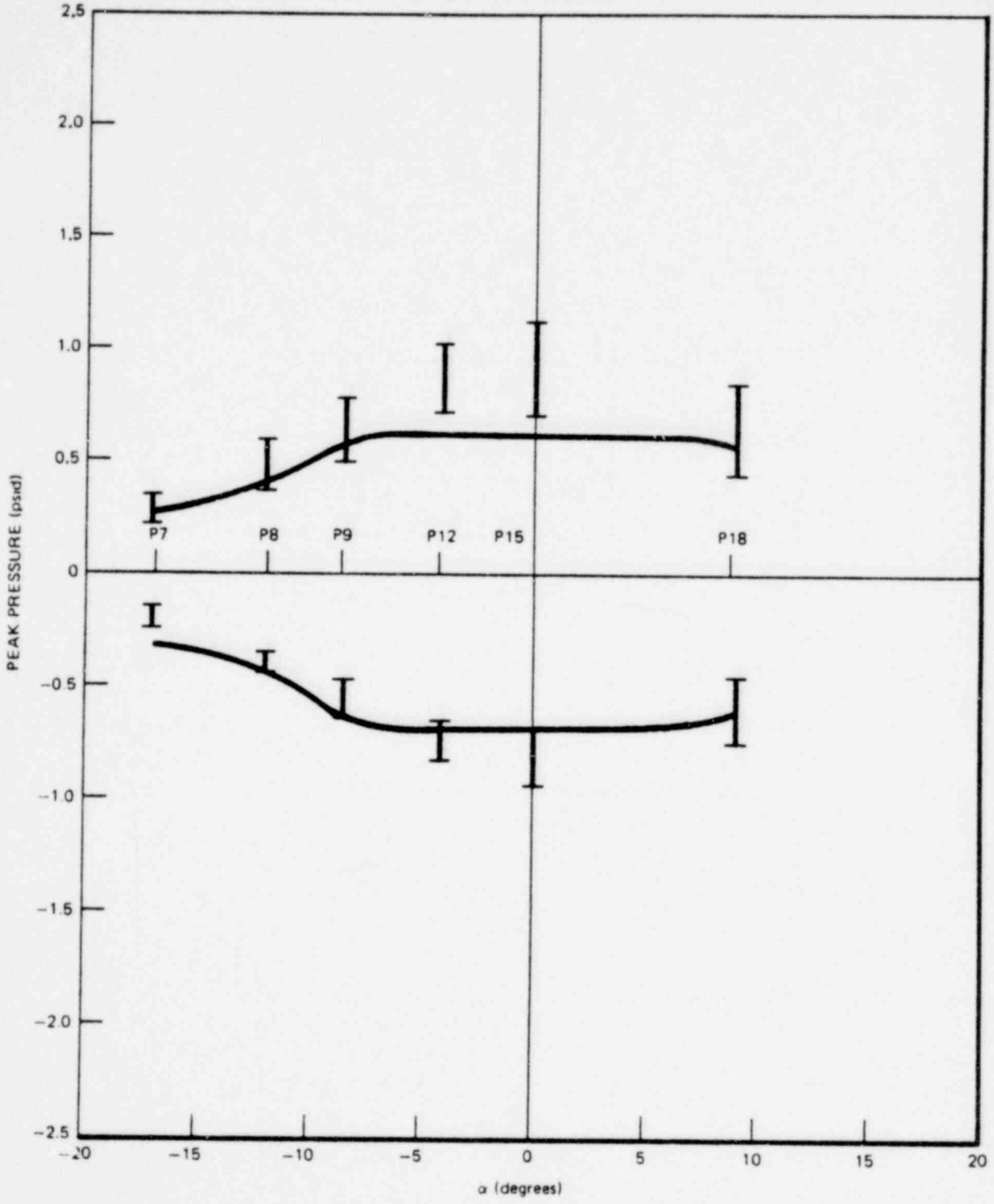

Figure 3-99. Peak Pressure Distribution For 1/4 Scale Test Case 15 @ β = 0.0

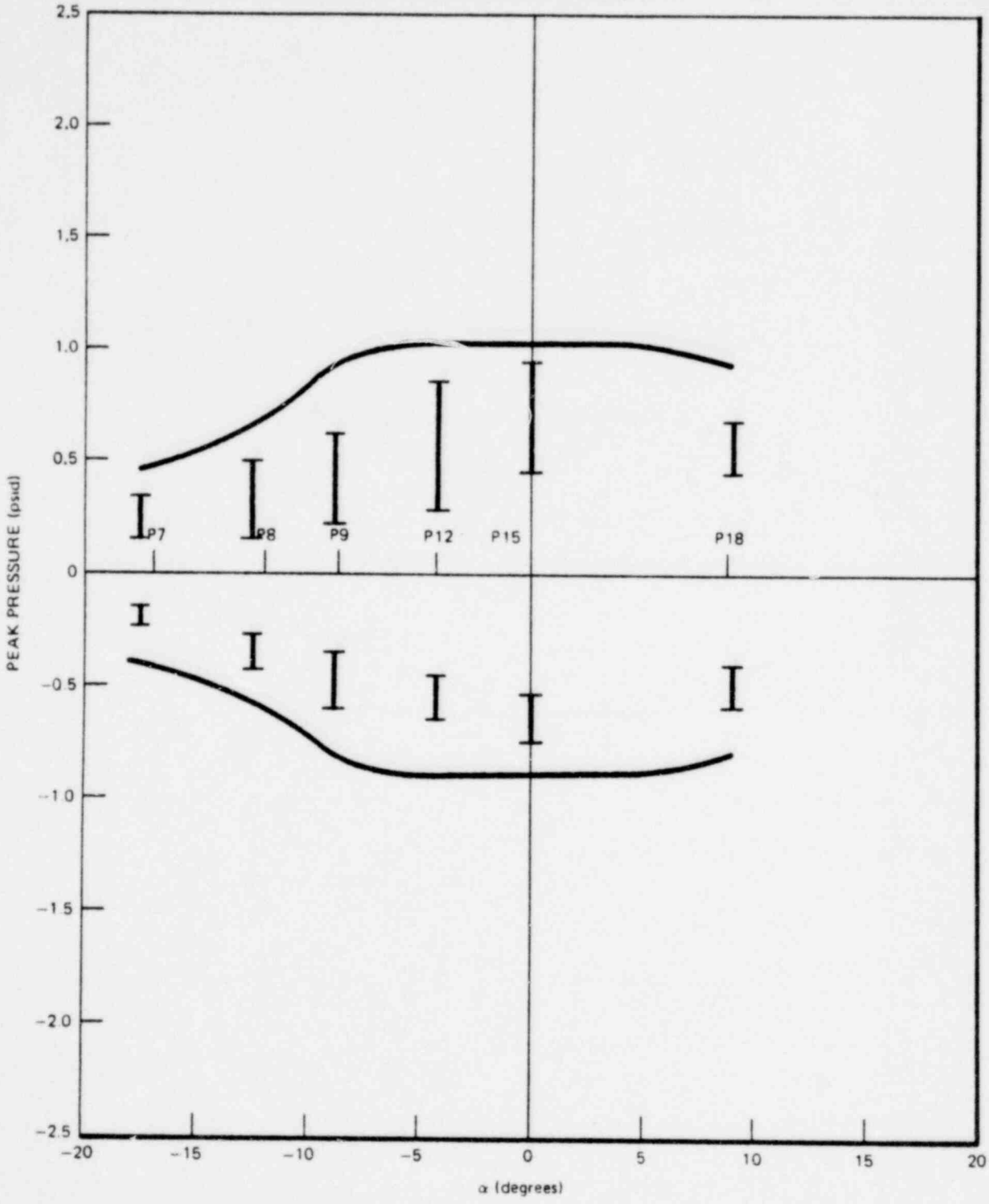

Figure 3-100. Peak Pressure Distribution For 1/4 Scale Test Case 16 @ β = 0.0

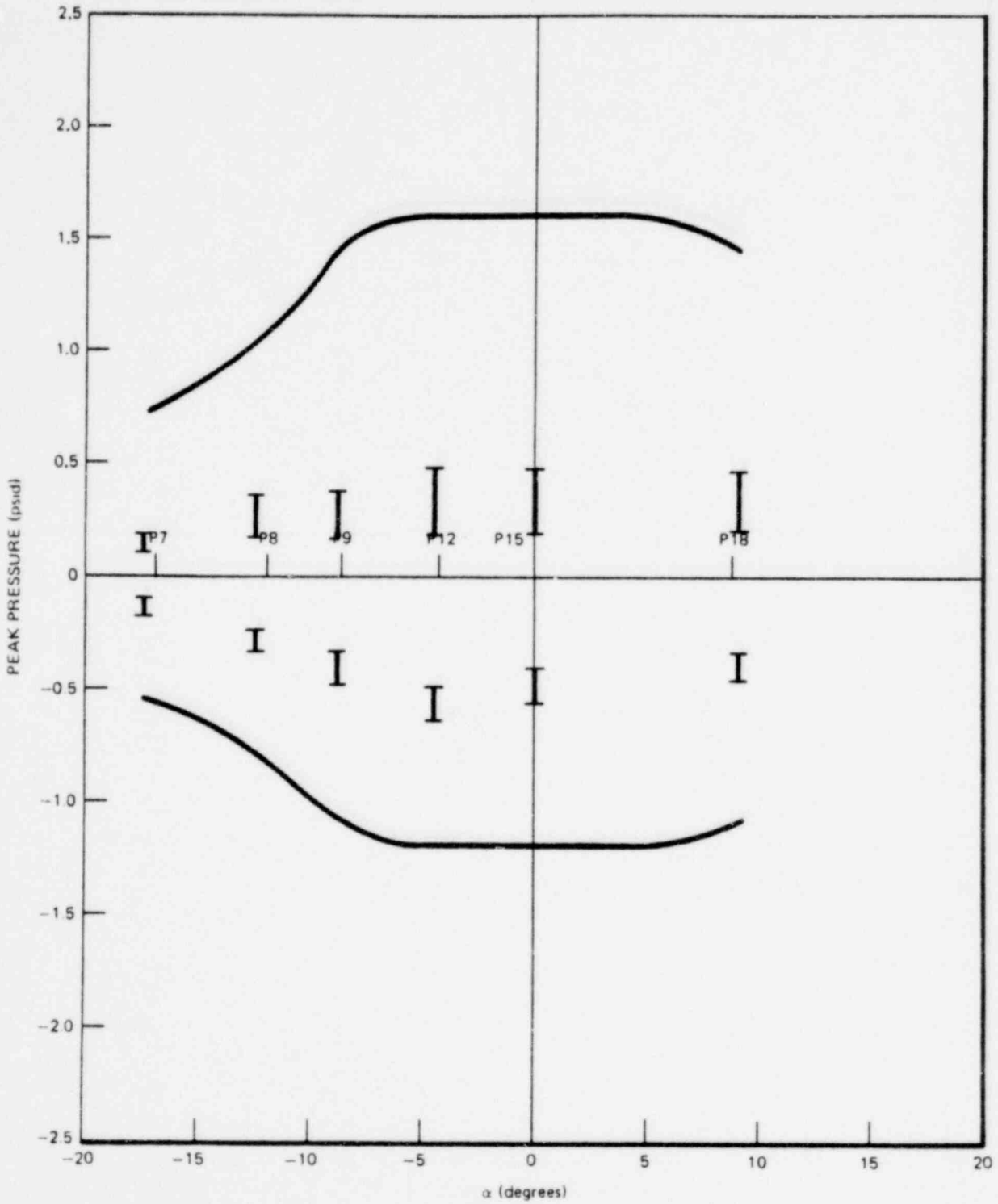

Figure 3-101. Peak Pressure Distribution For 1/4 Scale Test Case 17 @ β = 0.0

1764 324

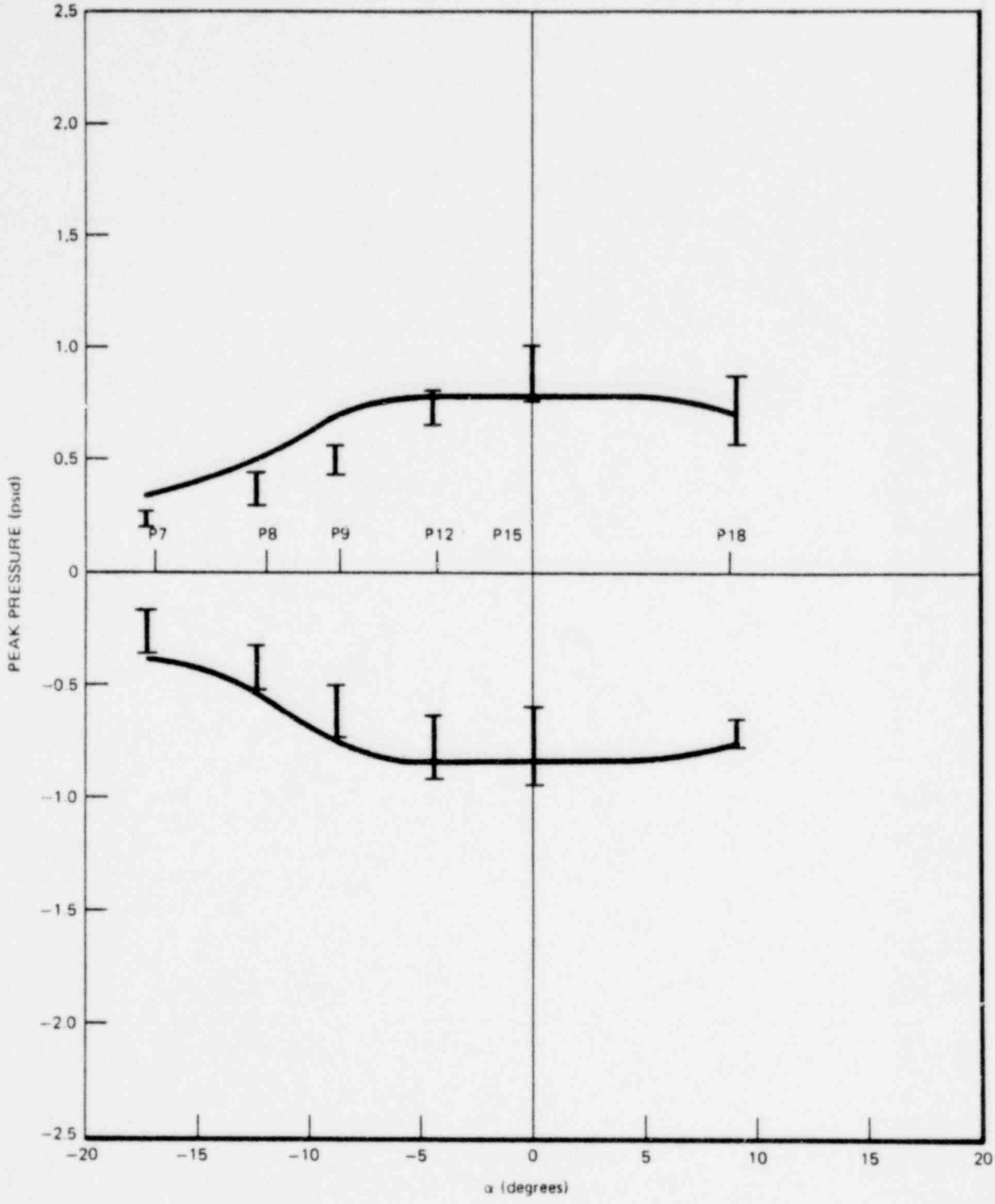

Figure 3-102. Peak Pressure Distribution For 1/4 Scale Test Case 18 @ β = 0.0

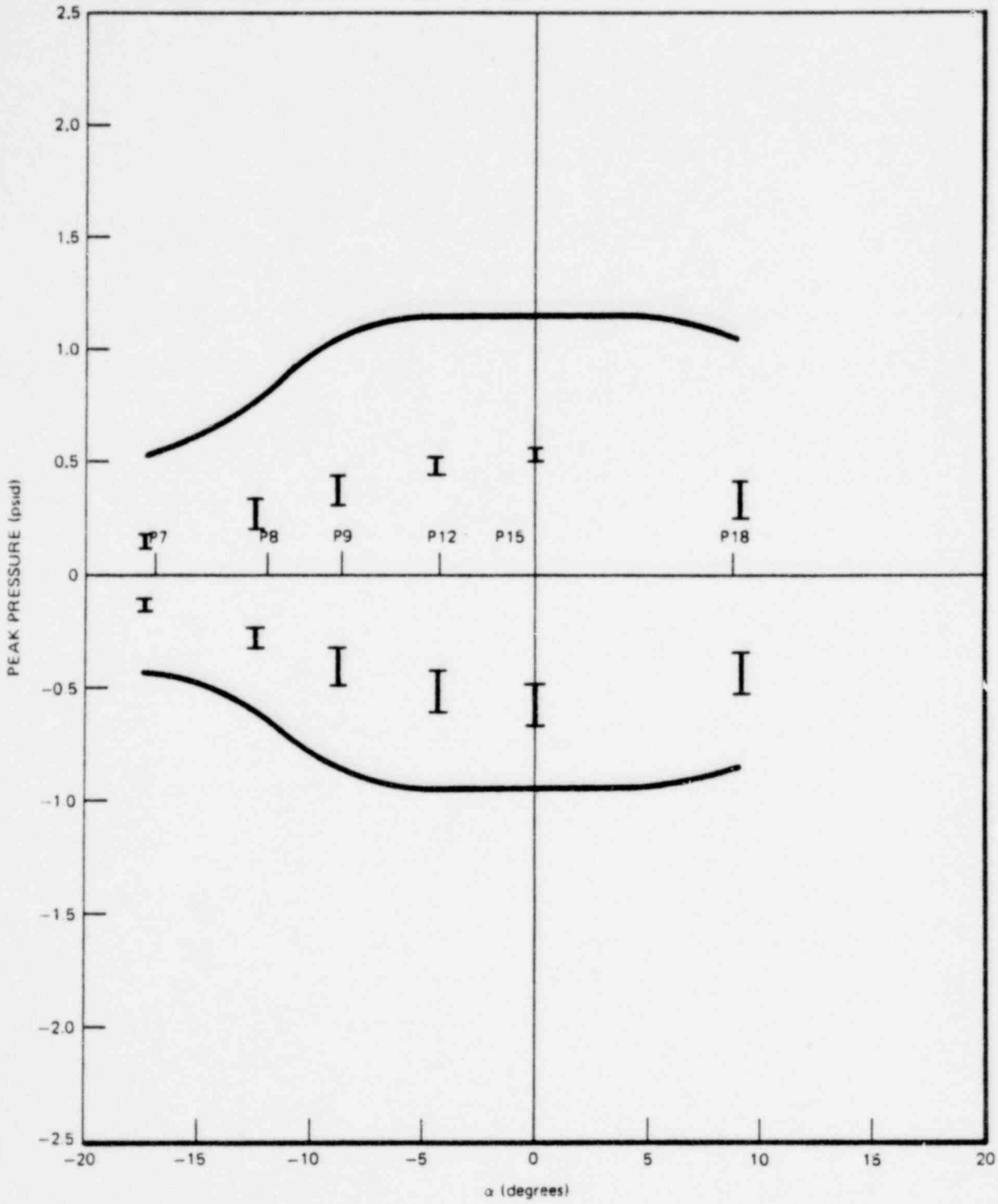

Figure 3-103. Peak Pressure Distribution For 1/4 Scale Test Case 19 @ β = 0.0

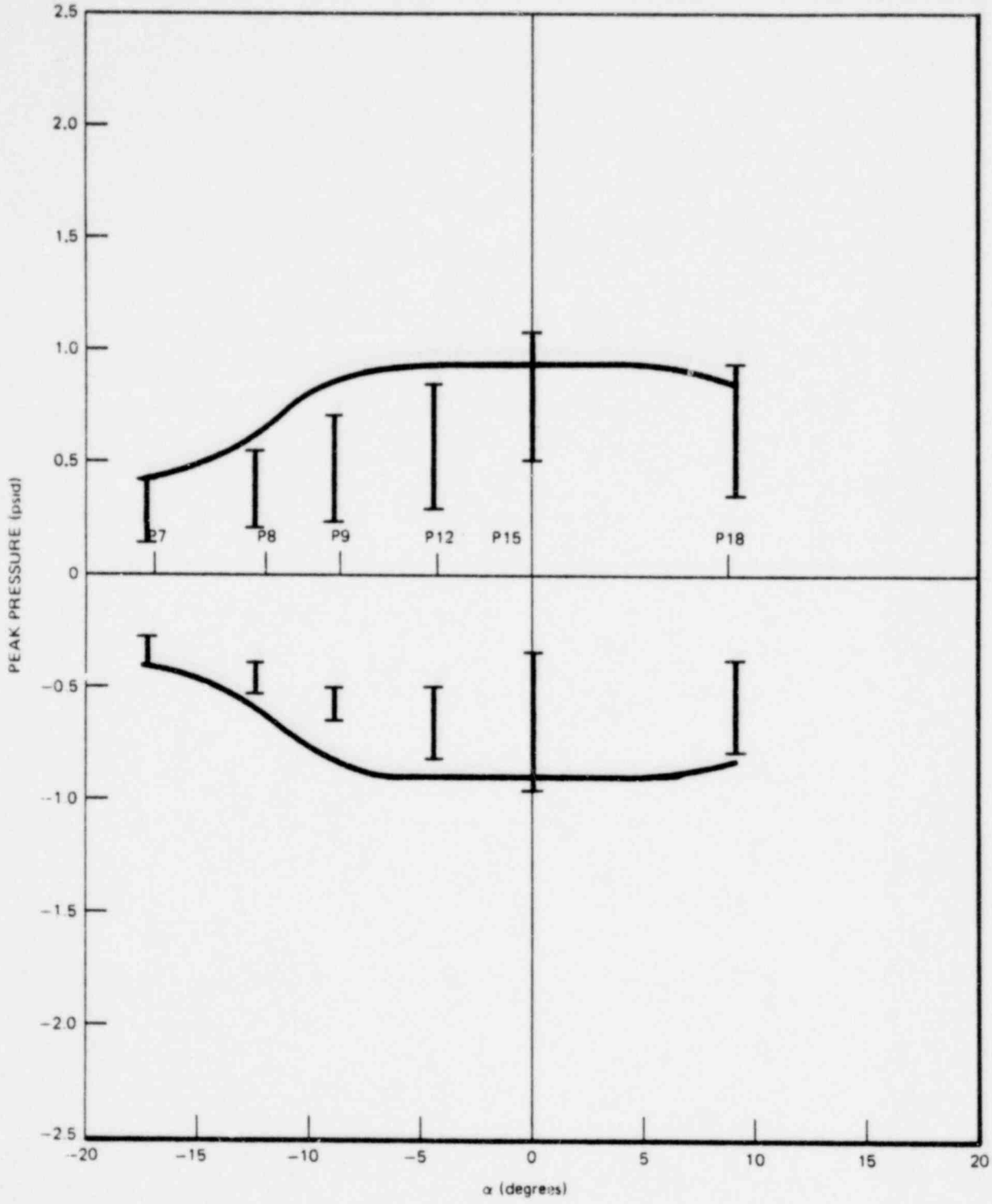

Figure 3-104. Peak Pressure Distribution For 1/4 Scale Test Case 20 @ β = 0.0

4.0 DISCUSSION

4.1 GENERAL

The bubble dynamics model, as described in Appendices A, B, C, D and outlined in Section 2 of this report, accurately predicts the dynamics of an oscillating bubble in a finite pool, provided the initial conditions are properly specified. The initial conditions are bubble size and bubble pressure, both of which are determined b the charging process. For a T-Quencher bubble, the charging process is n c amenable to exact analysis and can only be approximated by an idealized process that leads to initial conditions that are close to the actual ones.

The charging rate, i.e., the energy flow rate into the bubble, is a function of time and depends on the mass and the thermodynamic properties of the air, the dynamics of the water inside and outside of the quencher arm and the geometry of the quencher. It is possible to assume an idealized charging process that will give acceptable results for a given set of conditions. To ensure the validity of such assumptions, the model has been tested over the expected range of parameters.

The present model was developed and compared with the Monticello test results and later refined on the basis of the 1/4 scale data. The final model, as presented in this report, is in good agreement with test data over the entire range of parameters expected in the Mark I plants. This implies that, even though the water velocity and the air velocity assumptions may not be accurate, the combination of these assumptions leads to the correct enthalpy flux for all the cases where good agreement between measured and predicted data exists. The empirical pressure distribution model seems to apply to small scale as well as large scale geometry, and regardless of whether the torus is flexible (Monticello) or rigid (1/4 scale).

4.2 MONTICELLO COMPARISONS

Table 3-6 shows that the model predicts bubble pressure and frequency reasonably well for a variety of initial conditions, hot and cold pipe, elevated or depressed water level and normal or reduced air mass. Note that the air mass for hot pipe cases and the water level for the elevated and depressed water level cases were estimated.

The empirical pressure distribution model is not necessarily a best fit, but it is simple and follows the trend of the measured data in the radial and circumferential directions.

The 1.65 multiplier gives a conservative estimate of the pressure distribution and of the total force acting on the torus shell.

4.3 1/4 SCALE TEST

4.3.1 Scaling

The original 1/4 scale T-Quencher design was based on the scaling analysis of Reference 3. In that analysis, it was assumed that the flow of air through the quencher holes would be choked at all times. Based on this assumption, the quencher hole area must be scaled by a factor of $\lambda_x^{2.5}/\lambda_T^{0.5}$.

Test results showed bubble and shell pressures were significantly greater than the scaled down Monticello results. The average peak positive and peak negative bubble pressures for the Monticello cold pipe tests were 5.55 psid and -5.35 psid, which scales down to 1.39 psid and -1.34 psid. The corresponding values for the original 1/4 scale quencher were 2.58 psid and -1.63 psid. The source of the discrepancy was found to be the scaling of the quencher hole area. The analytical model predicted that geometric scaling of the quencher holes would improve the 1/4 scale test results. This meant scaling the quencher hole area according to λ_x^2 as opposed to $\lambda_x^{2.5}/\lambda_T^{0.5}$. In effect, the quencher hole area had to be approximately doubled. In addition, the cross-sectional

areas of the quencher arm and of the submerged portion of the discharge line had to be modified to maintain the scaling of the water clearing time (see Table 3-2 of Reference 2). A new quencher was designed and the necessary modifications were made based on geometric scaling of hole area. The base case was repeated and the results (1.50 psid and -1.10 psid) were in good agreement with the scaled down Monticello results. This quencher was used throughout the test program. Two additional tests were run with the original 1/4 scale T-Quencher at 7.7 psia and 11.25 psia initial pipe and wetwell pressures.

In Reference 2, these tests are designated as Tests B and C, respectively, and the base case is designated as Test A (see Table 6-1 of Reference 2). The purpose of these additional tests was to confirm that both quenchers give the same trend for the effect of initial pressure on shell pressures. The difference in the magnitude of the influence coefficients for the two quenchers was not statistically significant.

4.3.2 Sensitivity Studies

4.3.2.1 Effect of Steam Flow Rate — Results of Tests 1, 2, and 3 indicate that pressure amplitudes depend on the steam flow rate but frequency is insensitive to steam flow rate (see Figure 3-16 and 3-17). This is in agreement with the X-Quencher statistical correlation, which also predicts an increase in bubble pressure with increasing steam flow rate.

4.3.2.2 Effect of Initial Pipe and Wetwell Pressure — Figures 3-18, 3-20, and 3-22 show the effects of initial wetwell and pipe pressure on shell pressure magnitudes. For 26-ft and 52-ft lines, the negative pressures increase with increasing initial pressure, but the positive pressures decrease slightly or remain unchanged. For the 108-ft line, however, both positive and negative pressures increase with increasing initial pressure. Since air mass is proportional to initial pipe pressure, these results indicate that a general statement cannot be made regarding the effect of air mass on shell pressures. The effect of air mass depends on the mass flow rate of air into the pool. For instance, if the flow of air continues after the bubble has reached its first negative

peak pressure, the effect is a slowing down of the inflow of water and a decrease in the peak positive pressure. On the other hand, if the same amount of air is discharged while the bubble is expanding, an increase in the magnitude of the negative pressure will result. Therefore, the effect of air mass is closely related to the charging process.

The results of Test 1, 4A, 4, 5, 6, 7, and 8 (see Figures 3-19, 3-21, and 3-23) indicate an increase in bubble frequency due to increasing wetwell pressure. In fact, frequency is proportional to $\sqrt{P_\infty}$, which agrees with classical theory of an oscillating bubble in an infinite medium.

$$f = \frac{1}{2\ \P R}\sqrt{\frac{3k\ g_c\ P_\infty}{\rho}}$$

The model correctly predicts this effect. Note that bubble radium does not significantly change when both the initial pipe pressure and wetwell pressure are changed by the same amount.

4.3.2.3 Effect of Pipe Length — Since bubble frequency is inversely proportional to bubble radius, (See Equation (4-1), other parameters being the same, an increase in pipe length results in a decrease in bubble frequency as indicated by Figures 3-25, 3-27, and 3-29. However, the effect of pipe length on shell pressures is more complicated. Figures 3-24 and 3-26 show a slight decrease followed by an increase in pressure magnitudes as the pipe length is increased. Figure 3-28 does not include a point with a pipe length corresponding to an air volume of 0.4 ft^3, and hence it is not known whether or not it would also show the same trend as Figures 3-24 and 3-26. Pipe length has two opposing effects where bubble pressure is concerned. On the one hand, a shorter pipe gives higher pipe pressures and shorter water clearing time, both of which tend to give a higher bubble pressure. On the other hand, shorter pipe means less air mass and lower bubble pressure. It is therefore not surprising that both the model and the test data indicate a minimum for the pressure vs air volume curves.

4.3.2.4 Effect of Submergence — Figures 3-30 and 3-31 show a slight decrease in pressure magnitudes and a slight increase in frequency due to increased submergence. Since increasing submergence means increasing P_∞, and since frequency is proportional to $\sqrt{P_\infty}$, these results and predictions are reasonable. The changes in pressure and frequency are attributed to the changes in P_∞ and the hydrodynamic mass associated with the oscillating bubble.

4.3.2.5 Effect of Distance of Quencher From Floor — The model predicts a more pronounced increase in shell pressure than observed in Test 9 caused by a reduction in the distance of the quencher from the floor. (See Figure 3-32). The model is slightly conservative. There is no significant effect of distance from the floor on frequency (See Figure 3-33).

4.3.2.6 Effect of Pipe Diameter — The effect of pipe diameter (keeping the pipe length and all other parameters the same) on shell pressures appears to be dependent on the pipe length. For a 52-ft pipe, increasing the pipe size from 1 1/2 in. schedule 40 to 2 1/2 in. schedule 80 caused a 50% increase in peak shell pressures (see Figure 3-34), whereas the same change for a 26-ft pipe caused a 20% decrease. Frequency decreases in both cases, as expected (larger bubble radius).

4.3.2.7 Effect of Water Leg Length — To study the effect of increasing water leg length (Test Case 11), keeping submergence and other parameters constant, a horizontal section was added to the submerged portion of the discharge line (see Figure 4-1). The test results showed low bubble and shell pressures for this arrangement (See Figures 3-64, 3-65, and 3-95). The measured bubble pressures were one half of predicted values and the frequency was 2 Hz (~15%) lower than the prediction. (See Table 3-13). These anomalies were attributed to the particular geometry of the submerged portion of the pipe, which was not representative of any Mark I geometry, and to the increase in the wetted surface of the discharge line. To investigate the effect of wetted surface, Test 16 was conducted. This test was different from the base case only in that the inside surface of the discharge line was wetted up to a point

2.87 ft above the normal water level, prior to valve actuation. This increase in the wetted surface, which gave the same wetted areas as in Test 11, did not produce the expected reduction in loads. Only a 10% reduction in pressures was realized. It was concluded that the low pressures obtained in Test 11 were not due to the increased wetted surface alone. One possible reason may be the uneven and possibly slow clearing of the arms due to the geometry of the submerged portion of the line. Since this geometry was not representative of any Mark I plant geometry, it was decided to study the effect of long water leg, causing the same line geometry as in the base case. This was done in two different ways: in Test 15 the water leg length was increased by decreasing the pipe pressure and in Test 18 the wetwell pressure was raised. In both cases the water leg length was 6.25 ft compared with 3.38 ft for the base case. Both of these tests gave results that were not significantly different from the base case except for the frequencies that were higher (see Table 3-13). Test 18 was considered more meaningful in that it had about the same air mass as the base case whereas in Test 15, because of the reduced pipe pressure, the air mass was lower. This explains the higher frequency for Test 15. The higher frequency in Test 18 was caused by the higher wetwell pressure.

One possible explanation for this lack of sensitivity of shell pressures to water leg length is the increase in water clearing time associated with a long water leg. This longer water clearing time results in more mixing of air and steam and therefore a lower effective mass flow rate of air. The effect of increased wetted area of the discharge line also contributes somewhat, as indicated by the results of Test 16. The combination of these two effects balances with the effect of increased air-water interface pressure.

To further investigate the effect of water leg, two tests were conducted at a low submergence of 0.895 ft, corresponding to $\sim$ 3.6 ft full scale submergence, which is outside of the range of Mark I plants. Test 17 was conducted with nominal pipe and wetwell pressure and a water leg of 2.5 ft. In Test 19, the wetwell was pressurized to obtain a water leg of 3.38 ft (identical to the

base case). Because of the strong effect of the low submergence, the results of these tests could not be used to infer the effect of water leg length. The air-water interface pressures and the bubble and shell pressures were all well below predictions but frequencies were higher than predicted. Since such low submergence is not practical, the models were not modified to account for the effect of low submergence, thereby bringing the predictions closer to the measured data.

To isolate the effect of a short water leg, keeping all other parameters including submergence the same as for the base case, the inclination of the submergence portion of the discharge line was modified for Test 14 (see Figure 4-1). This case, with a short vertical water leg of 1.65 ft gave positive pressures that were 70% higher and negative pressures 40% higher than the base case. Readings of the transducers PT-19 and PT-20 (Figure 3-15) were observed to be closer than in the previous tests (see Table B-1), indicating a more symmetric clearing of the quencher arms. This observation suggested that the inclination of the submerged portion of the discharge line might be an important parameter to study. Test 20 was conducted with the same discharge line inclination as in Test 14 but with an increased submergence of 3.38 ft, giving a water leg of 3.38 ft. The results of this test were not significantly different from those of the base case, indicating that the inclination of the submerged portion of the discharge line is not an important factor if the water leg length remain the same.

4.3.3 Asymmetry

In general, both the bubble pressures and the shell pressures were higher on that side of the quencher where the discharge line was attached (see Table B-1 and Figure B-1). Note that the discharge line is attached to the opposite side of the quencher for Tests 15 through 19.

The asymmetry generally observed is attributed to asymmetric water clearing due to the shape of the air-water interface. This trend, which was also apparent in the Monticello test, was almost nonexistent in Test 14 where the discharge line entered the pool vertically. The opposite trend was observed in Test 11.

The pressure distribution model assumes symmetric pressure distribution and therefore usually overpredicts shell pressures on one side of the quencher.

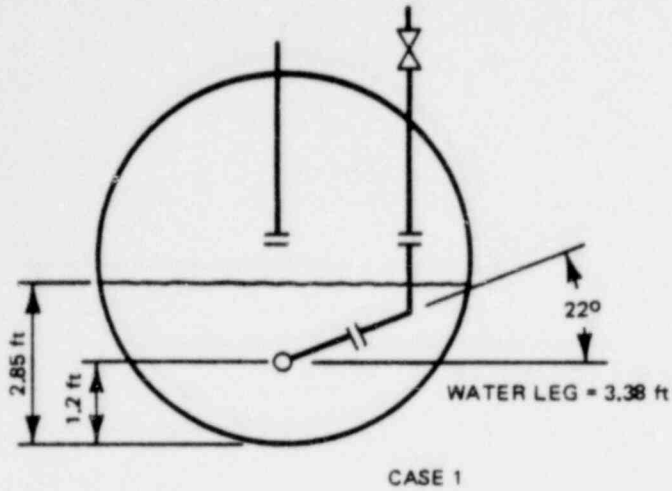

Figure 4-1. 1/4 Scale Test Water Leg Geometry

5.0 CONCLUSIONS

On the basis of the sensitivity studies and the comparisons presented, the following conclusions are reached:

a. The model accurately predicts the effect of all the important parameters on shell pressure magnitudes and frequencies over the range encountered in the Mark I plants. This conclusion is based on the 1/4 Scale Test results and predictions.

b. The model predicts the mean of shell pressures for the Monticello plant and for the most severe case (cold pipe) with reasonable accuracy and bounds the measured data with a multiplier of 1.65. The same multiplier also bounds the 1/4 Scale data.

c. Within the scaled up range of parameters, the model, with a 1.65 multiplier, gives bounding values for shell pressures, correct values for frequency and a conservative attenuation with time.

d. With a multiplier of 2.5 applied to flow rates of water and air, the model predicts bounding values for positive and negative bubble pressures and adjusts bubble radial velocity and acceleration accordingly.

e. The effect of air mass on shell pressures is complex and depends on pipe length, pipe diameter, and pipe pressure. The effects on pressure magnitudes and frequency are correctly predicted by the model.

f. It is difficult to study the effect of water leg length without changing other parameters such as submergence, wetwell or pipe pressure or the inclination of the submerged portion of the discharge line. For an inclination of 22 degrees, increasing the water leg lengths by either lowering the pipe pressure or raising

the wetwell pressure does not seem to significantly affect shell pressures. However, with a discharge line vertically entering the pool, a reduction in the water leg substantially increases the shell pressures. The model predicts these trends reasonably well.

g. Shell pressures depend strongly on the mass flow rate of steam. This trend, which is correctly predicted by the model, is also observed in X-quenchers.

h. Increasing the wetted inside area of the discharge line causes a reduction in the air clearing loads.

i. For submergences below four ft (full scale), the model overpredicts shell pressures and overpredicts frequencies. However, this is not of any practical concern since it does not correspond to any actual Mark I plant.

j. When the discharge line enters the pool at a slope, the shell pressures are generally greater on that side of the quencher where the discharge line joins the quencher. This is caused by the preferential uncovering of the quencher holes during water clearing transient.

k. Bubble frequency is proportional to the inverse of bubble radius and the square root of the absolute equilibrium pressure.

6.0 REFERENCES

1. "Mark I Containment Program - Final Report, Monticello T-Quencher Test, Task Number 5.1.2," R.A. Asai, et al. NEDO-21864, June 1979.

2. "Mark I Containment Program - Final Report, 1/4 Scale T-Quencher Test, Task 6.2.1," C.T. Sawyer, NEDO-24549, June 1979.

3. "Mark I Containment Program, Analytical Model for Computing Transient Pressures and Forces in the Safety/Relief Valve Discharge Line, Task Number 7.1.2," A.J. Wheeler, NEDO-23749, February 1978.

4. "Mark I Containment Program, Analytical Model for Computing Water Rise in a Safety/Relief Valve Discharge Line Following Valve Closure, Task 7.1.2.2," A.J. Wheeler, and D.A. Dougherty, NEDO-23898, August 1979.

5. "Mark I Containment Program Scaling Analysis for Modeling Initial Air-Clearing Caused by Reactor Safety/Relief Valve Discharge, Task Number 6.2.1," R. Schrum, NEDC-23713-P, GE Proprietary, January 1978.

6. "Mark II Containment Dynamic Forcing Functions," NEDO-21061, June 1978.

APPENDIX A

KINETIC ENERGY OF A FINITE POOL DUE TO AN OSCILLATING BUBBLE

APPENDIX A

KINETIC ENERGY OF A FINITE POOL DUE TO AN OSCILLATING BUBBLE

A.1 INFINITE POOL

If a bubble of radius R is oscillating in an infinite pool, the velocity potential is:

$$\phi = -\dot{R} R^2/r \qquad \text{(A-1)}$$

The kinetic energy of the pool is:

$$(KE)_\infty = \frac{\rho}{2}\int_V \left(\frac{\partial\phi}{\partial r}\right)^2 dV = \frac{\rho}{2}\int_S \left[\phi \frac{\partial\phi}{\partial n}\right]_S dS$$

where S = surface of the boundary which is the bubble surface. At the bubble surface:

$$\phi]_S = -\dot{R}R$$

and

$$\frac{\partial\phi}{\partial n}\Big]_S = -\frac{\partial\phi}{\partial r}\Big]_S = [-\dot{R} R^2/r^2]_S = -\dot{R}$$

$$(KE)_\infty = \frac{\rho}{2}\int_S R \dot{R}^2 dS = 2\pi \rho R^3 \dot{R}^2$$

$$(KE)_\infty = 2\pi \rho R^3 \dot{R}^2 \qquad \text{(A-2)}$$

A.2 SEMI-INFINITE POOL

Consider a bubble of radius R at a distance Z from the bottom of a semi-infinite pool (Figure A-1). If $R \ll Z$, the velocity potential can be written as.

$$\phi = \phi + \phi_1 + - \dot{R} R^2 (1/r + 1/r_1) \qquad \text{(A-3)}$$

where:

$$r_1 \quad (4 Z^2 + r^2 - 4 r Z \cos \theta)^{1/2} \qquad \text{(A-4)}$$

is the distance between the point of interest and the center of the image of the actual bubble, as shown in Figure A-1.

Substituting for r_1, in (A-3):

$$\phi = -\dot{R} R^2 \left(1/r + (4 Z^2 + r^2 - 4 r Z \cos \theta)^{-1/2}\right)$$

$$\frac{\partial \phi}{\partial r} = \dot{R} R^2 \left(1/r^2 + (r - 2 Z \cos \theta)(4 Z^2 + r^2 - 4 r Z \cos \theta)^{-3/2}\right)$$

On the surface of the bubble:

$$\phi]_S = - \dot{R} R^2 \left(1/R + (4 Z^2 + R^2 - 4 RZ \cos \theta)^{-1/2}\right) \qquad \text{(A-5)}$$

and

$$\frac{\partial \phi}{\partial n}\Big]_S = - \frac{\partial \phi}{\partial r}\Big]_S = - \dot{R} R^2 \left(1/R^2 + (R - 2Z \cos \theta)\right.$$

$$\left.(4 Z^2 + R^2 - 4 RZ \cos \theta)^{-3/2}\right)$$

$$\therefore KE = \frac{\rho}{2} \int_S \phi \frac{\partial \phi}{\partial n}\Big]_S d\zeta = \frac{\rho}{2} \int_o^{\pi} \dot{R}^2 R^4 \left(1/R + (4 Z^2 + R^2\right.$$

$$\left. - 4 RZ \cos \theta)^{-1/2}\right) \left(1/R^2 + (R - 2Z \cos \theta)\right.$$

$$\left.(4 Z^2 + R^2 - 4 RZ \cos \theta)^{-3/2}\right) 2\pi R^2 \sin \theta d\theta$$

The main point here is that for the same oscillating bubble, the KE of a finite pool is larger than that of an infinite pool. The deviation from infinite pool approximation depends on the ratio of bubble radius to the distance between the center of the bubble and the rigid boundaries.

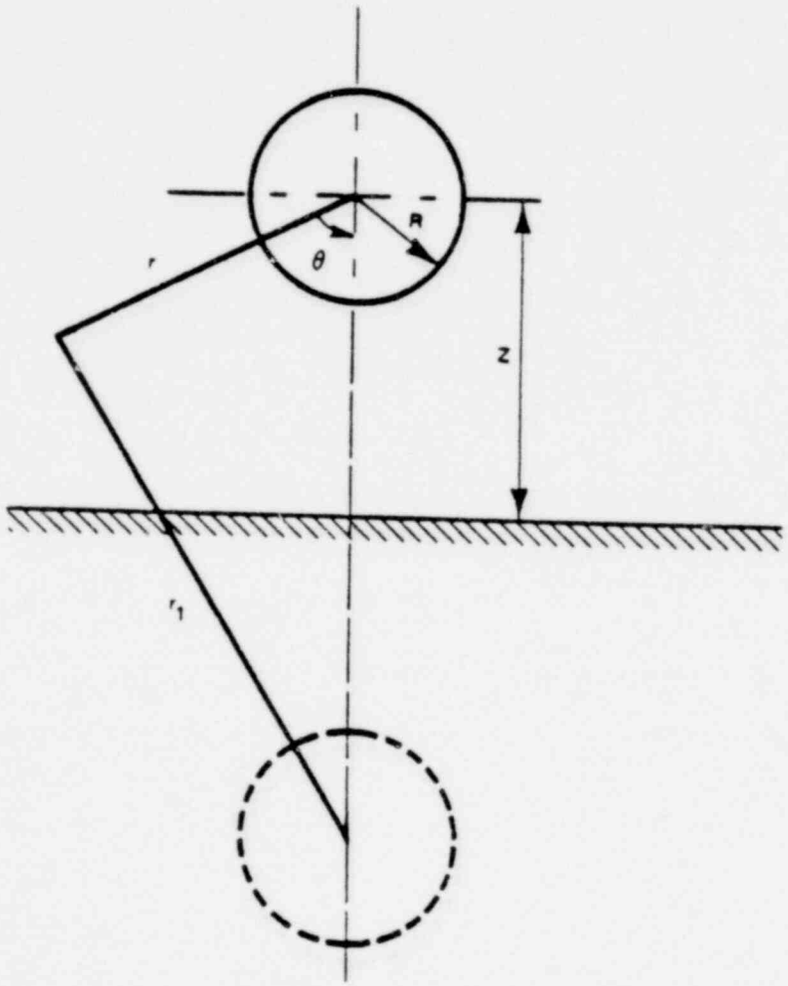

Figure A-1. Spherical Bubble in Semi-Infinite Pool

or

$$KE = KE_{\infty}\left[1 + \frac{\gamma}{2}\left(1 + \frac{1}{4}\ln\frac{2+\gamma}{2-\gamma} - \frac{\gamma^4 - \gamma^3 - 4\gamma^2 + 4\gamma}{(4-\gamma^2)^2}\right)\right]$$

where

$$\gamma = R/Z$$

and

$$(KE)_{\infty} = 2\pi\rho R^3 \dot{R}^2$$

For small values of γ one may approximate KE by the following expressions:

$$KE \simeq (KE)_{\infty}(1 + R/2Z) \qquad \text{(A-6)}$$

A.3 FINITE POOL

For small values of R/Z, it is reasonable to assume that the increase in the KE of the pool due to each wall can be estimated by using Equation (A-6) with the appropriate value of Z. For a square pool with a bubble in the middle, the distance between the center of the bubble and each wall is $\sqrt{A_p}/2$ where A_p is the free surface area of the pool. (Of course for a circular pool with a bubble in the middle, the distance is $\sqrt{A_p}/\sqrt{\pi}$). By the same token, the effect of the free surface can be approximated by including a term (-R/2(H-Z)). Therefore, an estimate of the kinetic energy of the pool is:

$$KE = KE_{\infty}\left(1 + R/2Z - R/2\,(H-Z) + 4\,R/\sqrt{A_p}\right)$$

or

$$KE = 2\pi\rho R^3 \dot{R}^2\left(1 + R/2Z - R/2\,(H-Z) + 4R/\sqrt{A_p}\right) \qquad \text{(A-7)}$$

APPENDIX B

RATE OF ENERGY DISSIPATION

BY ACOUSTIC RADIATION

APPENDIX B
RATE OF ENERGY DISSIPATION BY ACOUSTIC RADIATION

For a compressible fluid, the velocity potential function satisfies the following equation:

$$\nabla^2\phi - \frac{1}{C^2}\frac{\partial^2\phi}{\partial t^2} = \frac{1}{2c^2}\left(2\frac{\partial}{\partial t} + \nabla\phi \cdot \nabla\right)(\nabla\phi \cdot \nabla\phi)$$

which, for $|\nabla\phi| \ll C$ reduces to:

$$\nabla^2\phi - \frac{1}{C^2}\frac{\partial^2\phi}{\partial t^2} = 0 \qquad \text{(B-1)}$$

When the flow field is due to an oscillating bubble of radius R, Bernoulli's Equation, neglecting gravity, can be written as:

$$P = P_\infty - \rho\left(\frac{\partial\phi}{\partial t} + \frac{1}{2}\left(\frac{\partial\phi}{\partial r}\right)^2\right) \qquad \text{(B-2)}$$

Assuming a solution of the form:

$$\phi = f(\tau)/r \qquad \text{(B-3)}$$

where

$$\tau = t - (r - R)/C$$

R being the bubble radius:

$$\frac{\partial\phi}{\partial t} = f' \cdot (1 + \dot{R}/C)/r \qquad \text{(B-4)}$$

1764 346

$$\frac{\partial \phi}{\partial r} = -(f + r f'/C)/r^2 \qquad \text{(B-5)}$$

$$\frac{\partial \phi}{\partial r} = \dot{R} \text{ at } r = R \quad \text{(Boundary Condition)} \qquad \text{(B-6)}$$

Substituting Equations (B-4) and (B-6) in (B-2) and putting r = R:

$$P_B - P_\infty = -\rho\,[(1 + \dot{R}/C)\, f'/R + \dot{R}^2/2] \qquad \text{(B-7)}$$

or

$$f' = -[(P_B - P_\infty)/\rho + \dot{R}^2/2]\, RC/(\dot{R} + C) \qquad \text{(B-8)}$$

According to Equations (B-5) and (B-6):

$$\left.\frac{\partial \phi}{\partial r}\right]_{r=R} = \dot{R} = -(f + R f'/C)/R^2 \qquad \text{(B-9)}$$

Then

$$f' = -(R\ddot{R} + f/R)C \qquad \text{(B-10)}$$

Substituting (B-10) in (B-7) and rearranging:

$$f = R^2\,[((P_B - P_\infty)/\rho + \dot{R}^2/2)/(C + \dot{R}) - \dot{R}]$$

Differentiating

$$f' = 2R\dot{R}\,[((P_B - P_\infty)/\rho + \dot{R}^2/2)/(C + \dot{R}) - \dot{R}]$$

$$+ R^2((\dot{P}_B/\rho + \dddot{R}R)/(C + \dot{R}) - \ddot{R}) \qquad \text{(B-11)}$$

Where the term with $(C + \dot{R})^2$ in the denominator has been neglected. Substituting (B-11) in (B-8) and simplifying gives:

$$R\ddot{R} + 3/2\ \dot{R}^2 + \dot{R}^3/C - 2\dot{R}(P_B - P_\infty)/\rho C - R\dot{P}_B/\rho C = (P_B - P_\infty)/\rho \quad \text{(B-12)}$$

Comparing (B-12) with Raleigh's Equation:

$$R\ddot{R} + 3/2\ \dot{R}^2 = (P_B - P_\infty)/\rho$$

We notice that the last three terms on the left-hand side of Equation (B-12) are due to compressibility effects. To obtain the rate of acoustic radiation, both sides of Equation (B-12) may be multiplied by $4\pi R^2\dot{R}\rho$. The rate of energy dissipation due to acoustic radiation becomes:

$$\dot{E}_R = 4\pi R^2\dot{R}(\rho\dot{R}^3 - 2\dot{R}(P_B - P_\infty) - R\dot{P}_B)/C \quad \text{(B-13)}$$

Finally, assuming isentropic process:

$$\dot{P}_B = -3KP_B\ \dot{R}/R$$

$$\therefore\ \dot{E}_R = 4\pi R^2\dot{R}(\rho\dot{R}^3 - 2\dot{R}(P_B - P_\infty) + 3K\dot{R}P_B)/C$$

If we put $3K \cong 4$ above the equation reduces to:

$$\dot{E} = 4\ R^2\dot{R}^2(\rho\dot{R}^2 + 2(P_B + P_\infty))/C$$

APPENDIX C

THE IMPORTANCE OF ENTHALPY FLOW RATE AND HEAT TRANSFER

APPENDIX C

THE IMPORTANCE OF ENTHALPY FLOW-RATE AND HEAT TRANSFER

The dynamics of a "charging" air bubble in an infinite pool are described by the momentum equation (Raleigh's):

$$R\ddot{R} + 3/2\dot{R}^2 = (P_B - P_\infty)/\rho \qquad \text{(C-1)}$$

coupled with the energy equation:

$$\dot{U} = \dot{m}h_o - P_B\dot{V} + \dot{Q} \qquad \text{(C-2)}$$

where:

- $\dot{U}$ = Internal energy of bubble;
- $\dot{m}$ = Mass flow rate into the bubble;
- h_o = Stagnation enthalpy of entering air;
- P_b = Bubble pressure;
- V = Bubble volume;
- $\dot{Q}$ = Rate of heat received from the surroundings.

Equation (C-2) can be written as

$$\frac{d}{dt}(H - P_BV) = \dot{m}h_o - P_B\dot{V} + \dot{Q}$$

or

$$\dot{H} - V\dot{P}_B = \dot{m}h_o + \dot{Q} \qquad \text{(C-3)}$$

but:

$$H = \rho V h = V\rho KRT/(K-1) = VKP_B/(K-1)$$

$$\therefore \dot{H} = (K/(K-1)(V\dot{P}_B + P_B\dot{V})$$

Substituting in (C-3) and rearranging:

$$\dot{P}_B = (K-1)\dot{m}h_o/V - K P_B\dot{V}/V + (K-1)\dot{Q}/V$$

or:

$$\dot{P}_B = (K-1)\dot{m}h_o/V - 3KP_B\dot{R}/R + \frac{(K-1)\dot{Q}}{V} \qquad (C-4)$$

In the absence of heat transfer:

$$\frac{dP_B}{dt} = (K-1)\dot{m}h_o/V - 3KP_B\dot{R}/R \qquad (C-5)$$

It is immediately evident from Equation (C-4) that neglecting boundary effects, the dynamics of a charging bubble depend mainly on the product $\dot{m}h_o$, (the enthalpy flow rate) and the heat transfer rate ($\dot{Q}$).

Heat transfer becomes important if the vapor pressure of steam is substantially higher than the saturation pressure corresponding to pool temperature. Numerical calculations show that for a mixture of air and steam, it is possible to have an increase in the peak positive pressure for successive oscillations. In other words, if at the end of the first contraction the peak pressure is P_1, at the end of the second contraction, the peak pressure $P_2 > P_1$. This may continue for two or three oscillations and then the peak pressure begins to decline due to reduced bubble energy. The variations of peak pressure depend strongly on the percent steam and the heat transfer coefficient.

For the quencher where almost all of the steam is condensed before the bubble is formed, the term $\dot{Q}$ is negligible and the pressure becomes dependent mainly on $\dot{m}h_o$.

Neglecting heat transfer and assuming that the charging process is completed in one half cycle, i.e., by the time the bubble pressure reaches its first minimum, the only way that the magnitude of the minimum bubble pressure can be controlled is by controlling $\dot{m}h_o$ which in general is a function of time. In principle, it should be possible to produce any minimum pressure between the vapor pressure corresponding to pool temperature and the local hydrostatic pressure, provided $\dot{m}h_o$ can be controlled without restriction. In practice, however, there are restrictions on both $\dot{m}$ and h_o. One can assume that h_o (stagnation enthalpy) is fixed, then $\dot{m}$ is the only variable. However, the fact that the total mass of air is fixed requires that:

$$\int_0^\tau \dot{m}dt = m$$

where τ is the duration of flow. Other restrictions on $\dot{m}$ are due to limitations on the geometry of discharge device and the dynamics of the air clearing transient.

Although Equations (C-1) and C-5) cannot be solved analytically, even if $\dot{m}(t)$ is known, parametric studies show that generally the slower the rate of flow, the higher the minimum absolute pressure (i.e., the lower the pressure differential $P_\infty - P_{Bmin}$). If all the air is out by the time this minimum pressure is reached, then the maximum bubble pressure which occurs half a cycle later, will also be smaller for a lower flow rate. This fact will be shown for both isentropic and isothermal bubbles.

The point here is that reducing the flow rate of enthalpy to the bubble is the key to the reduction of air-clearing loads. That is the principle of operation of the quencher.

C.1 ISENTROPIC BUBBLE

If a bubble of fixed mass in a finite pool starts at a minimum pressure P_{min} and undergoes an isentropic compression to a maximum pressure P_{max}, this maximum pressure can be predicted as follows:

Conservation of energy applied to the pool:

$$E_2 - E_1 = \int_1^2 P_B \, dV - \int_1^2 P_a \, dV$$

where P_a = atmospheric pressure above the pool surface:

$$E_2 - E_1 = -(P_2V_2 - P_1V_1)/(K - 1) - P_a(V_2 - V_1) \qquad \text{(C-6)}$$

where:

P_1 = absolute minimum bubble pressure;

P_2 = absolute maximum bubble pressure;

P_∞ = absolute hydrostatic pressure

The change in the energy of the pool is simply the change in its potential energy (KE of pool is = 0 at both states):

$$E_2 - E_1 = (V_2 - V_1)\rho gH \qquad \text{(C-7)}$$

Where H = submergence of center of bubble.

1764 353

Substituting in (C-6):

$$(V_2 - V_1)\rho gH = - (P_2V_2 - P_1V_1)/(K - 1) - P_a(V_2 - V_1)$$

or

$$- (P_2V_2 - P_1V_1)/(K - 1) = (V_2 - V_1)P_\infty \qquad (C\text{-}8)$$

where

$$P_\infty = P_a + \rho gH$$

Using the isentropic correlation:

$$V_2 = V_1(P_1/P_2)^{1/K}$$

Equation (C-8) reduces to:

$$P_1/P_\infty = - (K - 1)[1 - (P_2/P_1)^{1/K}]/(P_2/P_1 - (P_2/P_1)^{1/K}) \qquad (C\text{-}9)$$

C.2 ISOTHERMAL BUBBLE

This is the same as C.1 except:

$$\int_1^2 P_B \, dV = P_1V_1 \ln (V_2/V_1)$$

and

$$P_1V_1 = P_2V_2$$

The final result is:

$$P_2/P_\infty = (P_2/P_1 - 1)/\ln(P_2/P_1)$$

1764 354

APPENDIX D

FORMULATION OF BUBBLE DYNAMICS

APPENDIX D

FORMULATION OF BUBBLE DYNAMICS

The dynamics of an oscillating and migrating bubble in a finite pool are formulated using the energy approach. Referring to Figure D-1 and considering the water as a closed thermodynamic system, the following energy balance equation applies.

$$\dot{W} + \dot{E}_s = Q \tag{D-1}$$

$\dot{W}$ is the rate of work done by the system, i.e., by the water on the surroundings:

$$\dot{W} = -(P_B - P_a)\, 4\pi R^2 \dot{R} + \dot{E}_R \tag{D-2}$$

where:

P_a = atmosphere pressure above the pool surface;

P_B = bubble pressure;

R = bubble radius;

$\dot{E}_R$ = rate of energy released by acoustic radiation (see Appendix B for derivation)

$$\dot{E}_R = (4\pi R^2 \rho \dot{R}^2/C)\,(\dot{R}^2 + 2\,(P_B + P_\infty)/\rho)$$

where:

$$P_\infty = P_a + (H - Z)\,\rho g \tag{D-4}$$

$\dot{E}_s$ = Rate of change of energy of the system:

$$\dot{E}_s = \frac{d}{dt}(PE)_s + \frac{d}{dt}(KE)_s + \frac{d}{dt}(U)_s \qquad \text{(D-5)}$$

where, using the pool bottom as the reference plane,

$$\frac{d}{dt}(PE)_s = \frac{d}{dt}\left[\rho g\left(A_p \frac{H^2}{2} + \frac{4}{3}\pi R^3 (H - Z)\right)\right]$$

Neglecting change of H with time:

$$\frac{d}{dt}(PE)_s = 4\pi R^2 \rho g\left[\dot{R}(H - Z) - R\dot{Z}/3\right] \qquad \text{(D-6)}$$

The kinetic energy of the system can be approximated by the following expression:

$$(KE)_s = \pi \rho R^3 \dot{Z}^2/3 + 2\pi \rho R^3 \dot{R}^2\left(1 + R/2Z - R/2(H-Z) + 4R/\sqrt{A_p}\right) \qquad \text{(D-7)}$$

The first term on the right-hand side is due to vertical motion of the bubble, using a hydrodynamic mass of $(2/3)\pi\rho R^3$. This term becomes significant only near the end of the transient when the bubble approaches the free surface. During the first few oscillations, which are of interest, this term is negligible compared with the second term, due to $\dot{Z}$ being much smaller than average absolute value of $\dot{R}$. The second term on the right-hand side of Equation (D-7) represents the kinetic-energy of the system due to radial motion of the bubble (see Appendix A for derivation). The terms $R/2Z$, $-R/2(H-Z)$ and $4R/\sqrt{A_p}$ are due to boundary and free surface effects. Without these terms, the KE of pool due to bubble oscillation reduces to $2\pi\rho R^3\dot{R}^2$, i.e., that due to an oscillating bubble in an infinite pool. Boundary effects become significant only when the bubble radius becomes comparable to the distance between the center of the bubble and the nearest solid boundary. A more rigorous treatment of the KE of the pool requires the

solution of the transient potential flow field for any given pool geometry at every time step, something which, except for very simple geometries is not practical.

Differentiating Equation (D-7) with respect to time, gives:

$$\frac{d}{dt}(KE)_S = \pi\rho[R^2\dot{R}z^{\cdot 2} + (2/3)R^3\dddot{z}z + (6R^2R^3 + 4R^3\dddot{R}R)$$

$$(1 + R/2z - R/2(H - z) + 4R/\sqrt{Ap})$$

$$+ 2R^3\dot{R}^2(\dot{R}/2z + 4\dot{R}/\sqrt{Ap} - R\dot{z}/2z^2 - \dot{R}/2(H - z)$$

$$+ R\dot{z}/2(H - z)^2] \qquad (D\text{-}8)$$

Finally, neglecting viscous dissipation the rate of increase of the internal energy of the system is equal to the rate of heat received at the bubble surface:

$$\frac{d}{dt}(U)_S = \dot{Q} \qquad (D\text{-}9)$$

Substituting Equations (D-6), (D-8), and (D-9) in (D-5) we obtain:

$$\dot{E}_s = 4\pi R^2\dot{R}\rho[g(H - z) - gR\dot{z}/3\dot{R} + \dot{z}^2/4 + R\dot{z}\ddot{z}/6\dot{R}$$

$$+ (3\dot{R}^2/2 + R\ddot{R})(1 + R/2z - R/2(H - z) + 4R/\sqrt{Ap})$$

$$+ (R\dot{R}/2)(\dot{R}/2z - \dot{R}/2(H - z) + R\dot{z}/2(H - z)^2$$

$$+ 4\dot{R}/\sqrt{Ap} - R\dot{z}/2z^2)] + \dot{Q}$$

1764 358

Simplifying:

$$\dot{E}_s = 4\pi R^2 \dot{R}\rho[g(H - z) - gR\dot{z}/3\dot{R} + \dot{z}^2/4$$

$$+ R\dot{z}\ddot{z}/6\dot{R} + R\ddot{R}(1 + R/2z - R/2(H - z)$$

$$+ 4R/\sqrt{Ap}) + \dot{R}^2(3/2 + R/z - R/(H - z) + 8R/\sqrt{Ap})$$

$$+ R^2\dot{R}\dot{z}/4(H - z)^2 - R^2\dot{R}\dot{z}/4z^2] + \dot{Q} \qquad \text{(D-10)}$$

Substituting (D-3) in (D-2):

$$\dot{w} = 4\pi R^2 \dot{R}(P_a - P_B) + (4\pi R^2 \dot{R}^2 \rho/c).$$

$$(\dot{R}^2 + 2(P_B + P_\infty)/\rho) \qquad \text{(D-11)}$$

Substituting (D-10) and (D-11) in (D-1):

$$4\pi R^2 \dot{R}\rho[g(H - z) - gR\dot{z}/3\dot{R} + \dot{z}^2/4 + R\dot{z}\ddot{z}/6\dot{R}$$

$$+ R\ddot{R}(1 + R/2z - R/2(H - z) + 4R/\sqrt{Ap})$$

$$+ \dot{R}^2(3/2 + R/z - R/(H - z) + 8R/\sqrt{Ap})$$

$$- R^2\dot{R}\dot{z}/4z^2 + R^2\dot{R}\dot{z}/4(H - z)^2 + (P_a - P_B)/\rho$$

$$+ (\dot{R}/C)(\dot{R}^2 + 2(P_B + P_\infty)/\rho)] + \dot{Q} = \dot{Q}$$

Simplifying and rearranging:

$$\ddot{R} = [(1/\rho)(P_B(1 - 2\dot{R}/C) - \dot{P}_\infty(1 + 2\dot{R}/C))$$

$$- \dot{R}^2(3/2 + R/z - R/(H - z) + 8R/\sqrt{Ap} + \dot{R}/C)$$

$$+ R\dot{z}(g/3\dot{R} + R\dot{R}/4z^2 - R\dot{R}/4(H - z)^2) - \dot{z}^2/4$$

$$- R\dot{z}\ddot{z}/6\dot{R}]/\left(\frac{R}{2}(2 + R/z - R/(H - z) + 8R/\sqrt{Ap})\right) \qquad \text{(D-12)}$$

Where P_∞ is the absolute pressure in the undisturbed pool at the elevation of the center of the bubble, therefore a function of time.

Equation (D-12) reduces to Raleigh's equation: $R\ddot{R} + 3/2\dot{R}^2 = (P_B - P_\infty)/\rho$ if the effects of compressibility, finite size, vertical motion, and gravity are neglected.

Numerical solution of Equation (D-12) poses a problem due to the fact that $\dot{R}$ appears in the denominator of two of the terms on the right-hand side. Although the sum of these two terms has a finite limit for $\dot{R} = 0$, each term becomes infinite when $\dot{R} = 0$. To avoid this difficultiy, $\ddot{z}$ is approximated for an oscillating spherical bubble and substituted in (D-12) as follows:

$$\text{Buoyancy} = (4/3)\pi R^3 \rho g$$

Momentum of water in the vertical direction $= 2\pi R^3 \rho \dot{z}/3$

Momentum of bubble is negligible (small mass):

$$\therefore (4/3)\pi R^3 \rho g = \frac{d}{dt}(2\pi R^3 \rho \dot{z}/3) = (2\pi\rho/3)(3R^2\dot{R}\dot{z} + R^3\ddot{z})$$

or

$$\ddot{z} = 2g - 3\dot{R}\dot{z}/R \qquad \text{(D-13)}$$

This convenient approximation does not affect the accuracy of the results, since Z and Z will be calculated accurately.

Substituting (D-13) in (D-12) gives:

$$\ddot{R} = [(1/\rho)(P_B(1 - 2\dot{R}/C) - P_\infty(1 + 2\dot{R}/C))$$

$$- \dot{R}^2(3/2 + R/z - R/(H - z) + 8R/\sqrt{Ap} + \dot{R}/C)$$

$$+ \dot{z}^2/4 + (R^2\ddot{R}z/4)$$

$$(1/z - 1/(H - z)^2]/\left(\frac{R}{2}(2 + R/z - R/(H - z) + 8R/\sqrt{Ap})\right) \quad (D\text{-}14)$$

It remains to define P_B and Z as functions of time to be able to solve Equation (D-14).

Bubble pressure P_B is calculated from Equation (C-5) (see Appendix C) which is coupled with Equation (D-14).

Finally, the vertical motion of the bubble needs to be defined (Figure D-2). Even though Equation (D-13) is a good approximation of the vertical acceleration of the bubble, strictly speaking it is only good for an infinite ocean. The hydrodynamic mass of a bubble in a finite pool may be substantially more than $2\pi R^3\rho/3$. The vertical motion of the bubble is calculated by considering the difference in the rate of expansion and contraction of the bubble in the positive and negative Z directions, due to the difference in the local values of P_∞. It is assumed that this preferential expansion (and contraction) only causes vertical motion of the bubble but the spherical shape of the bubble is maintained.

Referring to Figure (D-2)

$$\dot{z} = (\dot{R}_1 - \dot{R}_2)/2 \quad (D\text{-}15)$$

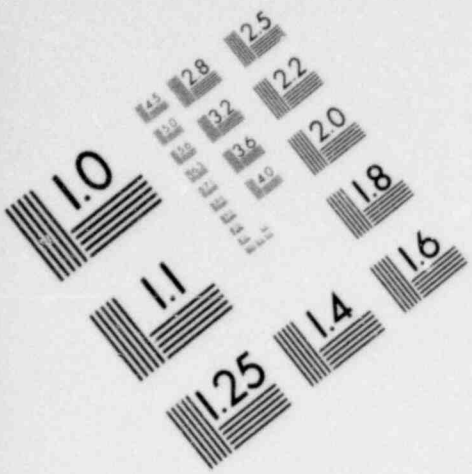

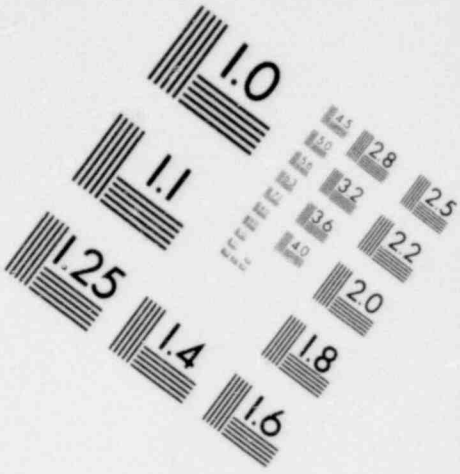

IMAGE EVALUATION
TEST TARGET (MT-3)

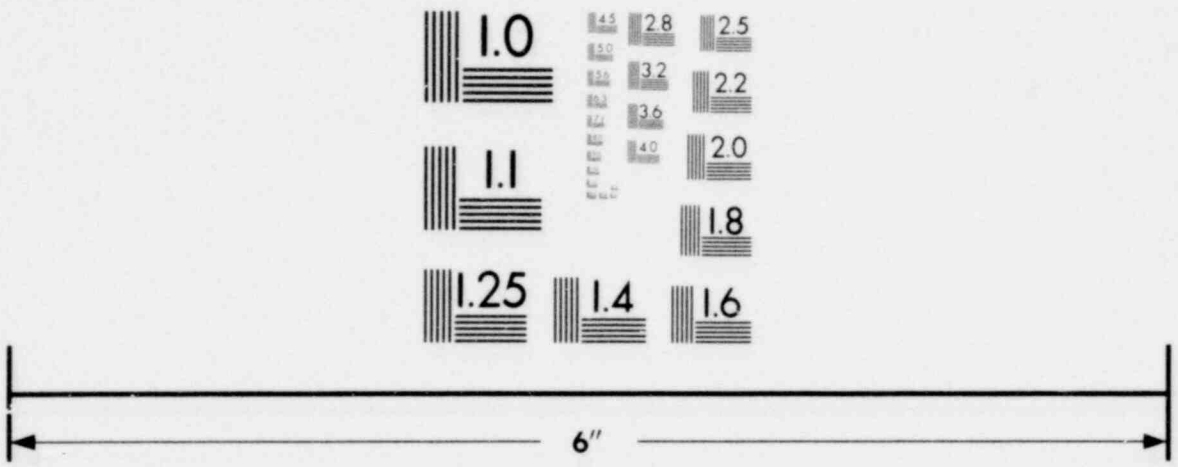

MICROCOPY RESOLUTION TEST CHART

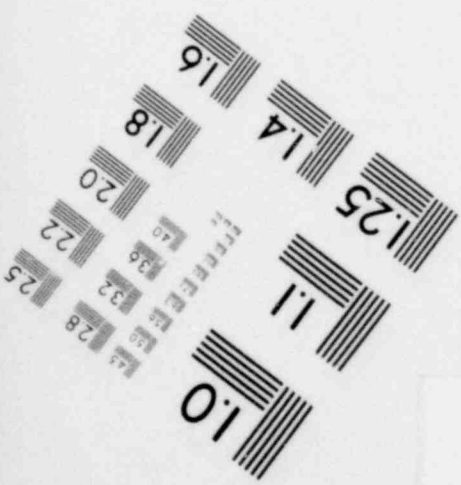

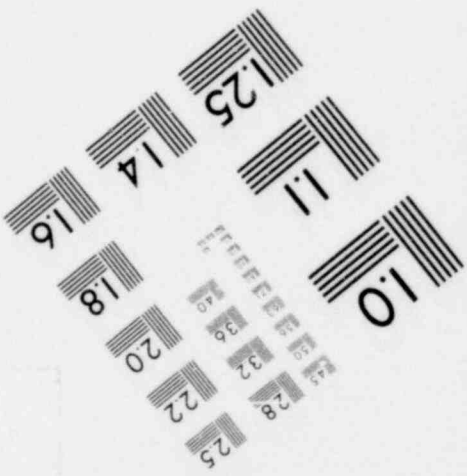

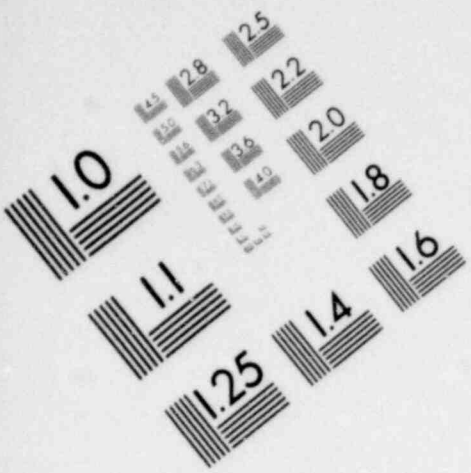

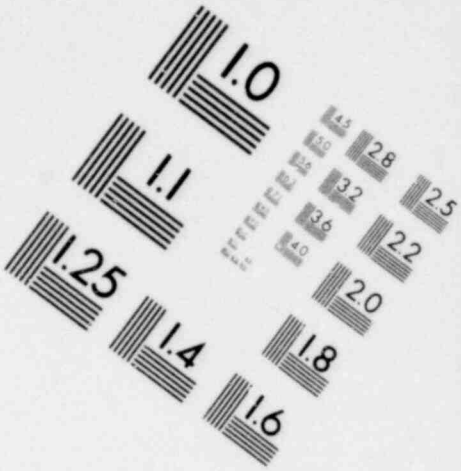

IMAGE EVALUATION
TEST TARGET (MT-3)

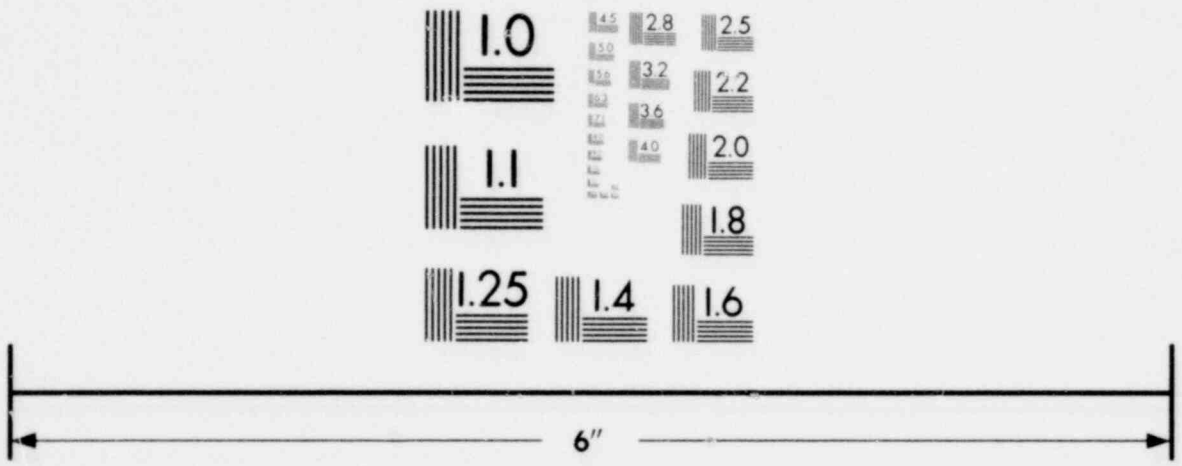

MICROCOPY RESOLUTION TEST CHART

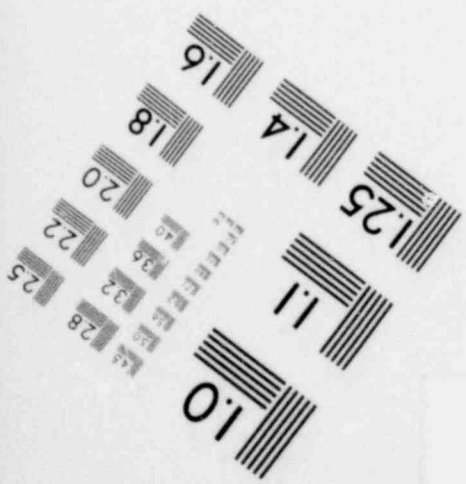

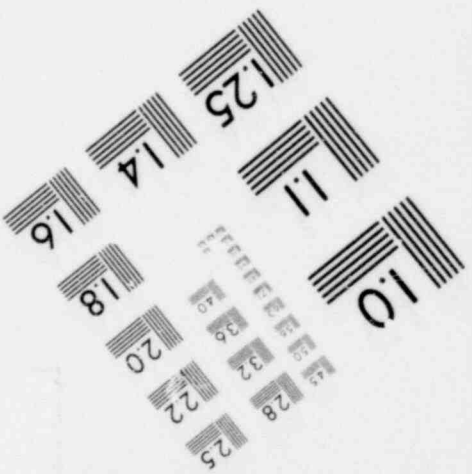

Also:

$$R = (R_1 + R_2)/2$$

$$\therefore \dot{R} = (\dot{R}_1 + \dot{R}_2)/2$$

or

$$\dot{R}_2 = 2\dot{R} - \dot{R}_1$$

Substituting for R_2 in (D-15):

$$\dot{z} = \dot{R}_1 - \dot{R} \qquad \text{(D-16)}$$

and

$$\ddot{z} = \ddot{R}_1 - \ddot{R} \qquad \text{(D-17)}$$

Equation (D-17) is used to define the vertical motion of the bubble. To calculate R_1, in equation similar to Equation (D-14) is employed, except:

$$P_{\infty 1} = P_\infty - R\rho g \qquad \text{(D-18)}$$

and, from Equation (D-16):

$$\dot{R}_1 = \dot{z} + \dot{R} \qquad \text{(D-19)}$$

are used in place of P_∞ and $\dot{R}$. This method predicts a slower rate of bubble rise than predicted by Equation (D-13).

This completes the formulation of the problem which involves three simultaneous differential equations in terms of radius (R), distance of center of bubble from a reference horizontal plant (Z) and bubble pressure (P_B).

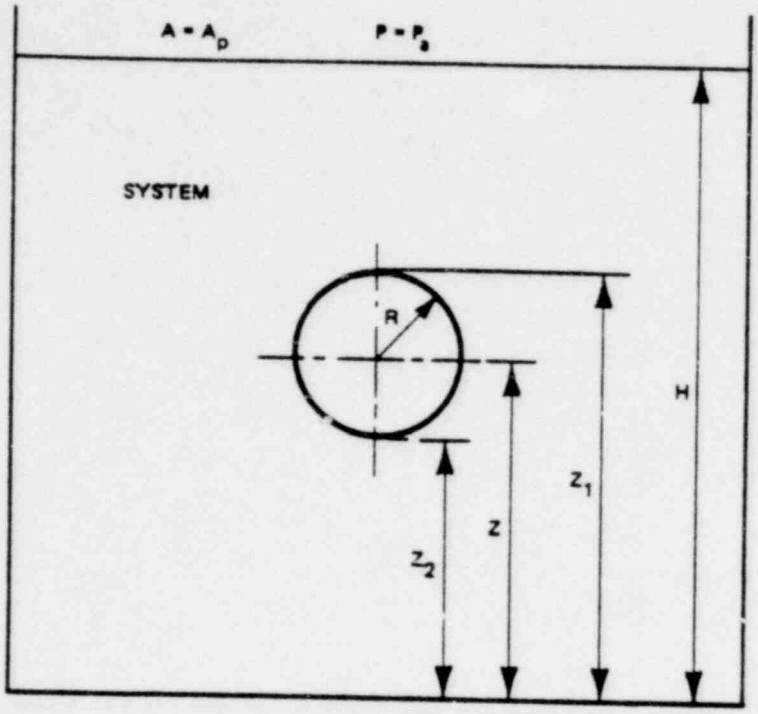

Figure D-1. Oscillating Bubble in Finite Pool

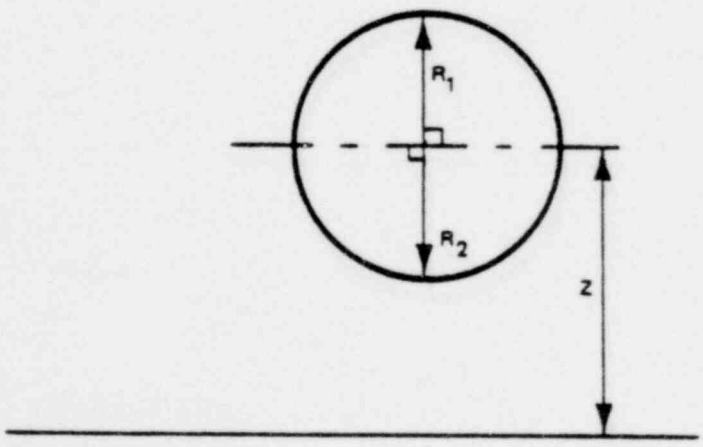

Figure D-2. Mechanism of Vertical Motion

1765 002

APPENDIX E

MONTICELLO SHELL PRESSURES

Table E-1

TORUS SHELL PRESSURES

Peak Positive/Peak Negative (psid)
(Sheet 1 of 8)

Run No.	Test No.	P12	P13	P14	P15	
2	2					
3	501					*
4	502					
5	801					
6	802					
7	901					
8	902					
9	903					
10	904					
11	905					
12	1101					
13	1102					
14	1103					
15	1104					
16	1105					
17	12					
18	1301					
18	1302					
18	1303					
19	14					
20	15					
21	1601					
21	1602					
21	1603					
21	1604					
21	1605					
22	18					
23	19					
24	21					
25	22					
26	2301					
28	2302					
30	2303					
31	2304					
31	2305					
31	2306					
31	2307					
32	24					

*Proprietary information has been deleted.

1765 004

Table E-1

TORUS SHELL PRESSURES
Peak Positive/Peak Negative (psid)
(Sheet 2 of 8)

Run No.	Test No.	P16	P17	P18	P19
2	2				
3	501				
4	502				
5	801				
6	802				
7	901				
8	902				
9	903				
10	904				
11	905				
12	1101				
13	1102				
14	1103				
15	1104				
16	1105				
17	12				
18	1301				
18	1302				
18	1303				
19	14				
20	15				
21	1601				
21	1602				
21	1603				
21	1604				
21	1605				
22	18				
23	19				
24	21				
25	22				
26	2301				
28	2302				
30	2303				
31	2304				
31	2305				
31	2306				
31	2307				
32	24				

*Proprietary information has been deleted.

1765 005

Table E-1

TORUS SHELL PRESSURES
Peak Positive/Peak Negative (psid)
(Sheet 3 of 8)

Run No.	Test No.	P20	P21	P22	P23	
2	2					
3	501					
4	502					
5	801					
6	802					***
7	901					
8	902					
9	903					
10	904					
11	905					
12	1101					
13	1102					
14	1103					
15	1104					
16	1105					
17	12					
18	1301					
18	1302					
18	1303					
19	14					
20	15					
21	1601					
21	1602					
21	1603					
21	1604					
21	1605					
22	18					
23	19					
24	21					
25	22					
26	2301					
28	2302					
30	2303					
31	2304					
31	2305					
31	2306					
31	2307					
32	24					

*Sensor 20 zero-shifted by -0.3 psid at test start (1302)

**Sensor 20 zero-shifted by +0.5 psid at test start (2307)

***Proprietary information has been deleted.

1765 006

Table E-1

TORUS SHELL PRESSURES

Peak Positive/Peak Negative (psid)

(Sheet 4 of 8)

Run No.	Test No.	P24	P26	P27	P29	
2	2					
3	501					*
4	502					
5	801					
6	802					
7	901					
8	902					
9	903					
10	904					
11	905					
12	1101					
13	1102					
14	1103					
15	1104					
16	1105					
17	12					
18	1301					
18	1302					
18	1303					
19	14					
20	15					
21	1601					
21	1602					
21	1603					
21	1604					
21	1605					
22	18					
23	19					
24	21					
25	22					
26	2301					
28	2302					
30	2303					
31	2304					
31	2305					
31	2306					
31	2307					
32	24					

*Proprietary information has been deleted.

Table E-1

TORUS SHELL PRESSURES
Peak Positive/Peak Negative (psid)
(Sheet 5 of 8)

Run No.	Test No.	P30	P31	P33	P34
2	2				
3	501				
4	502				
5	801				
6	802				
7	901				
8	902				
9	903				
10	904				
11	905				
12	1101				
13	1102				
14	1103				
15	1104				
16	1105				
17	12				
18	1301				
18	1302				
18	1303				
19	14				
20	15				
21	1601				
21	1602				
21	1603				
21	1604				
21	1605				
22	18				
23	19				
24	21				
25	22				
26	2301				
28	2302				
30	2303				
31	2304				
31	2305				
31	2306				
31	2307				
32	24				

*Proprietary information has been deleted.

1765 008

Table E-1
TORUS SHELL PRESSURES
Peak Positive/Peak Negative (psid)
(Sheet 6 of 8)

Run No.	Test No.	P35	P36	P37	P38
2	2				
3	501				
4	502				
5	801				
6	802				
7	901				
8	902				
9	903				
10	904				
11	905				
12	1101				
13	1102				
14	1103				
15	1104				
16	1105				
17	12				
18	1301				
18	1302				
18	1303				
19	14				
20	15				
21	1601				
21	1602				
21	1603				
21	1604				
21	1605				
22	18				
23	19				
24	21				
25	22				
26	2301				
28	2302				
30	2303				
31	2304				
31	2305				
31	2306				
31	2307				
32	24				

**

*P35 shifted at beginning of reading by +1.1 psid.
**Proprietary information has been deleted.

1765 009

Table E-1

TORUS SHELL PRESSURES
Peak Positive/Peak Negative (psid)
(Sheet 7 of 8)

Run No.	Test No.	P39	P40	P41	P42	
2	2					
3	501					*
4	502					
5	801					
6	802					
7	901					
8	902					
9	903					
10	904					
11	905					
12	1101					
13	1102					
14	1103					
15	1104					
16	1105					
17	12					
18	1301					
18	1302					
18	1303					
19	14					
20	15					
21	1601					
21	1602					
21	1603					
21	1604					
21	1605					
22	18					
23	19					
24	21					
25	22					
26	2301					
28	2302					
30	2303					
31	2304					
31	2305					
31	2306					
31	2307					
32	24					

*Proprietary information has been deleted.

1765 010

Table E-1

TORUS SHELL PRESSURES
Peak Positive/Peak Negative (psid)
(Sheet 8 of 8)

Run No.	Test No.	P43	P46
2	2		
3	501		
4	502		
5	801		
6	802		
7	901		
8	902		
9	903		
10	904		
11	905		
12	1101		
13	1102		
14	1103		
15	1104		
16	1105		
17	12		
18	1301		
18	1302		
18	1303		
19	14		
20	15		
21	1601		
21	1602		
21	1603		
21	1604		
21	1605		
22	18		
23	19		
24	21		
25	22		
26	2301		
28	2302		
30	2303		
31	2304		
31	2305		
31	2306		
31	2307		
32	24		

*

*Proprietary information has been deleted.

APPENDIX F

1/4 SCALE T-QUENCHER TEST BUBBLE AND WALL PRESSURES

Table F-1

1/4 SCALE T-QUENCHER TEST BUBBLE AND WALL PRESSURES (Sheet 1 of 3)

Test Identification		Bubble Pressures (psid) PT 19	Bubble Pressures (psid) PT 20	Tank Wall Pressures (psid) Pressure	Tank Wall Pressures (psid) *PT Numbers
Test A Runs 1-4 Baseline Case (Choked T-q) Piping Arr. A	Highest Value				11/15
	Mean				
	Std. Dev.				
	Std. Dev./Mean				
Test B Runs 1-5 P_{Tank} = 7.7 psia (Choked T-q) Piping Arr. A	Highest Value				11/15
	Mean				
	Std. Dev.				
	Std. Dev./Mean				
Test C Runs 1-4 P_{Tank} = 11.25 psia (Choked T-q) Piping Arr. A	Highest Value				11/12
	Mean				
	Std. Dev.				
	Std. Dev./Mean				
Test 1, Runs 1-4 Baseline Case Piping Arr. A	Highest Value				16/15
	Mean				
	Std. Dev.				
	Std. Dev./Mean				
Test 2 Runs 1-4 Low Steam Flow Piping Arr. A	Highest Value				11/15
	Mean				
	Std. Dev.				
	Std. Dev./Mean				
Test 3 Runs 1-4 High Steam Flow Piping Arr. A	Highest Value				15/15
	Mean				
	Std. Dev.				
	Std. Dev./Mean				
Test 4 Runs 1-5 P_{Tank} = 11.25 psia Piping Arr. A	Highest Value				11/15
	Mean				
	Std. Dev.				
	Std. Dev./Mean				
Test 4A Runs 1-4 P_{Tank} = 7.7 psia Piping Arr. A	Highest Value				11/15
	Mean				
	Std. Dev.				
	Std. Dev./Mean				
Test 5 Runs 1-6 Air Length = 26' Piping Arr. B	Highest Value				11/12
	Mean				
	Std. Dev.				
	Std. Dev./Mean				
Test 6 Runs 1-5 Air Length = 26' P_{Tank} = 11.25 psia Piping Arr. B	Highest Value				16/16
	Mean				
	Std. Dev.				
	Std. Dev./Mean				

*Proprietary information has been deleted.

1765 013

Table F-1

1/4 SCALE T-QUENCHER TEST BUBBLE AND WALL PRESSURES (Sheet 2 of 3)

Test Identification		Bubble Pressures (psid) PT 19	Bubble Pressures (psid) PT 20	Tank Wall Pressures (psid) Pressure	Tank Wall Pressures (psid) * PT Numbers
Test 7 Run 1, 3-5 Air Length = 108' Piping Arr. C	Highest Value Mean Std. Dev. Std. Dev./Mean				15/12 *
Test 8 Runs 1-4 Air Length = 108' P_{Tank} = 11.25 psia Piping Arr. C	Highest Value Mean Std. Dev. Std. Dev./Mean				11/13
Test 9 Runs 1-7 T-quencher Dist. to Tank Bottom = 0.7' Piping Arr. D	Highest Value Mean Std. Dev. Std. Dev./Mean				16/16
Test 10 Runs 1-4 Large Pipe (52') Piping Arr. E	Highest Value Mean Std. Dev. Std. Dev./Mean				16/15
Test 11 Runs 3-6 Waterleg = 6.25' Piping Arr. F	Highest Value Mean Std. Dev. Std. Dev./Mean				15/15
Test 12 Runs 1-4 Large Pipe (26') Piping Arr. G	Highest Value Mean Std. Dev. Std. Dev./Mean				12/15
Test 13 Runs 1-4 Submergence = 2.8' Piping Arr. H	Highest Value Mean Std. Dev. Std. Dev./Mean				16/16
Test 14, Runs 1-4 Waterleg = 1.65' Piping Arr. I	Highest Value Mean Std. Dev. Std. Dev./Mean				15/15
Test 15 Runs 2-5 $\Delta P_{Tank/Pipe}$ = 2 87' H_2O Piping Arr. I	Highest Value Mean STd. Dev. Std. Dev./Mean				17/17
Test 16 Runs 1-5 Wetted Pipe = 2.87' Piping Arr. K	Highest Value Mean Std. Dev. STd. Dev./Mean				15/17

*Proprietary information has been deleted.

1765 014

Table F-1

1/4 SCALE T-QUENCHER TEST BUBBLE AND WALL PRESSURES (Sheet 3 of 3)

Test Identification **		Bubble Pressures (psid)		Tank Wall Pressures (psid)		
		PT 19	PT 20	Pressure	* PT Numbers	
Test 17 Runs 1-5 Waterleg = 2.5' Minimum submergence Piping Arr. K	Highest Value Mean Std. Dev. Std. Dev./Mear				17/13	***
Test 18 Runs 1-4 ΔP_{Tank} = 4.9 + psia Piping Arr. J	Highest Value Mean Std. Dev. Std. Dev./Mean				15/15	
Test 19 Runs 1-4 $\Delta P_{Tank/Pipe}$ = 0.75' H_2O Piping Arr. K	Highest Value Mean Std. Dev. Std. Dev./Mean				13/13	
Test 20 Runs 1-5 Waterleg and Submergence = 3.38' Piping Arr. I	Highest Value Mean Std. Dev. Std. Dev./Mean				16/18	

* For sensors with highest positive and negative values.

** For piping arrangement see Figure B-1.

*** Proprietary information has been deleted.

1765 015

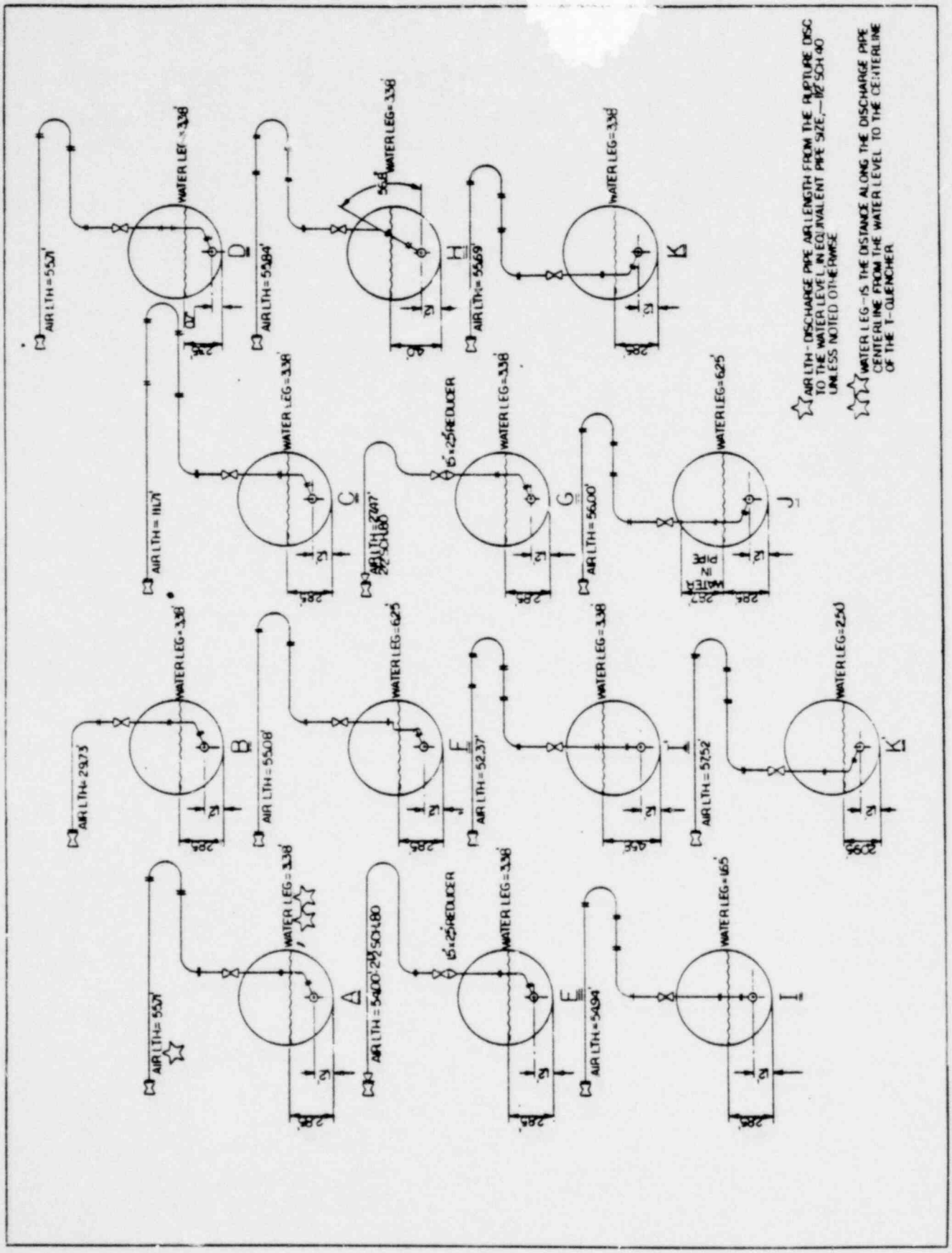

Figure F-1. Test Facility Piping (S/RVDL) Arrangements

NUCLEAR ENERGY DIVISIONS • GENERAL ELECTRIC COMPANY
SAN JOSE CALIFORNIA 95125

GENERAL ELECTRIC

TECHNICAL INFORMATION EXCHANGE

TITLE PAGE

AUTHOR	SUBJECT	TIE NUMBER
P. Valandani W. T. Hsiao	730	79NED71
		DATE: September 1979
TITLE: Analytical Model for Computing Air Bubble and Boundary Pressures Resulting from an S/RV Discharge Through a T-Quencher Device		GE CLASS: I
		GOVERNMENT CLASS: -
REPRODUCIBLE COPY FILED AT TECHNICAL SUPPORT SERVICES, R&UO, SAN JOSE, CALIFORNIA 95125 (Mail Code 211)		NUMBER OF PAGES: 213

SUMMARY

This report describes the methodology for calculating the loads on the boundaries of a pressure suppression pool due to safety/relief valve actuation. The methodology is applicable to Mark I plants equipped with T-Quencher discharge devices.

Model predictions are compared with full scale in-plant and 1/4 scale test data, the latter covering the range of the important parameters for Mark I plants.

By cutting out this rectangle and folding in half, the above information can be fitted into a standard card file.

DOCUMENT NUMBER NEDO-21878

INFORMATION PREPARED FOR Nuclear Power Systems Division

SECTION Containment Improvement Programs

BUILDING AND ROOM NUMBER PYD 409 MAIL CODE 905

GENERAL ELECTRIC